UNIVERSITÀ
DEGLI STUDI
DI PADOVA

Sede Amministrativa: Università degli Studi di Padova

Dipartimento di Salute della Donna e del Bambino – SDB

SCUOLA DI DOTTORATO DI RICERCA IN:

MEDICINA DELLO SVILUPPO E SCIENZE DELLA PROGRAMMAZIONE

INDIRIZZO: Ematooncologia, immunologia e genetica

CICLO XXVI

MECHANISMS OF CNS INFILTRATION IN T-CELL LEUKEMIA –A MOLECULAR STUDY OF ZEBRAFISH AND MOUSE MODELS

Direttore della Scuola: Ch.mo Prof. Giuseppe Basso

Coordinatore d'indirizzo: Ch.mo Prof. Giuseppe Basso

Supervisore: Dott.ssa Geertruy te Kronnie

Dottoranda: Chiara Borga

ABSTRACT

In 1970s, the introduction of presymptomatic central nervous system (CNS) therapy changed the prognosis of pediatic Acute Lymphoblastic Leukemia (ALL). Before that more than half of complete remissions obtained with systemic chemotherapy experienced CNS relapse. The contemporary use of risk-directed treatment has improved 5-year event-free survival to rates about 80% for childhood ALL. However, still CNS relapse remains an important cause of mortality occurring in about 3-8% of ALL patients. Recent clinical trials focus in reducing CNS relapse with the use of individualized therapy that can avoid both over- and under-treatment. Moreover, several studies aim to minimize secondary negative effects related to use of cranial irradiation, a treatment still recommended for ALL children at high risk of CNS relapse (i.e: patients with CNS leukemia at diagnosis or T-immuniphenotype with high White Blood Cell (WBC) count).

This project aims to deep insight into the mechanisms used by blast cells to infiltrate the CNS. We focused on T-ALL as in this leukemia the phenomenon of CNS disease is more recurrent than in B-ALL. To identify conserved molecular mechanisms that could be at the basis of CNS infiltration we started the analysis on animal models to move subsequently to human patients. To goal in this aim we used a gene expression profiling (GEP) approach.

Chapter 1 reports a study performed on two zebrafish models both developing T-ALL but that are genetically different; *hMYC-ER* line overexpresses human *C-MYC*, while *hlk* model carries an unknown mutation. We demonstrate for the first time that both these zebrafish model can mimic the phenomenon of CNS disease in T-ALL. Moreover, we found a different predisposition for *hMYC-ER* and *hlk* cancers to infiltrate the CNS. A whole transcriptome analysis of *hMYC-ER* and *hlk* T-ALL helped us to identify different molecular mechanisms that could control motility of blast cells. Particularly, we identified on *cxcr4/cxcl12* axis, an important mechanisms that could predispose T-lymphoblasts to infiltrate the CNS environment. In fact, we found a positive correlation between *cxcr4* expression levels and seriousness of CNS infiltration.

The importance of CXCR4/CXCL12 axis in determining extramedullary infiltration is still debated, as studies on pediatric ALL patients reveal conflicting results. In Chapter 2, we investigated the association of *CXCR4/*CXCR4 expression and CNS infiltration, using murine models xenoengrafted with human patients T-ALL cells. Also in this animal model we found diverse degree of CNS infiltration on xenografted mice derived by different human patients. Preliminary results seem to confirm that higher levels of *CXCR4* expression favour the migration of T-lmphoblasts towards the CNS environment. Further analyses of validation are ongoing on a larger cohort.

In Chapter 3 we switch to study the phenomenon of CNS infiltration on ALL patients. GEP analysis was used to compare patients with (CNS+) or without (CNS-) disease. However, this approach on human patients failed to find a strong signature that could identify CNS+ and CNS- patients. This result underlines the difficulty to study this phenomenon directly on human patients, as a high heterogeneity is present inside both T- and B-ALL group. Moreover, we could not find an association between *CXCR4* expression and CNS infiltration in a T-ALL cohort and that stress the idea that blasts cells can use different mechanisms to infiltrate the CNS and the high expression of *CXCR4* might be a predisposing factor that requires interaction with others mechanisms.

T-test analysis performed on zebrafish gene expression results revealed a significant different gene expression profile existing inside the zebrafish group overexpressing h*C-MYC* (*hMYC-ER*). This observation challenges us to clarify the importance and the role of *C-MYC* oncogene in T-ALL leukemogenesis. In Chapter 4 we were able to find a strong signature insight the group of patients with high expression of *C-MYC* that can discriminate patients with- and without- *C-MYC* rearrangements. In both Chapter 4 and 5 we tested the ability of gene expression profiling approach in identifying signature within specific subgroup of T-ALL patients. In fact also in Chapter 5 we showed the presence of a gene expression profile that characterize patients carrying *MLLT10* rearrangements inside the *HOXA* category of pediatric T-ALL.

RIASSUNTO

Fino agli anni ’70, la prognosi dei pazienti con Leucemie Linfoblastiche Acute (LAL) e coinvolgimentiìo del SNC era particolarmente infausta. Infatti circa il 70% dei pazienti presentava una ricaduta con coinvolgimento del SNC. L’introduzione di terapie mirate alla prevenzione/trattamento delle infiltrazioni blastiche nel Sistema Nervoso Centrale (SNC) all’inizio degli anni ’80 ha rivoluzionato il decorso clinico dei pazienti con ricaduta LAL e coinvolgimento del SNC. Attualmente, le ricadute LAL nel SNC rappresentano circa il 3-6% di tutte le ricadute e questo miglioramento si può ricondurre all’identificazione precoce dei pazienti ad alto rischio di ricaduta e l’uso di terapie specifiche per diverse categorie di rischio, che complessivamente, hanno permesso di raggiungere un tasso di guarigione che va oltre l’80%. Tuttavia, le ricadute nel SNC continuano ad essere un’importante causa di mortalità soprattutto in età pediatrica. Recentemente, numerosi *trials* clinici stanno cercando di ridurre il tasso di incidenza delle ricadute LAL che coinvolgono il SNC, attraverso l’uso di terapie individuali che permettano di evitare il sovra- o il sotto-dosaggio di chemioterapico per il paziente. Inoltre, molti studi stanno cercando di minimizzare gli effetti negativi dovuti all'uso di radioterapia, un trattamento ancora raccomandato nella cura delle LAL pediatriche ad alto rischio di ricaduta nel SNC (i.e. pazienti con infiltrazione del SNC già alla diagnosi o on LAL di tipo T associata ad un'alta conta di globuli bianchi).

In questa tesi, abbiamo impiegato lo studio del profilo di espressione genica al fine di individuare i possibili meccanismi molecolari che consentano alle cellule leucemiche di infiltrare il SNC, utilizzando 2 differenti modelli animali: zebrafish e topi NSG. I processi biologici identificati sono stati quindi validati in una corte di pazienti pediatrici alla diagnosi con leucemia limfobalstica acuta. Ci siamo focalizzati in particolar modo sulle LAL di tipo T, poichè in questo tipo di leucemie il coinvolgimento del SNC è più ricorrente rispetto alle LAL-B sia alla diagnosi che alla ricaduta.

Il capitolo 1 riporta uno studio effettuato su due modelli di zebrafish geneticamente differenti, in grado di riprodurre la LAL-T. La linea transgenica *hMYC-ER* sviluppa una leucemia LAL-T indotta dalla sovraespressione del gene umano *C-MYC*, mentre il modello zebrafish *hkl* è stato ottenuto tramite mutagenesi chimica non specifica. In

questo studio, abbiamo dimostrato come entrambe queste linee modello riescano a riprodurre il fenomeno dell infiltrazione delle cellule blastiche nel SNC con diverso grado di invasione a seconda del tipo di modello considerato. L'analisi dell'intero trascrittoma delle cellule leucemiche estratte dai due modelli di zebrafish, ci ha permesso di identificare diversi meccanismi molecolari che possono regolare la migrazione e l'infiltrazione delle cellule tumorali. In particolare, l'attivazione dell'asse *cxcr4/cxcl12* sembra conferire ai linfoblasti T una maggiore capacità di infiltrazione del SNC nel modello *hMYC-ER*, come dimostrato dalla sua maggiore invasivita nel SNC, rivelando una correlazione diretta tra l '*over-espressione* del *cxcr4* e il grado di invasione.

Nel capitolo 2, abbiamo studiato l'associazione tra espressione del *CXCR4* e l'infiltrazione del SNC in topi xenotrapiantati con cellule LAL-T provenienti da pazienti pediatrici. Risultati preliminari sembrano confermare la correlazione tra alti livelli di espressione del *CXCR4* e l'aumentata migrazione dei linfoblasti T nel SNC. Attualmente ulteriori analisi sono in corso, con lo scopo di validare la relazione "espressione *CXCR4*-infiltrazione del SNC" in una coorte più ampia.

Nel capitolo 3, considerando i risultati precedentemente ottenuti, abbiamo analizzato il profilo di espressione genica di pazienti pediatrici alla diagnosi di leucemia limfobalstica acuta con (SNC+) o senza (SNC-) coinvolgimento del SNC. Questo approccio non ha portato all'identificazione di una *signature* in grado di distinguere i due gruppi considerati e questo risultato è in parte dovuto al basso numero di pazienti analizzati con SNC+ e all'alta eterogenicità genetica presente all interno della corte studiata. La mancanza di una diretta correlazione tra l'espressione del *CXCR4* e l'infiltrazione nel SNC nei pazienti LAL-T suggerisce che più meccanismi molecolari possano cooperare per regolare il movimento delle cellule leucemiche e determinarne la capacità di infitrare tessuti extra-midollari. L'alta espressione del *CXCR4* potrebbe essere un fattore di predisposizione che tuttavia richiede l'interazione con altri mecanismi per consentire ai linfoblasti-T di entrare nel SNC.

Nel capitolo 4 ci siamo focalizzati sul significato biologico della diversa espressione del gene C-MYC in pazienti LAL-T in relazione alla varie aberrazioni genetiche che possono modulare l'espressione di questo oncogene. Tramite l'analisi dell'espressione genica abbiamo individuato una specifica signature in grado di distinguere pazienti con over espressione e riarrangiamenti citogenetici del gene C-MYC.

Abbiamo successivamente analizzato il profilo di espressione genica di pazienti LAL-T con riarrangiamenti citogentici *HNRNPH1-MLLT10* e *DDX3X-MLLT10* per determinare se questo sottogruppo di pazienti presentava caratteristiche comuni ad altri pazienti con riarrangiamenti del gene *MLLT10* all'interno della categoria *HOXA*.

Attraverso questo studio abbiamo dimostrato i vantaggi legati all'analisi del profilo di espressione genica per l'identificazione di particolari *signatures* che vadano a distinguere dei sottogruppi all'interno di specifiche categorie di pazienti affetti da LAL-T. Lo studio ha permesso inoltre, attraverso l'utilizzo in due diversi modelli animali, di identificare comuni specifici meccanismi molecolari legati all'infiltrazione delle cellule blastiche nel sistema nervoso centrale.

INDEX

LIST OF ABBREVIATIONS

AIEOP	- Associazione Italiana Ematologia-Oncologia Pediatrica
ALL	- Acute Lymphoblastic Leukemia
T-ALL	- T-cell Acute Lymphoblastic Leukemia
B-ALL	- B-cell Acute Lymphoblastic Leukemia
AML	- Acute Myeloid Leukemia
BM	- Bone Marrow
BBB	-Blood Brain Barrier
BRB	-Blood Retinal Barrier
cDNA	- complementary Deoxyribonucleic Acid
CI-FISH	- interphase fluorescence in situ hybridization
CNS	- Central Nervous System
CNS+	- Positive for Central Nervous System infiltration at diagnosis
CNS-	- Negative for Central Nervous System infiltration at diagnosis
CSF	- Cerebrospinal fluid
Ct	- Cycle threshold
DAVID	- Database for Annotation, Visualization and Integrated Discovery
DEPC	- Diethylpyrocarbonate
dpf	- days post-fertilization
dpi	- days post-injection
DNA	- Deoxyribonucleic Acid
EFS	- Event Free Survival
ENU	- ethylnitrosourea
FAB	- French–American–British
FACS	- fluorescence-activated cell sorting
FCM	- Flow cytometry
GEP	- Gene Expression Profiling
HG	- Human Genome
h	- human

hpi	- hours post-injection
H&E	- Hematoxiyin & Eosin
IgG	- Immunoglobulin G
IF	- Immunoflorescent
IHC	- Immunohistochemistry
IVT	- In Vitro Transcription
lfdr	- local false discovery rate
HSC	- Hematopoietic Stem Cells
MDS	- Myelodysplastic Syndromes
MILE	- Microarray Innovations in LEukemia study group
MNC	- Mononucleated Cells
MRD	- Minimal Residue Disease
N.D.	- No Data
NK	- natural killer cells
PB	- Peripheral Blood
PCR	- Polymerase Chain Reaction
PGR	- Prednisone Good Response
PPR	- Prednisone Poor Response
RIN	- Ribonucleic Acid Integrity Number
RMA	- Robust Multi-array Average
RNA	- Ribonucleic Acid
QC	- Quality Control
qPCR	- quantitative – Polymerase Chain Reaction
qRT-PCR	- quantitative Reverse Transcriptase – Polymerase Chain Reaction
ROIs	- Regions of interest
RT-PCR	- Reverse Transcriptase – Polymerase Chain Reaction
SAPE	- Streptavidin-phycoerythrin
SE	- Standard Error
STRING	- Search Tool for the Retrieval of Interacting Genes/Proteins
TAE	- Tris-Acetate-EDTA
TCR	- T-cell Receptor

TLP	- Traumatic Lumbar Punction
vs.	- Versus
WBC	- White Blood Count
Zf	- zebrafish

INTRODUCTION

ACUTE LYMPHOBLASTIC LEUKEMIA

Acute Lymphoblastic Leukemia (ALL) is a clonal aggressive malignancy of the bone marrow, characterized by abnormal proliferation of lymphoid progenitor cells that arrested at premature stage of differentiation, disrupting the normal haematopoiesis and infiltrating extramedullary organs. ALL constitutes the most common pediatric cancer, representing 80% of all leukemia that occur in children and adolescents [1,2]. This malignancy represents a heterogeneous group, characterized by different morphological, immunologic and cytogenetic features [3-5]. The malignant clones can originate both from the B-cell (85% ALL) and the T-cell lineage (15% ALL) [6-8] and often carry specific genetic alterations, such as chromosomal translocation that create specific fusion genes, aberrant expression of proto-oncogenes, chromosomal deletion and hypo- or hyper-diploidy (figure1).

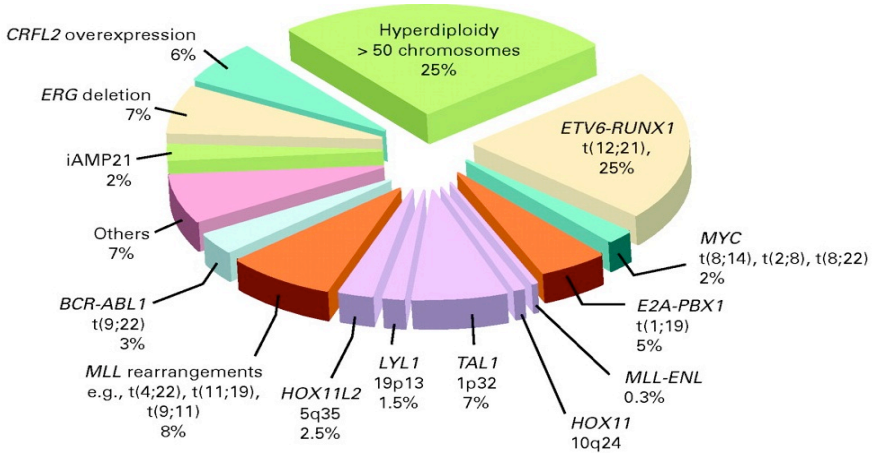

Figure 1: Estimated frequency of genetic abnormalities in ALL. Violet areas refer to T-ALL abnormalities; other colours indicate B ALL abnormalities (from Pui et al., 2011 [8]).

The presence of established genetic alterations in blasts cells allowed the identification of specific subtypes of disease related to different prognosis [9-12]. For this reason, nowadays, genetic aberrations are also used to stratify ALL patients into different risk-groups, ranging from standard-risk to high-risk. In the last years, multi-agent combination chemotherapy and the introduction of a risk-directed treatment allowed

ALL patients to receive more appropriate treatment and that resulted in a cure rate of more than 85% (5-year event free survival, EFS) in children with ALL [8,13,14]. Although the overall EFS have increased significantly over the past decades there are still groups of ALL patients that experience treatment resistance and relapse [8] and remain of major concern [15]. One of these unfavourable events, that position ALL-patients in the high-risk strata, is the presence of blast cells in the Central Nervous System (CNS) [16].

CNS INFILTRATION IN CHILDHOOD ALL

The Central Nervous System (CNS) was recognized as possible site of infiltration by leukemic cells in the early decades of childhood ALL therapy [17,18]. The presence of CNS infiltration (CNS+) is an event that can be present both at diagnosis (<5%) and relapse (~30-40%) in ALL pediatric patients and constitutes one of the main challenge in the cure of ALL. The ability to enter in the CNS gives an immediate advantage to blast cells: the CNS acts as a shelter for lymphoblasts preventing their exposure to chemotherapeutic compounds and serving as a reservoir for relapse [19,20]. The presence of blasts cells in the CNS can be related to pathological symptoms, such as symptoms of CNS haemorrhage (i.e. altered mental status, headache, neurological deficits, seizure) or spinal cord compression (paresthesias, weakness, back pain, bladder dysfunction), but most frequently patients experience asymptomatic CNS infiltration [16]. The current methodology for the diagnosis of CNS+ ALL is the cytopathological examination of a cytospin smear of cerebrospinal fluid (CSF) taken trough lumbar puncture. Nowadays, a patient is considered to have CNS infiltration (CNS+) at diagnosis with high risk of relapse, when more than 5 White Blood Cells (WBCs)/μL are detected in its CSF. In detail, there is a risk classification for CNS disease in ALL: CNS 1, identifies the absence of leukemic cells detectable in the CSF; CNS 2, denotes the presence of blast cells in a CSF sample with <5 WBCs/μL; CNS 3, refers to CSF samples with leukemic cells and >5 WBCs/μL [21]. A recent study stressed the importance to detect Minimal Residue Disease (MRD) in the CSF of CNS+ patients during treatment, to better recognise cases at high risk of leukemic relapses [22]. This study also proposed to use more sensitive techniques than cytopathological analysis of

the CSF, such as flow cytometry (FCM) or PCR-based methods [23,24]. In addition, several works showed that applying FCM or PCR methods in CSF analysis, many ALL patients at diagnosis resulted to have subclinical disease (CNS 2) in the CNS [23-27], an information very important as the presence of small numbers of leukocytes in the CSF at diagnosis (CNS 2) is still a controversial risk factor [21,28,29]. These considerations suggest that also patients that clinically are considered to be without CNS infiltration (CNS-) could partially experience this complication; we can easily understand the importance of introducing more sensitive techniques in the diagnosis of CNS disease in ALL to get deeper insight in the clinical significance of subclinical CNS infiltration in patients.

Molecular mechanisms used by ALL-cells to infiltrate the CNS are not well understood. Moreover, also the access way to enter in this environment is unknown and is hypothesized to be diverse; blast cells could enter the cerebrospinal fluid (CSF) through the choroid plexus, use the brain capillaries to invade the parenchyma, infiltrate the leptomeninges through bony lesions of the skull or enter through hemorrhages due to natural and iatrogenic processes (i.e: lumbar puncture)[16,30]. To understand the access way and the molecular mechanisms used by blasts cells to infiltrate the CNS, the study of CNS+ patients is not so easy. In fact, patients' material is few and it is currently not possible to study cells extracted from the CSF, as the sample often contains very few cells or no cells at all. Moreover, studying patients does not allow to analyze how CNS infiltration occurs at the anatomical level.

Two studies tried to investigate the molecular mechanisms used by ALL cells to infiltrate the CNS in pediatric patients; Cario and colleagues compared the transcriptome of children with- and without- CNS infiltration in ALL, they found the up-regulation of *interleukin-15* (*IL-15*) as a factor that predicted the ability of blasts to infiltrate the CNS [31]. Crazzolara and colleagues focused on the expression of CXCR4 in ALL pediatric patients, showing that higher levels of this chemokine receptor could be predictive of blasts ability to infiltrate extramedullary organs [32]. However, the results of these studies still need to be reproduced in validation studies.

Given the difficulties to study the phenomenon of CNS infiltration in patients, the

research of CNS leukemia has two important sources in 1) old histological studies performed on brains of CNS+ patients (post mortem) and 2) studies of animal models that mimic CNS+ ALL.

Studies of pathological anatomy on the brain of pediatric patients with acute leukemia were performed in the 1970s, when the blasts ability to infiltrate the CNS was just discovered and 70% of patients presented intracranial leukemia at time of death. An old histological study of intracranial leukemic infiltrates in the CNS of children with acute leukemia revealed the presence of different degrees of CNS infiltration that together could indicate the way used by blast-cells to infiltrate the CNS until reaching deeper sites: the parenchyma. Particularly, this study described CNS infiltration as a progressive arachnoid disease, identifying 1) an initial infiltration of the walls of superficial arachnoid veins and surrounding adventitia, with consequent disruption of arachnoid trabeculae and contamination of the CSF when the number of cells increased; 2) a following involvement of the deep arachnoid tissue in grey and white matter regions and 3) in association with perivascular arachnoid leukemia, pia-glial-membrane disruption and infiltration of parenchyma (figure 2).

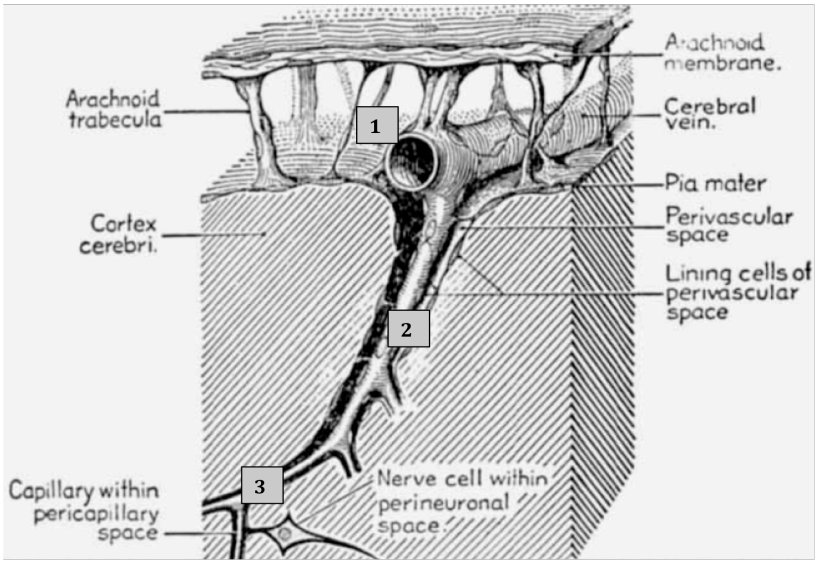

Figure 2. Diagram of leptomeninges (modified by *Weed, Am. J. Anat., Vol 31*).

In summary the study revealed how leukemia cells do not penetrate capillaries of CNS parenchyma, but infiltration of the neural tissue is a consequence of arahnoid leukemia

progression following disruption of the pia-glial-membrane [33]. In addition, another pathological study revealed how, in pediatric acute leukemia, there is a close relation between CNS disease (meningeal level) and the eye involvement at the level of both the optic nerve and retina [34]. Fortunately, the level of CNS infiltration that is found nowadays in most ALL patients is very different from that described in studies of the 1970s; never the less these "old" study are very informative, giving an overview of how blast cells can potentially infiltrate the CNS environment if the disease had develop when left untreated.

Another important source to study the phenomenon of the CNS infiltration is the use of animal models that can mimic CNS+ ALL disease. These models can be obtained through both the creation of transgenic models and xenotransplantations of human cells (from stable cell lines or directly from ALL patients) in immuno-suppressed animal recipients. In the previous decades, several murine models of ALL developing CNS infiltration have been created both for the B- and T- lineages; however, multiple incongruent results have been obtained from these studies. Buonamici and colleagues created a murine model xenografted with human T-ALL cell lines and found in the CCR7 expression a key signal for migration of T-lymphoblasts towards the CNS [35]. Holland and colleagues studied the presence of CNS infiltration in a mouse model, engrafted with human pre-B pediatric ALL cells, identifying an important role played by RAC2, AEP and ICAM1 in the process of CNS invasion [36]. Of note, in the latter murine model the CNS infiltration involved also the eye level, underlining the ability of this model to mimic infiltration found in patients [33]. Moreover, in another study performed in a pre-B ALL murine model, the down-regulation of CXCR4 was found in CNS-homing cells [37]. Summarizing, different results have been found in studies performed both on CNS+ ALL human patients and animal models and the mechanism/s used by ALL cell to infiltrate the CNS is/are still unknown.

In the absence of a clear understanding of the phatogenesis of CNS disease, the design of target therapies remains beyond reach. ALL-patients that present CNS infiltration are stratified in a high-risk group and usually receive an intensive treatment consisting in a combination of intrathecal chemotherapy followed by cranial irradiation. The main

benefit of intrathecal therapy is the avoidance of the blood brain barrier. Nowadays, one of the main challenge in the cure of ALL is the reduction of treatment-related late negative effects that involve about two third of long-term survivors [38]. This challenge mainly concerns ALL pediatric patients that present CNS infiltration, as a lot of secondary negative complications are associated to cranial irradiation (i.e: cognitive deficits, endocrinopathy, second cancers) [38-42]. In the last decades, many efforts have attempted to avoid or reduce the use of prophylactic cranial irradiation [43,44] and two clinical trials [30,45] demonstrated that cranial irradiation could be completely omitted using intensive triple (methotrezate, hydrocortisone and cytarabine) intrathecal therapy [46]. The combination of these drugs is highly effective in the treatment of CNS infiltration in pediatric patients. However, as CNS relapse still remains an important cause of mortality occuring in 3-6% of ALL patients that relapse [16,47,48], cranial irradiation is still recommended for 2-20% of patients at very high risk of CNS relapse [16]. Several risk factors have been associated to an increased risk to develop CNS relapse in ALL pediatric patients; a) the presence of leukemic cells in the CSF both for natural or iatrogenic introduction after traumatic lumbar punctures [29,49,50], b) T-cell immunophenotype, especially if accompanied by high leukocyte counts [16,51-53] and c) genetic abnormalities, such as t(9;22), t(1;19) and MLL rearrangements [16,54].

T-CELL ACUTE LYMPHOBLASTIC LEUKEMIA

T-cell Acute Lymphoblastic Leukemia (T-ALLs) is an aggressive hematologic tumor arising from the malignant transformation of hematopoietic progenitors of the T-lineage. T-ALL constitutes 10-15% of pediatric and 25% of adult ALL cases [55]. Clinically, T-ALL patients show an extended infiltration of the bone marrow by immature T cell lymphoblasts, often associated to high white cell counts, mediastinal masses with pleural effusion and increased risk of leptomeningeal infiltration at diagnosis [56]. T-ALL is a genetically heterogeneous disease resulting from a multistep oncogenic process in which several genetic alterations contribute to arrest the process of thymocyte differentiation at different stages of T-cell maturation and at the same time promote proliferation and survival of T-lymphoblasts. Below follow the main genetic alterations that have been associated to the pathogenesis of T-ALL.

Constitutive activation of NOTCH1signaling

The NOTCH signaling pathway plays a central role in T-ALL pathogenesis. NOTCH1, whose gene is localized on chromosome 9, is a transmembrane receptor involved in normal development of T-cell progenitors and thymocytes differentiation. Physiologic activation of NOTCH1 is due to the interaction with a DSL ligand that induces two proteolitic cleavages in the receptor. These proteolitic cleavages allow the release of the intracellular portion of NOTCH1 protein (ICN1) from the membrane to the cytoplasm [57]. Than, ICN1 translocates to the nucleus where it acts as transcription factor of specific target genes [58]. Aberrant NOTCH1 signaling in T-ALL was initially related to a rare chromosomal translocation [t(7;9)(q34;q34.3)] of *NOTCH1* with T-cell receptor B (*TCRB*) described in 1% of T-ALL and resulting in a truncated form of constitutively active NOTCH1 [59]. The subsequent identification of *NOTCH1* activating mutations in nearly 60% of T-ALL patients [60] underlines the central role of NOTCH1 in oncogenic T-cell transformation. *NOTCH1* mutations usually involve the heterodimerization domain (HD) or the C-terminal PEST domain [60]: mutations in the HD domain are present in ~40% of T-ALLs and result in a ligand-independent activation of the receptor, while mutations in the PEST domain involve ~15% of T-ALLs and impair ICN1 proteasomal degradation with consequence ICN1 stabilization in the nucleus. In both cases, the final effect for these mutations is the constitutive activation of the *NOTCH1* signaling pathway. Another event that contributes to NOTCH1 pathway activation in ~15% of T-ALL patients is the presence of inactivating mutations in the *FBXW7*, a gene that encodes for a protein involved in NOTCH1 degradation [61,62]. In the last years, several studies showed how NOTCH1 pathway activation in pediatric T-ALL was associated with improved early therapeutic response and increased sensitivity to glucocorticoids. However, different results were obtain in terms of clinical outcome; in fact, four studies showed an improved outcome in patient that present *NOTCH1/FBXW7* mutations [63-66], whereas two other studies failed to find this association [67,68]. All together these studies show that the prognostic impact of NOTCH1 activation seems to be therapy-related.

Deletions of the CDKN2A locus

More than 70% of T-ALL patients present deletions of the *CDKN2A* locus [69] (chromosomal band 9p21), which contains the *p16INK4A* and *p14ARF* tumor suppressor genes, which contributes to leukemia progress through loss of cell proliferation control [70,71]. The incidence of these deletions has not been investigated in large T-ALL cohorts and for the moment their prognostic significance remains unknown.

Chromosome rearrangements in T-ALL

Among genomic alterations at diagnosis of childhood T-ALL, chromosomal translocations that place oncogenic transcription factors (TLX1, TLX3, TAL1, LMO1, LMO2, HOXA) under the control of *TCR* genes (*TCRB* or *TCRA-TCRD*) have an incidence of 40-50%. In addition, also other non-TCR gene mediated translocations could produce fusion products and several genes can be activated or inactivated by the presence of somatic copy number variations (amplifications and/or deletions) or specific point- or insertion/deletion mutations [72].

In the light of these observations, T-ALL is a heterogeneous disease that can present multiple genetic aberrations. However, several studied have identified some major subtypes that are useful to classify the T-ALL. Particularly, these subtypes are associated to specific chromosomal rearrangements, distinct gene expression signatures (*TAL*-like, *TLX1/3*-like and *HOX*-like) and different stage of arrest during T cell development [7,55,73-75].

TAL1: Overexpression and aberrant activation of *TAL1* is present in about 60% of T-ALL cases as result of various chromosomal rearrangements [76]. In 20-30% of T-ALL, a small intracromosomal rearrangement placed *TAL1* under the control of the promoter region of *SIL*, resulting in the SIL-TAL1 fusion product. Moreover, the translocations t(1;14)(p32;q11) or the variant t(1;7)(p32;q35) juxtaposes *TAL1* under the control of *TCRA/D* enhancers, resulting in its ectopic expression in about 3% of TALL. Late-cortical T-ALL thymocytes (CD4+, CD8+, CD3+) have been shown to carry the activation of the *TAL1* transcription factor and this has been associated to a more favourable outcome [70,77-79].

LMO: Translocations involving the *LMO1* [t(11;14)(p15;q11)] and *LMO2*

[t(11;14)(p13;q21)] genes occur only in 9% of pediatric T-ALL cases. However, about 45% of T-ALL present an aberrant expression of *LMO2*, suggesting other still unknown mechanisms of activation, In most cases, the activation of *LMO1* and *LMO2* has been associated to over-expression of *TAL1* [55].

TLX1: The aberrant expression of *TLX1* is due to a translocation [t(10;14)(q24;q11)] that positions *TLX1* under the control of the *TCRA/D* enhancer [80-82], occurs in 5-10% of pediatric T-ALL and is usually associated with good prognosis and low risk of relapse [55,83].

TLX3: The overexpression of *TLX3* is present in 20-25% of pediatric ALL and result from the t(5;14)(q35;q32) translocation [84]. Both the expression of *TLX1* and *TLX3,* have been associated with early- cortical T-ALL [55]. In some studies the aberrant expression of *TLX3* has been associated to poor prognosis and high incidence of relapse [70,79].

HOXA: about 3% of T-ALL patients carry translocations of the *HOXA* cluster of *HOX* genes in *TCRB* and *TCRG* loci, with aberrant expression of the *HOXA10* and *HOXA9* genes [85]. In addition, over-expression of *HOXA* genes also characterized T-ALL patients that carry other chromosomal translocation generating other chimeric transcription factors [86,87]. These translocations include: the *PICALM-MLLT10* fusion oncogene [t(10;11)(p12;p14)] involving about 5-10% of T-ALL patients which has been associated with an adverse prognosis [85,88]; the *MLL* rearrangements (*MLL-AF4* and *MLL-ELN*) in 5% of T-ALL, whose prognostic significance remains to be defined [89] and the rare deletion del(9)(q34.11q34.13), resulting in the *SET-NUP214* fusion product [90].

Next to these rearrangements that characterize the main subgroups, there are also translocations involving proto-oncogenes, such as *c-MYB* and *c-MYC*. The t(6;7)(q23;q34) results in the activation of the *c-MYB* oncogene through a rearrangement with *TCRB*: this MYB translocation has been identified in very young children (<2 years old) and has been shown to be characterized by a peculiar gene expression profile [91]. Also *c-MYC* can be activated by translocations with the *TCR* [t(8;14)(q24;q11)] in 1% of T-ALL [92], but usually *c-MYC* activation is the result of different factors.

Deregulation of C-MYC expression

MYC is an important transcription factor controlling several cell functions, such as energy metabolism, proliferation and survival [93] and it is also a potent oncogene, whose deregulation is present in about 70% of cancers [94-96]. In addition, MYC is a complex factor with a dual functional role: while it promotes cell growth and cell cycle progression, it can also promote apoptosis through the P53/ARF and BIM pathways. So in physiological conditions, the extra cell divisions caused by MYC overexpression is balanced by an increased cell-death [97,98].

In T-ALL, *C-MYC* plays a critical role in determining tumor growth and maintenance and its deregulation at transcriptional level is frequently associated to $NOTCH1^{m}$, as *C-MYC* is a direct target gene of NOTCH1 [99-101]. Notably, most of the genes controlled by NOTCH1 that regulate cell growth, proliferation and metabolism are also target of MYC [99,102,103]. This *NOTCH1-MYC* transcriptional regulatory loop position the control of anabolic cell growth pathways as an important mechanism in mediating T-Cell malignant transformation by NOTCH1. In addition to $NOTCH1^{m}$, there are several other physiologic pathways that regulate MYC at transcriptional and posttranscriptional levels [236], so alternative routes can induce MYC activation independently from $NOTCH1^{m}$. One of these alternative mechanisms are *FBXW7* mutations ($FBXW7^{m}$) that can occur both in the presence (~20%) or absence (~5%) of $NOTCH1^{m}$. By preventing degradation of several proteins (among them NOTCH1 and MYC), $FBXW7^{m}$ can contemporary induce NOTCH1-dependent *MYC* transcriptional activation and MYC stabilization at the protein level [61,62,104]. Moreover, *C-MYC* expression can also be modulated by *LEF1* inactivation (~11%) [105] and *C-MYC* rearrangements with *TCR* or unknown partner genes, even if these genetic alterations are rare in T-ALL (~5%) [106]. In addition, another major cause of MYC activation in T-ALL is the downregulation of PTEN (consequent to *PTEN* deletion or mutations), an event that causes the release of AKT-induced inhibition of GSK-3β, preventing MYC phosphorilation and degradation [107] (figure 3). A recent study in a murine model showed that activation of Wnt/β-catenin pathway can induce the development of a Notch1-independent T-ALL, characterized by high expression of *Myc* due to *Myc*

rearrangements and loss of Pten activity [108]. Interestingly, several different networks converge to induce the up-regulation of MYC, suggesting a critical role of this oncogene in T-ALL leukemogenesis [100,107,109,110].

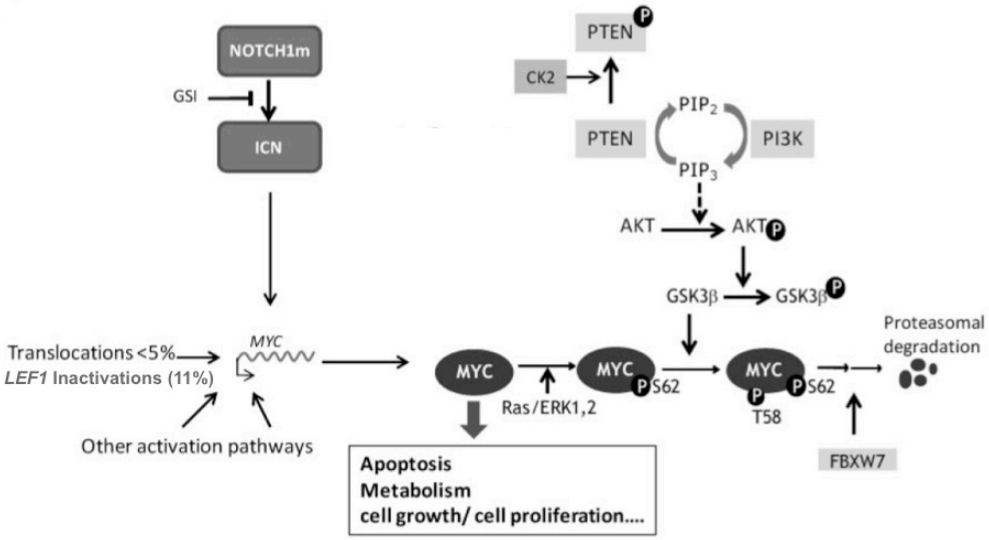

Figure 3. MYC transcription and postranscription modulation. Schematic representation of a few regulators/effectors that modulate MYC expression. (modified from [107]).

The oncogenic potential of MYC in leukemic initiation was demonstrated in many animals models [111-115], however, several other studies demonstrated that the overexpression of MYC by itself is not sufficient to cause T-ALL and additional events are required to initiate leukemogenesis [116-118].

Alterations in signal transduction pathway

In addition to chromosomal rearrangements previously described, genetic aberration can interest also genes that have important functions in controlling and regulating pathways related to T-cell proliferation that are frequently deregulated in T-ALL.

Genetic alterations that involve the tumor suppressor *PTEN* cause the aberrant activation of the PI3K-AKT pathway, as PTEN is a critical negative regulator of this pathway [119]. Deletion of *PTEN* is present in 5-10% of T-ALL, but ~17% of T-ALL lack PTEN protein expression [120].

About 5-10% of T-ALL carry *RAS*-activating mutations that result in accumulation of Ras in its active conformation [121-123]. In addition, about 3% of T-ALL present

mutations or deletions of a negative regulator of the Ras pathway: the *NF1* gene [124]. Moreover, several studies have described mutations of the oncogene *IL7R* in 10% of T-ALL (gain-of-function exon 6 mutations) [125] and recently it has been demonstrated that mutations of this oncogene promote tumor formation through constitutive activation of the JAK-STAT signaling pathway [126].

In conclusion, T-ALLs constitute a complex and heterogeneous group of disease, resulting from numerous combinations of multigenic aberrations and oncogenic cooperation [87] that have been extensively characterized. However, the association between genetic alterations and prognostic impact is often not clear. Moreover, although current therapies achieve five years-relapsed-free survival rates for about 75% in children, still 30% of patients relapse [127,128]. The high number of relapses stresses the importance of gaining deeper insights into molecular mechanisms that control malignant transformation and drug resistance, to eventually develop effective targeted therapies. However, one of the main obstacle to achieve this aim lies in T-ALL heterogeneity: in fact, in each patient multiple genetic alterations can occur and cooperate, determining the activation of particular oncogenic processes that determine a specific prognostic significance.

GENE EXPRESSION PROFILING

Microarray technology is a powerful technique that allows the simultaneous analyses of the expression of ten of thousands of genes in a sample of interest. In the field of leukemia diagnosis and research, microarray gene expression analysis consents to study the "whole transcriptome" of cancer cells and help the discovery of genes or gene networks that can be related to disease processes. This technology can have multiple applications, not only in basic research to investigate molecular mechanisms that contribute to disease development, but also to find prognostic marker that can be used in the clinic through the building of a 'prognostic' classifier for patients.

Microarrays technology

In this project we used the GeneChip Human Genome U133 Plus 2.0 Array and the Zebrafish Genome Array (Affymetrix, Santa Clara, CA). This type of microarray

platforms can evaluate the expression of coding sequences of genes by assessment of the amount of RNA transcription (gene expression profiling, GEP). GeneChips consist of a small surface of silicon wafer containing immobilized short (25-30 mer) oligonucleotides probes synthesized in situ by photolithographic techniques. The pool of transcripts of a sample of interest is labeled with a fluorescent dye and hybridized to the microarray. The fluorescent signal bound to the probe is an indicator of the expression levels of the corresponding transcript. The use of short oligonucleotides probes minimizes the risk of cross-hybridization, consenting high levels of specificity of the signal [129,130]. To accurately measure the expression level of a particular transcript, a probe set containing 11 probe pairs, is used. All probe sets are redundant and distributed all over the GeneChip.

Several types of arrays are commercialy available that are specific for different species (Human, Mouse, Zebrafish etc). For human samples, each array contains more than 54.000 probe sets, which cover more than 47.000 transcripts and variants representing approximately 38.500 human genes. Currently, commercial arrays have reached whole transcriptome coverage. Often results of mircoarray results are validated using other techniqus such as qRT-PCR.

Several controls are assessed in order to validate the quality of each GeneChip:

Scale factor: This factor is the mean value of all numbers that are applied by the Command Expression Console Software to each signal present on the array to adjust them to a target value (default = 100). The Scale Factor is used to assess the comparability between GeneChips. We used a maximum of 3-fold difference between the highest and lowest Scale Factor.

Background and Noise: The background represents non-specific binding and auto-fluorescence of the surface of the array. The noise factor is related to the background and represents the variation within the background signal. For the comparison of GeneChips with each other, these values should be really similar for each array. The mean 10x standard deviation is used.

Present calls: This control represents the percentage of present probe sets (hybridized transcripts) in a GeneChip. Within an experiment we expect that the percentage of

present calls remain equal across different GeneChips. The percentage of present calls in human tissue should always be higher than 30%.

Internal probe calls: Oligo B2 spiked controls: *bioB*, *bioC*, *bioD* and *CRE* were added to the hybridization. We used this control to judge the hybridization procedure, meaning that the probe sets targeting these Oligo B2 transcripts always should be present.

Poly-A controls: This control represent RNA from 4 different genes derived from B. *subtilis* (*LYS*, *PHE*, *THR* and *DAP*) that are not transcribed in human beings. This control was used to judge if there was no bias during transcription. We expected that both human genes and the Poly-A control were retro transcribed in the same ratio. The RNA of the 4 genes had different concentration, whereby *DAP* represents the highest concentration and *LYS* the lowest.

Ratio GAPDH/β-actin 3'/5': These housekeeping genes were used to assess the extent to which the samples were degraded. Therefore the ratio of the probe sets for the 3' and 5' site were analyzed. When the reverse transcriptase synthesis went well, a ratio of 1 was expected since only then the reverse transcriptase enzyme fully synthesized complete cDNA. We used a ratio of maximal 3 as acceptable.

Data analysis

The output of a microarray experiments consist of a large amount of data corresponding to the expression levels of thousands of genes. Data analysis requires sophisticated computational methods. Before analysis data need to be normalized to allow comparison between microarrays to control possible variation among experiments. For normalization, we used the robust multi-array average (RMA) approach, a method that uses a transformation to correct arrays for background, normalizes them using a formula based on a normal distribution and uses a linear model to estimate expression values on a log scale.

Classification algorithms are used to discover new categories within a data set (class discovery: unsupervised classification) or to assign objects to a priori defined categories (class prediction; supervised classification). Specifically for analysis of gene expression, unsupervised classification (Class Discovery) is a learning algorithm that clusters

unspecified data based on a similar gene expression pattern; supervised analysis (Class Comparison, Class Prediction) is a learning algorithm that uses already defined (labeled) data in order to identify a set of genes that characterize the pre-specified data. The list of differentially expressed genes that constitute a gene expression signature is accompanied by a false discovery rate (FDR) [131] or a *P*-value corrected for multiple testing to give a measure of significance for the results. Hierarchical cluster analysis is the most common unsupervised classification algorithm used in microarray analysis and allows to graphically represent results of unsupervised or supervised analysis in a tree diagram (dendogram) [132].

Supervised classification is also used to construct predictive algorithms. Predictive algorithms are developed on a "training" data set, where the categories to which objects belongs are known and evaluated on an independent "test" data set, in which objects are assigned to previously defined categories. To keep in mind, the gene lists obtained from hypothesis testing do not necessarily provide the best prediction. Different methods can be used to construct predictor algorithms (i.e: a SVM_support vector machine; PAM_predictive analysis of microarrays; kTSP_k-top scoring pairs).

Power of Gene Expression classification in leukemia

A decade ago, gene expression profiling (GEP) was successfully introduces in haematological research. Golub and colleagues were the first pioneers that showed the power to use a class discovery method to distincguish AML and ALL as well as B- and T-ALL [133]. From this first work, a new word started to rise and nowadays, gene expression profiling is widely used in science. Yeoh et al. showed that distinct expression profiling could identify all leukemia subtypes that were important at that time for clinical classification (T-ALL, E2A-PBX1, BCR-ABL, TEL-AML1, MLL rearrangements, hyperdiploid >50 chromosomes) and could be used for risk-stratification of pediatric ALL patients [9]. Nowadays, microarray technology is a powerful approach to improve diagnosis in haematological malignancies [134,135], and to discover new therapeutic targets [136] for the development of new therapies. Several studies confirmed that leukemia subtypes are characterized by specific gene expression patterns (class prediction) [9,133,137,138], while others were able to identify new categories (class discovery) [55,139,140,141].

In ALL, microarray technology was able to discriminate patients, according to the B- and T-lineage, different stage of maturation or carrying specific genomic rearrangements. These studies showed the potential of GEP to facilitate the identification of specific leukemia subtypes.

The international Microarray Innovations in Leukemia (MILE) Study Group has been the largest gene expression profiling study in haematology. MILE was a collaborative project, designed to assess the clinical accuracy of gene expression profiles for 16 acute and chronic leukemia subclasses, myelodysplastic syndromes (MDSs) and the control group (non-malignant disorders and normal bone marrow). In stage I of the MILE study, gene expression profiling of 2,143 patients (with leukemia and myelodysplastic syndromes) were generated with the aim to identify class signatures. In stage II, the gene expression profiling-based diagnostic accuracy was validated in an independent cohort of 1,191 patient samples, revealing a robust performance of this method to classify patients. This study demonstrated for the first time, the possibility to integrate the microarray technology in routine diagnostic procedures.

The following studies were able to identified new categories (class discovery) that allow the prediction of patients categories related to prognosis [55,142-144]. Both in B- and T- lineage ALL, gene expression based classifiers have been created for the prediction of prognosis, revealing the clinical heterogeneity that characterized distinct genetic leukemia subgroups.

Concerning T-ALL, Ferrando and colleagues revealed that distinct gene expression signatures were strongly associated to aberrant expression of main oncogenic transcription factors and this division seemed to reflect a specific stage of T cell developmental arrest. However, these specific signatures clustered also patients lacking the activation of known oncogenes, revealing that other unknown transcription factors could raise similar patterns of gene expression. In addition, in this work each group revealed by hierarchical clustering was associated with response to treatment and prognostic significance [55]. A following study identified the “early T-cell precursor” ALL cases showing the increased genomic instability and poor outcome for this subgroup that maintained stem cell-like features [86]. Moreover, a new subgroup of patients with *CASP8AP2* deletion and poor early treatment response in T-ALL was identified [145].

Nowadays, numerous efforts are made to successfully integrate microarray technology with haematological diagnostic procedures. A recent study used combined interphase fluorescence in situ hybridization (CI-FISH), single nucleotide polymorphism (SNP), and gene expression profiles (GEP) in T-ALL children stratified according to minimal residual disease (MRD) risk categories (AIEOP-BFM ALL2000). This approach provided an accurate, genomic diagnosis and a complementary GEP-based classification of T-ALL in children, showing a successful diagnosis in over 90% of cases and improving patients risk stratification [146].

ANIMAL MODELS

Model organisms have been shown to be very useful for studies of human diseases and biological processes during development and differentiation. The high degree of evolutionary conservation of genome and basic cellular processes among both vertebrate and invertebrate organisms, allow using animals as models to study many human diseases. Of these, vertebrate models have been widely used to gain insight in understanding human leukemia.

Zebrafish model

In the last decades, *D.rerio* (zebrafish) emerged as a useful model to study human diseases, owing to its numerous advantageous features: zebrafish (zf) can develop spontaneous tumors [147-149], most oncogenes and tumor suppressors are conserved between zf and human [150,151] and it can be easily genetically manipulated. In comparison with the murine model, the high fecundity (hundreds of fertilized eggs per couple) and the low maintenance cost of zebrafish allow to use this model to perform also large-scale forward genetic screens and pharmacological tests in a high-throughput manner. Zebrafish embryos develop externally facilitating observations and manipulation at different stages during development. Moreover, zf embryos and larvae are transparent, a characteristic that makes them an excellent model for real-time monitoring of internal organ development as well as for transplantation. In addition, the introduction of a stable transparent transgenic line allows real-time monitoring also in adult organisms [152]. Multiple approaches can be used in zebrafish to induce

leukemia, such as the creation of transgenic models, (xeno)transplantations, chemical or insertional mutagenesis.

One of the main strategies to induce cancer in zf is through the creation of transgenic animals that express activated oncogenes (usually mammalian oncogenes) in a tissue-specific manner, thus mimicking the human disease. The first transgenic model developed in zebrafish was a T-cell leukemia: the *rag2* promoter was used to drive mouse *Myc* overexpression in zf lymphoid cells [111]. To visualize cells carrying the oncogene, a chimeric EGFP-*mMyc* trangene was created. Wild-type fish embryos were microinjected with the vector with the transgene and 50% of F0 fish developed T-cell leukemia. Tumor cells initially grow in the thymus and than disseminate to other organs. Moreover these tumor cells could engraft irradiated wild-type adult zebrafish. Following studies aimed to improved this model which resulted in the establishment of a stable *mMyc* transgenic line [153] and a conditional line under heat shock control [154]. Numerous transgenic models have been developed using the same approach: a transgenic line over-expressing bcl2 fused to EGFP under the *rag2* promoter was developed to block apoptosis in T-ALL cells [155]; a pre-B ALL model was generated by induced over-expression of the *TEL-AML1* fusion gene [156] and another T-ALL model was established by over-expression of human *NOTCH1* under the rag2 promoter [157]. Recently, another T-ALL transgenic model was created by over-expression of human *MYC* under the *rag2* promoter [112] and also two lines for the study of Acute Myeloid Leukemia (AML) have been established [158,159]. Moreover, several transgenic zf models have been created for the study of solid tumors, such as melanoma [160] and rhabdomyosarcoma [161].

Transplantation of tumor cells from a donor- to recipient-animal provides information about the malignancy of the tumor and this assay has been used to test the ability of zf leukemic cells to propagate in a host [111]. This approach is very useful to study migration, homing, survival, and proliferation of tumor cells post-transplantation. In this context, xenotransplantation provides the opportunity to study human tumor cells *in vivo*. Zebrafish was largely used for transplantation and xenotransplantation of different human cells. As already underlined, the transparency of both embryos/larval fishes and the stable *casper* line are a great advantage, because they allow real-time observation of

injected cells. Of note, in transplants to zebrafish embryos immunosupression has not been used, as immature T- and B- cells are not present until 3-4 day post fertilization [162]. In addition, the zebrafish immune system starts to be functional at 28 days [163]. Instead, irradiation is often used to suppress the immune system of adult fish to prevent rejection of transplanted cells. Several studies have already demonstrated how almost all zebrafish models of leukemia created until now present leukemic cells that can engraft and perpetuate the tumor in zf recipients [111,156,157,164]. Concerning xenografting, the ability of mammalian cancer cells to successfully engraft in the zebrafish was established for solid tumors [165,166]. Moreover in a recent paper it has been shown that Jurkat cells could be successfully transplanted in the yolk/blood circulation of zebrafish embryos [167], showing that zebrafish embryos can be successfully used to perform xenotransplantion of hALL cell lines.

Tumor initiation and progression usually require genetic mutations and/or chromosomal translocations, resulting in the activation of oncogenes or inactivation of tumor suppressors. Genomic instability is considered a risk factor for tumor initiation and increasing cancer susceptibility. Forward genetic screens performed in zebrafish are useful to study the phenomenon of genomic instability and cancer susceptibility. This type of study uses chemical or insertional mutagenesis of zebrafish. Chemical mutagenesis is used to mutagenize the genome; wild-type male zebrafish are treated with a chemical mutagen (ethylnitrosourea, ENU) that causes genomic mutations in the premeiotic germ cells. ENU-treated males are then coupled to wild-type females to produce a F1 offspring carrying the genomic mutations. At this point eggs can be collected by squeezing of a F1 female and fertilization with UV-inactivated sperm to produce haploid F2 embryos in which ENU induced mutations can be found (figure 4). ENU usually causes point mutations that could result in altered protein sequence, truncated proteins, impaired splicing of mRNA precursors or mRNA degradation.

Instead, insertional mutagenesis requires the use of a retrovirus as insertional mutagen. The efficiency of the latter method is lower compared to chemical mutagenesis, however, the important advantage the rapid detection of the gene effected by the insertion using the retroviral sequence as a “tag”.

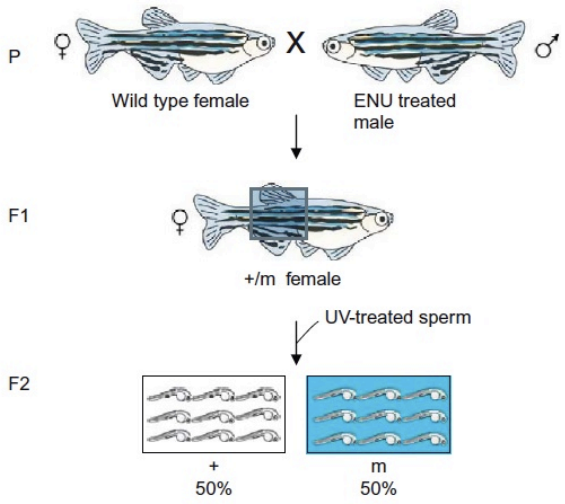

Figure 4. Schematic representation of a haploid screen *(from Zebrafish_Fish_Physiology_Vol. 29; 2010).*

These screening approaches aim to discover new mechanisms that can be involved in cancer biology. Using these approaches, two studies identified new interesting genes implicate in cancer development; in fact, the presence of heterozygosis mutations in *b-myb*, a transcriptional regulator [168] and *separase*, a mitotic regulator [169] have been shown to be related to increased cancer susceptibility in adult fish. Moreover, with the use of chemical mutagenesis, a study identified multiple lines with heritable predisposition to T cell malignancy, recapitulating human T cell neoplasia and showing heritable transmission [164].

Another advantage of the zebrafish model is the possibility to perform high-throughput chemical screening. In these screens, thousands of embryos are arrayed in multi-well-plates and are treated with chemicals during certain stage of development. Embryos are allowed to grow and scored for desired phenotype. At the same time also the toxicity of the compound is monitored. Of note, this approach allows also small drug discoveries without knowing the specific molecular targets [170-172].

Murine model

The mouse has been shown to have numerous advantages as organismal model to study human diseases; in fact, it shares physiological, anatomical and genomic similarities

with humans and it is relatively easy to genetically manipulate. Targeting specific genes by homologous recombination in mouse embryonic stem (ES) cells allows the creation of transgenic murine models theoretically capable of mimicking the human disease driven by the introduced gene. Moreover, transgenic technology allows the creation of models that over-expresses oncogenes in a tissue-specific manner and/or with a temporal control. Despite these numerous advantages, the prohibitive maintenance cost of mouse colonies forms a limitation for experiments such as large-scale genetic screens.

The main techniques used to induce leukemia in the murine model are: 1) the creation of a transgenic line; 2) the use of retroviral transduction/transplantation; 3) transplantations. Nowadays, mostly transgenic mouse models are generated using a "knock-in" approach [173], in which a chromosomal translocation is generated *de novo* in a conditional manner. An example is the use of the Cre-lox system to produce tissue-specific and/or inducible transgene expression. The Cre recombinase recognizes and catalyzes DNA recombination between recognition sequences referred to as loxP sites [174,175]. Any DNA sequence flanked by loxP sites will be excised by recombination if Cre is present in the cell. This approach requires independent lines of transgenic animals: the first transgene must contain the gene of interest flanked by loxP sites, while the second transgene contains the coding sequences for the Cre recombinase protein placed under the control of tissue-specific regulatory elements. Crossing of transgenic animals will result in an animal model each offspring harbouring the transgene and activation of the gene of interest only in those cells that express the Cre recombinase (tissue-specific).

An alternative approach to created murine model of leukemia is the use of bone marrow (BM) transduction/transplantation (BMT). In this case, BM progenitors are isolated, transduced *ex vivo* with a retrovirus carrying the oncogene of choice. After characterization of effects on proliferation, differentiation and self-renewal, the BM progenitors can be transplanted into syngeneic recipient mice to observe the leukemogenic potential *in vivo* [76].

Transplantations and Xenotransplantation models (from human to mouse) are very important not only for assaying tumor cell malignancy, but also to testing *in vivo* pharmacological inhibitors. The first experiments of human hematopoietic cells

xenotransplantation in irradiated, athymic nude (nu/nu) mice were not successful, as the immune system was not completely silenced (mice still had B cells producing antibodies, complement and natural killer (NK) cells). The introduction of two new murine models changed the world of xenotransplantations; the bg/nu/xid (BNX) was a mouse with three recessive mutations (beige/nude/X-linged immunodeficiency) to generate a more immuno-deficient model, while the SCID mice carried homozygous *scid* mutations. This mutation resulted in unsuccessful DNA rearrangement that impaired the rearrangement of immunoglobulin and *T*-cell receptor genes, resulting in T- and B- cells deficiency. The residual immunity in SCID mouse was due to the NK cells, complements and myeloid cells. The SCID model was improved by the development of non-obese diabetic (NOD)/SCID mice [177]: this mouse had less residual immunity since NOD mice had defects in the complement pathway and macrophage function. Xenotransplants in (NOD)/SCID mice presented high levels of human cells engraftment [178] and this murine model was largely used for studies of human malignancies *in vivo*. Moreover, the injected primary human ALL and AML cells were able to engraft the host organism maintaining the characteristics of the original leukemia [179,180]. Several studies used the (NOD)/SCID xenografted model and interesting results have been found regarding the biology of leukemia. Particularly, a correlation between xeno-engraftment potential and leukemia aggressiveness in humans has been reported [181,182] and the kinetics of human cells engraftment in the mouse has been shown to reflect the human disease (migration of leukemic cells from the BM to the spleen, PB an other organs) [179,182].

A further recent improvement was obtained with the introduction of the NSG murine model, in which a deletion in the γ-common chain in NOD/SCID mice resulted in the elimination of the residual NK cell activity, improving the environment for human cells engraftment [184]. Using this new murine model, Soulier and colleagues showed how xenograft leukemias appear to arise from minor aggressive subclones of T-ALL patients at diagnosis which after transplantation often resemble human leukemias at relapse [185].

Although the use of zebrafish or murine models is very useful to gain insight in the research of leukemic disease, we have to keep in mind that these animal models mimic a leukemia that resembles but cannot perfectly reproduce the human disease and that is

due to the insuperable differences between animal and human BM microenvironments. Thus, studies on animal models can help to identify important conserved events of leukemogenesis or target genes that can be useful for developing therapy, but results need to be contextualized in human patients.

CXCR4 IN LEUKEMIA

CXCR4 was described for the first time in 1994 as a seven-transmembrane domain receptor expressed on the surface of white blood cells [186]. Further studies revealed that CXCR4 was highly expressed on the surface of lymphocytes, neutrophils, monocyte and Hematopoietic Stem Cells (HSCs). CXCR4 belongs to the G-protein coupled chemokine receptor superfamily and selectively binds the CXC chemokine Stromal Cell-Derived Factor 1 (SDF-1) also know as CXCL12 [187,188]. CXCL12 is produced by stromal cells in the bone marrow (BM), lymph nodes, spleen, vessels and brain [189]. The interaction between CXCR4 and CXCL12 has been shown to be essential for development, organogenesis, vascularization and normal hematopoiesis [190-195]. Particularly, *CXCR4*-deficient mice show a marked decrease in B lymphopoiesis, myelopoiesis, bone marrow colonization and die during the perinatal period [192], while *CXCL12*-deficient mice have defects in myelopoiesis [190]. T-lineage lymphopoiesis is not affected in mutant embryos, indicating that thymocyte maturation does not depend on the CXCL12/CXCR4 axis. The interaction between CXCR4 and CXCL12 is known to regulate the retention and migration of CD34+ HSCs within niches in the bone marrow [195-197], the egress of immature B and T lymphocytes from the BM into the Peripheral Blood (PB) and lymphoid tissues [198] and direct naïve leukocyte trafficking [199]. In fact, CXCL12 is a chemokine that induces the migration of monocytes, neuthophils, pro- and pre-B lymphocytes and T-lymphocytes [200-202]. Interesting, when B-cells develop into mature cells, they progressively lose the ability to respond to the CXCL12, even if CXCR4 continues to be expressed at high levels on the surface membrane [203-204]. On the contrary, T-lymphocytes do not lose the responsiveness to CXCL12, and also in this case CXCR4 is expressed in higher percentages on the surface of immature- compared to mature T lymphocytes [205].

CXCR4 transcription is mainly regulated by two transcription factors; Nuclear

Respiratory Factor-1 (NRF-1) positively regulates *CXCR4* transcription [206,207], while Yin-Yang 1 (YY1) is a negative transcription factor for *CXCR4* [208]. Interestingly, several studies have shown an increase in YY1 activity in the presence of decreased expression levels of MYC, a natural suppressor of YY1 [209].

However, multiple external factors can influence the expression of CXCR4 on the surface membrane. Cytokines, including TGF-1β, IL-2, IL-4, IL-6, IL-7, IL-10 and IL-15, and growth factors, such as EGF, VEGF, basic FGF and stem cell factor, and hypoxia (via hypoxia-inducible factor 1-α) all induce up-regulation of *CXCR4* [210,211]. While contact with CXCL12, phorbol esters, pertussis toxin and inflammatory cytokines, including TNF-α and IFN-γ, cause down-regulation of surface CXCR4 [210-212].

The binding of CXCL12 to CXCR4 determines the activation of the chemokine receptor. This activation results in phosphorylation and internalization of CXCR4 via clathrin-coated pits. After internalization, CXCR4 can either be ubiquitinated and degradated in the lysosome [213], or recycled back to the cell surface [210,214]. Leukocytes have been shown to have large amounts of intracellular CXCR4 in store for prompt responses [214]. Upon activation of CXCR4, there is an increase of intracellular calcium levels [216] and diverse G-protein dependent and independent signalling pathway are activated leading to multiple biological responses [211,215], such as migration, adhesion and transcriptional activation (figure 5). The overall result of CXCR4 activation is increased chemotaxis toward its ligand CXCL12 in a dose dependent manner [189]. Particularly, high expression of CXCR4 increased the ability of T-lymphocytes to migrate towards a CXCL12 chemo-attracting gradient and this phenomenon has been shown to occur also in several solid cancers and hematopoietic malignancies [216]. However, the functional consequence of CXCR4 expression on cancer cells is still not completely understood; in fact, through CXCL12/CXCR4-mediated chemotaxis leukemia cells could migrate into niches within the bone marrow, with consequent increased proliferation and survival; whereas the chemokine CXCL12 could function as chemo-attractant, facilitating adhesion, migration and metastasis of cancer cells in tissues that express this chemokine. In fact, several studies have demonstrated that CXCL12 can influence

integrin activity enhancing cell rolling and adhesion under blood flow conditions and consequent cessation of cellular locomotion [217-220]. For the moment, studies attempting to correlate CXCR4 expression with metastatic potential reported differing results.

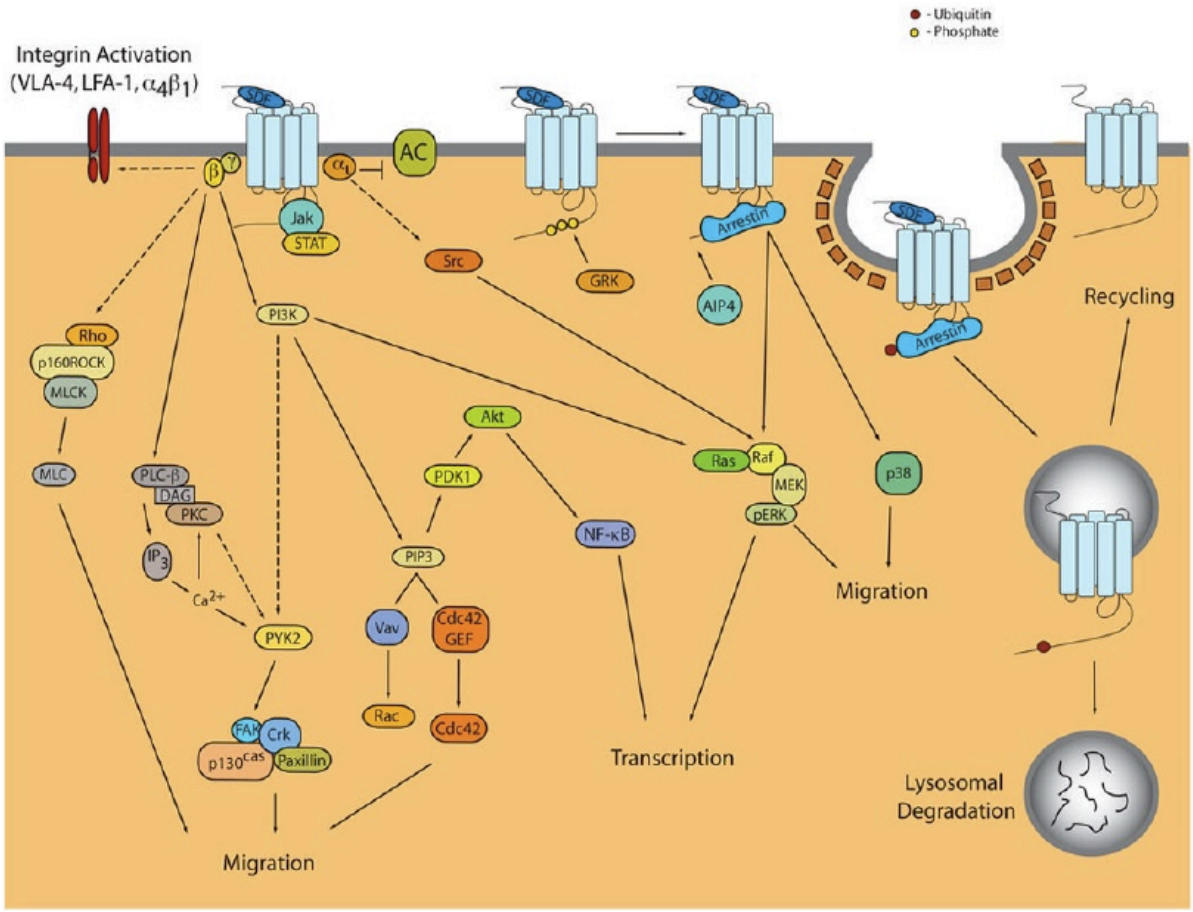

Figure 5. General Signal Transduction Pathways and Regulation of CXCR4 [211]

Concerning leukemia, CXCR4 is expressed both in lymphoid and myeloid leukemia. At the molecular level, CXCR4 activation promotes leukemia progression. In fact, the binding of CXCL12 to the receptor promotes activation of the PI3K/AKT and MAPK pathways, which mediate the survival and proliferation of leukemia cells [221]. Moreover, the activation of NF-κB pathway is also induced as well as the production of matrix metalloproteinases, IL-8 and VEGF, that can help to disrupt the extracellular matrix [221,222]. Several studies have suggested that increased CXCR4 expression may be associated to poor prognosis in various types of leukemia [223,224], as leukemia

cells can migrate into bone marrow niches that confer resistance to chemotherapy. A potential therapeutic strategy to overcome this phenomenon could be the use of specific inhibitors for CXCR4. Inhibition of CXCR4 may allow leukemia cells to be released from the protective niches of the bone marrow. In acute leukemias, CXCR4 levels are highest in acute promyelocytic leukemia (French–American–British [FAB] subtype M3), myelomonocytic AML (FAB subtypes M4 and M5) and B-lineage ALL [225], even if B-cells lose receptor functionality during the maturation process. Several studies have suggested that increased levels of CXCR4 expression have a prognostic significance in childhood ALL [32], adult AML [226-229] and B-cell CLL [230]. *In vitro* experiments using specific CXCR4 inhibitors (T140, TC140012, T134 and AMD3100) on pre-B cell ALL cells resulted in inhibition of CXCL12-induced chemotaxis and migration into bone marrow [231]. Moreover, a study on a mouse model of pediatric pre-B ALL suggested that the use of CXCR4 inhibitors could mobilize leukemic cells into the peripheral blood, impairing metastasis [232]. Moreover, CXCR4 inhibition may also be useful in the treatment of high-risk ALL, infant *MLL*-rearranged [233] or ALL carrying the fusion protein BCR–ABL [234].

Of note, the importance and the role played by the CXCR4/CXCL12 axis in relation to extramedullary leukemia (testicles, CNS, spleen, liver, ovaries) is less understood. The first work that investigated this phenomenon indicated that the CXCR4 expression could be predictive of extramedullary disease [32]. However, CNS-homing cells presented CXCR4 down-regulation in a mouse model of CNS pre-B ALL [37]. In addition, another study showed that in children with ALL relapses associated to testicles or CNS leukemia blast cells had a significantly lower CXCR4 levels than blasts from children with relapsed disease isolated to the bone marrow [235], suggesting that blasts were not tightly retained in the bone marrow and allowed to metastasize to the testicles and the CNS. Further studies are necessary to clarify the importance of the CXCR4/CXCL12 axis in determining extramedullary infiltration by blast cells.

REFERENCES

1. Poplack D. Acute lymphoblastic leukemia, in Pizzo P, Poplack D (eds):Principles and Practice of Pediatric Oncology (ed 2). Philadelphia, PA, Lippincott 1993; p 431
2. Young, Jr, J.L., Ries, L.G., Silverberg, E., Horm, J.W. & Miller, R.W. (1986) Cancer incidence, survival, and mortality for childrenyounger than age 15 years. Cancer, 58, 598±602.
3. Greaves MF. Differentiation-linked leukemogenesis in lymphocytes. Science 1986; 234:697.
4. Smith LJ, Curtis JE, Messner HA, Senn JS, Furthmayr H, McCulloch EA. Lineage infidelity in acute leukemia. Blood 1983; 61:1138.
5. Swerdlow, S.H., Campo, E., Harris, N.L., Jaffe, E.S., Pileri, S.A., Stein, H., Thiele, J., Vardiman, J.W, WHO Classification of Tumours of Haematopoietic and Lymphoid Tissues, Fourth Edition, Lyon, France, IARC Press: 2008
6. Greaves M. Infection, immune responses and the aetiology of childhood leukaemia. Nat Rev Cancer 2006; 6(3):193-203.
7. Pui CH, Robison LL, Look AT. Acute lymphoblastic leukaemia. Lancet 2008; 371(9617):1030-43.
8. Pui CH, Carroll WL, Meshinchi S, Arceci RJ. Biology, risk stratification, and therapy of pediatric acute leukemias: an update. J Clin Oncol 2011; 29(5):551-65.
9. Yeoh EJ, Ross ME, Shurtleff SA, Williams WK, Patel D, Mahfouz R, Behm FG, Raimondi SC, Relling MV, Patel A, Cheng C, Campana D, Wilkins D, Zhou X, Li J, Liu H, Pui CH, Evans WE, Naeve C, Wong L, Downing JR. Classification, subtype discovery, and prediction of outcome in pediatric acute lymphoblastic leukemia by gene expression profiling. Cancer Cell 2002; 1(2):133-43.
10. Armstrong SA, Staunton JE, Silverman LB, Pieters R, den Boer ML, Minden MD, Sallan SE, Lander ES, Golub TR, Korsmeyer SJ. MLL translocations specify a distinct gene expression profile that distinguishes a unique leukemia. Nat Genet. 2002;30(1):41-7.
11. Ferrando AA, Armstrong SA, Neuberg DS, Sallan SE, Silverman LB, Korsmeyer SJ, Look AT. Gene expression signatures in MLL-rearranged T-lineage and B-precursor acute leukemias: dominance of HOX dysregulation. Blood 2003; 102(1):262-8.
12. Lu J, Getz G, Miska EA, Alvarez-Saavedra E, Lamb J, Peck D, Sweet-Cordero A, Ebert BL, Mak RH, Ferrando AA, Downing JR, Jacks T, Horvitz HR, Golub TR. MicroRNA expression profiles classify human cancers. Nature 2005; 435(7043):834-8.
13. J Formos Med Assoc. 2010 Nov; 109(11):777-87. Recent research advances in childhood acute lymoholastic leukemia. Pui CH.
14. Pui CH, Mullighan CG, Evans WE, Relling MV, Pediatric acute lymphoblastic leukemia: where are we going and how do we get there? Blood, 2012 August 9;120(6);1165-1174. DOI: 10.1182/blood-2012-05-378943
15. Marta Pillon MD, Maurizio Aricò MD, Giuseppe Basso MD, Franco Locatelli MD, Marco Citterio MD, Concetta Micalizzi MD, Anna Maria Testi MD, Elena Barisone MD, Margherita Nardi MD, Alessandra Lombardi MD, Roberto Rondelli MD, Angelo Rosolen MD, On behalf of the NHL-Committee of the Italian Association of Pediatric Hematology, Oncology (AIEOP), Long-term results of AIEOP-8805 protocol for acute B-cell lymphoblastic leukemia of childhood, Pediatric Blood & Cancer, 2011 April;56(4):544–550. DOI: 10.1002/pbc.22787
16. Pui CH, Howard SC, Current management and challenges of malignant disease in the CNS in pediatric leukemia, The Lancet Oncology, 2008 March;9(3):257-268. DOI:10.1016/S1470-2045(08)70070-6
17. Aur RJ, Simone J, Hustu HO, et al. Central nervous system therapy and combination chemotherapy of childhood lymphocytic leukemia. Blood 1971;37:272–281.
18. Simone JV. History of the treatment of childhood ALL: A paradigm for cancer cure. Best Pract Res Clin Haematol 2006;19: 353–359; review.
19. Akers SM, Rellick SL, Fortney JE, et al. Cellular elements of the subarachnoid space promote ALL survival during chemotherapy Leuk Res 2011;35:705– 711.
20. Jahnukainen K, Saari T, Salmi TT, et al. Reactions of Leydig cells and blood vessels to lymphoblastic leukemia in the rat testis. Leukemia 1995;9:908–914.

21. Mahmoud HH, Rivera GK, Hancock ML, Krance RA, Kun LE, Behm FG, et al. Low leukocyte counts with blast cells in cerebrospinal fluid of children with newly diagnosed acute lymphoblastic leukemia. N Engl J Med.1993;329:314-9.

22. Martínez-Laperche C, Gómez-García AM, Lassaletta Á, Moscardó C, Vivanco JL, Molina J, Fuster JL, Couselo JM, de Toledo JS, Bureo E, Madero L, Ramírez M. Detection of occult cerebrospinal fluid involvement during maintenance therapy identifies a group of children with acute lymphoblastic leukemia at high risk for relapse. Am J Hematol. 2013 May;88(5):359-64. doi: 10.1002/ajh.23407. Epub 2013 Mar 7.

23. de Haas V, Vet RJ, Verhagen OJ, et al. Early detection of central nervous system relapse by polymerase chain reaction in children with B-precursor acute lymphoblastic leukemia. Ann Hematol 2002;81:59–61.

24. Subir_a D, Casta~n_on S, Rom_an A, et al. Flow cytometry and the study of central nervous disease in patients with acute leukaemia. Br J Haematol 2001;112:381–384.

25. Biojone E, Queir_oz RD, Valera ET, et al. Minimal residual disease in cerebrospinal fluid at diagnosis: A more intensive treatment protocol was able to eliminate the adverse prognosis in children with acute lymphoblastic leukemia. Leuk Lymphoma 2012;53:89–95.

26. Scrideli CA, Queiroz RP, Takayanagui OM, et al. Polymerase chain reaction on cerebrospinal fluid cells in suspected leptomeningeal involvement in childhood acute lymphoblastic leukemia: Comparison to cytomorphological analysis. Diagn Mol Pathol 2003;12:124–127.

27. Pine SR, Yin C, Matloub YH, et al. Detection of central nervous system leukemia in children with acute lymphoblastic leukemia by real-time polymerase chain reaction. J Mol Diagn 2005;7:127–132.

28. Smith M, Arthur D, Camitta B, et al. Uniform approach to risk classification and treatment assignment for children with acute lymphoblastic leukemia. J Clin Oncol 1996;14:18–24.

29. Burger B, Zimmermann M, Mann G, Kü hl J, Löning L, Riehm H, et al. Diagnostic cerebrospinal fluid examination in children with acute lymphoblastic leukemia: significance of low leukocyte counts with blasts or traumatic lumbar puncture. J Clin Oncol. 2003;21: 184-8.

30. Pui CH, Campana D, Pei D, Bowman WP, Sandlund JT, Kaste SC, Ribeiro RC, Rubnitz JE, Raimondi SC, Onciu M, Coustan-Smith E, Kun LE, Jeha S, Cheng C, Howard SC, Simmons V, Bayles A, Metzger ML, Boyett JM, Leung W, Handgretinger R, Downing JR, Evans WE, Relling MV, Treating childhood acute lymphoblastic leukemia without cranial irradiation, The New England Journal of Medicine, 2009 Jun 25;360: 2730-2741. DOI: 10.1056/NEJMoa0900386

31. Gunnar Cario, Shai Izraeli, Anja Teichert, Peter Rhein, Julia Skokowa, Anja Möricke, Martin Zimmermann, Andre Schrauder, Leonid Karawajew, Wolf-Dieter Ludwig, Karl Welte, Holger J. Schünemann, Brigitte Schlegelberger, Martin Schrappe and Martin Stanulla, High Interleukin-15 Expression Characterizes Childhood Acute Lymphoblastic Leukemia With Involvement of the CNS, Journal of Clinical Oncology, 2007 Oct 20;25:4813-4820. DOI: 10.1200/JCO.2007.11.8166

32. Crazzolara R, Kreczy A, Mann G, Heitger A, Eibl G, Fink FM, Möhle R, Meister B. High expression of the chemokine receptor CXCR4 predicts extramedullary organ infiltration in childhood acute lymphoblastic leukaemia. Br J Haematol. 2001 Dec;115(3):545-53.

33. Price RA, Johnson WW. The central nervous system in childhood leukemia. I. The arachnoid. Cancer. 1973 Mar;31(3):520-33.

34. Robb RM, Ervin LD, Sallan SE. A pathological study of eye involvement in acute leukemia of childhood. Trans Am Ophthalmol Soc. 1978;76:90-101.

35. Buonamici S, Trimarchi T, Ruocco MG, Reavie L, Cathelin S, Mar BG, Klinakis A, Lukyanov Y, Tseng JC, Sen F, Gehrie E, Li M, Newcomb E, Zavadil J, Meruelo D, Lipp M, Ibrahim S, Efstratiadis A, Zagzag D, Bromberg JS, Dustin ML, Aifantis I.CCR7 signalling as an essential regulator of CNS infiltration in T-cell leukaemia. Nature. 2009 Jun 18;459(7249):1000-4. doi: 10.1038/nature08020.

36. Holland M, Castro FV, Alexander S, Smith D, Liu J, Walker M, Bitton D, Mulryan K, Ashton G, Blaylock M, Bagley S, Connolly Y, Bridgeman J, Miller C, Krishnan S, Dempsey C, Masurekar A, Stern P, Whetton A, Saha V, RAC2, AEP, and ICAM1 expression are associated with CNS disease in a mouse model of pre-B childhood acute lymphoblastic leukemia, Blood, 2011 May 23;118(3):638-649. DOI: 10.1182/blood-2010-09-307330.

37. Christina Halsey, Mark TS Williams, Yasar Yousafzai, Klaus Rehe, Olaf Heidenreich, Josef Vormoor, Brenda Gibson[3]and Gerard Graham, Central Nervous System Involvement in a Xenograft Model of Pre-B

Acute Lymphoblastic Leukaemia Is Associated with Dysfunctional CXCR4 Expression and Upregulation of the Neurotropic Chemokine Receptors CCR6 and CX3CR1, Blood, 2011: Abstract 3449.

38. Oeffinger KC, Mertesn AC, Sklar CA, et al. Chronic health conditions in adult survivors of childhood cancer. N Engl J Med 2006;355:1572–1582. [PubMed: 17035650].

39. Pui CH, Cheng C, Leung W, et al. Extended follow-up of long-term survivors of childhood acute lymphoblastic leukemia. N Engl J Med 2003;349:640–649. [PubMed: 12917300]

40. Hijiya N, Hudson MM, Lensing S, et al. Cumulative incidence of secondary neoplasms as a first event after childhood acute lymphoblastic leukemia. JAMA 2007;297:1207–1215. [PubMed: 17374815]

41. Geenen MM, Cardous-Ubbink MC, Kremer LCM, et al. Medical assessment of adverse health outcomes in long-term survivors of childhood cancer. JAMA 2007;297:2705–2715. [PubMed: 17595271]

42. Waber DP, Turek J, Catania L, et al. Neuropsychological outcomes from a randomized trial of triple intrathecal chemotherapy compared with 18 Gy cranial radiation as CNS treatment in acute lymphoblastic leukemia: findings from Dana-Farber Cancer Institute ALL Consortium Protocol 95–01. J Clin Oncol 2007;25:4914–4921. [PubMed: 17971588]

43. Vilmer E, Suciu S, Ferster A, et al. Long-term results of three randomized trials (58831, 58832, 58881) in childhood acute lymphoblastic leukemia: a CLCG-EORTC report. Leukemia 2000;14:2257–2266. [PubMed: 11187917]

44. Manera R, Ramirez I, Mullins J, Pinkel D. Pilot studies of species-specific chemotherapy of childhood acute lymphoblastic leukemia using genotype and immunophenotype. Leukemia 2000;14:1354–1361. [PubMed: 10942229]

45. Veerman AJ, Kamps WA, van den Berg H, van den Berg E, Bökkerink JP, Bruin MC, van den Heuvel-Eibrink MM, Korbijn CM, Korthof ET, van der Pal K, Stijnen T, van Weel Sipman MH, van Weerden JF, van Wering ER, van der Does-van den Berg A; Dutch Childhood Oncology Group, Dexamethasone-based therapy for childhood acute lymphoblastic leukaemia: results of the prospective Dutch Childhood Oncology Group (DCOG) protocol ALL-9 (1997-2004), The Lancet Oncology, 2009 Oct;10(10):957-966. DOI:10.1016/S1470-2045(09)70228-1

46. Pui CH, Central Nervous System Disease in acute lymphoblastic leukemia: Prophylaxis and Treatment, ASH Education Book, 2006 Jan 1;2006(1):142-146. DOI: 10.1182/asheducation-2006.1.142

47. Silverman LB, Declerck L, Gelber RD, et al. Results of Dana-Farber Cancer Institute Consortium protocols for children with newly diagnosed acute lymphoblastic leukemia (1981–1995). Leukemia 2000;14:2247–2256.

48. Pui CH, Boyett JM, Rivera GK, et al. Long-term results of Total Therapy studies 11, 12 and 13A for childhood acute lymphoblastic leukemia at St Jude Children's Research Hospital. Leukemia 2000;14:2286–2294.

49. te Loo DM, Kamps WA, van der Does-van den Berg A, van Wering ER, de Graaf SS. Prognostic significance of blasts in the cerebrospinal fluid without pleiocytosis or a traumatic lumbar puncture in children with acute lymphoblastic leukemia: experience of the Dutch Childhood Oncology Group. J Clin Oncol. 2006;24: 2332-6.

50. Gajjar A, Harrison PL, Sandlund JT, Rivera GK, Ribeiro RC, Rubnitz JE, et al. Traumatic lumbar puncture at diagnosis adversely affects outcome in childhood acute lymphoblastic leukemia. Blood. 2000;96:3381-4.

51. Conter V, Schrappe M, Aricü M, Reiter A, Rizzari C, Dördelmann M, et al. Role of cranial radiotherapy for childhood T-cell acute lymphoblastic leukemia with high WBC and good response to prednisone. J Clin Oncol. 1997;15:2786-91.

52. Schrappe M, Reiter A, Ludwig WD, Harbott J, Zimmermann M, Hiddemann W, et al. Improved outcome in childhood acute lymphoblastic leukemia despite reduced use of anthracyclines and cranial radiotherapy: results of trial ALL-BFM 90. German-Austrian-Swiss ALLBFM Study Group. Blood. 2000;95:3310-22.

53. Goldberg JM, Silverman LB, Levy DE, Dalton VK, Gelber RD, Lehmann L, et al. Childhood T-cell acute lymphoblastic leukemia: the Dana-Farber Cancer Institute acute lymphoblastic leukemia consortium experience. J Clin Oncol. 2003;21:3616-22.

54. Pui CH, Evans WE. Treatment of acute lymphoblastic leukemia. N Engl J Med. 2006;354:166-78.

55. Ferrando AA, Neuberg DS, Staunton J, Loh ML, Huard C, Raimondi SC, Behm FG, Pui CH, Downing JR, Gilliland DG, Lander ES, Golub TR, Look AT. Gene expression signatures define novel oncogenic

pathways in T cell acute lymphoblastic leukemia. Cancer Cell. 2002;1(1):75-87.

56. Pui CH, Relling MV, Downing JR. Acute lymphoblastic leukemia. N Engl J Med 2004; 350(15):1535-48.

57. Struhl G, Greenwald I. Presenilin-mediated transmembrane cleavage is required for Notch signal transduction in Drosophila. Proc Natl Acad Sci U S A. 2001 Jan 2;98(1):229-34.

58. Hansson EM, Lendahl U, Chapman G. Notch signaling in development and disease. Semin Cancer Biol. 2004 Oct;14(5):320-8.

59. Ellisen LW, Bird J, West DC, Soreng AL, Reynolds TC, Smith SD, Sklar J. TAN-1, the human homolog of the Drosophila notch gene, is broken by chromosomal translocations in T lymphoblastic neoplasms. Cell 1991; 66(4):649-61.

60. Weng AP, Ferrando AA, Lee W, Morris JP 4th, Silverman LB, Sanchez-Irizarry C, Blacklow SC, Look AT, Aster JC. Activating mutations of NOTCH1 in human T cell acute lymphoblastic leukemia. Science 2004; 306(5694):269-71.

61. O'Neil J, Grim J, Strack P, Rao S, Tibbitts D, Winter C, Hardwick J, Welcker M, Meijerink JP, Pieters R, Draetta G, Sears R, Clurman BE, Look AT. FBW7 mutations in leukemic cells mediate NOTCH pathway activation and resistance to gamma-secretase inhibitors. J Exp Med 2007; 204(8):1813-24.

62. Thompson BJ, et al. The SCFFBW7 ubiquitin ligase complex as a tumor suppressor in T cell leukemia. *J Exp Med*. 2007;204(8):1825–1835.

63. Breit S, Stanulla M, Flohr T, Schrappe M, Ludwig WD, Tolle G, et al. Activating NOTCH1 mutations predict favorable early treatment response and long-term outcome in childhood precursor T-cell lymphoblastic leukemia. Blood 2006;108 (4):1151–7.

64. Park MJ, Taki T, Oda M, Watanabe T, Yumura-Yagi K, Kobayashi R, et al. FBXW7 and NOTCH1 mutations in childhood T cell acute lymphoblastic leukaemia and T cell non-Hodgkin lymphoma. Br J Haematol 2009;145(2):198–206.

65. Kox KZ, Stanulla M, Leibe S, Schrappe M, Ludwig WD, Koehler R, et al. The favorable effect of activating NOTCH1 receptor mutations on long-term out come in T-ALL patients treated on the ALL-BFM 2000 protocol can be separated from FBXW7 loss of function. Leukemia 2010;24(12):2003–4.

66. Clappier E, Collette S, Grardel N, Girard S, Suarez L, Brunie G, et al. NOTCH1 and FBXW7 mutations have a favorable impact on early response to treatment but not on outcome in children with T-cell acute lymphoblastic (T-ALL) leukemia treated on EORTC trials 58881 and 58951. Leukemia 2010;24(12):2323–31.

67. van Grotel M, Meijerink JP, Beverloo HB, Langerak AW, Buys-Gladdines JG, Schneider P, et al. The outcome of molecular-cytogenetic subgroups in pediatric T-cell acute lymphoblastic leukemia: a retrospective study of patients treated according to DCOG or COALL protocols. Haematologica 2006;91(9):1212–21.

68. Zuurbier L, Homminga IC V, teWinkelML, Buijs-Gladdines J, Kooi C, SmitsWK, et al. NOTCH1 and/or FBXW7mutations predict for initial good prednisone response but not for improved outcome in pediatric T-cell Acute Lymphoblastic Leukemia patients treated on DCOG or COALL protocols. Leukemia 2010;24(12):2014–22.

69. Hebert J, Cayuela JM, Berkeley J, Sigaux F. Candidate tumor-suppressor genes MTS1 (p16INK4A) and MTS2 (p15INK4B) display frequent homozygous deletions in primary cells from T- but not from B-cell lineage acute lymphoblastic leukemias. *Blood*. 1994;84(12):4038–4044.

70. van Grotel M, Meijerink JP, van Wering ER, Langerak AW, Beverloo HB, Buijs-Gladdines JG, Burger NB, Passier M, van Lieshout EM, Kamps WA, Veerman AJ, van Noesel MM, Pieters R. Prognostic significance of molecular-cytogenetic abnormalities in pediatric TALL is not explained by immunophenotypic differences. Leukemia 2008; 22(1):124-31

71. Larson Gedman A, Chen Q, Kugel Desmoulin S, Ge Y, LaFiura K, Haska CL, Cherian C, Devidas M, Linda SB, Taub JW, Matherly LH. The impact of NOTCH1, FBW7 and PTEN mutations on prognosis and downstream signaling in pediatric T-cell acute lymphoblastic leukemia: a report from the Children's Oncology Group. Leukemia 2009; 23(8):1417-25.

72. Murre C. Intertwining proteins in thymocyte development and cancer. Nat Immunol 2000; 1(2):97-8.

73. Clappier E, Cuccuini W, Kalota A, Crinquette A, Cayuela JM, Dik WA, et al. The C-MYB locus is involved in chromosomal translocation and genomic duplications in human T-cell acute leukemia (T-ALL), the translocation defining a new T-ALL subtype in very young children. Blood 2007;110:1251–61.

74. Bergeron J, Clappier E, Radford I, et al. Prognostic and oncogenic relevance of TLX1/ HOX11 expression level in T-ALLs. Blood. 2007; 110(7):2324-2330.

75. Homminga I, Pieters R, Langerak AW, et al. Integrated transcript and genome analyses reveal NKX2-1 and MEF2C as potential oncogenes in T cell acute lymphoblastic leukemia. Cancer Cell. 2011;19(4):484-497.

76. Van Vlierberghe P, Ferrando A. The molecular basis of T cell acute lymphoblastic leukemia. J Clin Invest. 2012 Oct 1;122(10):3398-406. doi: 10.1172/JCI61269. Epub 2012 Oct 1.

77. Kikuchi A, et al. Clinical significance of TAL1 gene alteration in childhood T-cell acute lymphoblastic leukemia and lymphoma. *Leukemia*. 1993; 7(7):933–938.

78. Bash RO, et al. Clinical features and outcome of T-cell acute lymphoblastic leukemia in childhood with respect to alterations at the TAL1 locus: a Pediatric Oncology Group study. *Blood*. 1993; 81(8):2110–2117.

79. Cavé H, Suciu S, Preudhomme C, Poppe B, Robert A, Uyttebroeck A, Malet M, Boutard P, Benoit Y, Mauvieux L, Lutz P, Méchinaud F, Grardel N, Mazingue F, Dupont M, Margueritte G, Pages MP, Bertrand Y, Plouvier E, Brunie G, Bastard C, Plantaz D, Vande Velde I, Hagemeijer A, Speleman F, Lessard M, Otten J, Vilmer E, Dastugue N. Clinical significance of HOX11L2 expression linked to t(5;14)(q35;q32), of HOX11 expression, and of SIL-TAL fusion in childhood T-cell malignancies: results of EORTC studies 58881 and 58951. Blood 2004; 103(2):442-50.

80. Dube ID, et al. A novel human homeobox gene lies at the chromosome 10 breakpoint in lymphoid neoplasias with chromosomal trans location t(10;14). *Blood*. 1991;78(11):2996–3003.

81. Hatano M, Roberts CW, Minden M, Crist WM, Korsmeyer SJ. Deregulation of a homeobox gene, HOX11, by the t(10;14) in T cell leukemia. *Science*. 1991;253(5015):79–82.

82. Kennedy MA, et al. HOX11, a homeobox-containing T-cell oncogene on human chromosome 10q24. *Proc Natl Acad Sci U S A*. 1991;88(20):8900–8904.

83. Ferrando AA, et al. Prognostic importance of TLX1 (HOX11) oncogene expression in adults with T-cell acute lymphoblastic leukaemia. *Lancet*. 2004;363(9408):535–536.

84. Bernard OA, et al. A new recurrent and specific cryptic translocation, t(5;14)(q35;q32), is associated with expression of the Hox11L2 gene in T acute lymphoblastic leukemia. *Leukemia*. 2001; 15(10):1495–1504.

85. Soulier J, Clappier E, Cayuela JM, Regnault A, García-Peydró M, Dombret H, et al.HOXA genes are included in genetic and biologic networks defining humanacute T-cell leukemia (T-ALL). Blood 2005;106:274–86.

86. Coustan-Smith E, Mullighan CG, Onciu M, Behm FG, Raimondi SC, Pei D, Cheng C, Su X, Rubnitz JE, Basso G, Biondi A, Pui CH, Downing JR, Campana D. Early T-cell precursor leukaemia: a subtype of very high-risk acute lymphoblastic leukaemia. Lancet Oncol 2009; 10(2):147-56.

87. Van Vlierberghe P, Pieters R, Beverloo HB, Meijerink JP. Molecular-genetic insights in paediatric T-cell acute lymphoblastic leukaemia. Br J Haematol 2008; 143(2):153-68.

88. Asnafi V, et al. CALM-AF10 is a common fusion transcript in T-ALL and is specific to the TCRgammadelta lineage. *Blood*. 2003;102(3):1000–1006.

89. Ferrando AA, Look AT. Clinical implications of recurring chromosomal and associated molecular abnormalities in acute lymphoblastic leukemia. *Semin Hematol*. 2000;37(4):381–395.

90. Van Vlierberghe P, et al. The recurrent SET-NUP214 fusion as a new HOXA activation mechanism in pediatric T-cell acute lymphoblastic leukemia. Br J Haematol 2008; 143(2):153-68.

91. Clappier E, Cuccini W, Cayuela JM, Vecchione D, Baruchel A, Dombret H, Sigaux F, Soulier J. Cyclin D2 dysregulation by chromosomal translocation to TCR loci in T-cell acute lymphoblastic leukemia. Leukemia 2006; 20:82-86.

92. Erikson J, et al. Deregulation of c-myc by trans location of the alpha-locus of the T-cell receptor in T-cell leukemias. *Science*. 1986;232(4752):884–886.

93. Dang CV, O'Donnell KA, Zeller KI, Nguyen T, Osthus RC, Li F. The c-Myc target gene network. *Semin Cancer Biol.* 2006;16(4):253-264.

94. Albihn A, Johnsen JI, Henriksson MA. MYC in oncogenesis and as a target for cancer therapies. *Adv Cancer Res.* 2010;107:163-224.

95. Junttila MR, Westermarck J. Mechanisms of MYC stabilization in human malignancies. *Cell Cycle.* 2008;7(5):592-596.

96. Meyer N, Penn LZ. Reflecting on 25 years with MYC. *Nat Rev Cancer.* 2008;8(12):976-990.

97. Hemann MT, Bric A, Teruya-Feldstein J, et al. Evasion of the p53 tumour surveillance network by tumour-derived MYC mutants. *Nature.* 2005; 436(7052):807-811.

98. Berns A. Cancer: two in one. *Nature.* 2005; 436(7052):787-789.

99. PalomeroT, LimWK, Odom DT, et al. NOTCH1 directly regulates c-MYC and activates a feed-forwardloop transcriptional network promoting leukemic cell growth. Proc Natl Acad Sci U S A 2006;103: 18261^6.

100. Weng AP, Millholand JM, Yashiro-Ohtani Y, Arcangeli ML, Lau A, Wai C, Del Bianco C, Rodriguez CG, Sai H, Tobias J, Li Y, Wolfe MS, Shachaf C, Felsher D, Blacklow SC, Pear WS, Aster JC. c-Myc is an important direct target of Notch1 in T-cell acute lymphoblastic leukemia/lymphoma. Genes Dev 2006; 20:2096-2109.

101. SharmaVM, CalvoJA, Draheim KM, et al. Notch1 contributes tomouseT-cell leukemia by directly inducing the expression of c-myc. Mol Cell Biol 2006;26: 8022^31.

102. PalomeroT, Sulis ML, Cortina M, et al. Mutational loss of PTENinduces resistance to NOTCH1inhibition inT-cell leukemia. Nat Med 2007;13:1203^10. Epub 2007 Sep 16.

103. Margolin AA, Palomero T, Sumazin P, Califano A, Ferrando AA, Stolovitzky G. ChIP-on-chip significance analysis reveals large-scale binding and regulation by human transcription factor oncogenes. Proc Natl Acad Sci USA 2009;106(1): 244–9.

104. Asnafi V, Buzyn A, Le Noir S, et al. NOTCH1/ FBXW7 mutation identifies a large subgroup with favorable outcome in adult T-cell acute lymphoblastic leukemia (T-ALL): a Group for Research on Adult Acute Lymphoblastic Leukemia (GRAALL) study. *Blood.* 2009;113(17):3918-3924.

105. Gutierrez A, Sanda T, Ma W, Zhang J, Grebliunaite R, Dahlberg S, Neuberg D, Protopopov A, Winter SS, Larson RS, Borowitz MJ, Silverman LB, Chin L, Hunger SP, Jamieson C, Sallan SE, Look AT. Inactivation of LEF1 in T-cell acute lymphoblastic leukemia. Blood. 2010 Apr 8;115(14):2845-51. doi: 10.1182/blood-2009-07-234377. Epub 2010 Feb 1.

106. Boyer J. t(8;14) (q24;q11) Atlas Genet Cytogenet Oncol Haematol. http://AtlasGeneticsOncology.org/Anomalies/t0814ID1061.html. Accessed April 2001.

107. Bonnet M, Loosveld M, Montpellier B, Navarro JM, Quilichini B, Picard C, Di Cristofaro J, Bagnis C, Fossat C, Hernandez L, Mamessier E, Roulland S, Morgado E, Formisano-Tréziny C, Dik WA, Langerak AW, Prebet T, Vey N, Michel G, Gabert J, Soulier J, Macintyre EA, Asnafi V, Payet-Bornet D, Nadel B. Posttranscriptional deregulation of MYC via PTEN constitutes a major alternative pathway of MYC activation in T-cell acute lymphoblastic leukemia. Blood. 2011 Jun 16;117(24):6650-9. doi: 10.1182/blood-2011-02-336842. Epub 2011 Apr 28.

108. Kaveri D, Kastner P, Dembélé D, Nerlov C, Chan S, Kirstetter P. β-Catenin activation synergizes with Pten loss and Myc overexpression in Notch-independent T-ALL. Blood. 2013 Aug 1;122(5):694-704. doi: 10.1182/blood-2012-12-471904. Epub 2013 Jun 25.

109. Palomero T, Lim WK, Odom DT, Sulis ML, Real PJ, Margolin A, Barnes KC, O'Neil J, Neuberg D, Weng AP, Aster JC, Sigaux F, Soulier J, Look AT, Young RA, Califano A, Ferrando AA. NOTCH1 directly regulates c-MYC and activates a feed-forward-loop transcriptional network promoting leukemic cell growth. Proc Natl Acad Sci 2006; 103:18261-18266.

110. Sharma VM, Draheim KM, Kelliher MA. 2007. The Notch1/c-Myc pathway in T cell leukemia. Cell Cycle 6:927–930.

111. Langenau DM, Traver D, Ferrando AA, Kutok JL, Aster JC, Kanki JP, Lin S, Prochownik E, Trede NS, Zon LI, Look AT. 2003. Myc-induced T cell leukemia in transgenic zebrafish. Science 299:887–890.

112. Gutierrez A, Grebliunaite R, Feng H, Kozakewich E, Zhu S, Guo F, Payne E, Mansour M, Dahlberg SE, Neuberg DS, Hertog J, Prochownik EV, Testa JR, Harris M, Kanki JP, Look AT. 2011. Pten mediates Myc oncogene dependence in a conditional zebrafish model of T cell acute lymphoblastic leukemia. J Exp Med 208:1595–1603.

113. Smith DP, Bath ML, Metcalf D, Harris AW, Cory S. 2006. MYC levels govern hernatopoietic tumor type and latency in transgenic mice. Blood 108:653–661.

114. Guo W, Lasky JL, Chang CJ, Mosessian S, Lewis X, Xiao Y, Yeh JE, Chen JY, Iruela-Arispe ML, Varella-Garcia M, Wu H. 2008. Multi-genetic events collaboratively contribute to Pten-null leukaemia stem-cell formation. Nature 453:529–533.

115. Li X, Gounari F, Protopopov A, Khazaie K, von Boehmer H. 2008. Oncogenesis of T-ALL and nonmalignant consequences of overexpressing intracellular NOTCH1. J Exp Med 205:2851–2861.

116. Felsher , D.W. , and J.M. Bishop. 1999 . Reversible tumorigenesis by MYC in hematopoietic lineages. Mol. Cell . 4 : 199 – 207 .

117. Girard , L. , Z. Hanna , N. Beaulieu , C.D. Hoemann , C. Simard , C.A. Kozak , and P. Jolicoeur. 1996 . Frequent provirus insertional mutagenesis of Notch1 in thymomas of MMTVD/myc transgenic mice suggests a collaboration of c-myc and Notch1 for oncogenesis. Genes Dev. 10 : 1930 – 1944.

118. Loosveld M, Bonnet M, Gon S, Montpellier B, Quilichini B, Navarro JM, Crouzet T, Goujart MA, Chasson L, Morgado E, Picard C, Hernandez L, Fossat C, Gabert J, Michel G, Nadel B, Payet-Bornet D. MYC fails to efficiently shape malignant transformation in T-cell acute lymphoblastic leukemia. Genes Chromosomes Cancer. 2014 Jan;53(1):52-66. doi: 10.1002/gcc.22117. Epub 2013 Oct 12.

119. Cully M, You H, Levine AJ, Mak TW. Beyond PTEN mutations: the PI3K pathway as an integrator of multiple inputs during tumorigenesis. *Nat Rev Cancer*. 2006;6(3):184–192.

120. Palomero T, et al. Mutational loss of PTEN induces resistance to NOTCH1 inhibition in T-cell leukemia. *Nat Med*. 2007;13(10):1203–1210.

121. Van Vlierberghe P, et al. ETV6 mutations in early immature human T cell leukemias. *J Exp Med*. 2011; 208(13):2571–2579.

122. Zhang J, et al. The genetic basis of early T-cell precursor acute lymphoblastic leukaemia. *Nature*. 2012;481(7380):157–163.

123. Bar-Eli M, Ahuja H, Foti A, Cline MJ. N-RAS mutations in T-cell acute lymphocytic leukaemia: analysis by direct sequencing detects a novel mutation.*Br J Haematol*. 1989;72(1):36–39.

124. Balgobind BV, et al. Leukemia-associated NF1 inactivation in patients with pediatric T-ALL and AML lacking evidence for neurofibromatosis. *Blood*. 2008; 111(8):4322–4328.

125. Shochat C, Tal N, Bandapalli OR, Palmi C, Ganmore I, te Kronnie G, Cario G, Cazzaniga G, Kulozik AE, Stanulla M, Schrappe M, Biondi A, Basso G, Bercovich D, Muckenthaler MU, Izraeli S. Gain-of-function mutations in interleukin-7 receptor-α (IL7R) in childhood acute lymphoblastic leukemias. J Exp Med 2011; 208(5):901-8.

126. Zenatti PP, Ribeiro D, Li W, Zuurbier L, Silva MC, Paganin M, Tritapoe J, Hixon JA, Silveira AB, Cardoso BA, Sarmento LM, Correia N, Toribio ML, Kobarg J, Horstmann M, Pieters R, Brandalise SR, Ferrando AA, Meijerink JP, Durum SK, Yunes JA, Barata JT. Oncogenic IL7R gain-of-function mutations in childhood T-cell acute lymphoblastic leukemia. Nat Genet 2011; 43(10):932-9.

127. Pieters R, Carroll WL. Biology and treatment of acute lymphoblastic leukemia. Pediatr Clin North Am 2008; 55: 1–20, ix.

128. Pui CH, Evans WE. Treatment of acute lymphoblastic leukemia. N Engl J Med 2006; 354: 166–178.

129. Southern E, Mir K, Shchepinov M. Molecular interactions on microarrays. Nat Genet. 1999 Jan;21(1 Suppl):5-9.

130. Lipshutz RJ, Fodor SP, Gingeras TR, Lockhart DJ. High density synthetic oligonucleotide arrays. Nat Genet. 1999 Jan;21(1 Suppl):20-4.

131. Storey H. A direct approach to false discovery rates. J R Statist Soc Ser B 2002; 4 (Part3): 479-498.

132. Eisen MB, Spellman PT, Brown PO, Botstein D. Cluster analysis and display of genome-wide expression patterns. Proc Natl Acad Sci U S A. 1998 Dec 8;95(25):14863-8.

133. Golub TR, Slonim DK, Tamayo P, Huard C, Gaasenbeek M, Mesirov JP, Coller H, Loh ML, Downing JR, Caligiuri MA, Bloomfield CD, Lander ES. Molecular classification of cancer: class discovery and class prediction by gene expression monitoring. Science. 1999 Oct 15;286(5439):531

134. Wouters BJ, Löwenberg B, Delwel R. A decade of genome-wide gene expression profiling in acute myeloid leukemia: flashback and prospects. Blood. 2009 Jan 8;113(2):291-8. doi: 10.1182/blood-2008-04-153239. Epub 2008 Aug 14.

135. Willman CL. Has gene expression profiling improved diagnosis, classification, and outcome prediction in AML? Best Pract Res Clin Haematol. 2008 Mar;21(1):21-8. doi: 10.1016/j.beha.2007.11.008.

136. Iqbal J, Liu Z, Deffenbacher K, Chan WC. Gene expression profiling in lymphoma diagnosis and management. Best Pract Res Clin Haematol. 2009 Jun;22(2):191-210. doi: 10.1016/j.beha.2009.05.001.

137. Valk PJ, Verhaak RG, Beijen MA, Erpelinck CA, Barjesteh van Waalwijk van Doorn-Khosrovani S, Boer JM, Beverloo HB, Moorhouse MJ, van der Spek PJ, Löwenberg B, Delwel R. Prognostically useful gene-expression profiles in acute myeloid leukemia. N Engl J Med. 2004 Apr 15;350(16):1617-28.

138. Haferlach T, Kohlmann A, Schnittger S, Dugas M, Hiddemann W, Kern W, Schoch C. Global approach to the diagnosis of leukemia using gene expression profiling. Blood. 2005 Aug 15;106(4):1189-98. Epub 2005 May 5.

139. Bullinger L, Döhner K, Bair E, Fröhling S, Schlenk RF, Tibshirani R, Döhner H, Pollack JR. Use of gene-expression profiling to identify prognostic subclasses in adult acute myeloid leukemia. N Engl J Med. 2004 Apr 15;350(16):1605-16.

140. Radmacher MD, Marcucci G, Ruppert AS, Mrózek K, Whitman SP, Vardiman JW, Paschka P, Vukosavljevic T, Baldus CD, Kolitz JE, Caligiuri MA, Larson RA, Bloomfield CD; Cancer and Leukemia Group B. Independent confirmation of a prognostic gene-expression signature in adult acute myeloid leukemia with a normal karyotype: a Cancer and Leukemia Group B study. Blood. 2006 Sep 1;108(5):1677-83. Epub 2006 May 2.

141. Mullighan CG, Goorha S, Radtke I, Miller CB, Coustan-Smith E, Dalton JD, Girtman K, Mathew S, Ma J, Pounds SB, Su X, Pui CH, Relling MV, Evans WE, Shurtleff SA, Downing JR. Genome-wide analysis of genetic alterations in acute lymphoblastic leukaemia. Nature. 2007 Apr 12;446(7137):758-64.

142. Willenbrock H, Juncker AS, Schmiegelow K, Knudsen S, Ryder LP. Prediction of immunophenotype, treatment response, and relapse in childhood acute lymphoblastic leukemia using DNA microarrays. Leukemia. 2004 Jul;18(7):1270-7.

143. Bhojwani D, Kang H, Menezes RX, Yang W, Sather H, Moskowitz NP, Min DJ, Potter JW, Harvey R, Hunger SP, Seibel N, Raetz EA, Pieters R, Horstmann MA, Relling MV, den Boer ML, Willman CL, Carroll WL; Children's Oncology Group Study; Dutch Childhood Oncology Group; German Cooperative Study Group for Childhood Acute Lymphoblastic Leukemia. Gene expression signatures predictive of early response and outcome in high-risk childhood acute lymphoblastic leukemia: A Children's Oncology Group Study [corrected]. J Clin Oncol. 2008 Sep 20;26(27):4376-84. doi: 10.1200/JCO.2007.14.4519.

144. Chiaretti S, Li X, Gentleman R, Vitale A, Vignetti M, Mandelli F, Ritz J, Foa R. Gene expression profile of adult T-cell acute lymphocytic leukemia identifies distinct subsets of patients with different response to therapy and survival. Blood. 2004 Apr 1;103(7):2771-8. Epub 2003 Dec 18.

145. Remke M, Pfister S, Kox C, Toedt G, Becker N, Benner A, Werft W, Breit S, Liu S, Engel F, Wittmann A, Zimmermann M, Stanulla M, Schrappe M, Ludwig WD, Bartram CR, Radlwimmer B, Muckenthaler MU, Lichter P, Kulozik AE. High-resolution genomic profiling of childhood T-ALL reveals frequent copy-number alterations affecting the TGF-beta and PI3K-AKT pathways and deletions at 6q15-16.1 as a genomic marker for unfavorable early treatment response. Blood. 2009 Jul 30;114(5):1053-62. doi: 10.1182/blood-2008-10-186536. Epub 2009 Apr 30.

146. La Starza R, Lettieri A, Pierini V, Nofrini V, Gorello P, Songia S, Crescenzi B, Te Kronnie G, Giordan M, Leszl A, Valsecchi MG, Aversa F, Basso G, Biondi A, Conter V, Cazzaniga G, Mecucci C. Linking genomic lesions with minimal residual disease improves prognostic stratification in children with T-cell acute lymphoblastic leukaemia. Leuk Res. 2013 Aug;37(8):928-35. doi: 10.1016/j.leukres.2013.04.005. Epub 2013 Jun 2.

147. Kent, M., Bishop-Stewart, J., Matthews, J., and Spitsbergen, J. (2002). Pseudocapillaria tomentosa, a nematode pathogen, and associated neoplasms of zebrafish. Comp. Med. 52, 354–358.

148. Smolowitz, R., Hanley, J., and Richmond, H. (2002). A three-year retrospective study of abdominal tumors in zebrafish maintained in an aquatic laboratory animal facility. Biol. Bull. 203, 265–266.

149. Matthews, J. (2004). Common diseases of laboratory zebrafish. Meth. Cell Biol. 77, 617–643.

150. Postlethwait, J., Woods, I., Ngo-Hazelett, P., Yan, Y., Kelly, P., Chu, F., Huang, H., Hill- Force, A., and Talbot, W. (2000). Zebrafish comparative genomics and the origins of vertebrate chromosomes. Genome Res. 10, 1890–1902.

151. Liu, T., Zhou, Y., Kanki, J., Deng, M., Rhodes, J., Yang, H., Sheng, X., Zon, L., and Look, A. (2002). Evolutionary conservation of zebrafish linkage group 14 with frequently deleted regions of human chromosome 5 in myeloid malignancies. Proc. Natl Acad. Sci. USA 99, 6136–6141.

152. White, R., Mark, Sessa, A., Burke, C., Bowman, T., LeBlanc, J., Ceol, C., Bourque, C., Dovey, M., Goessling, W., Burns, C., Erter, et al. (2008). Transparent adult zebrafish as a tool for in vivo transplantation analysis. Cell Stem Cell 2, 183–189.

153. Langenau, D. M., Feng, H., Berghmans, S., Kanki, J. P., Kutok, J. L., and Look, A. T. (2005a). Cre/lox-regulated transgenic zebrafish model with conditional myc-induced T cell acute lymphoblastic leukemia. Proc. Natl Acad. Sci. USA 102, 6068–6073.

154. Feng, H., Langenau, D. M., Marge, J., Quinkertz, A., Gutierrez, A., Neuberg, D., Kanki, J. P., and Look, A. T. (2007). Heat-shock induction of T-cell lymphoma/leukaemia in conditional Cre/lox-regulated transgenic zebrafish. Br. J. Haematol. 138, 169–175.

155. Langenau, D. M., Jette, C., Berghmans, S., Palomero, T., Kanki, J. P., Kutok, J. L., and Look, A. T. (2005b). Suppression of apoptosis by bcl-2 overexpression in lymphoid cells of transgenic zebrafish. Blood 105, 3278–3285.

156. Sabaawy, H., Azuma, M., Embree, L., Tsai, H., Starost, M., and Hickstein, D. (2006). TELAML1 transgenic zebrafish model of precursor B cell acute lymphoblastic leukemia. Proc. Natl Acad. Sci. USA 103, 15166–15171.

157. Chen, J., Jette, C., Kanki, J. P., Aster, J. C., Look, A. T., and Griffin, J. D. (2007). NOTCH1- induced T-cell leukemia in transgenic zebrafish. Leukemia 21, 462–471.

158. Zhuravleva J, Paggetti J, Martin L, Hammann A, Solary E, Bastie JN et al. MOZ/TIF2-induced acute myeloid leukaemia in transgenic fish. Br J Haematol 2008; 143: 378–382.

159. Alghisi E, Distel M, Malagola M, Anelli V, Santoriello C, Herwig L, Krudewig A, Henkel CV, Russo D, Mione MC. Targeting oncogene expression to endothelial cells induces proliferation of the myelo-erythroid lineage by repressing the Notch pathway. Leukemia. 2013 Nov;27(11):2229-41. doi: 10.1038/leu.2013.132. Epub 2013 Apr 29.

160. Patton, E. E., Widlund, H. R., Kutok, J. L., Kopani, K. R., Amatruda, J. F., Murphey, R. D., Berghmans, S., Mayhall, E. A., Traver, D., Fletcher, C. D. M., et al. (2005). BRAF mutations are sufficient to promote nevi formation and cooperate with p53 in the genesis of melanoma. Curr. Biol. 15, 249–254.

161. Langenau, D. M., Keefe, M. D., Storer, N. Y., Guyon, J. R., Kutok, J. L., Le, X., Goessling, W., Neuberg, D. S., Kunkel, L. M., and Zon, L. I. (2007). Effects of RAS on the genesis of embryonal rhabdomyosarcoma. Genes Dev. 21, 1382–1395.

162. Traver D, Herbomel P, Patton EE, Murphey RD, Yoder JA, Litman GW, Catic A, Amemiya CT, Zon LI, Trede NS. The zebrafish as a model organism to study development of the immune system. Adv Immunol. 2003;81:253-330.

163. Lam SH, Chua HL, Gong Z, Lam TJ, Sin YM. Development and maturation of the immune system in zebrafish, Danio rerio: a gene expression profiling, in situ hybridization and immunological study. Dev Comp Immunol. 2004 Jan;28(1):9-28.

164. Frazer JK, Meeker ND, Rudner L, Bradley DF, Smith AC, Demarest B, Joshi D, Locke EE, Hutchinson SA, Tripp S, Perkins SL, Trede NS. Heritable T-cell malignancy models established in a zebrafish phenotypic screen. Leukemia. 2009 Oct;23(10):1825-35. doi: 10.1038/leu.2009.116. Epub 2009 Jun 11.

165. Nicoli, S., Ribatti, D., Cotelli, F., and Presta, M. (2007). Mammalian tumor xenografts induce neovascularization in zebrafish embryos. Cancer Res. 67, 2927–2931.

166. Stoletov, K., Montel, V., Lester, R. D., Gonias, S. L., and Klemke, R. (2007). High-resolution imaging of the dynamic tumor cell vascular interface in transparent zebrafish. Proc. Natl Acad. Sci. USA 104, 17406–17411.

167. Pruvot B, Jacquel A, Droin N, Auberger P, Bouscary D, Tamburini J, Muller M, Fontenay M, Chluba J, Solary E. Leukemic cell xenograft in zebrafish embryo for investigating drug efficacy. Haematologica. 2011 Apr;96(4):612-6. doi: 10.3324/haematol.2010.031401. Epub 2011 Jan 12.

168. Shepard, J. L., Amatruda, J. F., Stern, H. M., Subramanian, A., Finkelstein, D., Ziai, J., Finley, K. R., Pfaff, K. L., Hersey, C., Zhou, Y., et al. (2005). A zebrafish bmyb mutation causes genome instability and increased cancer susceptibility. Proc. Natl Acad. Sci. USA 102, 13194–13199.

169. Shepard, J. L., Amatruda, J. F., Finkelstein, D., Ziai, J., Finley, K. R., Stern, H. M., Chiang, K., Hersey, C., Barut, B., Freeman, J. L., et al. (2007). A mutation in separase causes genome instability and increased susceptibility to epithelial cancer. Genes Dev. 21, 55–59.

170. Peterson, R. T., Shaw, S. Y., Peterson, T. A., Milan, D. J., Zhong, T. P., Schreiber, S. L., MacRae, C. A., and Fishman, M. C. (2004). Chemical suppression of a genetic mutation in a zebrafish model of aortic coarctation. Nat. Biotechnol. 22, 595–599.

171. Stern, H., Murphey, R., Shepard, J., Amatruda, J., Straub, C., Pfaff, K., Weber, G., Tallarico, J., King, R.,

and Zon, L. (2005). Small molecules that delay S phase suppress a zebrafish bmyb mutant. Nat. Chem. Biol. 1, 366–370.

172. North, T., Goessling, W., Walkley, C., Lengerke, C., Kopani, K., Lord, A., Weber, G., Bowman, T., Jang, I., Grosser, T., et al. (2007). Prostaglandin E2 regulates vertebrate haematopoietic stem cell homeostasis. Nature 447, 1007–1011.

173. Forster A, Pannell R, Drynan LF, Codrington R, Daser A, Metzler M, Lobato MN, Rabbitts TH. The invertor knock-in conditional chromosomal translocation mimic. Nat Methods. 2005 Jan;2(1):27-30.

174. Hamilton, D. L., and Abremski, K. (1984). Site-specific recombination by the bacteriophage P1 lox-Cre system. Cre-mediated synapsis of two lox sites. J. Mol. Biol. 178(2), 481–486.

175. Hoess, R. H., and Abremski, K. (1984). Interaction of the bacteriophage P1 recombinase Cre with the recombining site loxP. Proc. Natl Acad. Sci. USA 81(4), 1026–1029.

176. Lavau C, Szilvassy SJ, Slany R, Cleary ML. Immortalization and leukemic transformation of a myelomonocytic precursor by retrovirally transduced HRX-ENL. EMBO J. 1997 Jul 16;16(14):4226-37.

177. Shultz LD, Schweitzer PA, Christianson SW, Gott B, Schweitzer IB, Tennent B, McKenna S, Mobraaten L, Rajan TV, Greiner DL, et al. Multiple defects in innate and adaptive immunologic function in NOD/LtSz-scid mice. J Immunol. 1995 Jan 1;154(1):180-91.

178. Dick JE. Normal and leukemic human stem cells assayed in SCID mice. Semin Immunol. 1996 Aug;8(4):197-206.

179. Kamel-Reid S, Letarte M, Sirard C, Doedens M, Grunberger T, Fulop G, Freedman MH, Phillips RA, Dick JE. A model of human acute lymphoblastic leukemia in immune-deficient SCID mice. Science. 1989 Dec 22;246(4937):1597-600.

180. Lapidot T, Sirard C, Vormoor J, Murdoch B, Hoang T, Caceres-Cortes J, Minden M, Paterson B, Caligiuri MA, Dick JE. A cell initiating human acute myeloid leukaemia after transplantation into SCID mice. Nature. 1994 Feb 17;367(6464):645-8.

181. Uckun FM, Waurzyniak BJ, Sather HN, Sensel MG, Chelstrom L, Nachman J, Gaynon PS, Bostrom B, Ek O, Sarquis M, Steinherz PG, Reaman GH. Prognostic significance of T-lineage leukemic cell growth in SCID mice: a Children's Cancer Group study. Leuk Lymphoma. 1999 Feb;32(5-6):475-87.

182. Pearce DJ, Taussig D, Zibara K, Smith LL, Ridler CM, Preudhomme C, Young BD, Rohatiner AZ, Lister TA, Bonnet D. AML engraftment in the NOD/SCID assay reflects the outcome of AML: implications for our understanding of the heterogeneity of AML. Blood. 2006 Feb 1;107(3):1166-73. Epub 2005 Oct 18.

183. Nijmeijer BA, Mollevanger P, van Zelderen-Bhola SL, Kluin-Nelemans HC, Willemze R, Falkenburg JH. Monitoring of engraftment and progression of acute lymphoblastic leukemia in individual NOD/SCID mice. Exp Hematol. 2001 Mar;29(3):322-9.

184. Feuring-Buske M, Gerhard B, Cashman J, Humphries RK, Eaves CJ, Hogge DE.Improved engraftment of human acute myeloid leukemia progenitor cells in beta 2-microglobulin-deficient NOD/SCID mice and in NOD/SCID mice transgenic for human growth factors. Leukemia. 2003 Apr;17(4):760-3.

185. Clappier E, Gerby B, Sigaux F, Delord M, Touzri F, Hernandez L, Ballerini P, Baruchel A, Pflumio F, Soulier J. Clonal selection in xenografted human T cell acute lymphoblastic leukemia recapitulates gain of malignancy at relapse. J Exp Med. 2011 Apr 11;208(4):653-61. doi: 10.1084/jem.20110105. Epub 2011 Apr 4.

186. Loetscher M, Geiser T, O'Reilly T, Zwahlen R, Baggiolini M, Moser B. Cloning of a human seven-transmembrane domain receptor, LESTR, that is highly expressed in leukocytes. J. Biol. Chem. 1994; 269(1):232–237. [PubMed: 8276799]

187. Murphy PM, Baggiolini M, Charo IF, Hebert CA, Horuk R, Matsushima K, Miller LH, Oppenheim JJ, Power CA. International union of pharmacology. XXII. Nomenclature for chemokine receptors. Pharmacol Rev 2000;52(1):145–76. [PubMed: 10699158]

188. Fredriksson R, Lagerstrom MC, Lundin LG, Schioth HB. The G-protein-coupled receptors in the human genome form five main families. Phylogenetic analysis, paralogon groups, and fingerprints. Mol Pharmacol 2003;63(6):1256–72. [PubMed: 12761335]

189. Mueller, A., Homey, B., Soto, H., Ge, N., Carton, D., Buchanan, M.E., McClanahan, T., Murphy, E., Yuan, W., Wagner, S.N., Barrera, J.L., Mohar, A., Verastegui, E. & Zlotnik, A. (2001) Involvement of chemokine receptors in breast carcinoma metastasis. Nature, 410, 50±56.

190. Nagasawa T, Hirota S, Tachibana K, Takakura N, Nishikawa S, Kitamura Y, Yoshida N, Kikutani H, Kishimoto T. Defects of B-cell lymphopoiesis and bone-marrow myelopoiesis in mice lacking the CXC chemokine PBSF/SDF-1. Nature 1996;382(6592):635–8. [PubMed: 8757135]

191. Zou YR, Kottmann AH, Kuroda M, Taniuchi I, Littman DR. Function of the chemokine receptor CXCR4 in haematopoiesis and in cerebellar development. Nature 1998;393(6685):595–9. [PubMed: 9634238]

192. Ma Q, Jones D, Borghesani PR, Segal RA, Nagasawa T, Kishimoto T, Bronson RT, Springer TA. Impaired B lymphopoiesis, myelopoiesis, and derailed cerebellar neuron migration in CXCR4- and SDF-1-deficient mice. Proc Natl Acad Sci U S A 1998;95(16):9448–53. [PubMed: 9689100]

193. McGrath KE, Koniski AD, Maltby KM, McGann JK, Palis J. Embryonic expression and function of the chemokine SDF-1 and its receptor, CXCR4. Dev Biol 1999;213(2):442–56. [PubMed: 10479460]

194. Nagasawa T, Tachibana K, Kishimoto T. A novel CXC chemokine PBSF/SDF-1 and its receptor CXCR4: their functions in development, hematopoiesis and HIV infection. Semin Immunol 1998;10 (3):179–85. [PubMed: 9653044]

195. SchenW, Bendall LJ, Gottlieb DJ, Bradstock KF (2001) The chemokine receptor CXCR4 enhances integrin-mediated *in vitro* adhesion and facilitates engraftment of leukemic precursor-B cells in the bone marrow. *Exp Hematol* 29: 1439–1447.

196. Lapidot T, Kollet O (2002) The essential roles of the chemokine SDF-1 and its receptor CXCR4 in human stem cell homing and repopulation of transplanted immune-deficient NOD/SCID and NOD/SCID/B2mnull mice. *Leukemia* 16: 1992–2003.

197. Méndez-Ferrer S, Frenette PS. Hematopoietic stem cell trafficking: regulated adhesion and attraction to bone marrow microenvironment. Ann. NY Acad. Sci. 2007; 1116:392–413. [PubMed: 18083941]

198. Ma, Q., Jones, D., Borghesani, P.R., Segal, R.A., Nagasawa, T., Kishimoto, T., Bronson, R.T. & Springe, R.T.A. (1998) Impaired Blymphopoiesis, myelopoiesis, and derailed cerebellar neuron migration in CXCR4- and SDF-1-deficient mice. Proceedings of the National Academy of Sciences of the United States of America, 95, 9448±9453.

199. Rossi D, Zlotnik A. The biology of chemokines and their receptors. Annu Rev Immunol 2000;18:217–42.

200. D'Apuzzo M, Rolink A, Loetscher M, et al. The chemokine SDF-1, stromal cell-derived factor 1, attracts early stage B cell precursors via the chemokine receptor CXCR4. Eur. J. Immunol. 1997; 27(7):1788–1793. [PubMed: 9247593]

201. Bleul CC, Fuhlbrigge RC, Casasnovas JM, Aiuti A, Springer TA. A highly efficacious lymphocyte chemoattractant, stromal cell-derived factor 1 (SDF-1). J. Exp. Med. 1996; 184(3):1101–1109. [PubMed: 9064327]

202. Oberlin E, Amara A, Bachelerie F, et al. The CXC chemokine SDF-1 is the ligand for LESTR/ fusin and prevents infection by T-cell-line-adapted HIV-1. Nature. 1996; 382(6594):833–835. [PubMed: 8752281]

203. Fedyk ER, Ryyan DH, Ritterman I, Springer TA. Maturation decreases responsiveness of human bone marrow B lineage cells to stromal-derived factor 1 (SDF-1). J Leukoc Biol 1999;66(4):667–73. [PubMed: 10534124]

204. Honczarenko M, Douglas RS, Mathias C, Lee B, Ratajczak MZ, Silberstein LE. SDF-1 responsiveness does not correlate with CXCR4 expression levels of developing human bone marrow B cells. Blood 1999;94(9):2990–8. [PubMed: 10556181]

205. Kitchen SG, Zack JA. CXCR4 expression during lymphopoiesis: implications for human immunodeficiency virus type 1 infection of the thymus. J. Virol. 1997; 71(9):6928–6934. [PubMed: 9261420]

206. Wegner SA, Ehrenberg PK, Chang G, Dayhoff DE, Sleeker AL, Michael NL. Genomic organization and functional characterization of the chemokine receptor CXCR4, a major entry coreceptor for human immunodeficiency virus type 1. J. Biol. Chem. 1998; 273(8):4754–4760. [PubMed: 9468539] 57. Bleul CC, Wu L, Hoxie

207. Moriuchi M, Moriuchi H, Turner W, Fauci AS. Cloning and analysis of the promoter region of CXCR4, a coreceptor for HIV-1 entry. J Immunol 1997;159(9):4322–9. [PubMed: 9379028]

208. Moriuchi M, Moriuchi H, Margolis DM, Fauci AS. Cloning and analysis of the promoter region of CXCR4, a coreceptor for HIV-1 entry. USF/c-Myc enhances, while Yin-Yang 1 suppresses, the promoter activity of CXCR4, a coreceptor for HIV-1 entry. J. Immunol. 1999; 162(10):5986– 5992. [PubMed: 10229837]

209. Hasegawa A, Yasukawa M, Sakai I, Fujita S. Transcriptional down-regulation of CXC chemokine receptor 4 induced by impaired association of transcription regulator YY1 with c-Myc in human herpesvirus 6-infected cells. J Immunol 2001;166(2):1125–31. [PubMed: 11145693]

210. Signoret N, Oldridge J, Pelchen-Matthews A, et al. Phorbol esters and SDF-1 induce rapid endocytosis and down modulation of the chemokine receptor CXCR4. J. Cell Biol. 1997; 139(3): 651–664. [PubMed: 9348282]

211. Busillo JM, Benovic JL. Regulation of CXCR4 signaling. Biochim. Biophys. Acta. 2007; 1768(4): 952–963. [PubMed: 17169327] • Very well-written review that summarizes the signaling pathways involving CXCR4 and the regulation of CXCR4 expression.

212. Hesselgesser J, Liang M, Hoxie J, et al. Identification and characterization of the CXCR4 chemokine receptor in human T cell lines: ligand binding, biological activity, and HIV-1 infectivity. J. Immunol. 1998; 160(2):877–883. [PubMed: 9551924]

213. Marchese A, Benovic JL. Agonist-promoted ubiquitination of the G protein-coupled receptor CXCR4 mediates lysosomal sorting. J. Biol. Chem. 2001; 276(49):45509–45512. [PubMed: 11641392]

214. Förster R, Kremmer E, Schubel A, et al. Intracellular and surface expression of the HIV-1 coreceptor CXCR4/fusin on various leukocyte subsets: rapid internalization and recycling upon activation. J. Immunol. 1998; 160(3):1522–1531. [PubMed: 9570576]

215. Kucia M, Jankowski K, Reca R, Wysoczynski M, Bandura L, Allendorf DJ, Zhang J, Ratajczak J, Ratajczak MZ. CXCR4-SDF-1 signalling, locomotion, chemotaxis and adhesion. J Mol Histol 2004;35(3):233–45. [PubMed: 15339043]

216. Balkwill F. Cancer and the chemokine network. Nat Rev Cancer 2004;4(7):540–50. [PubMed: 15229479]

217. Laudana C, Kim JY, Constantin G, Butcher E. Rapid leukocyte integrin activation by chemokines. Immunol. Rev. 2002; 186:37–46. [PubMed: 12234360]

218. Campbell JJ, Hedrick J, Zlotnik A, Siani MA, Thompson DA, Butcher EC. Chemokines and the arrest of lymphocytes rolling under flow conditions. Science 1998;279(5349):381–4. [PubMed: 9430588]

219. Glodek AM, Honczarenko M, Le Y, Campbell JJ, Silberstein LE. Sustained activation of cell adhesion is a differentially regulated process in B lymphopoiesis. J Exp Med 2003;197(4):461–73. [PubMed: 12591904]

220. Wright N, Hidalgo A, Rodriguez-Frade JM, Soriano SF, Mellado M, Parmo-Cabanas M, Briskin MJ, Teixido J. The chemokine stromal cell-derived factor-1 alpha modulates alpha 4 beta 7 integrinmediated lymphocyte adhesion to mucosal addressin cell adhesion molecule-1 and fibronectin. J Immunol 2002;168(10):5268–77. [PubMed: 11994484]

221. Tavor S, Petit I. Can inhibition of the SDF-1/CXCR4 axis eradicate acute leukemia? Semin. Cancer Biol. 2010; 20(3):178–185. [PubMed: 20637871]

222. Scupoli MT, Donadelli M, Cioffi F, et al. Bone marrow stromal cells and the upregulation of interleukin-8 production in human T-cell acute lymphoblastic leukemia through the CXCL12/CXCR4 axis and the NF-κB and JNK/AP-1 pathways. Haematologica. 2008; 93(4):524–532. [PubMed: 18322253]

223. Burger JA, Tsukada N, Burger M, Zvaifler NJ, Dell'Aquila M, Kipps TJ. Blood-derived nurse-like cells protect chronic lymphocytic leukemia B cells from spontaneous apoptosis through stromal cell-derived factor-1. Blood 2000;96(8):2655–63. [PubMed: 11023495]

224. Damiano JS, Cress AE, Hazlehurst LA, Shtil AA, Dalton WS. Cell adhesion mediated drug resi stance (CAM-DR): role of integrins and resistance to apoptosis in human myeloma cell lines. Blood 1999;93(5):1658–67. [PubMed: 10029595]

225. Möhle R, Schittenhelm M, Failenschmid C, et al. Functional response of leukaemic blasts to stromal cell-derived factor-1 correlates with preferential expression of the chemokine receptor CXCR4 in acute myelomonocytic and lymphoblastic leukaemia. Br. J. Haematol. 2000; 110(3): 563–572. [PubMed: 10997965]

226. Konoplev S, Rassidakis GZ, Estey E, et al. Overexpression of CXCR4 predicts adverse overall and event-free survival in patients with unmutated Flt3 acute myeloid leukemia with normal karyotype. Cancer. 2007; 109(6):1152–1156. [PubMed: 17315232] • One of several studies that suggests that high CXCR4 expression is associated with poor outcome.

227. Spoo AC, Lü bbert M, Wierda WG, Burger JA. CXCR4 is a prognostic marker in acute myelogenous leukemia. Blood. 2007; 109(2):786–791. [PubMed: 16888090]

228. Peled A, Tavor S.Role of CXCR4 in the pathogenesis of acute myeloid leukemia. Theranostics. 2013;3(1):34-9. doi: 10.7150/thno.5150. Epub 2013 Jan 13.

229. Rombouts EJ, Pavic B, Löwenberg B, Ploemacher RE. Relation between CXCR-4 expression, Flt3 mutations, and unfavorable prognosis of adult acute myeloid leukemia. Blood. 2004; 104(2): 550–557. [PubMed: 15054042]

230. Barretina J, Juncà J, Llano A, et al. CXCR4 and SDF-1 expression in B-cell chronic lymphocytic leukemia and stage of the disease. Ann. Hematol. 2003; 82(8):500–505. [PubMed: 12783211]

231. Juarez J, Bradstock KF, Gottlieb DJ, Bendall LJ. Effects of inhibitors of the chemokine receptor CXCR4 on acute lymphoblastic leukemia cells *in vitro*. Leukemia. 2003; 17(7):1294–1300. [PubMed: 12835717]

232. Juarez J, Dela Pena A, Baraz R, et al. CXCR4 antagonists mobilize childhood acute lymphoblastic leukemia cells into the peripheral blood and inhibit engraftment. Leukemia. 2007; 21(6):1249– 1257. [PubMed: 17410186]

233. Brown, P.; McIntyre, E.; Li, L.; Small, D. Disruption of leukemia stem cell (LSC) interactions with bone marrow stromal niche enhances efficacy of FLT3 tyrosine kinase inhibitors (TKI) *in vivo*; Presented at: 50th American Society of Hematology Annual Meeting and Exposition; SanFrancisco, CA, USA. 2008; December 6–9. Abstract 383

234. Fielding AK. How I treat Philadelphia chromosome-positive acute lymphoblastic leukemia. Blood. 2010; 116(18):3409–3417. [PubMed: 20656928]

235. Wu S, Gessner R, Taube T, et al. Chemokine IL-8 and chemokine receptor CXCR3 and *CXCR4* gene expression in childhood acute lymphoblastic leukemia at first relapse. J. Pediatr. Hematol. Oncol. 2006; 28(4):216–220. [PubMed: 16679918]

236. Wierstra I, Alves J. The c-myc promoter: still MysterY and challenge. *Adv Cancer Res.* 2008;99:113-333.

AIM OF THE PROJECT

Central nervous system (CNS) leukemia at diagnosis and CNS relapse continues to pose a significant challenge in the research of an efficient cure for children with Acute Lymphoblastic Leukemia (ALL). The prognosis of patients with isolated and mixed CNS relapse is particularly poor and treatments used for the cure are very invasive (intratechal chemotherapy and cranial irradiation). As CNS irradiation causes a lot of secondary negative effects (second cancers, neurocognitive deficits, endocrinphathy), efforts are made to improve haematological control and to reduce or avoid the use of cranial irradiation using alternative intrathecal treatment. However, CNS irradiation is still necessary for patients at high risk of relapse within the CNS, especially for those with leukemic involvement of CNS at diagnosis.

Because little is know about how leukemic cells can invade the CNS, our studies aims to deepen the knowledge of molecular mechanisms that regulate this event. We used a gene expression profiling approach to gain in this aim. Moreover, our efforts addressed potential conserved molecular mechanisms in animal models to be translated to human patients.

With the help of two T-ALL zebrafish models that develop CNS leukaemia, we were able to perform whole transcriptome profiles of leukemic cells identifying interesting genes that could explain different mechanisms used by leukemic cells to infiltrate the CNS. Among these genes the importance of *cxcr4* expression in predisposing T-ALL cells to infiltrate the CNS was investigated in zebrafish/murine models as well as in pediatric human patients. Moreover, the strong signature found in zebrafish group overexpressing hu*C-MYC* (*huMYC-ER*) challenged us to clarify the importance and the role of the *C-MYC* oncogene in T-ALL using a GEP approach that we had shown to be successful in identifying signatures inside a specific T-ALL subgroup (i.e: T-ALL patients carrying *MLLT10* rearrangements inside the *HOXA* subgroup).

CHAPTER 1

Discovery of Central Nervous System Infiltration in Zebrafish T Cell Leukemia

Chiara Borga[1], Lance Batchelor[2], Silvia Bresolin[1], Ilaria Bronzini[1], Kimberly Dobrinski[3], Charles Lee[4], Giuseppe Basso[1], J. Kimble Frazer[2] , Geertruy te Kronnie[1]

1Department of Women's and Children's Health, Padua, Italy; 2Pediatric Hematology-Oncology, University of Oklahoma Health Sciences Center, Oklahoma City, OK, USA; 3Pathology & Cell Biology, University of South Florida College of Medicine, Tampa, FL, USA; 4Pathology, Brigham and Women's Hospital, Boston, MA, USA

Manuscript in preparation

ABSTRACT

Central nervous system (CNS) leukemia at diagnosis and relapse continue to pose significant challenges toward more effective treatment of Acute Lymphoblastic Leukemia (ALL). To determine if zebrafish could model CNS disease in T-ALL, we performed histological analyses of CNS involvement in two *D. rerio* lines [*hlk* (n=10) and *hMYC-ER* (n=10)] with GFP^+ T-ALL. Histological analyses of fish at the most advanced stage of disease showed both *hlk* and *hMYC-ER* lines had lymphoblastic infiltration of the CNS, in the meninges, in the optic nerve and retina, and in some animals, the brain parenchyma as well. Moreover, the degree of CNS infiltration was higher in *hMYC-ER* compared to *hlk* groups (*p*-value:0,04). FACS-purified cells from each fish with CNS involvement (by sorting for GFP) were analyzed for gene expression (GeneChip Zebrafish Genome Arrays, Affymetrix, Santa Clara, CA, USA), revealing significantly different profiles between *hlk* and *hMYC-ER* cancers. Particularly, an activation of *cxcr4/cxcl12* axis and *wnt/β-cathenin* pathway was found in *hMYC-ER* and *hlk* cancers, respectively. Interesting, the *cxcr4* expression positively correlated with the degree of CNS invasion, suggesting that higher expression of *cxcr4* increased the migratory response of T-lymphoblatsts towards the CNS environment. CNS involvement in *hlk* and *hMYC-ER* zebrafish cancers position both lines as useful models for studying CNS^+ T-ALL and the different ability for *hMYC-ER* and *hlk* T-lymphoblasts to infiltrate the CNS suggests that these lines can be used to explore different molecular mechanisms that drive CNS invasion in T-ALL.

INTRODUCTION

Central nervous system (CNS) leukemia at diagnosis and relapse continues to pose a significant challenge in the research of an efficient cure for children with Acute Lymphoblastic Leukemia (ALL) [1,2,7]. The prognosis of patients with isolated and mixed CNS relapse is particularly poor and treatments used for the cure are very invasive (intrathecal chemotherapy and cranial irradiation). As CNS irradiation causes a lot of secondary negative effects (second cancers, neurocognitive deficits, endocrinopathy), numerous efforts are made to improve haematological control and to reduce or avoid the use of cranial irradiation using alternative intrathecal treatment [3-6]. However, CNS irradiation is still necessary for patients at high risk of relapse within the CNS, especially for those presenting CNS leukemia at diagnosis [7]. Because little is know about how leukemic cells can invade the CNS, our studies aims to deepen the knowledge of molecular mechanisms that regulate this event. Leukemic cells can infiltrate the CNS both at diagnosis and relapse in hALLs and this event is more frequent in T-ALL compared to B-ALL [7]. For this reason, we focused this project on T-ALL and we decided to study the phenomenon of CNS infiltration with the help of zebrafish models. Zebrafish (zf) is an attractive model organism for studying cancer; in fact, zebrafish can develop spontaneous tumours that resemble those in humans [8-12] and this model allows large-scale genetic screens that can be useful to identify conserved cancer pathways. In addition, tumor suppressors and oncogenes are conserved between human and zebrafish genomes [12,14]. Regarding our specific topic, leukemia is not a spontaneous tumor that spreads in zebrafish. However, next to spontaneous occurring tumors, malignancies can also be induced in the zebrafish model through chemical- (ethylnitrosourea, ENU) and retrovirus insertional- mutagenesis [15,16] or through the development of transgenic models that over-express tumor genes in a tissue-specific manner [17,18]. In the last ten years, several transgenic zebrafish models that develop leukemia have been created, both for T-ALL [17,19-23], pre-B-ALL [24] and AML [25,26]. Moreover, the transparency of zebrafish embryos and the introduction of a transparent stable zebrafish line (*casper*) [27] give a big advantage for real-time monitoring of labelled tumor cells engraftment after transplantation. For our study, it is important to know that there are significant similarities between the anatomical structures of the CNS (i.e: Blood Brain Barrier (BBB), Blood Retinal

Barrier (BRB), meninges) of adult and 3 days post fertilisation (dpf) larval zebrafish and that of higher vertebrates [28,29]. To determine if the zebrafish can be a good model to study CNS disease in T-ALL, we used two approaches: first, we tried to establish an *in vivo* model of CNS leukemic invasion through serial xenotransplantations with human pediatric T-ALL cell lines in wild-type (wt) zebrafish of 3 dpf; second, we performed histological analysis of the CNS of two stable T-ALL *D.rerio* lines (*hMYC-ER* [23] and *hlk* [30]) developing GFP^+ T-ALL. Concerning the first approach, the ability of mammalian cancer cells to successfully engraft zf embryos and induce neovascularisation is well described for solid tumors [31,32], even if human metastatic melanoma cells transplanted in zebrafish embryos move, proliferate and survive without engrafting the host tissues [33]. A recent paper showed successful Jurkat cells transplants in the yolk/blood circulation of zebrafish embryos [34], supporting our choice to perform xenotransplantion of hALL cell lines. Injection of labelled human leukemic T-ALL cell lines was performed in wt larval zf at 3 dpf, divided in two groups depending on the injection site: CNS ventricle/parenchyma or yolk/blood circulation (figure1).

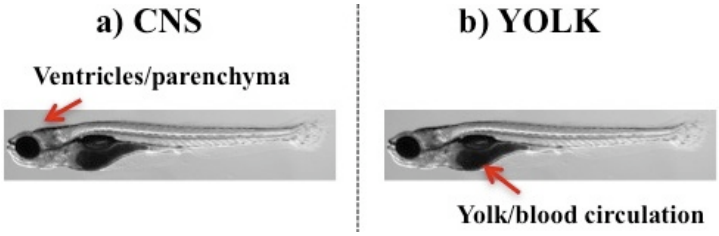

Figure 1. Site of injection of Jurkat cells in larval zebrafish of 3 dpf. Larval fishes were divided in two groups depending on the site of injection that could be at CNS (a) or Yolk (b) site. Red arrows indicate the site of injections in the two groups.

Both injection sites were important to observe the ability of human leukemic cells to move and invade other tissues apart from the injection site. Moreover, CNS injection (in the ventricles/parenchyma) gave immediate insight in the ability of leukemic cells to survive in this environment. For xenotransplantation larval fishes at 3 dpf were used to avoid rejection of transplanted cells by the zebrafish immune system, which starts to be functional from 28 dpf [38].

With the second approach, we analyzed the presence of T-lymphoblastic infiltration in the CNS of two stable zf lines (*hlk* and *hMYC-ER*) that both develop GFP+ T-ALL disease. Even if the time to leukemia is different in *hlk* and *hMYC-ER* lines (6-8 months and 3-4 months respectively), these two zf lines present a similar phenotype regarding the spread of disease; in fact, for both lines it is possible to distinguish a stage of "localized disease", in which GFP+ bright masses arise from the thymic region and a "final stage" of disease, where GFP+ cells are spread in the entire fish (figure 2).

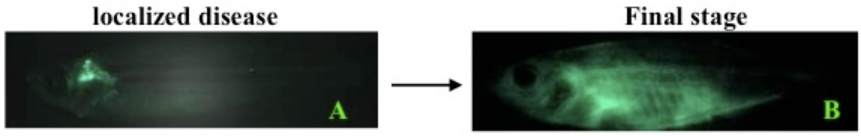

Figure 2. Whole mount fluorescent microscopy images exemplary of the localized and final stage of the disease. Stages were monitored in both *hMYC-ER* and *hlk* zebrafish models. (A) At the stage of localized disease, T-lymphoblasts (GFP+) had proliferated and were localized at the site of the thymus; (B) in the final stage of the disease, leukemic cells had spread to most parts of the body.

Summarizing, in both zf models T-malignant cells originate in the thymus, spread to the peripheral blood, invading gills, retro-orbital area and disseminate into abdominal organs, such as the kidney-marrow (zf bone marrow equivalent), spleen, gut, muscles, skin and fat. *hlk* and *hMYC-ER* lines both develop T-ALL, but they are genetically different. Chemical (ENU) mutagenesis (not further characterized) was used to establish the *hlk* zf line, characterized by a dominant heritable predisposition to develop a clonal and transplantable T-ALL [30]. Instead, in the transgenic *hMYC-ER* T-ALL model, the *rag2* promoter was used to drive the expression of human *C-MYC* oncogene in zebrafish lymphoid cells; also in this case, malignant cells were clonal and could engraft irradiated hosts [23]. Even if both these models have been well characterized, the presence of CNS infiltraton by T-ALL cells had not been investigated in these zf lines. We decided to perform histological analysis of heads of fishes and found for both zf lines the involvement of CNS. The discovery of CNS involvement in *hlk* and *hMYC-ER* zebrafish cancers position both lines as useful models for the study of CNS^{+} T-ALL. Moreover, the degree of CNS infiltration was different comparing *hMYC-ER* and *hlk* cancers, indicating a different ability of these zf T-ALL cells to infiltrate the CNS. Gene expression profiling (GEP) analysis on zebrafish T-ALL cells revealed distinct

expression signatures between *hMYC-ER* and *hlk* cancers; this observation let us to speculate on the presence of different molecular mechanisms that control the invasion of *hMYC-ER* and *hlk* T-ALL cells in the CNS environment.

MATERIAL AND METHODS

Zebrafish Care and Maintenance

Fish were kept in colony at 28.5°C on a 12/12 hour (hr) circadian cycle. For all procedures, fish were anesthetized with 0.02% tricaine methanesulfonate (MS222). After xenotransplantation, larval fishes were maintain 1h at 28°C and than at 33°C to allow survival of both human leukemic cells and larval fishes.

Leukemic Cells preparation and Transplants

Xenotransplants (Table 1) were performed using leukemia derived cell lines (CCRF-CEM, P12-ICHIKAWA, DND-41, TALL-1 and Jurkat). ~$3*10^6$ cells were centrifuged and re-suspended in 1 ml of RPMI 1640 medium (10% FBS, 1% ampicilline and 1% glutamine). Cells were incubated at 37°C for 30 minutes with label CM-DiI, a lipophilic fluorescent tracking dye (Invitrogen, Paisley, UJ) according to the manufacturer's instruction. Larval fish at 3 days post fertilisation (dpf) were used for xenotransplants. ~50-200 labelled (CM-DiI) leukemic cells were injected per larval fish using a microinjector. Larval fishes were divided in two groups depending on the injection site: brain ventricle/parenchyma or yolk (Figure1a/b). Each group included 30-80 larval fishes. Microscopic observations were made with Leica DMR microscope, equipped with a digital camera DC500. Fishes were observed by fluorescent microscopy daily and ~5 fishes of each group were fixed in 4% paraformaldehyde at 2, 3, 4, 5, 6, 7 dpi for immunohistochemical analysis. All remaining fishes were fixed at 7 days post injection (dpi).

Table 1. Number of xenotransplantations of 5 human T-ALL cell lines performed per site of injection.

Human Cell lines	1° Transplant	2° Transplant	3° Transplant	4° Transplant
TALL1	30 CNS	30 CNS/30YOLK	30 CNS/30YOLK	
DND-41	30 CNS/30YOLK	30 CNS/30YOLK	30 CNS/30YOLK	
P12-ICHIKAWA	30 CNS/30YOLK	30 CNS/30YOLK	30 CNS/30YOLK	
CCRF-CEM	30 CNS/30YOLK	30 CNS/30YOLK	30 CNS/30YOLK	
Jurkat	30 CNS/30YOLK	60 CNS/60YOLK	60 CNS/60YOLK	110CNS/130YOLK

In addition, injection of labelled Jurkat cells was performed in 30 *Tg(fli1:EGFP)y1* larval zebrafish of 3dpf for each group (injection in brain ventricle or yolk). In *Tg(fli1:EGFP)y1* zebrafishes the vascular system is labelled with GFP. For confocal microscopy, fixed embryos were embedded with 0.7% low-melting agarose and placed on a Petri capsule. Stacks were recorded using ×40 immersion objective (SP5 spectral confocal system; Leica). All images were analyzed with ImageJ software (http://rsb.info.nih.gov/ij/). Using confocal microscopy injected fishes were monitored for real-time monitoring of malignant cells behaviour.

Histology, Immunoflorescent analysis (IF) and Immunohistochemistry (IHC)

Xenotransplanted larval fishes for each group (injected in CNS or yolk) were fixed at 2, 3, 4, 5, 6 and 7 dpi in 4% paraformaldehyde, paraffin-embedded and sectioned (5μm). For IF, whole-mount antibody staining for Ki67 [1:200 mouse monoclonal anti-human Ki-7 #M7240 (Dako, Denmark, EU)], HDAC1 [1:200 rabbit polyclonal anti-human nuclei #sc-7872 (Santa Cruz Biotechnology, Dallas, TX)] and DAPI [1:10000 (Sigma-Aldrich, Milano, Italy)] staining was performed. IF images were obtained on a video-confocal microscope (Vico, Ecliple Ti80, Nikon), equipped with a digital camera.

5 WIK *lck::EGFP*$^{+/+}$ (used like healthy controls), 5 *hMYC-ER* and 5 *hlk* fishes at the stage of localized disease and the heads of 10 *hMYC-ER* and 10 *hlk* fishes at the last stage of disease, were fixed in 4% paraformaldehyde, paraffin-embedded and sectioned (5μm). Hematoxylin and eosin (H&E) staining was performed using standard

procedures. For IHC, staining was performed using an anti-GFP antibody [1:400 dilution; mouse monoclonal antibody #sc- 9996 (Santa Cruz Biotechnology, Dallas, TX)] with resolution of GFP+ tissues using a DAB detection kit (Dako, Denmark, EU).

Microscopy and analysis of quantitative microscopy

Adult *hMYC-ER* and *hlk* fishes were screened for abnormal GFP patterns with an Olympus szx 12 fluorescent microscope and camera (Center Valley, PA) and Optronics Picture frame software (Goleta, CA). H&E, HIC and IF images were obtained on a video-confocal microscope (Vico, Ecliple Ti80, Nikon), equipped with a digital camera. For quantitative microscopy analyses images were analyzed with the software open source ImageJ. To obtain a comparable measure of the degree of infiltration, we analyzed IHC stained slides at the level of the optic chiasm for each specimen. Images at the same resolution (10X) were converted to 8-bit greyscale images, and then a threshold was applied. ROIs (regions of interest) were manually selected and the percentage of CNS infiltration was measured as the ratio between the area involved by lymphoblast infiltration (the only area detected in black) and the total area of the CNS (considering the total area delimited by the zebrafish skull).

Flow Cytometry

The body (except the head) of 10 *hMYC-ER* and 10 *hlk*- sacrificed fishes at the last stage of disease was placed in PBS1X. Cells were dissociated through pestle mechanic movements and passed two times trough 35μm filters (Becton Dickinson (BD), San Jose, CA) before analysis. GFP+ positive cells were isolated using a BD fluorescence-activated cell sorting (FACS) Vantage Instrument (Becton Dickinson). GFP intensity, forward-and side-scatter were used for gating. After sorting, cells were centrifuged and immediately put on Trizol (Invitrogen, Karlsruhe, Germany).

RNA extraction and Microarray whole transcriptome expression analysis

Total RNA from single fish was extracted from FACS GFP+ purified cells using Trizol according to the manufacturer's instruction (Invitrogen, Karlsruhe, Germany). RNA concentration was determined using QBit 2.0 Fluorometer (Life Technology, Carlsbad, California, U.S.). Total RNA was stored at -80°C. To perform microarray experiments,

RNA quality and purity control was assessed on the Agilent Bioanalyzed 2100 (Agilent Technologies, Waldbronn, Germany) using "Eukaryote total RNA Assay". Only RNA samples that passed quality controls (6 *hMYC-ER* and 3 *hlk* samples) were used to perform microarray (Affymetrix GeneChip Zebrafish Genome Arrays) analysis. *In vitro* transcription, hybridization and biotin labelling were performed according to GeneChip 3'IVT Express kit protocol (Affymetrix, Santa Clara, CA). Microarrays data (.CEL files) were generated using Affymetrix GeneChip Command Console Software (AGCC). All microarrays passed the quality controls: scale factor, number of present calls, internal probe calls, Poly-A controls and the ratio GAPDH/β-actin 3'/5'.

Statistical analysis

Microarray data (.CEL files) were analyzed using Command Expression Console (Affymetrix). The .CEL files were normalized using the justRMA algorithm and analyzed for supervised and unsupervised analysis, using R-Bioconductor (Version 2.15.3). Unsupervised analysis (Class Discovery) clusters together unspecified (new) specimens based on similar gene expression patterns and filtering only for probe sets that present a variance >90%. Supervised analysis (Class Comparison, Class Prediction) is a learning algorithm that uses already defined (labelled) data in order to identify a set of genes that characterize the pre-specified data. In order to find differently expressed probe sets between two groups of interest (in our case *hMYC-ER* and *hlk*), we applied a Shrinkage t-test on the normalized .CEL files [56]. We used a local false discovery rate (lfdr) as correction of the p-value. A lfdr < 0,05 was considered significant for genes differently expressed between the two groups. Differently expressed probe sets derived from the Shrinkage t-test were used for clustering analysis. Hierarchical clustering analysis was used to cluster the specimens in an unsupervised manner using Euclidean Distance and Ward's Method.

GraphPad Prism 5 software program (GraphPhad Software, La Jolla, CA, U.S.A.) was used to perform Pearson correlation analysis, between expression levels of *cxcr4a* and *cxcr4b* and degree of CNS infiltration.

Search Tool for the Retrieval of Interacting Genes/Proteins (STRING) v9.05. STRING, based on text mining, was used in order to investigate potential gene/protein networks within the list of differently expressed genes between *hMYC-ER* and *hlk* groups.

Reverse-transcription and real-time polymerase chain reaction

250 ng of RNA extracted from GFP+ cells of single fishes, was reverse transcribed using Superscript II (Invitrogen, Karlsruhe, Germany) and random primers following standard techniques. SYBR-Green Real-time quantitative PCR (qRT-PCR) was performed using the Platinum SYBR-Green qPCR SuperMix UDG (Invitrogen, Karlsruhe, Germany) and the 7900 HT Fast Real-Time PCR System (Applied Biosystems, Foster City, CA). qRT-PCR was performed in triplicates (both for housekeeping and genes of interest) for each sample and standard curve of 3 serial dilutions was used as control for each plates. qRT-PCR was executed for detecting expression level of *cxcr4a*, *cxcr4b* and *hMYC* genes, while *β-actin* was used as housekeeping gene to normalize gene expression data. Primers are listed in the table 2. The specificity of the primers was examined with the corresponding dissociation curve. To allow comparison between samples, transcript quantification was performed after normalization with *β-actin* using the Ct method and results were calculated according to the following formula $2^{-\Delta ct}$ [46]. Analysis of expression was performed using the GraphPad Prism 5 software and statistical significance was calculates as a *P* value using non-parametric Mann-Whitney test. Two tailed 95% confidence intervals were used to assess the significance of the data ($P < .05$).

RESULTS

Testing the possibility to establish a model of CNS leukemic infiltration in zebrafish

The first efforts of this project focused on the establishment of an *in vivo* model in zebrafish that could mimic the phenomenon of leukemic infiltration into the CNS in T-ALL patients. A total number of ~100-200 transplantations of 5 pediatric T-ALL cell lines (table 1) have been performed in larval fishes at 3 days post-fertilization (dpf) as previously described (Figure1). Among cell lines injected, Jurkat cells showed a clear predisposition to move away from the site of injection invading other loci. On the

contrary, CCRF-CEM, DND-41, P12-ICHIKAWA and TALL-1 cell lines did not show this ability to move from the site of injection and after 7 days post injection human labelled cells were no longer detected in 70-80% of injected larval fishes. Moreover, whole-mount analysis on larval fishes injected with T-ALL1 and DND-41 excluded the hypothesis of an increased proliferation of these cells causing the loss of the membrane dye; no human cells were detected in larval fishes analyzed (data not shown). These data suggest that these cell lines are not fit to survive in the zebrafish environment. Instead, larval fishes of both groups (injection at the CNS or yolk) transplanted with Jurkat, already after 6 hours post-injection (hpi) showed labelled cells both at the site of injection (100% larval fish transplanted) and in blood vessels circulating together with zebrafish blood cells or accumulated in the ventral caudal region (50% and 10% of larval fishes xenotransplanted in the yolk and CNS, respectively) (Figure 3A/4A). To better localize the position of Jurkat cells, xenotransplants with Jurkat cells were performed in 30 *Tg(fli1:EGFP)y1* zebrafish at 3 dpf for both groups: at the CNS site and at the yolk. In vivo confocal microscopy showed the presence of Jurkat cells in the blood vessels and capillaries from 6 hours onwards and Jurkat cells that were blocked or stayed adhered to the wall of blood vessels (Figure 5A and B). Similar results were obtained for both groups after longer times post cell injections. Interesting, at 7 days post-injection (dpi) 10% of larval fishes of both groups presented Jurkat cells at several sites away from the original site of injection, showing the ability of Jurkat cells to survive and circulate in zebrafish tissues (Figure 3B/4B). Whole body immunofluorescence analysis on larval fishes injected in the CNS or yolk and fixed at different time points after injection, where performed. Analysis on larval fishes fixed at 2 (figure 6 A and B) and 7 dpi revealed the presence of Jurkat cells positive for anti-Ki67 (marker of proliferating cells) [47] and HDAC (marker of human nuclei) staining. However, the total number of cells had not increased from 2 to 7 dpi (data not shown) so we can assume that cell death of Jurkat cells had also occurred.

Lymphoblastic CNS infiltration in hMYC-ER and hlk T-ALL zebrafish models

To understand if *hMYC-ER* and *hlk* zebrafish lines could be good models for the study of CNS infiltration by T-ALL cells, we performed detailed histological analysis of the CNS at the “localized” and “final” stages of the disease in both zebrafish T-ALL lines

(figure 2). First, we performed histological analysis of the CNS for 5 *hMYC-ER* and 5 *hlk* fishes at the stage of localized disease and we observed signs of T-ALL cell infiltration. At this early stage of the disease, the sites and extend of CNS infiltration were different from one fish to the other. In fact T-ALL cells could be present in the neural tube, the parenchyma, the pineal gland and meninges. However, all fishes presented CNS involvement to some extend. (figure 7). Histological analysis performed at the last stage of the disease for 9 *hMYC-ER* and 8 *hlk* fishes, showed a more sizeable infiltration of the CNS for both zebrafish lines, with involvement of meninges, optic nerve, retina and some infiltration of the parenchyma (figure 8). We found CNS infiltration in 8/9 *hMYC-ER* fishes, compared to 5/8 *hlk* fishes. For fishes presenting CNS involvement, we observed a distinct trend of lymphoblastic infiltration among the groups: the *hMYC-ER* fishes showed a more massive infiltration of the CNS compared to the *hlk* line, while the latter presented a thin layer of CNS infiltration but important signs of infiltration under the skin (figure 9). We proceeded with quantitative microscopy image analysis to measure the level of CNS infiltration in the two zebrafish lines (9 *hMYC-ER* fishes and 8 *hlk* fishes), and we found a significant difference in the degree of CNS infiltration between the *hMYC-ER* and the *hlk* group (Mann-Whitney T-test, *p*-value: 0,04) (figure10).

Gene expression signatures and networks activated in hMYC-ER and hlk models

To identify active networks that could explain the different ability of *hMYC-ER* and *hlk* cancers to infiltrate the CNS, we performed whole transcriptome analysis of T-ALL cells extracted from the body of *hMYC-ER* and *hlk* fishes, of which the heads were used for histological analysis. Suitable RNA was available for 6 *hMYC-ER* and 3 *hlk* fishes all with CNS infiltration. Using a class discovery approach, unsupervised hierarchical cluster analysis separated *hMYC-ER* and *hlk* groups, underlining a strong gene expression profile distinction between *hlk* and *hMYC-ER* cancers (figure 11). Class comparison analysis, using shrinkage T-test revealed 683 probe sets differently expressed between *hMYC-ER* and *hlk* lines (lfdr<0,05) (figure 12). Considering genes with >1,2-fold change of expression, a set of 317 genes with human homologous genes was identified. Among these 215 and 102 human homologous genes were up-regulated in the *hMYC-ER* and *hlk* group, respectively (table 3). Using STRING (Search Tool for

the Retrieval of Interacting Genes/Proteins) analysis, on genes up-regulated in the *hMYC-ER* and *hlk* group separately, the human homologous gene list revealed to be enriched for genes related to motility, cell adhesion and leukocyte transendothelial migration (KEGGs pahways). In particular, for the *hMYC-ER* group, we found an activation of the *cxcr4/cxcl12* axis, whereas for the *hlk* group, activation of the *wnt/β-catenin* pathway was revealed (figure 13). Specifically, a >2-fold change in *cxcr4a* and >1,3-fold change in *cxcr4b* expression was observed in *hMYC-ER* vs. *hlk* cancers. The up-regulation of two distinct gene networks related to cell motility support the hypothesis that molecular mechanisms underlying extramedullary organ infiltration in *hMYC-ER* and *hlk* zebrafish may be different.

Expression levels of cxcr4a and cxcr4b reflect degree of CNS infiltration

Here we focused at first on the *cxcr4/cxcl12* axis in the two zebrafish lines. Data of gene expression profiling on *cxcr4a/b* expression from array analysis, were validated by qRT-PCR. Moreover, we were able to increase the number of samples, by adding 3 *hMYC-ER* and 4 *hlk* samples. These samples had been included also in the quantitative microscopy image analysis. qRT-PCR results confirmed the presence of a significant different expression of *cxcr4a* and *cxcr4b* (p-value 0,0004) between *hMYC-ER* and *hlk* cancers (figure 14). Importantly, the expression levels of both *cxcr4a* and *cxcr4b* positively correlated with the degree of CNS infiltration measured by quantitative microscopy image analysis (Pearson Correlation R^2=0,039 and R^2=0,069 respectively) (figure 15).

High expression levels of hMYC are associated with increased cxcr4 transcription

T-ALL cells presenting high expression of *cxcr4a* and *cxcr4b* derived from the *hMYC-ER* zebrafish line. This transgenic model presents an induced over-expression of h*MYC*. We analyzed by qRT-PCR the expression levels of h*MYC* and confirmed that T-lymphoblasts from the *hMYC-ER* zebrafish line expressed high levels of human *C-MYC* (data not shown). Several works already showed how hMYC could physically interact with hYY1, mutually inhibiting their biological functions in a dose dependent manner [35]. As the transcription factor YY1 is the main repressor of *CXCR4* transcription [36], we speculated that the induced over-expression of hMYC in *hMYC-ER* zebrafish T-

lymphoblasts sequestered zfYy1, with consequent increased transcription of *cxcr4a* and *cxcr4b* (figure 16). To support this hypothesis, alignment of the protein sequence, revealed a high identity between hYY1 and zfYy1 (76% identity) and the domain of interaction with MYC, was shown to be completely conserved between h- and zf-YY1 [35] (figure17).

Expression of hMYC modifies zf* Yy1 *activity in the hMYC-ER model

YY1 can function both as transcriptional activator or repressor of specific target genes [35]. Unsupervised hierarchical analysis considering target genes that are activated or repressed by YY1 [37] revealed separate clustering of *hMYC-ER* and *hlk* groups (figure 18) and target genes follow the expected direction (activation or repression) in the *hlk* comparing to the *hMYC-ER* cancer. These analyses of gene expression profiling supported our hypothesis: in the *hMYC-ER* zebrafish line, the biological function of zfYy1 is inhibited by the induced over-expression of hMYC and through this meachnism zfYy1 target genes are differently expressed compared to the *hlk* group, where zfYy1 maintains its transcriptional activator or repressor function. This assumption is supported not only by YY1 target gene expression data from a single target gene (like *cxcr4a* and *cxcr4b*), but by considering all main YY1 target genes that are homologous between human and zebrafish (table 4). Interestingly, *hMYC-ER* and *hlk* groups present the same expression level of *yy1a* and *yy1b* (data not shown).

DISCUSSION

Although numerous efforts are made to improve haematological control and to reduce or avoid the use of cranial irradiation using alternative intrathecal treatment [5], CNS irradiation is still necessary for 2-20% of patients at high risk of CNS relapse [2]. The molecular mechanisms that allow ALL cells to enter and infiltrate the CNS are still largely unknown. In this study we aimed at identifying a beneficial *D.rerio* model that could mimic CNS infiltration by T-ALL cells, which may be used to deepen our insight into the biological mechanisms that regulate this phenomenon. First, we tried to establish an *in vivo* model through xenotransplants of childhood T-ALL cell lines in larval fishes at 3 dpf. Only Jurkat cells showed a clear predisposition to move from the original site of injection, circulate, invade other loci and survive in the host organism.

The ability of Jurkat cells to survive in the recipients was clear; fluorescent cells were detectable in all fishes transplanted both at 2 and 7 dpi. At these time points, labelled cells were visualized both at the site of injection (100% larval fishes xenotransplanted in yolk or CNS) and circulating in vessels or blocked/adhered in the ventral caudal vein or capillaries (50% of larval fishes xenotransplanted in yolk and 10% larval fishes xenotransplanted in the CNS). As yolk at 3 dpf is largely vascularised, the presence of circulating cells in 50% larval fishes injected in the yolk is not so surprising. Contrary, the presence of circulating cells in 10% of larval fishes injected in the brain ventricles, indicated the ability of Jurkat cells to migrate. Moreover, the presence of Jurkat cells, which was still detected at 7 dpi in the head of 100% of larval fishes injected in the ventricles, underlines the ability of Jurkat cells to survive in the zf CNS environment. However, the observation that the number of Ki67 positive cells was higher in larval fishes fixed at 2 compared to 7 dpi and that the number of HDAC positive cells did not increase from 2 to 7 dpi (data not shown), indicated that there was also considerable cell death/apoptosis of Jurkat cells. In conclusion, Jurkat cells can survive, circulate and infiltrate zf tissues, however, the number of cells does not increase and Jurkat cells are not able to really engraft the host organs. Moreover, even if it has been established that the immune system started to be functional at 28 dpf, there are also studies that showed the presence of immature T-lymphocyte moving towards the thymus at 4 dpf [39]. The latter could explain the death of injected Jurkat cells in our experiments. All together these data suggest that the model of xenografted zebrafish is not useful for studying the mechanisms that allow T-ALL cells to infiltrate the CNS. However, xenografting in zebrafish can be useful as recipient of human leukemic cells with a possible application for testing new experimental inhibitors of circulating human leukemia *in vivo* using high through-put approaches. Using such approaches bypasses the problem of the presence of T-lymphocytes at 4 dpf, as chemotherapeutic compounds act in leukemic cells but also repress the zf immune system at the same time [40].

At this point, to study the phenomenon of CNS infiltration by T-ALL cells, we decided to proceed using a different approach. We performed histological analysis of the CNS of two stable T-ALL *D.rerio* lines ([*hMYC-ER* [23] and *hlk* [30]) that developed GFP^+ T-ALL. Histological analysis performed at the stage of localized disease showed the firs

signs of lymphoblastic infiltration in the CNS (meninges, pineal gland, neural tube, parenchyma) for both groups, indicating a genetic predisposition of these leukemic cells to also invade the CNS. Histological analysis at the last stage of disease also revealed the presence of CNS involvement (meninges, pineal gland, optic nerve, retina, parenchyma). Interestingly, the type of CNS invasion found at this stage in these models was very similar to CNS infiltration found in pediatric patients at time to death in the 1970s. In fact, we found different degrees of infiltration at the meningeal level [48], always correlated to optic nerve involvement [49]. These data underline the ability of these zf models to mimic the human CNS disease. Moreover, at this stage we observed that this event was more frequent in *hMYC-ER* (88,8%) compared to the *hlk* (62,5%) line and the degree of CNS infiltration was higher in *hMYC-ER* compared to *hlk* groups (*p*-value:0,04). These data suggested a different ability for *hMYC-ER* and *hlk* T-lymphoblasts to infiltrate the CNS. This assumption was supported by whole transcriptome analysis performed on FACS-purified cells (through sorting for GFP) from the body of each fish presenting CNS infiltration. In fact, Gene Expression Profiling (GEP) analysis revealed the presence of two distinct activated motility networks and specific gene expression signatures in *hMYC-ER* and *hlk* cancers respectively. The different trend of CNS infiltration and the different gene expression profiles suggested the presence of different mechanisms that regulate and drive motility and invasiveness of *hMYC-ER* and *hlk* T-lymphoblasts. Particularly, Search Tool for the Retrieval of Interacting Genes/Proteins (STRING) analyses showed an activation of *cxcr4/cxcl12* axis and *wnt/β-cathenin* pathway in *hMYC-ER* and *hlk* cancers, respectively. The discovery of CNS involvement in *hMYC-ER* and *hlk* zebrafish cancers position both lines as useful models for CNS^+ T-ALL and different pathways may be explored for relevant molecular mechanisms that drive CNS invasion.

For the moment, we focused on *cxcr4/cxcl12*, the axis activated in the group with a higher degree of CNS infiltration. GEP analysis showed a >2-fold change (FC) and a >1,3 FC in *cxcr4a* and *cxcr4b* expression in *hMYC-ER* vs. *hlk* cancers respectively and analysis of qRT-PCR for *cxcr4a* and *cxcr4b* validated arrays data. The zebrafish model presents two copies of mammalian *CXCR4* (*cxcr4a* and *cxcr4b*) deriving from genomic duplication, which occurred during teleost evolution. The observation that during zf

embryogenesis *cxcr4a* and *cxcr4b* expression patterns are similar to those of the single mammalian *CXCR4* gene [41] suggested that zebrafish gene pairs spited mammalian gene functions between the two copies [42]. Particularly, *cxcr4a* conserved the majority of *CXCR4* functions, while *cxcr4b* seems to have acquired also other functions in early development [41]. Of note, in this study we found that both the expression of *cxcr4a* and *cxcr4b* positively correlated (R^2=0,039 and R^2=0,069 respectively) with the degree of CNS infiltration found through quantitative microscopy image analysis in *hMYC-ER* and *hlk* histological preparations. CXCR4 is a chemokine receptor, particularly important for haematopoiesis and also for trafficking T-lymphocytes [43]. The higher CXCR4 expression and activation in T-lymphocyte increased the migratory response of these cells towards its specific ligand CXCL12 gradient. One could speculate that the expression level of CXCR4 in leukemic cells could influence the migratory response of these cells towards tissues/organs that express the CXCL12, such as bone marrow, lymph nodes, spleen and brain [50]. In zebrafish, the expression of both *cxcr4a* and *cxcr4b* and *cxcl12a* and *cxcl12b* in the brain of adult fish has been documented [51]. A link between the over-expression of CXCR4 and the increased motility of leukemic cells is well documented for AML and CML [52-54]. However, the role of CXCR4/CXCL12 axis is not so clear in ALL. In fact, there are discordant hypotheses regarding the role of the CXCR4/CXCL12 axis and CNS infiltration in ALL: high levels of CXCR4 expression by childhood lymphoblasts have been associated with extra-medullary organ infiltration [44]. Alternatively, CNS-homing cells showed CXCR4 down-regulation in a mouse xenograft model of CNS pre-B leukaemia with levels of CXCR4 expression inversely proportional to the rapidity of CNS disease development [45]. Moreover, another study showed that in children with ALL relapses associated to testicles or CNS leukemia blast cells had a significantly lower CXCR4 level than blasts from children with relapsed disease isolated to the bone marrow [55]. Further analyses are necessary to clarify the role of CXCR4 expression in predicting the ability of hALL cells to infiltrate the CNS. For the moment, with this work we showed that higher levels of *cxcr4a* and *cxcr4b* seem to confer to T-lymphoblasts an increased ability to infiltrate the CNS.

Another aspect we investigated was the identification of a possible role of MYC in regulating *cxcr4a* and *cxcr4b* transcription. Several works already showed the physical interaction of hMYC with hYY1, mutually inhibiting their biological functions in a dose dependent manner [35,36]. We speculated that the induced over-expression of hMYC in *hMYC-ER* zebrafish T-lymphoblast caused the total sequestering of the zfYy1 transcription factor (the main transcriptional repressor of *CXCR4*) with consequent increased levels of *cxcr4a* and *cxcr4b* transcription. This hypothesis was supported by the unsupervised analysis considering only hYY1 target genes [37], in which *hMYC-ER* and *hlk* cancers cluster separately: we observed that YY1 target genes moved in opposite directions between the two zebrafish lines. Particularly, in the *hMYC-ER* fishes zfYy1 seems not be functional, while in the *hlk* group zfYy1 target genes move in the expected way (activated or repressed). Our data suggest a possible role for c-MYC in regulating *cxcr4a* and *cxcr4b* transcription and consequently in determining the migration of T-ALL cells towards the CNS. High levels of *C-MYC* could increase *CXCR4* transcription, conferring to these cells a predisposition to invade tissues expressing the CXCL12, such as the brain.

In conclusion, with this work we found two stable zf lines (*hMYC-ER* and *hlk*) that are good models of CNS+ T-ALL; these zf lines can have useful applications not only in the study of mechanisms used by T-lymphoblasts to infiltrate the CNS, but also for testing specific pharmacological inhibitors that can block this phenomenon. This discovery is very important, because it allows to bypass the problem of lack of human patient material available for such studies. Moreover, these two zf lines presented different active gene networks suggesting the presence of two diverse mechanisms that regulate the motility of their T-lymphoblasts and resulting in different abilities to infiltrate the CNS. These results revealed the presence of more than one molecular mechanisms that can determine CNS infiltration, giving a different predisposition to T-ALL cells to invade the CNS. Particularly, we observed that *cxcr4a* ad *cxcr4b* expression is not necessary to infiltrate the CNS, but higher expression levels of these chemokine receptors significantly increase the ability of T-ALL cells to invade the CNS. Moreover, we found in hMYC a modulator of zfYy1 transcriptional function with consequent effects on *cxcr4a* ad *cxcr4b* transcription. Further studies are necessary to

better characterize the molecular mechanisms found in these zf lines (*cxcr4/cxcl12* axis and *wnt/β-cathenin* pathway) in relation to CNS invasion also in human patients.

FIGURES

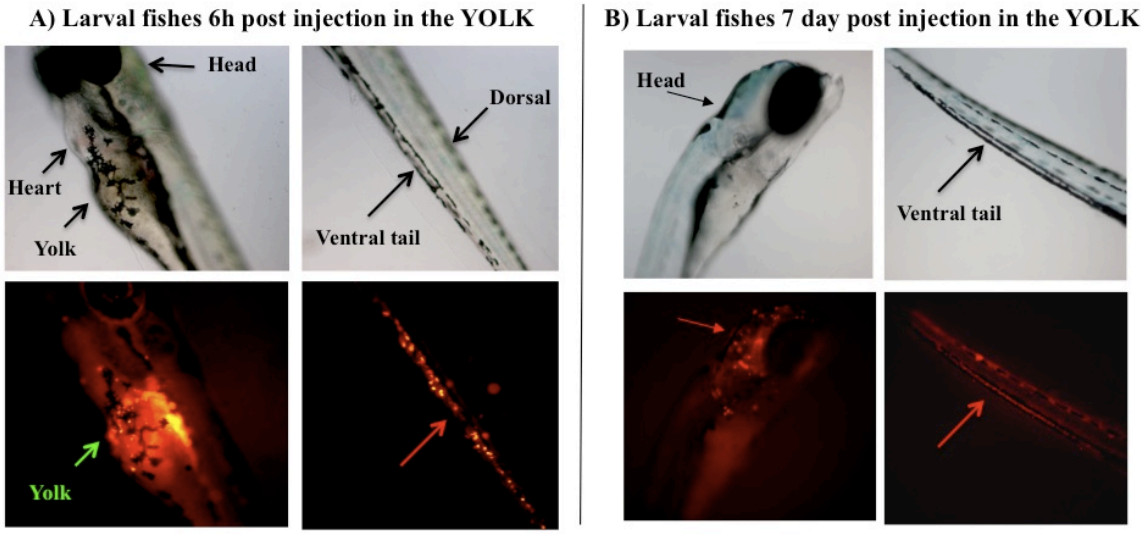

Figure 3: Fluorescent microscopy images show larval fishes injected with labelled Jurkat cells at the site of the yolk at 6 hours (panel A) and at 7 days (panel B) post-injection: (A) At 6 hour post injections in 50% of larval fishes Jurkat cells had moved away from the site of injection (green arrow) and were detected in the ventral caudal region (red arrow). (B) At 7 days post injection, Jurkat cells had continued to move and were detected in the ventral caudal vein and in the 10% of larval fishes also in the head (red arrows).

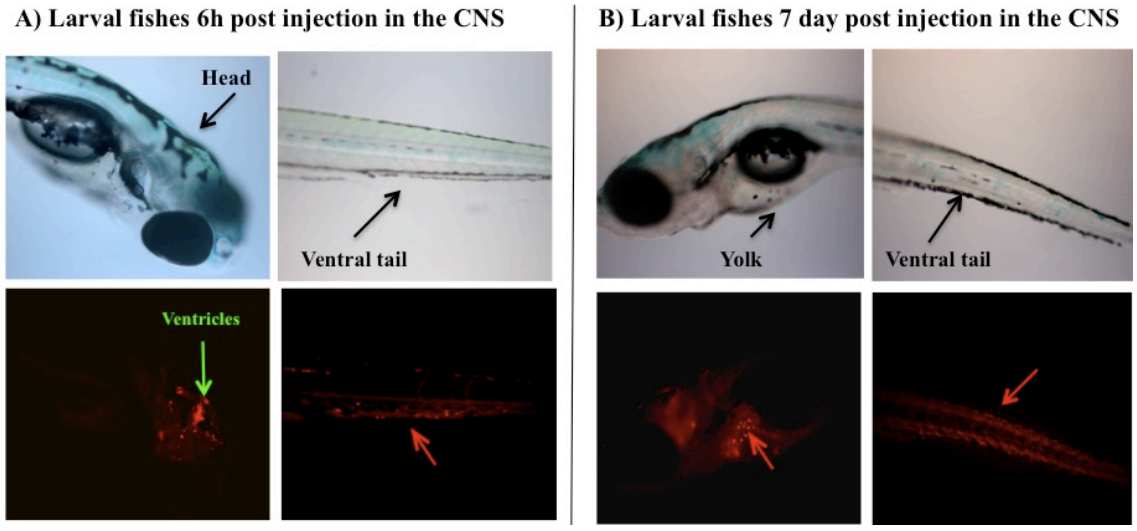

Figure 4: Fluorescent microscopy images show larval fish injected with labelled Jurkat cells in the ventricles/parenchyma at 6 hours (panel A) and at 7 days (panel B) post-injection: (A) At 6 hours post injections, Jurkat cells had moved away from the site of injection (green arrow) and were detected in the ventral caudal region (red arrow) in the 10% of larval fishes injected. (B) At 7 days post injection in 10% of larval fishes Jurkat cells were detected at various sites away from the site of injection, like the ventral caudal region and near the yolk (red arrows).

***In vivo* confocal images show Jurkat cells in zf blood vessel**

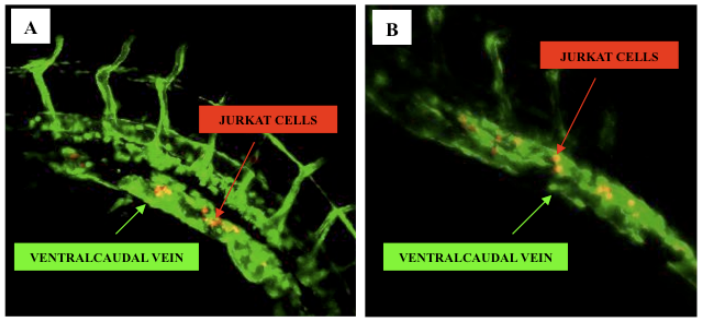

Figure 5A/B: *In vivo* confocal images show Jurkat cells (labelled in red) in blood vessels (labelled in green) of zebrafish *Tg(flil:EGFP)* larval fishes at 6 hours post injection. Figures show the majority of Jurkat cells adherent to the wall of vessels (at this position only few Jurkat cells move/circulate) at the level of the ventral caudal vein.

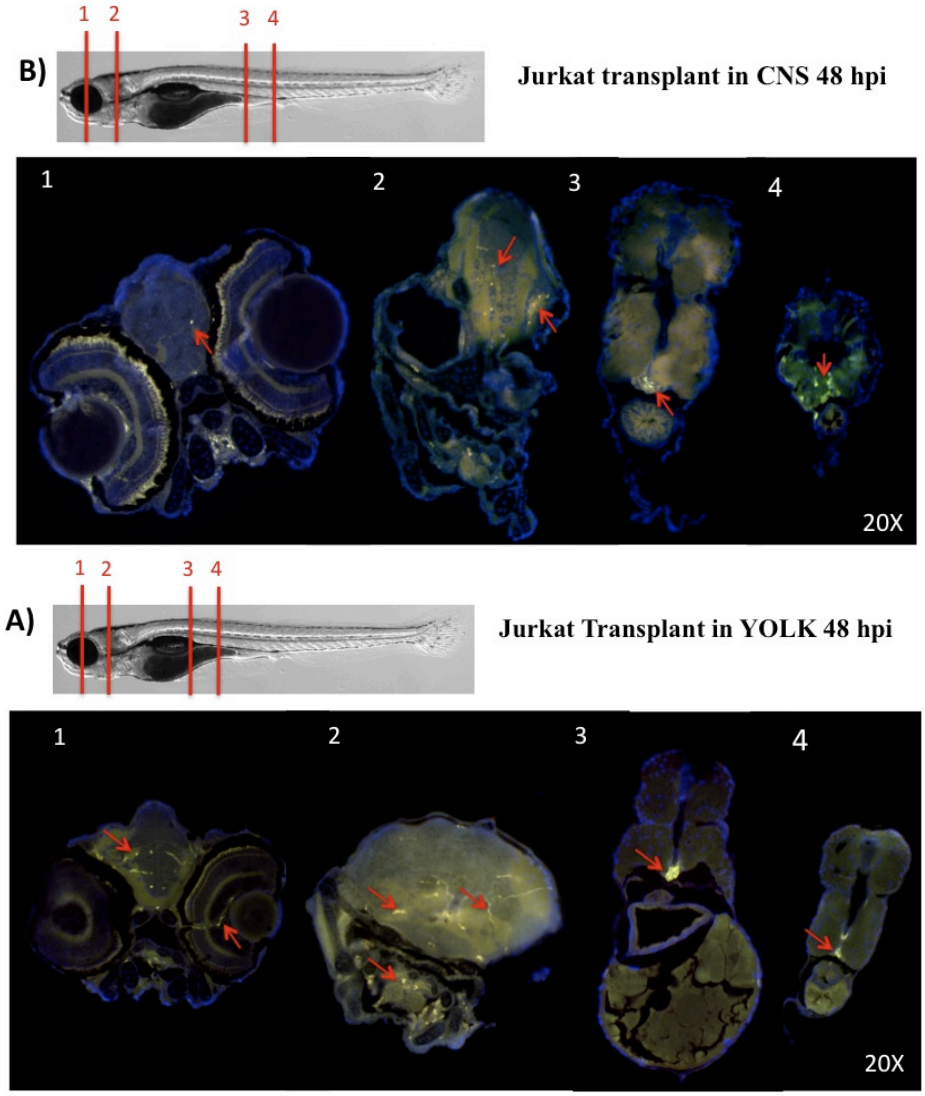

Figure 6: Whole body immunofluorescent analysis of larval fishes transplanted with Jurkat cell line after 2 dpi. Panel A: exemplar fluorescent microscopy images show the presence of Jurkat cells (some underlined with red arrow) at different section levels in larval fishes injected in the YOLK (1, 2, 3, 4). These images show the presence of many circulating labelled cells that pass also through the brain blood vessels (1, 2). Panel B: exemplar fluorescent microscopy images reveal the presence of Jurkat cells (red arrow) at different section levels in larval fishes injected in the CNS (1, 2, 3, 4). There are few cells seen in blood vessels, but Jurkat cells are detectable in the CNS (1, 2) and also in the tail (4).

IHC analyses reveal the presence of CNS infiltration at different stages of the disease in zf T-ALL models

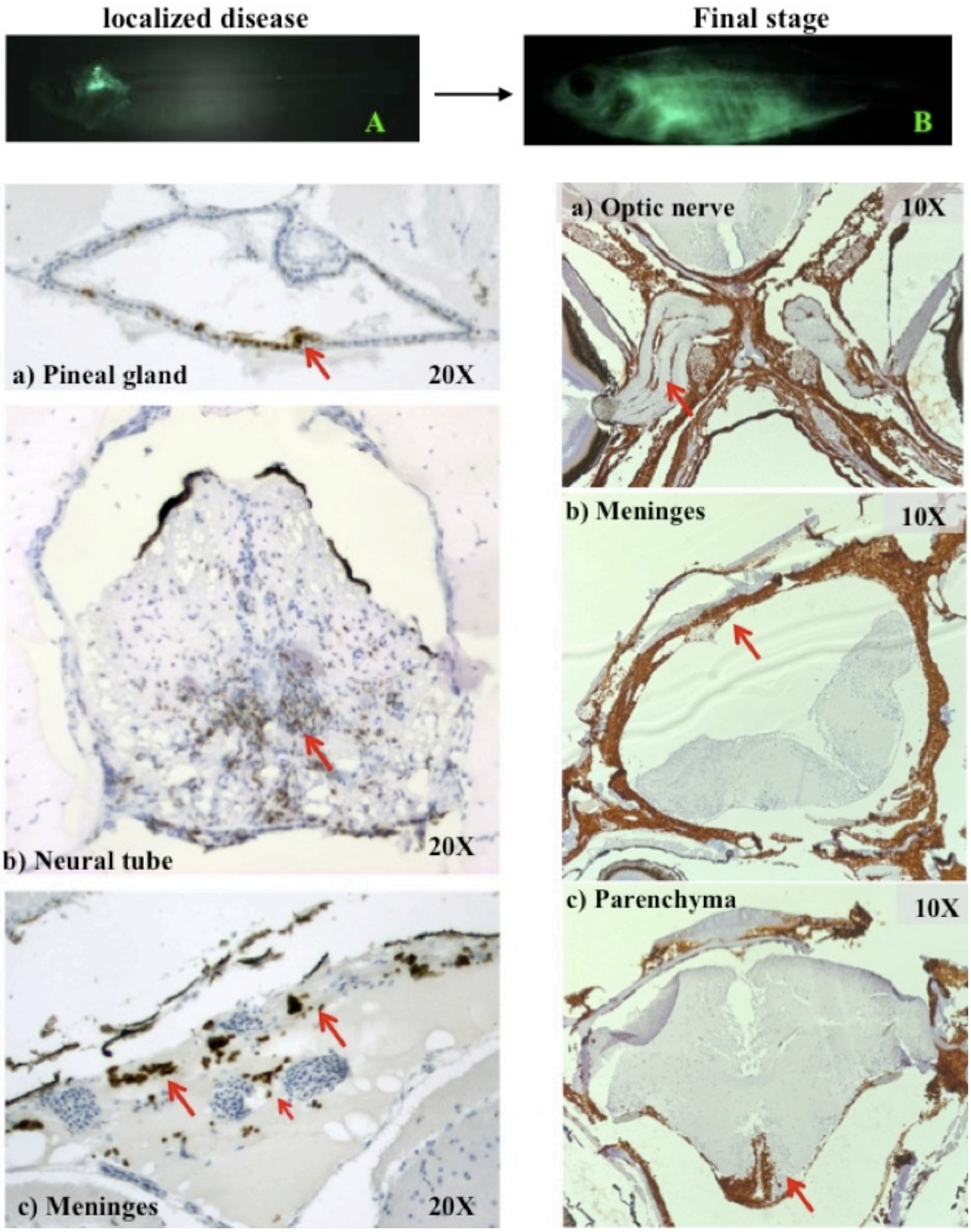

Figure 7 (left pannel): Transversal sections of CNS of fish at the stage of localized disease. Exemplar pictures of T-lymphoblast (DAB stained with PO-anti-GFP) infiltration (red arrows) in the CNS at several sites: pineal gland (a), neural tube (b), meninges (c).

Figure 8 (right pannel): Images of histological preparations (transversal section) of CNS of fishes at the last stage of disease. Exemplar pictures of T-lymphoblast (DAB stained with PO-anti-GFP) infiltration (red arrows) involving the optic nerve (a) the meninges (b) and the parenchyma (c) near the ventricles.

Different degree of CNS infiltration between *hMYC-ER* and *hlk* zebrafish models

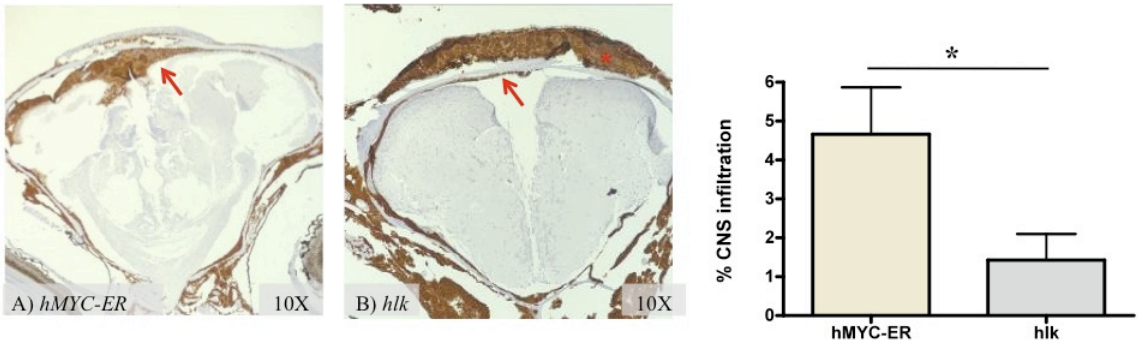

Figure 9 (left pannel) : Comparison of CNS infiltration between *hMYC-ER* (A) and *hlk* (B) zebrafish models at the same section level (optic nerve). Pictures underline the different T-lymphoblast (DAB stained with PO- anti-GFP) infiltration at the meningeal level (red arrows): *hMYC-ER* showed important meningeal infiltration (A) compared to the thin layer infiltrated in the *hlk* group (B). On the other hand *hlk* T-lymphoblasts had consistently infiltrated the skin (*).

Figure 10 (right graphic): Significant different degree of CNS infiltration between *hMYC-ER* and *hlk* zebrafish models at the last stage of disease. CNS infiltration was analyzed by quantitative microscopy image analysis of microscopic sections at the level of the optic nerve (Mann-Whitney T-test, *p*-value: 0,04). Y-axis shows the % of CNS infiltration measured by quantitative microscopy analyses.

Whole-transcriptome analysis reveals a different signature between *hMYC-ER* and *hlk* cancers

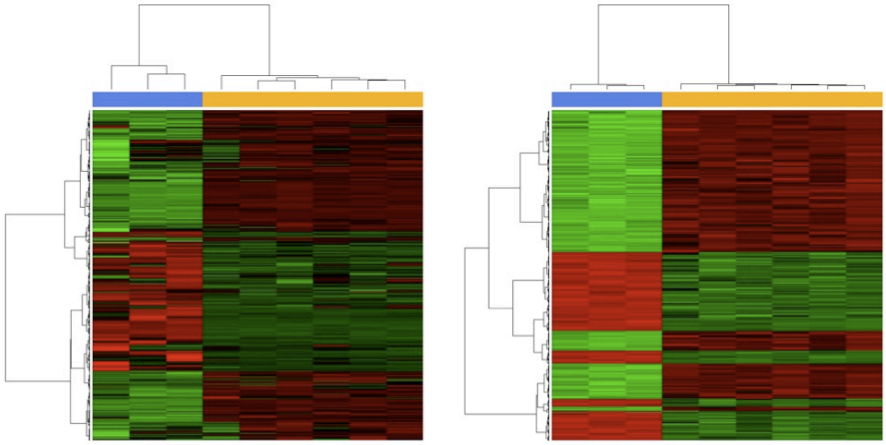

Figure 11 (left): The heatmap shows the results of unsupervised hierarchical clustering analysis, filtering for probe sets that present a variance >90%. Unsupervised analysis clustered the 6 *hMC-ER* (orange) and 3 *hlk* (blue) samples in two arms, revealing distinct gene expression signatures that separated the two zf lines.

Figure 12 (right): Supervised analysis, using Shrinkage T-test, identified 683 probe sets differently express between *hMYC-ER* (orange) and 3 *hlk* (blue) groups. The heatmap was created using only probe sets with a significant different expression from the comparison between groups (lfdr<.05)..

Different networks related to cell motility are active in *hMYC-ER* and *hlk* zf models

hMYC-ER

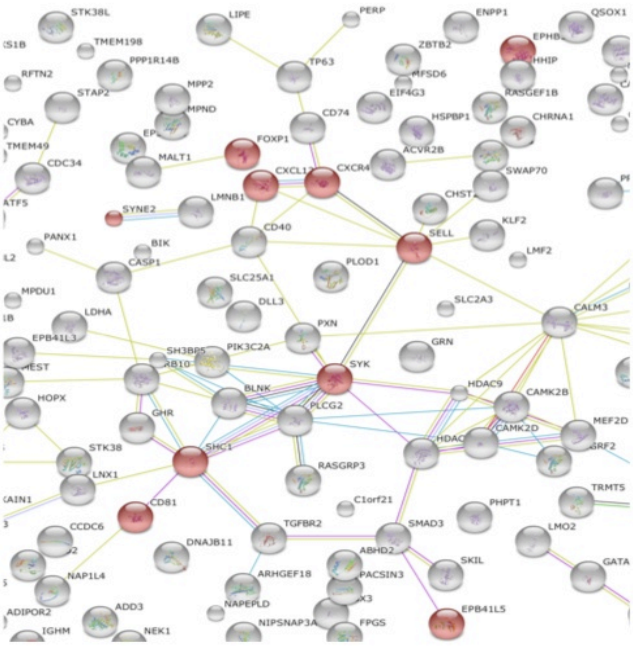

hlk

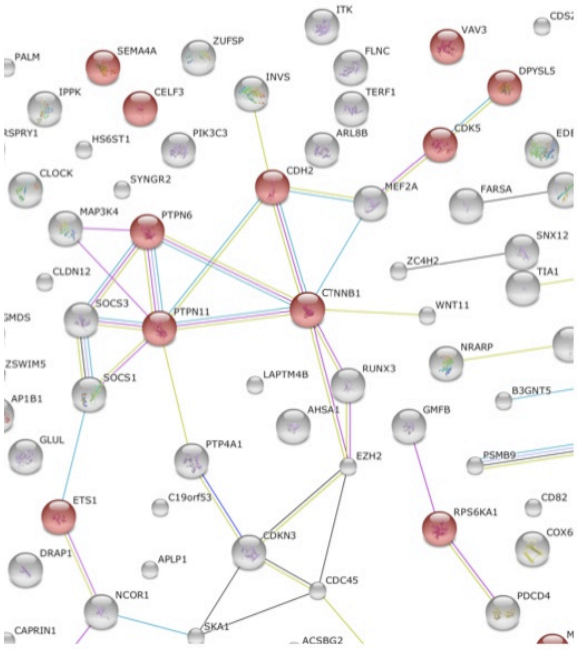

Figure 13: Using STRING (Search Tool for the Retrieval of Interacting Proteins) two distinct protein-protein interaction networks both related to cell motility were retrieved for *hMYC-ER* (first figure) and *hlk* (second figure) cancers respectively. Differentially expressed cell motility related genes were identified for the two fish lines by GEP analysis and homologous human counter parts were analyzed for protein-protein interactions.

hMYC-ER expresses higher levels of both _cxcr4_ and _cxcr4b_ compared to the _hlk_ group

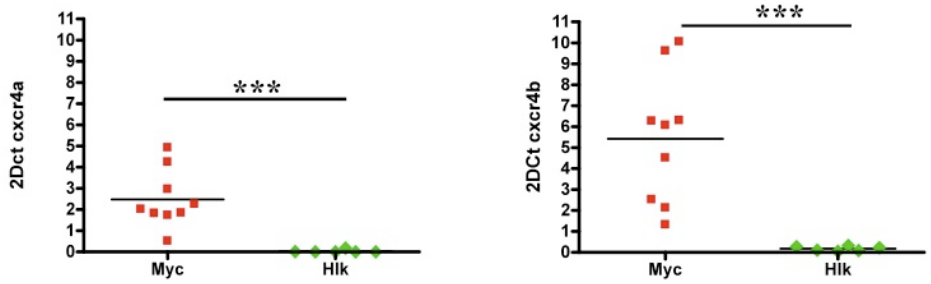

Figure 14: Validation of gene expression data of *cxcr4a* and *cxcr4b* expression by qRT-PCR. *hMYC-ER* (red) lymphoblasts expressed higher levels of both *cxcr4a* (left graphic) and *cxcr4b* (right graphic) compared to the *hlk* samples (green) (Mann Whitney T-test, *p*-value: 0,0004).

Expression levels of _cxcr4_ and _cxcr4b_ correlate with the degree of CNS infiltration in _hMYC-ER_ and _hlk_ models

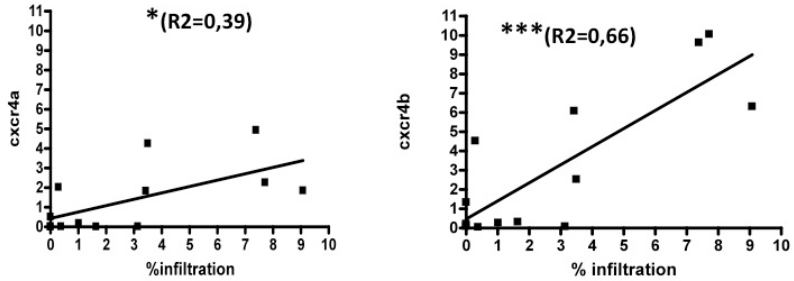

Figure 15: Positive correlation between the expression levels of *cxcr4a* (left) and *cxcr4b* (right) measured by qRT-PCR and the percentage of CNS infiltration (measured by quantitative microscopy image analysis) (Spearman Correlation).

Hypothesis of mechanism that regulate _cxcr4_ transcription in _hMYC-ER_ group

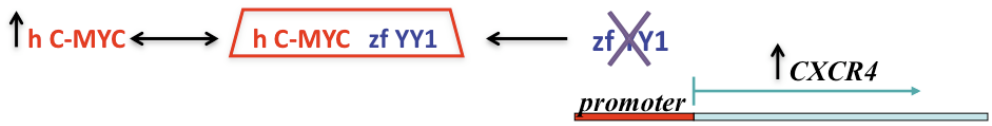

Figure 16: Hypothesis of the mechanism of regulation of *cxcr4a* and *cxcr4b* transcription in *hMYC-ER* fishes. The induced over-expression of hMYC sequestered all zfYY1, inhibiting its biological function as a transcriptional repressor of *cxcr4*. The absence of free zfYy1 allowed an increase in *cxcr4* transcription.

High identity between human and zebrafish YY1

Figure 17: Protein alignement of Human-Zebrafish-Mouse YY1 sequence revealed a high identity between human and zebrafish YY1 (76% identity). Moreover, the domain necessary for the interaction of YY1 with MYC is completely conserved (red cube) between the two species [35].

Hierarchical clustering based on main YY1 target genes separate *hMYC-ER* and *hlk* models

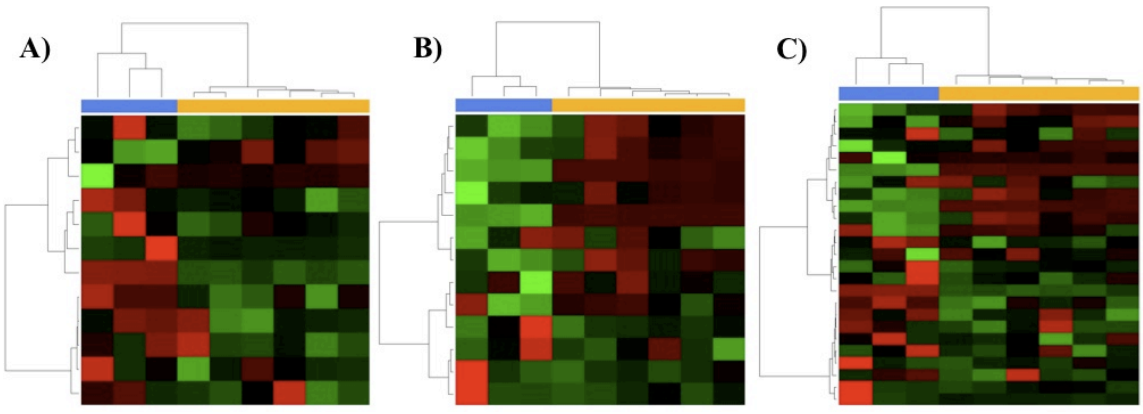

Figure 18: Unsupervised hierarchical analysis considering all main YY1 target genes (C) or separately target genes that are upregulated (A) or downregulated (B) by YY1, divide *hMYC-ER* (orange) and *hlk* (blue) cancers. Of note, in *hMYC-ER* group the function of Yy1 seems to be impaired and target genes behave in the opposite way compared to the the *hlk* group.

TABLES

Table 2. Primers used for qRT-PCR

GENES	PRIMERS
cxcr4a	Forward: 5'-TCATCATCTCCAAGCTGTCG-3'
	Reverse: 5'-CTCCGTCACGAAGATCCATT-3'
cxcr4b	Forward: 5'-CTTATTGCGCCTTTTTGAGC-3'
	Reverse: 5'-ATCCCGTATACTGTAGGGAGGAA-3'
hMYC	Forward: 5'-CCCTCAACGTTAGCTTCACC-3'
	Reverse: 5'-CCTCCTCGTCGCAGTAGAAA-3'
β-actin	Forward-5'-AAATCGCTGCCCTGGTCGTT-3'

Table 4. Probe sets of the main YY1 target genes homologous between human and zebrafish

zf gene	Probe sets target genes up-regulated by YY1
creb1a	Dr.19426.1.S1_at
myca	Dr.1.1.S1_at
mycb	Dr.16048.1.S1_at
col1a1a	Dr.20097.1.S1_s_at
hspa5	Dr.26116.1.S1_at
Msxa	Dr.5754.1.S1_at
Msxd	Dr.5789.1.S1_at
p53	Dr.2052.1.S1_at
parp1	Dr.17254.1.A1_at
erbb2	Dr.20789.1.A1_at
	Dr.22611.1.A1_at
ccl13	Dr.15125.1.A1_at
zf gene	**Probe sets target genes down-regulated by YY1**
acta1a	Dr.4837.1.A1_at
cat	Dr.1079.1.S1_at
sp1	Dr.9235.1.A1_at
cxcr4a	Dr.15055.1.S1_at
cxcr4b	Dr.6798.1.S1_at
cxma	Dr.18267.1.S1_at
cxmb	Dr.24950.1.S1_at
serpine1	Dr.383.1.A1_at
id1	Dr.541.1.S1_at
CXCR4	Dr.12986.3.S1_a_at
	Dr.12986.1.A1_a_at
	Dr.12986.2.S1_at

Table 3. Genes differently expressed between the *hMYC-ER* and the *hlk* group with a FC>1.2 that have a human homologous gene

Zf Probe Set	Group UP	zf gene	FC	human gene
Dr.23942.1.S1_at	*hlk*	b3gnt5a	2,96	*B3GNT5*
Dr.8297.1.S1_at	*hlk*	wnt11r	2,81	*WNT11*
Dr.2836.1.A1_at	*hlk*	zgc:63523	2,77	*PALM*
Dr.596.1.S1_at	*hlk*	itk	2,48	*ITK*
Dr.613.1.S2_at	*hlk*	stom	2,47	*STOM*
Dr.637.1.S2_at	*hlk*	cdh2	2,35	*CDH2*
Dr.9345.1.A1_at	*hlk*	sb:cb474	2,23	*ARPP21*
Dr.3413.1.S1_at	*hlk*	dachc	2,14	*DACH1*
Dr.3713.1.A1_at	*hlk*	flncb	2,11	*FLNC*
Dr.23460.1.S1_at	*hlk*	spred1	2,02	*SPRED1*
Dr.12882.1.A1_at	*hlk*	hs6st1a	2,00	*HS6ST1*
Dr.8281.1.S1_at	*hlk*	odz3	1,98	*ODZ3*
Dr.4763.1.S1_at	*hlk*	sox11a	1,93	*SOX11*
Dr.10688.1.S1_at	*hlk*	cdk5	1,91	*CDK5*
Dr.8094.1.S1_at	*hlk*	sema4e	1,89	*SEMA4*
Dr.4763.1.S2_at	*hlk*	sox11a	1,85	*SOX11*
Dr.17853.1.A1_at	*hlk*	fam49a	1,85	*FAM49A*
Dr.12590.1.S1_at	*hlk*	jag1a	1,83	*JAG1*
Dr.25676.1.A1_at	*hlk*	zgc:73142	1,79	*HMP19*
Dr.22955.1.A1_at	*hlk*	rilpl1	1,77	*RILPL1*
Dr.21814.1.S1_at	*hlk*	zgc:136864	1,76	*C19orf53*
Dr.13952.1.A1_at	*hlk*	ptpn11b	1,76	*PTPN11*
Dr.4876.1.A1_at	*hlk*	myo9b	1,75	*MYO9B*
Dr.1.1.S1_at	*hlk*	myca	1,73	*MYC*
Dr.11290.1.A1_at	*hlk*	midn	1,72	*MIDN*
Dr.9200.1.A1_at	*hlk*	laptm4b	1,70	*LAPTM4B*
Dr.4980.1.S1_at	*hlk*	glulb	1,68	*GLUL*
Dr.266.1.S1_at	*hlk*	mef2a	1,65	*MEF2A*
Dr.12366.2.A1_at	*hlk*	ets1a	1,60	*ETS1*
Dr.10668.1.S1_a_at	*hlk*	runx3	1,59	*RUNX3*
Dr.11398.1.A1_at	*hlk*	fam172a	1,59	*FAM172A*
Dr.6944.1.A1_at	*hlk*	pppde1	1,59	*DESI2*
Dr.24743.1.A1_at	*hlk*	syngr2b	1,55	SYNGR2
Dr.7099.2.A1_at	*hlk*	rnasekb	1,54	*RNASEK*
Dr.6531.1.A1_at	*hlk*	socs1	1,54	*SOCS1*
Dr.16940.2.A1_at	*hlk*	rab11bb	1,54	*RAB11B*
Dr.9266.1.A1_at	*hlk*	zgc:92321	1,52	*SKA1*
Dr.10638.1.A1_at	*hlk*	ssbp4	1,52	*SSBP4*
Dr.18474.1.A1_at	*hlk*	dclre1c	1,51	*DCLRE1C*
Dr.8004.1.A1_at	*hlk*	farsa	1,50	*FARSA*
Dr.22195.1.A1_at	*hlk*	si:dkeyp-8h3.5	1,49	*ZNF654*
Dr.4716.1.A1_at	*hlk*	nrarpa	1,49	*NRARP*

Dr.11133.1.A1_at	*hlk*	dpysl5b	1,47	*DPYSL5*
Dr.8323.1.S1_at	*hlk*	celf3	1,46	*CELF3*
Dr.4592.1.A1_at	*hlk*	galnt1	1,44	*GALNT1*
Dr.18194.1.A1_at	*hlk*	pik3c3	1,44	*PIK3C3*
Dr.24317.1.S1_at	*hlk*	cdkn3	1,42	*CDKN3*
Dr.11064.1.A1_at	*hlk*	aplp	1,42	*APLP1*
Dr.7859.1.A1_at	*hlk*	syne1	1,42	*SYNE1*
Dr.7862.1.A1_at	*hlk*	acsbg2	1,41	*ACSBG2*
Dr.7086.1.A1_at	*hlk*	mapk8ip3	1,40	*MAPK8IP3*
Dr.10952.1.A1_at	*hlk*	cdr2l	1,40	*CDR2L*
Dr.1542.1.A1_at	*hlk*	zgc:77734	1,39	*DBI*
Dr.7322.1.A1_at	*hlk*	spsb1	1,38	*SPSB1*
Dr.14306.1.S1_a_at	*hlk*	pdcd4b	1,37	*PDCD4*
Dr.6437.1.S1_at	*hlk*	ptpn6	1,35	*PTPN6*
Dr.10031.1.A1_at	*hlk*	wu:fk86g11	1,34	*VAV3*
Dr.18898.1.S1_at	*hlk*	ezh2	1,34	*EZH2*
Dr.13269.1.A1_at	*hlk*	rspry1	1,33	*RSPRY1*
Dr.5299.1.S1_at	*hlk*	snx12	1,33	*SNX12*
Dr.7974.1.S1_at	*hlk*	cdc45	1,32	*CDC45*
Dr.25346.1.A1_at	*hlk*	ppapdc1b	1,32	*PPAPDC1B*
Dr.956.1.S1_at	*hlk*	zgc:92631	1,32	*COX6B1*
Dr.12148.1.S1_at	*hlk*	invs	1,32	*INVS*
Dr.25287.1.A1_at	*hlk*	tia1	1,32	*TIA1*
Dr.719.1.S1_at	*hlk*	drap1	1,32	*DRAP1*
Dr.8212.1.S1_at	*hlk*	psmb9a	1,32	*PSMB9*
Dr.25530.1.A1_s_at	*hlk*	terf1	1,32	*TERF1*
Dr.3866.1.A1_at	*hlk*	caprin1a	1,30	*CAPRIN1*
Dr.13912.1.S1_at	*hlk*	ncor1	1,30	*NCOR1*
Dr.21065.1.S1_at	*hlk*	vps36	1,29	*VPS36*
Dr.16319.1.A1_at	*hlk*	clock	1,28	*CLOCK*
Dr.280.1.S1_at	*hlk*	ctnnb2	1,27	*CTNNB1*
Dr.10563.1.S1_at	*hlk*	msi2a	1,27	*MSI2*
Dr.20073.1.A1_at	*hlk*	ptbp1b	1,26	*PTBP1*
Dr.3142.1.S1_at	*hlk*	zswim5	1,26	*ZSWIM5*
Dr.25916.1.A1_at	*hlk*	dok2	1,26	*DOK2*
Dr.16111.1.S1_at	*hlk*	tshz1	1,25	*TSHZ1*
Dr.4987.1.A1_at	*hlk*	ahsa1	1,25	*AHSA1*
Dr.10301.1.A1_at	*hlk*	cd82b	1,25	*CD82*
Dr.3412.1.A1_at	*hlk*	ap1b1	1,25	*AP1B1*
Dr.11486.1.S1_at	*hlk*	edem1	1,25	*EDEM1*
Dr.20230.1.S1_at	*hlk*	gmfb	1,25	*GMFB*
Dr.19049.1.A1_at	*hlk*	dkk3	1,24	*DKK3*
Dr.26533.1.A1_at	*hlk*	zgc:112095	1,24	*SDE2*
Dr.4760.1.A1_at	*hlk*	psmb10	1,24	*PSMB10*
Dr.21796.1.A1_at	*hlk*	rps6ka1	1,24	*RPS6KA1*

Dr.9617.1.A1_at	*hlk*	socs3b	1,24	*SOCS3*
Dr.7628.1.A1_a_at	*hlk*	zufsp	1,23	*ZUFSP*
Dr.835.1.A1_at	*hlk*	pdxka	1,23	*PDXK*
Dr.3771.1.S2_at	*hlk*	cldn12	1,22	*CLDN12*
Dr.4179.1.S1_at	*hlk*	ptp4a1	1,22	*PTP4A1*
Dr.2695.1.A1_at	*hlk*	gmds	1,22	*GMDS*
Dr.10804.1.S1_at	*hlk*	zc4h2	1,22	*ZC4H2*
Dr.7615.1.A1_at	*hlk*	arl8ba	1,22	*ARL8B*
Dr.2200.1.A1_at	*hlk*	map3k4	1,21	*MAP3K4*
Dr.14727.1.A1_at	*hlk*	pi4k2b	1,21	*PI4K2B*
Dr.13218.1.A1_at	*hlk*	ino80db	1,21	*INO80D*
Dr.12295.2.A1_at	*hlk*	bop1	1,20	*BOP1*
Dr.2504.1.A1_at	*hlk*	ippk	1,20	*IPPK*
Dr.10676.1.S1_at	*hlk*	cds2	1,20	*CDS2*
Dr.2405.1.A1_at	*hlk*	rabl3	1,20	*RABL3*
DrAffx.1.53.S1_at	*hMYC-ER*	zgc:65749	1,21	*LYAR*
Dr.7638.1.S2_at	*hMYC-ER*	calm3a	1,21	*CALM3*
Dr.25350.1.A1_at	*hMYC-ER*	adoa	1,21	*ADO*
Dr.18811.2.A1_at	*hMYC-ER*	zgc:92799	1,21	*FAM204A*
Dr.15362.1.S1_at	*hMYC-ER*	zgc:110256	1,21	*TMEM256*
Dr.22607.1.S1_at	*hMYC-ER*	lactb	1,22	*LACTB*
Dr.10519.1.A1_at	*hMYC-ER*	trim71	1,22	*TRIM71*
Dr.13263.1.A1_at	*hMYC-ER*	elac1	1,22	*ELAC1*
Dr.9123.1.A1_at	*hMYC-ER*	foxk1	1,22	*FOXK1*
Dr.2475.1.A1_at	*hMYC-ER*	si:dkey-24l11.7	1,22	*PIK3C2A*
Dr.23775.1.A1_at	*hMYC-ER*	nap1l4a	1,22	*NAP1L4*
Dr.3539.1.A1_at	*hMYC-ER*	zgc:85789	1,22	*C11orf54*
Dr.982.1.S1_at	*hMYC-ER*	vmp1	1,22	*VMP1*
Dr.17125.1.A1_at	*hMYC-ER*	zgc:158603	1,22	*CREB3L2*
Dr.13752.1.S1_at	*hMYC-ER*	smfn	1,23	*REX2*
Dr.7688.1.A1_at	*hMYC-ER*	plod1a	1,23	*PLOD1*
Dr.15402.1.A1_a_at	*hMYC-ER*	mrps5	1,23	*MRPS5*
Dr.24923.1.S1_at	*hMYC-ER*	perp	1,24	*PERP*
Dr.13084.1.A1_at	*hMYC-ER*	hdac4	1,24	*HDAC4*
Dr.12720.1.S1_at	*hMYC-ER*	zdhhc8b	1,24	*ZDHHC8*
Dr.8060.1.S1_at	*hMYC-ER*	mest	1,24	*MEST*
Dr.10742.1.S1_at	*hMYC-ER*	zgc:55259	1,24	*HSPBP1*
Dr.25912.1.A1_at	*hMYC-ER*	ghra	1,24	*GHR*
Dr.10216.1.S1_a_at	*hMYC-ER*	zgc:112015	1,24	*CIB1*
Dr.10050.1.A1_at	*hMYC-ER*	adipor2	1,25	*ADIPOR2*
Dr.19378.1.S1_at	*hMYC-ER*	smad3a	1,25	*SMAD3*
Dr.14479.1.S1_at	*hMYC-ER*	zw10	1,25	*ZW10*
Dr.5906.1.A1_at	*hMYC-ER*	trmt5	1,25	*TRMT5*
Dr.26096.1.S1_x_at	*hMYC-ER*	hacl1	1,25	*HACL1*
Dr.18836.2.A1_at	*hMYC-ER*	foxp1a	1,26	*FOXP1*

Dr.18422.1.A1_a_at	*hMYC-ER*	fcho2	1,26	*FCHO2*
Dr.7738.1.A1_at	*hMYC-ER*	aldh18a1	1,26	*ALDH18A1*
Dr.7439.1.A1_at	*hMYC-ER*	mef2d	1,26	*MEF2D*
Dr.11512.1.A1_at	*hMYC-ER*	plcg2	1,26	*PLCG2*
Dr.17005.1.A1_at	*hMYC-ER*	rasgrf2	1,26	*RASGRF2*
Dr.3011.1.A1_at	*hMYC-ER*	ldlrad3	1,27	*LDLRAD3*
Dr.18403.1.S1_at	*hMYC-ER*	zgc:55572	1,27	*STK38*
Dr.17242.1.A1_at	*hMYC-ER*	zfp36l2	1,27	*ZFP36L2*
Dr.12509.1.S1_at	*hMYC-ER*	si:dkeyp-84a8.8	1,27	*FAM207A*
Dr.23652.1.A1_at	*hMYC-ER*	mpdu1b	1,28	*MPDU1*
Dr.4212.1.S1_at	*hMYC-ER*	ldha	1,28	*LDHA*
Dr.25770.1.S1_at	*hMYC-ER*	ctps	1,28	*CTPS1*
Dr.7073.1.A1_at	*hMYC-ER*	cbx3b	1,28	*CBX3*
Dr.3774.1.A1_at	*hMYC-ER*	nek1	1,29	*NEK1*
Dr.15262.1.S1_at	*hMYC-ER*	stk38l	1,29	*STK38L*
Dr.3629.1.A1_at	*hMYC-ER*	atp2a2b	1,29	*ATP2A2*
Dr.26460.1.S1_at	*hMYC-ER*	ttll1	1,30	*TTLL1*
Dr.23041.1.A1_at	*hMYC-ER*	camk2b1	1,30	*CAMK2B*
Dr.13069.1.A1_at	*hMYC-ER*	zc3h7b	1,30	*ZC3H7B*
Dr.15966.1.S1_at	*hMYC-ER*	dennd2d	1,30	*DENND2D*
Dr.10524.1.S1_at	*hMYC-ER*	rbfox2	1,30	*RBFOX2*
Dr.12113.1.A1_at	*hMYC-ER*	si:dkey-246i14.4	1,31	*SHC1*
Dr.14893.1.A1_at	*hMYC-ER*	exog	1,31	*EXOG*
Dr.12546.1.S1_at	*hMYC-ER*	upf3a	1,31	*UPF3A*
Dr.20346.1.S1_at	*hMYC-ER*	stk35l	1,31	*stk35l*
Dr.7780.1.S1_at	*hMYC-ER*	cd74	1,31	*CD74*
Dr.745.1.A1_at	*hMYC-ER*	zgc:56116	1,31	*PDLIM5*
Dr.24989.1.S1_at	*hMYC-ER*	myl10	1,31	*MYL10*
Dr.15781.1.S1_at	*hMYC-ER*	vrk2	1,33	*VRK2*
Dr.13994.2.A1_x_at	*hMYC-ER*	phpt1	1,33	*PHPT1*
Dr.14169.1.A1_at	*hMYC-ER*	slc25a32a	1,33	*SLC25A32*
Dr.4535.1.S1_at	*hMYC-ER*	ptp4a3	1,35	*PTP4A3*
Dr.5565.1.S1_at	*hMYC-ER*	selm	1,35	*SELM*
Dr.10216.2.S1_at	*hMYC-ER*	zgc:112015	1,35	*CIB1*
Dr.6798.1.S1_at	*hMYC-ER*	cxcr4b	1,35	*CXCR4*
Dr.5809.1.A1_at	*hMYC-ER*	grna	1,36	*GRN*
Dr.2550.1.S1_s_at	*hMYC-ER*	ctbp2	1,36	*CTBP2*
Dr.14639.1.S1_at	*hMYC-ER*	pcbd1	1,36	*PCBD1*
Dr.7471.1.A1_at	*hMYC-ER*	tmem198b	1,36	*TMEM198*
Dr.9667.1.S1_at	*hMYC-ER*	dnajb11	1,36	*DNAJB11*
Dr.17394.1.A1_at	*hMYC-ER*	lmf2b	1,38	*LMF2*
Dr.25730.1.S1_at	*hMYC-ER*	tes	1,38	*TES*
Dr.19486.1.A1_at	*hMYC-ER*	zgc:103750	1,38	*BFSP2*
Dr.17258.1.A1_at	*hMYC-ER*	abce1	1,39	*ABCE1*
Dr.13990.1.A1_at	*hMYC-ER*	slc25a1	1,39	*SLC25A1*

Dr.2705.1.A1_at	*hMYC-ER*	si:dkey-8l13.4	1,40	*SWAP70*
Dr.9086.1.A1_at	*hMYC-ER*	arhgef18a	1,40	*ARHGEF18*
Dr.9220.1.S1_at	*hMYC-ER*	mak16	1,41	*MAK16*
Dr.537.1.S1_a_at	*hMYC-ER*	ephb3a	1,41	*EPHB3*
Dr.18416.1.A1_at	*hMYC-ER*	selenbp1	1,41	*SELENBP1*
Dr.12480.1.S1_at	*hMYC-ER*	im:6902407	1,41	*SIVA1*
Dr.1233.1.A1_at	*hMYC-ER*	glsb	1,42	*GLS*
Dr.7691.1.A1_at	*hMYC-ER*	zgc:101761	1,43	*GNA11*
Dr.19227.1.S1_at	*hMYC-ER*	tp63	1,43	*TP63*
Dr.1180.1.S1_at	*hMYC-ER*	nccrp1	1,43	*NCCRP1*
Dr.18198.1.A1_at	*hMYC-ER*	si:dkeyp-	1,43	*EPS15L1*
Dr.3266.1.A1_at	*hMYC-ER*	napepld	1,43	*NAPEPLD*
Dr.938.2.S1_a_at	*hMYC-ER*	cyp3c1	1,44	*CYP3A4*
Dr.14120.1.A1_at	*hMYC-ER*	nkain1	1,44	*NKAIN1*
Dr.19236.1.S1_at	*hMYC-ER*	lmo4b	1,44	*LMO4*
Dr.23294.1.S1_at	*hMYC-ER*	lxn	1,44	*LNX*
Dr.19584.1.S1_at	*hMYC-ER*	ccdc125	1,44	*CCDC125*
Dr.26000.1.A1_at	*hMYC-ER*	grb10a	1,45	*GRB10*
Dr.21187.1.A1_at	*hMYC-ER*	slc2a3	1,45	*SLC2A3*
Dr.3945.1.A1_at	*hMYC-ER*	epb41l5	1,45	*EPB41L5*
Dr.486.1.S1_at	*hMYC-ER*	ppp1r14bb	1,45	*PPP1R14B*
Dr.18074.1.S1_at	*hMYC-ER*	cd99l2	1,45	*CD99L2*
Dr.21394.1.S1_at	*hMYC-ER*	xirp2a	1,46	*XIRP2*
Dr.17452.1.S1_at	*hMYC-ER*	zgc:56466	1,47	*NIPSNAP3A*
Dr.9110.1.A1_at	*hMYC-ER*	wu:fc14a10	1,48	*ATF5*
Dr.5981.1.S1_at	*hMYC-ER*	atp6v1b2	1,48	*ATP6V1B2*
Dr.1168.1.S1_at	*hMYC-ER*	caspa	1,48	*CASP1*
Dr.16195.1.A1_at	*hMYC-ER*	sell	1,48	*SELL*
Dr.15170.1.S1_s_at	*hMYC-ER*	zbtb2a	1,48	*ZBTB2*
Dr.20910.1.S1_at	*hMYC-ER*	sox19a	1,48	*SOX15*
Dr.9982.1.A1_at	*hMYC-ER*	tox	1,49	*TOX*
Dr.13472.1.A1_at	*hMYC-ER*	rasgrp3	1,49	*RASGRP3*
Dr.17141.1.A1_at	*hMYC-ER*	skilb	1,50	*SKIL*
Dr.18495.1.A1_at	*hMYC-ER*	si:dkey-49h9.6	1,50	*IGSF9*
Dr.25051.1.S1_at	*hMYC-ER*	lmnb1	1,51	*LMNB1*
Dr.4884.1.S1_at	*hMYC-ER*	rgrb	1,53	*RGR*
Dr.9976.1.S1_at	*hMYC-ER*	klf2b	1,53	*KLF2*
Dr.8291.1.S1_s_at	*hMYC-ER*	acvr2b	1,53	*ACVR2B*
Dr.8301.1.S1_a_at	*hMYC-ER*	hsf1	1,53	*HSF1*
Dr.14982.1.A1_at	*hMYC-ER*	si:dkey-3n22.7	1,54	*LIPE*
Dr.681.1.A1_at	*hMYC-ER*	rasd1	1,55	*RASD1*
Dr.14063.1.A1_at	*hMYC-ER*	eml2	1,55	*ELM2*
Dr.25398.1.S1_at	*hMYC-ER*	zgc:86759	1,56	*LPPR1*
Dr.5515.1.A1_at	*hMYC-ER*	epb41l3b	1,57	*EPB41L3*
Dr.13862.1.S1_at	*hMYC-ER*	bik	1,58	*BIK*

Dr.16752.1.A1_at	*hMYC-ER*	cpped1	1,58	*CPPED1*
Dr.7643.1.S1_at	*hMYC-ER*	fam116b	1,58	*DENND6B*
Dr.25608.1.A1_at	*hMYC-ER*	fhit	1,58	*FHIT*
Dr.13791.1.A1_at	*hMYC-ER*	cadm2a	1,59	*CADM2*
Dr.5573.1.S1_at	*hMYC-ER*	arl11	1,59	*ARL11*
Dr.18672.1.A1_at	*hMYC-ER*	si:ch211-69i14.7	1,59	*PANX1*
Dr.23928.1.A1_at	*hMYC-ER*	fhl3	1,60	*FHL3*
Dr.7467.1.S1_at	*hMYC-ER*	serinc5	1,60	*SERINC5*
Dr.7102.1.S1_at	*hMYC-ER*	ppdpfb	1,61	*PPDPF*
Dr.17137.1.S1_at	*hMYC-ER*	rorab	1,62	*RORA*
Dr.11161.1.A1_at	*hMYC-ER*	si:dkey-1a7.2	1,62	*EIF4G3*
Dr.555.1.S1_at	*hMYC-ER*	neurog1	1,62	*NEUROG1*
Dr.6833.1.A1_at	*hMYC-ER*	wee2	1,63	*WEE2*
Dr.4262.1.S1_at	*hMYC-ER*	igf2bp2b	1,63	*IGF2BP2*
Dr.8065.1.S1_at	*hMYC-ER*	lmo2	1,64	*LMO2*
Dr.7417.1.S1_at	*hMYC-ER*	sh3bp5	1,64	*SH3BP5*
Dr.23376.2.A1_at	*hMYC-ER*	pdlim1	1,66	*PDLIM1*
Dr.17749.2.A1_a_at	*hMYC-ER*	cyba	1,66	*CYBA*
Dr.10070.1.A1_at	*hMYC-ER*	fbp1a	1,67	*FBP1*
Dr.123.1.S1_at	*hMYC-ER*	chrna1	1,68	*CHRNA1*
Dr.15212.1.A1_at	*hMYC-ER*	zgc:92140	1,68	*C1orf21*
Dr.10705.1.S1_at	*hMYC-ER*	malt1	1,70	*MALT1*
Dr.5994.1.A1_at	*hMYC-ER*	hibadha	1,71	*HIBADH*
Dr.21774.1.A1_at	*hMYC-ER*	camk2d1	1,72	*CAMK2D*
Dr.17552.1.S1_at	*hMYC-ER*	ccdc6b	1,72	*CCDC6*
Dr.15824.1.S1_at	*hMYC-ER*	zgc:154070	1,73	*CHST2*
Dr.19516.1.S1_at	*hMYC-ER*	mfsd6b	1,75	*MFSD6*
Dr.9446.1.A1_a_at	*hMYC-ER*	pxn	1,75	*PXN*
Dr.10904.1.S1_a_at	*hMYC-ER*	add3a	1,76	*ADD3*
Dr.6782.1.A1_at	*hMYC-ER*	mpnd	1,76	*MPND*
Dr.17817.1.A1_at	*hMYC-ER*	lrig1	1,77	*IRIG1*
Dr.19395.1.A1_at	*hMYC-ER*	si:dkey-39n1.2	1,77	*QSOX1*
Dr.18112.2.A1_at	*hMYC-ER*	zgc:101072	1,78	*RAI14*
Dr.1118.1.A1_at	*hMYC-ER*	gfod2	1,78	*GFOD2*
Dr.17085.1.A1_at	*hMYC-ER*	ighm	1,79	*IGHM*
Dr.3012.1.A1_at	*hMYC-ER*	kif1b	1,79	*KIF1B*
Dr.12778.1.S1_at	*hMYC-ER*	auts2	1,80	*AUTS2*
Dr.22781.1.A1_at	*hMYC-ER*	calb1	1,80	*CALB1*
Dr.14235.1.S1_at	*hMYC-ER*	cd40	1,81	*CD40*
Dr.12565.1.A1_at	*hMYC-ER*	vat1	1,81	*VAT1*
Dr.2634.1.A1_at	*hMYC-ER*	enpp1	1,82	*ENPP1*
Dr.4725.1.A1_at	*hMYC-ER*	jam3b	1,83	*JAM3*
DrAffx.1.11.S1_at	*hMYC-ER*	syk	1,84	*SYK*
Dr.8080.1.S1_at	*hMYC-ER*	mitfa	1,84	*MITF*
Dr.18341.1.S1_at	*hMYC-ER*	nrp2b	1,86	*NRP2*

Dr.6362.1.A1_at	*hMYC-ER*	deptor	1,87	*DEPTOR*
Dr.17189.1.A1_at	*hMYC-ER*	ctdspla	1,87	*CTDSPL*
Dr.16423.1.S1_at	*hMYC-ER*	thrap6	1,88	*MED30*
Dr.6328.1.A1_at	*hMYC-ER*	myo1e	1,88	*MYO1E*
Dr.18158.1.A1_at	*hMYC-ER*	slc4a4b	1,89	*SLC4A4*
Dr.9633.1.A1_at	*hMYC-ER*	rftn2	1,91	*RFTN2*
Dr.14159.1.A1_at	*hMYC-ER*	hdac9b	1,92	*HDAC9*
Dr.13142.1.A1_at	*hMYC-ER*	stap2a	1,93	*STAP2*
Dr.17200.1.S1_at	*hMYC-ER*	metrnl	1,94	*METRNL*
Dr.17692.1.A1_at	*hMYC-ER*	prkcha	1,94	*PRKCH*
Dr.8153.1.S1_at	*hMYC-ER*	cldng	1,94	*CLDN4*
Dr.11977.1.A1_at	*hMYC-ER*	lrrc33	1,95	*LRRC33*
DrAffx.1.70.S1_at	*hMYC-ER*	hopx	1,95	*HOPX*
Dr.73.1.A1_at	*hMYC-ER*	si:dkey-76k16.7	1,96	*RRBP1*
Dr.11222.1.A1_at	*hMYC-ER*	anks1b	1,96	*ANKS1B*
Dr.13972.1.S1_at	*hMYC-ER*	zgc:64114	1,98	*DDIT4*
Dr.356.1.S1_at	*hMYC-ER*	gata2a	1,98	*GATA2*
Dr.8176.1.S1_at	*hMYC-ER*	pax5	1,98	*PAX5*
Dr.7257.1.A1_at	*hMYC-ER*	rasgef1ba	2,00	*RASGEF1B*
Dr.7801.1.A1_at	*hMYC-ER*	zgc:110586	2,00	*TSPAN2*
DrAffx.1.26.S1_at	*hMYC-ER*	blnk	2,00	*BLNK*
Dr.6285.1.S1_at	*hMYC-ER*	gcshb	2,02	*GCSH*
Dr.16183.1.S1_at	*hMYC-ER*	dlc	2,04	*DLL3*
Dr.21888.1.S1_at	*hMYC-ER*	jam2a	2,04	*JAM2*
Dr.4095.1.A1_at	*hMYC-ER*	ass1	2,05	*ASS1*
Dr.61.1.A1_at	*hMYC-ER*	cxcl12b	2,06	*CXCL12*
Dr.14004.1.S1_at	*hMYC-ER*	cdc34a	2,07	*CDC34*
Dr.10542.1.S1_at	*hMYC-ER*	hsd3b7	2,08	*HSD3B7*
Dr.6382.1.A1_at	*hMYC-ER*	hhip	2,10	*HHIP*
Dr.16892.1.A1_at	*hMYC-ER*	mpp2b	2,10	*MPP2*
Dr.1815.1.A1_at	*hMYC-ER*	macf1	2,10	*MACF1*
Dr.16393.1.A1_at	*hMYC-ER*	abhd2b	2,14	*ABHD2*
Dr.1164.1.S1_at	*hMYC-ER*	cyfip1	2,15	*CYFIP1*
Dr.4661.1.A1_at	*hMYC-ER*	syne2b	2,15	*SYNE2*
Dr.6407.1.A1_at	*hMYC-ER*	tgfbr2	2,17	*TGFBR2*
Dr.12020.1.A1_at	*hMYC-ER*	cdk16	2,18	*CDK16*
Dr.15055.1.S1_at	*hMYC-ER*	cxcr4a	2,19	*CXCR4*
Dr.24262.1.A1_at	*hMYC-ER*	plekhh1	2,19	*PLEKHH1*
Dr.17776.1.A1_at	*hMYC-ER*	tph1b	2,21	*TPH1*
Dr.18562.2.A1_at	*hMYC-ER*	fpgs	2,27	*FPGS*
Dr.15089.1.S1_at	*hMYC-ER*	rem1	2,28	*REM1*
Dr.21550.1.S1_at	*hMYC-ER*	dpysl5a	2,29	*DPYSL5*
Dr.13058.1.A1_at	*hMYC-ER*	slc12a7b	2,36	*SLC12A7*
Dr.15634.1.S1_at	*hMYC-ER*	tcea3	2,38	*TCEA3*
Dr.8025.2.A1_at	*hMYC-ER*	wu:fa11d03	2,49	*PACSIN3*

Dr.14510.1.A1_at	*hMYC-ER*	prmt2	2,55	*PRMT2*
Dr.25140.4.S1_at	*hMYC-ER*	cd81	2,58	*CD81*
Dr.5264.1.A1_at	*hMYC-ER*	pdzrn3	2,59	*PDZRN3*
Dr.9870.1.A1_at	*hMYC-ER*	zdhhc2	2,60	*ZDHHC2*
Dr.7612.1.A1_at	*hMYC-ER*	spi1	2,69	*SPI1*

REFERENCES

1. C.H., Pui, Central Nervous System Disease in acute lymphoblastic leukemia: Prophylaxis and Treatment, ASH Education Book, 2006 Jan 1;2006(1):142-146. DOI: 10.1182/asheducation-2006.1.142
2. Pui CH, Robison LL, Look AT. Acute lymphoblastic leukaemia. Lancet 2008; 371(9617):1030-43.
3. Vilmer E, Suciu S, Ferster A, et al. Long-term results of three randomized trials (58831, 58832, 58881) in childhood acute lymphoblastic leukemia: a CLCG-EORTC report. Leukemia 2000;14:2257–2266. [PubMed: 11187917]
4. Manera R, Ramirez I, Mullins J, Pinkel D. Pilot studies of species-specific chemotherapy of childhood acute lymphoblastic leukemia using genotype and immunophenotype. Leukemia 2000;14:1354–1361. [PubMed: 10942229]
5. Pui CH, Campana D, Pei D, Bowman WP, Sandlund JT, Kaste SC, Ribeiro RC, Rubnitz JE, Raimondi SC, Onciu M, Coustan-Smith E, Kun LE, Jeha S, Cheng C, Howard SC, Simmons V, Bayles A, Metzger ML, Boyett JM, Leung W, Handgretinger R, Downing JR, Evans WE, Relling MV, Treating childhood acute lymphoblastic leukemia without cranial irradiation, The New England Journal of Medicine, 2009 Jun 25;360: 2730-2741. DOI: 10.1056/NEJMoa0900386
6. Veerman AJ, Kamps WA, van den Berg H, van den Berg E, Bökkerink JP, Bruin MC, van den Heuvel-Eibrink MM, Korbijn CM, Korthof ET, van der Pal K, Stijnen T, van Weel Sipman MH, van Weerden JF, van Wering ER, van der Does-van den Berg A; Dutch Childhood Oncology Group, Dexamethasone-based therapy for childhood acute lymphoblastic leukaemia: results of the prospective Dutch Childhood Oncology Group (DCOG) protocol ALL-9 (1997-2004), The Lancet Oncology, 2009 Oct;10(10):957-966. DOI:10.1016/S1470-2045(09)70228-1
7. Pui CH, Howard SC, Current management and challenges of malignant disease in the CNS in pediatric leukemia, The Lancet Oncology, 2008 March;9(3):257-268. DOI:10.1016/S1470-2045(08)70070-6
8. Beckwith LG et al., Ethylnitrosourea induces neoplasia in zebrafish (Danio rerio). Lab Invest. 2000 Mar;80(3):379-85.
9. Amatruda JF et al., Zebrafish as a cancer model system. Cancer Cell. 2002 Apr;1(3):229-31.
10. Kent, M., Bishop-Stewart, J., Matthews, J., and Spitsbergen, J. (2002). Pseudocapillaria tomentosa, a nematode pathogen, and associated neoplasms of zebrafish. Comp. Med. 52, 354–358.
11. Smolowitz, R., Hanley, J., and Richmond, H. (2002). A three-year retrospective study of abdominal tumors in zebrafish maintained in an aquatic laboratory animal facility. Biol. Bull. 203, 265–266.
12. Matthews, J. (2004). Common diseases of laboratory zebrafish. Meth. Cell Biol. 77, 617–643.
13. Postlethwait, J., Woods, I., Ngo-Hazelett, P., Yan, Y., Kelly, P., Chu, F., Huang, H., Hill- Force, A., and Talbot, W. (2000). Zebrafish comparative genomics and the origins of vertebrate chromosomes. Genome Res. 10, 1890–1902.
14. Liu, T., Zhou, Y., Kanki, J., Deng, M., Rhodes, J., Yang, H., Sheng, X., Zon, L., and Look, A. (2002). Evolutionary conservation of zebrafish linkage group 14 with frequently deleted regions of human chromosome 5 in myeloid malignancies. Proc. Natl Acad. Sci. USA 99, 6136–6141.
15. Solnica-Krezel L, Schier AF, Driever W. Efficient recovery of ENU-induced mutations from the zebrafish germline. Genetics 1994 Apr;136(4):1401–20. [PubMed: 8013916]
16. Shepard, J. L., Amatruda, J. F., Stern, H. M., Subramanian, A., Finkelstein, D., Ziai, J., Finley, K. R., Pfaff, K. L., Hersey, C., Zhou, Y., et al. (2005). A zebrafish bmyb

mutation causes genome instability and increased cancer susceptibility. Proc. Natl Acad. Sci. USA 102, 13194–13199.
17. Langenau, D. M., Traver, D., Ferrando, A. A., Kutok, J. L., Aster, J. C., Kanki, J. P., Lin, S., Prochownik, E., Trede, N. S., Zon, L. I., et al. (2003). Myc-induced T cell leukemia in transgenic zebrafish. Science 299, 887–890.
18. Patton, E. E., Widlund, H. R., Kutok, J. L., Kopani, K. R., Amatruda, J. F., Murphey, R. D., Berghmans, S., Mayhall, E. A., Traver, D., Fletcher, C. D. M., et al. (2005). BRAF mutations are sufficient to promote nevi formation and cooperate with p53 in the genesis of melanoma. Curr. Biol. 15, 249–254.
19. Langenau, D. M., Feng, H., Berghmans, S., Kanki, J. P., Kutok, J. L., and Look, A. T. (2005a). Cre/lox-regulated transgenic zebrafish model with conditional myc-induced T cell acute lymphoblastic leukemia. Proc. Natl Acad. Sci. USA 102, 6068–6073.
20. Feng, H., Langenau, D. M., Marge, J., Quinkertz, A., Gutierrez, A., Neuberg, D., Kanki, J. P., and Look, A. T. (2007). Heat-shock induction of T-cell lymphoma/leukaemia in conditional Cre/lox-regulated transgenic zebrafish. Br. J. Haematol. 138, 169–175.
21. Langenau, D. M., Jette, C., Berghmans, S., Palomero, T., Kanki, J. P., Kutok, J. L., and Look, A. T. (2005b). Suppression of apoptosis by bcl-2 overexpression in lymphoid cells of transgenic zebrafish. Blood 105, 3278–3285.
22. Chen, J., Jette, C., Kanki, J. P., Aster, J. C., Look, A. T., and Griffin, J. D. (2007). NOTCH1- induced T-cell leukemia in transgenic zebrafish. Leukemia 21, 462–471.
23. Gutierrez A, Grebliunaite R, Feng H, Kozakewich E, Zhu S, Guo F, Payne E, Mansour M, Dahlberg SE, Neuberg DS, Hertog J, Prochownik EV, Testa JR, Harris M, Kanki JP, Look AT. 2011. Pten mediates Myc oncogene dependence in a conditional zebrafish model of T cell acute lymphoblastic leukemia. J Exp Med 208:1595–1603.
24. Sabaawy, H., Azuma, M., Embree, L., Tsai, H., Starost, M., and Hickstein, D. (2006). TELAML1 transgenic zebrafish model of precursor B cell acute lymphoblastic leukemia. Proc. Natl Acad. Sci. USA 103, 15166–15171.
25. Zhuravleva J, Paggetti J, Martin L, Hammann A, Solary E, Bastie JN et al. MOZ/TIF2-induced acute myeloid leukaemia in transgenic fish. Br J Haematol 2008; 143: 378–382.
26. Alghisi E, Distel M, Malagola M, Anelli V, Santoriello C, Herwig L, Krudewig A, Henkel CV, Russo D, Mione MC. Targeting oncogene expression to endothelial cells induces proliferation of the myelo-erythroid lineage by repressing the Notch pathway. Leukemia. 2013 Nov;27(11):2229-41. doi: 10.1038/leu.2013.132. Epub 2013 Apr 29.
27. White, R., Mark, Sessa, A., Burke, C., Bowman, T., LeBlanc, J., Ceol, C., Bourque, C., Dovey, M., Goessling, W., Burns, C., Erter, et al. (2008). Transparent adult zebrafish as a tool for in vivo transplantation analysis. Cell Stem Cell 2, 183–189.
28. Jeong JY, Kwon HB, Ahn JC, Kang D, Kwon SH, Park JA, Kim KW. Functional and developmental analysis of the blood-brain barrier in zebrafish. Brain Res Bull. 2008 Mar 28;75(5):619-28. Epub 2007 Nov 20.
29. Wang et al., Cranial meninges of goldfish:ager related changes in morphology of meningeal cells and accumulation of sur et al.Cranial meninges of goldfish: agerelated changes in morphology of surfactant-like multilamellar bodies. Cell Tissue Res. 1995 Aug;281(2):349-58.
30. Frazer JK et al., Heritable T-cell malignancy models established in a zebrafish phenotypic screen. Leukemia. 2009 Oct;23(10):1825-35. doi: 10.1038/leu.2009.116. Epub 2009 Jun 11.
31. Nicoli, S., Ribatti, D., Cotelli, F., and Presta, M. (2007). Mammalian tumor xenografts induce neovascularization in zebrafish embryos. Cancer Res. 67, 2927–2931.
32. Stoletov, K., Montel, V., Lester, R. D., Gonias, S. L., and Klemke, R. (2007). High-resolution imaging of the dynamic tumor cell vascular interface in transparent zebrafish.

Proc. Natl Acad. Sci. USA 104, 17406–17411.
33. Haldi, M., and Hopkins, N. (1999). A large-scale insertional mutagenesis screen in zebrafish. Genes Dev. 13(20), 2713–2724.
34. Pruvot B, Jacquel A, Droin N, Auberger P, Bouscary D, Tamburini J, Muller M, Fontenay M, Chluba J, Solary E. Leukemic cell xenograft in zebrafish embryo for investigating drug efficacy. Haematologica. 2011 Apr;96(4):612-6. doi: 10.3324/haematol.2010.031401. Epub 2011 Jan 12.
35. Shrivastava A, Yu J, Artandi S, Calame K. YY1 and c-Myc associate in vivo in a manner that depends on c-Myc levels. Proc Natl Acad Sci U S A. 1996 Oct 1;93(20):10638-41.
36. Hasegawa A, Yasukawa M, Sakai I, Fujita S.Transcriptional down-regulation of CXC chemokine receptor 4 induced by impaired association of transcription regulator YY1 with c-Myc in human herpesvirus 6-infected cells. J Immunol. 2001 Jan 15;166(2):1125-31.
37. Gordon S, Akopyan G, Garban H, Bonavida B. Transcription factor YY1: structure, function, and therapeutic implications in cancer biology. Oncogene. 2006 Feb 23;25(8):1125-42.
38. Lam SH, Chua HL, Gong Z, Lam TJ, Sin YM. Development and maturation of the immune system in zebrafish, Danio rerio: a gene expression profiling, in situ hybridization and immunological study. Dev Comp Immunol. 2004 Jan;28(1):9-28.
39. Traver D, Herbomel P, Patton EE, Murphey RD, Yoder JA, Litman GW, Catic A, Amemiya CT, Zon LI, Trede NS. The zebrafish as a model organism to study development of the immune system. Adv Immunol. 2003;81:253-330.
40. Stoletov, K., Montel, V., Lester, R. D., Gonias, S. L., and Klemke, R. (2007). High-resolution imaging of the dynamic tumor cell vascular interface in transparent zebrafish. Proc. Natl Acad. Sci. USA 104, 17406–17411.
41. Chong SW, Emelyanov A, Gong Z, Korzh V. Expression pattern of two zebrafish genes, cxcr4a and cxcr4b. Mech Dev. 2001 Dec;109(2):347-54.
42. Force A, Lynch M, Pickett FB, Amores A, Yan YL, Postlethwait J. Preservation of duplicate genes by complementary, degenerative mutations. Genetics. 1999 Apr;151(4):1531-45.
43. Rossi D, Zlotnik A. The biology of chemokines and their receptors. Annu Rev Immunol 2000;18:217–42.
44. Crazzolara R, Kreczy A, Mann G, et al. High expression of the chemokine receptor CXCR4 predicts extramedullary organ infiltration in childhood acute lymphoblastic leukaemia. Br. J. Haematology. 2001; 115(3):545–553.
45. Christina Halsey, Mark TS Williams, Yasar Yousafzai, Klaus Rehe, Olaf Heidenreich, Josef Vormoor, Brenda Gibson[3]and Gerard Graham, Central Nervous System Involvement in a Xenograft Model of Pre-B Acute Lymphoblastic Leukaemia Is Associated with Dysfunctional CXCR4 Expression and Upregulation of the Neurotropic Chemokine Receptors CCR6 and CX3CR1, Blood, 2011: Abstract 3449.
46. Meyer LH, Eckhoff SM, Queudeville M, Kraus JM, Giordan M, Stursberg J, Zangrando A, Vendramini E, Möricke A, Zimmermann M, Schrauder A, Lahr G, Holzmann K, Schrappe M, Basso G, Stahnke K, Kestler HA, Te Kronnie G, Debatin KM. Early relapse in ALL is identified by time to leukemia in NOD/SCID mice and is characterized by a gene signature involving survival pathways. Cancer Cell. 2011 Feb 15;19(2):206-17. doi: 10.1016/j.ccr.2010.11.014. Epub 2011 Feb 3.
47. Scholzen T, Gerdes J. The Ki-67 protein: from the known and the unknown. J Cell Physiol. 2000 Mar;182(3):311-22.
48. Akers SM, Rellick SL, Fortney JE, et al. Cellular elements of the subarachnoid space promote ALL survival during chemotherapy Leuk Res 2011;35:705– 711.

49. Robb RM, Ervin LD, Sallan SE. A pathological study of eye involvement in acute leukemia of childhood. Trans Am Ophthalmol Soc. 1978;76:90-101.
50. Mueller, A., Homey, B., Soto, H., Ge, N., Carton, D., Buchanan, M.E., McClanahan, T., Murphy, E., Yuan, W., Wagner, S.N., Barrera, J.L., Mohar, A., Verastegui, E. & Zlotnik, A. (2001) Involvement of chemokine receptors in breast carcinoma metastasis. Nature, 410, 50±56.
51. Diotel N, Vaillant C, Gueguen MM, Mironov S, Anglade I, Servili A, Pellegrini E, Kah O. Cxcr4 and Cxcl12 expression in radial glial cells of the brain of adult zebrafish. J Comp Neurol. 2010 Dec 15;518(24):4855-76. doi: 10.1002/cne.22492.
52. MoÈhle, R., Bautz, F., Rafii, S., Moore, M.A., Brugger, W. & Kanz, L. (1998) The chemokine receptor CXCR4 is expressed on CD341 hematopoietic progenitors and leukemic cells and mediates transendothelial migration induced by stromal cell-derived factor-1. Blood, 91, 4523±4530.
53. MoÈhle, R., Failenschmid, C., Bautz, F. & Kanz, L. (1999) Overexpression of the chemokine receptor CXCR4 in B cell chronic lymphocytic leukemia (B-CLL) is associated with increased functional response to stromal cell-derived factor-1. Leukemia, 13, 1954±1959.
54. Mohle, R., Schittenhelm, M., Failenschmid, C., Bautz, F., Kratz- Albers, K., Serve, H., Brugger, W. & Kanz, L. (2000) Functional response of leukaemic blasts to stromal cell-derived factor-1 correlates with preferential expression of the chemokine receptor CXCR4 in acute myelomonocytic and lymphoblastic leukaemia. British Journal of Haematology, 110, 563±572.
55. Wu S, Gessner R, Taube T, et al. Chemokine IL-8 and chemokine receptor CXCR3 and CXCR4 gene expression in childhood acute lymphoblastic leukemia at first relapse. J. Pediatr. Hematol. Oncol. 2006; 28(4):216–220. [PubMed: 16679918]
56. Biojone E, Queir_oz RD, Valera ET, et al. Minimal residual disease in cerebrospinal fluid at diagnosis: A more intensive treatment protocol was able to eliminate the adverse prognosis in children with acute lymphoblastic leukemia. Leuk Lymphoma 2012;53:89–95.

CHAPTER 2

CXCR4 expression and CNS infiltration: a study of murine models xenografted with human T-ALL cells

ABSTRACT

The CXCR4/CXCL12 axis seems to be particularly important for metastasis of different epithelial, mesenchymal and haemopoietic cancers. Activation of CXCR4 increased direct migration of cancer cells towards its specific ligand CXCL12 gradient. As CXCL12 is expressed in different type of tissues/organs (bone marrow, liver, spleen, kidney, lymph node and CNS), we can speculate that the expression level of CXCR4 in leukemic cells, could influence the ability of these cells to infiltrate extramedullary tissues, such as the CNS. At the moment, there are discordant hypotheses regarding the role of the CXCR4/CXCL12 axis and CNS infiltration in ALL. Through this study, we aimed to better clarify the importance of CXCR4/*CXCR4* expression in determining the ability of T-lymphoblasts to infiltrate the CNS. We decided to use mice xenografted with primary pediatric T-ALL cells as we found that also this xenografted murine model can present infiltration at the meningeal level with different seriousness. Preliminary data revealed that also in the murine model, the expression levels of *CXCR4* in T-ALL cells have a tendency to correlate with the degree of CNS infiltration at the meningeal level. This data underline the importance of *CXCR4* expression as a possible conserved mechanism able to predispose T-lymphoblasts to enter the CNS. Further studies on a larger cohort of xenografted mice are actually ongoing.

INTRODUCTION

Acute Lymphoblastic Leukemia (ALL) is the most frequent type of childhood malignancy [1] characterized by an uncontrolled growth of immature cells of the T- or B- lymphoid lineage. Leukemic cells colonize the bone marrow (BM) and often also extramedullary organs, such as ~30-50% spleen or liver [2] and < 5% Central Nervous System, CNS [3-4]. The ability to infiltrate the CNS gives a great advantage to lymphoblastic cells; in fact, the presence of the Blood Brain Barrier (BBB) impairs the entrance of chemotherapeutic compounds and malignant cells that escape into the CNS are protected from therapy. The presence of leukemic cells that survive to chemotherapy in extramedullary organs is problematic, because it can easily result in leukemic relapse. T-cell Acute Lympholastic Leukemia (T-ALL) represents 15% of pediatric ALLs and forms a high-risk group of patients. In fact, T-ALL is often associated to increased white cell counts, hepatosplenomegaly, increased risk of leptomeningeal infiltration at diagnosis [5] and high risk of CNS relapse [6-7]. For this reason, T-ALL patients usually receive intrathecal chemotherapy associate to cranial irradiation, a treatment that can result in a number of complications (secondary tumours, growth impairment, neurocognitive deficits and endocrinopathy) [7]. The introduction of intensified treatment protocols has improved the outcome of children with T-ALL (five-year relapse-free survival rates of about 75%), and numerous efforts have been made to reduce or avoid the use of cranial irradiation [8]. However, cranial irradiation is still necessary for patients at high risk, especially for those that present CNS involvement already at diagnosis as well as at relapse [7]. Little is know about how leukemic cells can infiltrate the CNS; several studies claimed the discovery of 'the key mechanism' that allowed ALL cells to invade, survive and colonize the CNS, but results are diverse. Holland et al. showed an important role for RAC2, AEP and ICAM1 expression in their study of a murine model of childhood pre-B ALL that developed CNS leukemia [9]. Buonamici et al. found a direct relation between CCR7 expression and the ability to infiltrate the CNS in a murine model xenografted with human T-ALL cell lines [10]. Moreover, there are discordant hypothesis regarding the importance of the CXCR4/CXCL12 axis and CNS infiltration; high levels of CXCR4 expression in lymphoblasts seem to be predictive of extramedullary organ infiltration in childhood ALL patients [11], however CNS-homing cells showed CXCR4 down-regulation in a

mouse model of CNS pre-B ALL [12] and children with ALL relapse associated to testicles or CNS leukemia showed blast cells with lower CXCR4 levels than blasts from cases with isolated bone marrow-relapses [13]. As we also found a positive correlation between *cxcr4* expression levels and the degree of CNS infiltration in two T-ALL zebrafish models (chapter 1 of this thesis), we were particularly interested in studying the importance of the CXCR4/CXCL12 axis in human T-ALL metastatic behavior. The CXCL12/CXCR4 axis plays an important role in regulating the engraftment of CD34+ haematopoietic stem cells into the bone marrow [14-15], the egress of preB and T lymphocytes from the BM into the Peripheral Blood (PB) and lymphoid tissues [16] and in directing naïve leukocyte trafficking [17]. The interaction of CXCR4 with CXCL12 activates the receptor, increasing the ability of cells to migrate towards a CXCL12 chemo-attracting gradient and this is true for cancer cells as well [18-19]. At this point, we suppose that the deregulation of CXCR4 expression in T-ALL cells could increased the homing of malignant cells towards tissues expressing CXCL12. CXCL12 is constitutively expressed in several human organs, particularly in extramedullary tissues that are often found to be involved in leukemic infiltration: bone marrow, lymph nodes, liver, spleen, kidney and brain [19-20]. The metastatic role of CXCR4 is well documented for both solid tumors [18] and haematological diseases, such as malignant CD34+ Acute Myeloid Leukemia (AML) and Chronic Lymphoblastic Leukemia (CLL) [21-23]. However, the importance of this axis for T-ALL is not clear. Through this study, we aimed to better clarify the importance of CXCR4 expression in determining the ability of T-lymphoblasts to infiltrate the CNS. We decided to study this phenomenon using NSG, or NOD/SCID gamma, (NOD.Cg-*Prkdc*^{scid} *Il2rg*^{tm1Wjl}/SzJ) murine models xenografted with a set of primary T-ALL cells of pediatric patients.

MATERIALS AND METHODS

T-ALL xenografts establishment

Primary T-ALL cells were obtained from bone marrow (BM) of newly diagnosed pediatric patients, according to the guidelines of the local ethics committees. For xenografts establishment, 6- to 9-weeks-old mice were injected intravenously (i.v.) with

10 x 10^6 T-ALL cells in 300 µl of Dulbecco's Phosphate Buffer Saline (PBS). NSG mice were purchased from Charles River (Wilmington, MA). Procedures involving animals and their care were conform institutional guidelines that comply with national and international laws and policies (EEC Council Directive 86/609, OJ L 358, 12 December, 1987). T-ALL engraftment was monitored by periodic blood drawings and flow cytometric analysis of CD5 and CD7 markers over a 5-month period. Mice were sacrificed when more than 40% of cells in the PB resulted positive for the CD7 or CD5.

TCR analysis

The recombination, insertion and deletion of Immunoglobulin (Ig) and T-cell receptor (TCR) gene segments results in an individual gene sequence unique for each lymphocyte, named N-region. This genes junctional region can be considered a fingerprint-marker specific of each lymphocytes and consequentially, of each lymphoid neoplasia. We used this biological characteristic to check that xenografted cells from each mouse maintained the rearrangement of the leukemia of the patient of origin.

Histology and scoring system

Skulls of sacrificed xenotransplanted mice were fixed in 4% paraformaldehyde, decalcified, paraffin-embedded and sectioned (5µm) according to standard procedures. Hematoxylin and eosin (H&E) staining was performed using standard protocols. Histopathological examination was performed in a blind fashion and details concerning experimental design were revealed only at the end of the analysis. T-lymphoblasts infiltration was found in the bone marrow of the skull, in dental alveoli, oral and rhinopharingeal mucosa, orbital space, middle ear and meninges.

The following scoring system was used to classify the degree of lymphoblastic infiltration:

<u>*Bone marrow*</u>

0. No invasion/colonization
1. Focal or multifocal invasion/colonization with partial effacement of preexisting hematopoietic population
2. Diffuse invasion with almost complete or complete effacement of preexisting hematopoietic population and focal disruption of bony encasement

3. Diffuse invasion with complete effacement of preexisting hematopoietic population and extensive disruption of bony encasement

Dental alveoli

0. No invasion
1. Focal or multifocal invasion with partial effacement of periodontal ligament and dental pulp
2. Diffuse invasion with almost complete or complete effacement of periodontal ligament and dental pulp
3. Diffuse invasion with complete effacement and disruption of the alveolar socket

Oral and rhinopharingeal mucosa

0. No invasion
1. Focal or multifocal infiltration and expansion of lamina propria and submucosa
2. Segmental infiltration and expansion of lamina propria and submucosa
3. Diffuse infiltration and expansion of lamina propria and submucosa with disruption of mucosal architecture and multiple infiltrative extension into the surrounding soft tissues

Orbital space

0. No invasion
1. Focal or multifocal infiltration with partial obliteration of orbital soft tissues
2. Diffuse invasion with almost complete or complete obliteration of orbital soft tissues and focal invasion of extraorbital structures
3. Diffuse invasion with almost complete or complete obliteration of the orbits and extensive invasion of extraorbital structures

Middle ear

0. No invasion
1. Focal or multifocal infiltration and expansion of lamina propria and submucosa
2. Diffuse infiltration and expansion of lamina propria and submucosa
3. Diffuse infiltration and expansion of lamina propria and submucosa with with disruption of mucosal architecture and multiple infiltrative extension into the surrounding soft tissues

Meninges

0. No invasion
1. Focal or multifocal infiltration of dura mater with partial expansion and obliteration of arachnoid space
2. Segmental to diffuse infiltration of dura mater with extensive expansion and obliteration of arachnoid space

3. Diffuse infiltration of dura mater with extensive expansion and obliteration of arachnoid space and focal/multifocal compression and degeneration of the subjacent neuroparenchyma

Flow Cytometry and CXCR4 expression analysis

Cells derived from both the spleen and the peripheral blood of 29 xenoengrafted mice were analyzed, by Flow cytometry (FCM) for CXCR4 expression. Briefly, $5*10^5$ cells both from the mice spleen and PB, after haemolysis with ACK Lysis buffer (8.29 g/L NH_4Cl, 1mM EDTA and 1g/L $KHCO_3$), were stained with FITC-conjugated antibody against human CD45, a PE-coniugated antibody against human CXCR4, a PC5-conjugated antibody against human CD7 and an APC-conjugated antibody against human CD3, following manufacture's instructions. Unlabeled cells were first acquired to ensure labeling specificity. Jurkat cells were used to test the efficient staining of all antibodies. Relative percentages of different subpopulations were calculated based on live- gated cells (as measured by the physical parameters of side scatter and forward scatter). In particular the percentage of CXCR4 positive cells was calculated on the gated human CD45+ population. All antibodies were provided by BD (Becton Dickinson, San Jose, CA) and all samples were analyzed on the Navios Flow cytometer (Beckman Coulter, Brea, CA).

RNA extraction, Reverse-transcription and Real-time polymerase chain reaction

Total RNA from ~ $5*10^5$ cells extracted from the spleen of each mouse using Trizol, according to the manufacturer's instruction (Invitrogen, Karlsruhe, Germany). RNA concentration was determined using NanoDrop ND-1000 Spectrophotometer (NanoDrop Technologies Inc, Wilmington, DE). RNA quality and purity control was assessed with the Agilent Bioanalyzed 2100 (Agilent Technologies, Waldbronn, Germany) using "Eukaryote total RNA Assay". 1 μg of RNA was reverse transcribed using Superscript II (Invitrogen, Karlsruhe, Germany), and random primers following standard techniques. SYBR-Green Real-time quantitative PCR (qRT-PCR) was performed using the Platinum SYBR-Green qPCR SuperMix UDG (Invitrogen, Karlsruhe, Germany) and the 7900 HT Fast Real-Time PCR System (Applied Biosystems, Foster City, CA). qRT-PCR was executed for detecting expression level of

human *CXCR4*, while *GUS* was used as housekeeping gene to normalize gene expression data. qRT-PCR was performed in triplicates (both for housekeeping and genes of interest) for each sample and standard curve of 3 serial dilutions was used as control for each plates. Primers are listed in table 2. The specificity of the primers was examined with the corresponding dissociation curve. To allow comparison between samples, transcript quantification was performed after normalization with *GUS* using the Ct method and results were calculated according to the following formula $2^{-\Delta ct}$, as previously described [24]. Analysis of expression was performed using the GraphPad Prisim 5 software.

Mice xenografted with Jurkat cells

NOD-SCID-common γ chain knock-out mice were obtained from Jackson Laboratory, USA and maintained in specific pathogen-free (spf) animal facility. Ten week old mice were injected with $10x10^6$ Jurkat cells i.v. and sacrificed after 21 days.

Spleens were homogenized and the recovered cell suspension was washed in Complete Medium (RPMI 1640 containing 10% FBS, sodium pyruvate, glutamax, 2-mercaptoethanol, non-essential aminoacids, penicillin and streptomycin) (GIBCO). Reb blood cells were lysed with ACK Lysis buffer (8.29 g/L NH_4Cl, 1mM EDTA and 1g/L $KHCO_3$). Blood was treated with ACK Lysis buffer and the leukocytes fraction washed in complete medium.

For FACS analysis, ex-vivo cells were pre-incubated with blocking anti-FCγ Receptor mab (HB197 hybridoma supernatant) prior to labeling with appropriate antibodies. Mabs conjugated with biotin, FITC, allophycocyanin, or allophycocyanin-Cy7 specific for the following antigens were used: hCD45 (LuBioScience GmbH); mLy6G and mLy6C (Becton Dickinson AG); mCD11b and hCD184 (CXCR4) (BioLegend). All samples were acquired with a BD LSR Fortessa™ FACS (BD Biosciences) and analyzed with FlowJo software (Tree Star).

RESULTS

Murine models xenografted with pediatric T-ALL cells and CNS lymphoblastic infiltration

The first efforts of this work investigated if murine models xenografted with pediatric T-ALL cells developed lymphoblastic CNS infiltration. We started with histological analysis of a first set of 18 xenografted mice heads. This analysis showed that xenografted mice developed T-ALL CNS disease to variable extends. Infiltration was observed in the bone marrow of the skull (BM), dental alveoli, oral and rhinopharingeal mucosa, middle ear, orbital space and meninges. The meningeal infiltration was of particular interest for this study where meningeal infiltration was used as a measure of the ability of T-ALL cells to eventually infiltrate the CNS. For each location analyzed mice presented different degrees of infiltration (figure 1A and B). A score for the degree of infiltration was applied ranging from 1-3 (table 1) according to the scoring system described in *Material and Methods*. Once we knew that, like the zebrafish model, also the murine model xenografted with pediatric T-ALL cells could be useful to study the phenomenon of CNS infiltration, we proceeded with the analysis of a second set of histological preparations of 29 xenografted mice heads. This second set of analysis is still ongoing.

Murine models xenografted with pediatric T-ALL expressed variable levels of **CXCR4**

We found that also mice xenografted with pediatric T-ALL cells developed CNS disease with variable degrees of infiltration. At this point, we decided to use the murine model to better understand the importance of CXCR4/*CXCR4* (protein and mRNA) expression in relation to extramedullary infiltration in T-ALL. For all 29 mice included in the second set of histological analysis we measured CXCR4 expression both at protein and mRNA levels. The aim of this analysis was to clarify the biological meaning for human T-ALL cells to have high or low levels of CXCR4 in relation to their ability to infiltrate the CNS in an *in vivo* murine model.

Flow Cytometry (FCM) was used to detect human (CD45+) CXCR4 positive cells in samples derived both from mice spleen and Peripheral Blood (PB). With this analysis we wanted to investigate the relation between the percentage of human CXCR4+ cells and the seriousness of CNS infiltration. Data revealed among mice the presence of variable percentages of hT-ALL cells that were double positive (CD45+/CXCR4+) in specimens of the spleen and PB (figure 2A and B). However, we have to consider that the amount of CXCR4 at T-cells surface can be influenced by the presence of CXCL12 in mouse spleen and vessels. As the binding of CXCL12 to CXCR4 causes the internalization of the chemokine receptor, the human cells (CD45+) that were found to be negative for CXCR4 can be attributed to interactions with CXCL12 in the murine environment and not to a real absence of CXCR4.

Levels of* CXCR4 *in Jurkat cells xenografted in the mouse

To have an idea of the influence of the mouse microenvironment on CXCR4 expression, we evaluated the percentage of CD45+/CXCR4+ cells in a murine model xenografted with the Jurkat cell line. Jurkat cells derived from *in vitro* culture expressed high levels of CXCR4 and cells were 100% double positive (CD45+ /CXCR4+) by FCM analysis. After xenografting, Jurkat cells extracted from spleen and PB showed partial loss of positivity, strongly suggesting the influence of murine CXCL12 on CXCR4 protein expression at the human T-cell surface (figure 3).

Variable amount of CXCR4 are expressed by leukemic cells infiltrating mouse spleen

At this point, we decided to measure *CXCR4* expression using qRT-PCR to obtain a measure of chemokine receptor quantifications that would be less dependent on short-term dynamic interactions with the microenvironment (e.g. CXCL12 levels). qRT-PCR was performed on samples extracted from mice spleen. Also for *CXCR4* transcription we found a range of expression levels among mice (figure 4). Interestingly, no correlation was found between the expression of CXCR4 at the protein and mRNA level.

CXCR4 transcription tends to reflect the degree of CNS infiltration (preliminary results)

For the moment, data of both histological analysis and qRT-PCR were available for 7 matched sample pairs of the first set of 18 xenografted mice heads analyzed. Preliminary results show how *CXCR4* expression levels tend to correlate with the degree of CNS infiltration (figure 5). Further analysis will be performed when histological analysis data will be completed also for the new set of 29 xenografted mice.

DISCUSSION

The ability of lymphoblasts to infiltrate the CNS continues to represent a great challenge in the cure of patients with ALL that present this complication. To deepen insight into the mechanisms that allowed ALL cells to invade the CNS is very important but also difficult at the same time. In fact, little material coming from ALL patients is available for studies, especially for material directly extracted from the cerebrospinal liquor of ALL patients with CNS involvement. To overcome these limitations, we decided to use NSG (NOD.Cg-*Prkdc*^{scid} *Il2rg*^{tm1Wjl}/SzJ) murine models xenografted with primary T-ALL cells of a set of pediatric patients. It has been largely shown how primary leukemic cells transplanted into murine recipients (NSG) cause the development of a disease, which is very similar to human leukemia. The first efforts of this study were focused in understanding if the T-ALL xenografted NSG murine model could also mimic the phenomenon of CNS disease. In a first set of histological analysis of mice, we found the presence of human T-ALL cells in the meninges of 12/18 samples. Moreover, we found different degrees of infiltration (figure 1), that we divided in 3 levels depending on the meningeal layer interested and the amount of T-lymphoblasts infiltrated in the meninges (table 1). These data showed that also the xenografted murine model can be a useful model for the study of CNS infiltration by human T-ALL cells. However, we have to underline that the presence of CNS involvement was more frequent in the mouse models compared to the pediatric T-ALL patients' cohorts. Indeed, the mouse model could present CNS infiltration even if this situation had not presented itself in the donor patient at diagnosis. However, even if this xenografted model does not directly reflect the situation in the matched human patients,

it is very useful to deepen insight into mechanisms that regulate CNS homing by human T-ALL cells. Different results have been obtained by studies on mechanisms that allow CNS leukemia: particular importance was given to RAC2, AEP and ICAM1 expression in the pre-B mouse model [9] and to CCR7 expression in a T-ALL xenografted murine model [10]. Moreover, the expression levels of CXCR4 have been shown to give discordant results in determining CNS infiltration by blast cells [11-13].

As we also found a positive correlation between *cxcr4* expression levels and the degree of CNS infiltration in two T-ALL zebrafish models (chapter 1 of this thesis), we decided to use the murine model to understand if CXCR4 expression levels might predict the ability of T-ALL cells to infiltrate the CNS. Data of flow cytometry revealed the presence of different percentages of human (CD45+) CXCR4 positive cells in the peripheral blood and Spleen among mice (figure 2A/B). However, we have shown that CXCR4 protein expression levels are affected by dynamic changes due to the presence of the ligand CXCL12 in the mouse microenvironment. That is not surprising considering that human and murine CXCL12 present a high identity at the protein level (~92%) and that also in mice CXCL12 is produced by stromal cells at different sites, such as BM, lymph nodes, spleen, vessels and brain [29]. When CXCL12 binds the CXCR4, the chemokine receptor is temporary internalized from the surface membrane of cells and no longer detectable by FCM. The latter can explain the presence of human cells that result to be CXCR4 "negative" by flowcytometry. To understand the influence of the microenvironment on CXCR4 surface membrane expression, we observed flow data obtained from a mouse model xenografted with Jurkat cells (figure 3). Also in this case, Jurkat cells that are 100% CXCR4 positive during *in vitro* culture showed diminished positivity of CXCR4 in an *in vivo* model (data of Spleen and Peripheral blood). These data underline the notion that CXCR4 surface expression in T-ALL cells is indeed highly variable and under direct influence of the microenvironment of an *in vivo* model. This influence makes it difficult to quantify the real amount of CXCR4 expression in T-ALL cells. To have a measure of the intrinsic CXCR4 expression we decided to measure *CXCR4* mRNA transcription through qRT-PCR analysis. qRT-PCR analysis revealed that in general T-ALL cell have a high expression of *CXCR4,* however also at the transcriptional level we found variability among samples (figure 4).

Interestingly, preliminary data for 7 samples included in the first set of histological analysis revealed that in the murine model, *CXCR4* expression of T-ALL cells have a tendency to correlate with the degree of CNS infiltration at the meningeal level (figure 5). These data seem to confirm previous results obtained in the zebrafish model (Chapter 1 of this thesis) and underline the importance of *CXCR4* expression levels as a conserved mechanism able to predispose T-ALL cells to enter the CNS. These preliminary results will be validated when histological analysis of the new set of 29 cases will be concluded.

FIGURES

Figure 1. Histological analysis of two xenografted murine models with different degrees of CNS infiltration

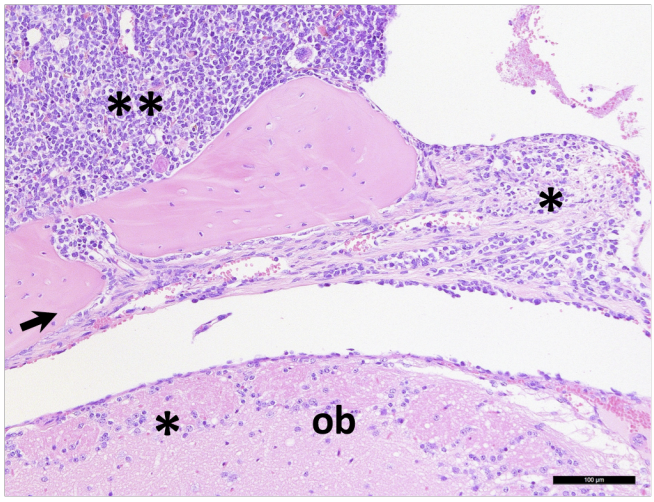

Figure1A: Meningeal infiltration level 1; Diffuse bone marrow invasion by leukemic cells (**) with almost complete effacement of preexisting hematopoietic population (a residual megakaryocyte is denoted by the arrowhead) and focal disruption of bony encasement (arrow). The underlying dura mater and arachnoid (*) are also infiltrated by scattered leukemic elements. H&E staining. Compact bone, cb; olfactory bulb, ob.

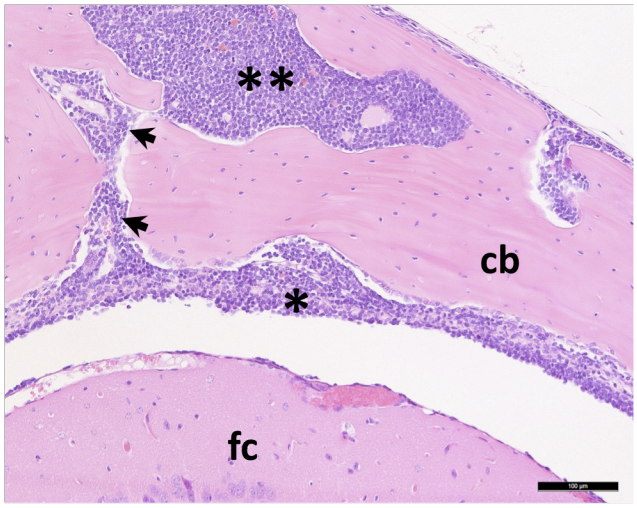

Figure1B : Meningeal infiltration level 3; Diffuse bone marrow invasion by leukemic cells (**) with complete effacement of preexisting hematopoietic population and focal disruption of bony encasement (arrows). The underlying dura mater and arachnoid (*) are also diffusely expanded by dense infiltrates of leukemic elements. H&E staining. Compact bone, cb; frontal cortex, fc.

Variable amount of human CXCR4 positive T-ALL cells in murine model

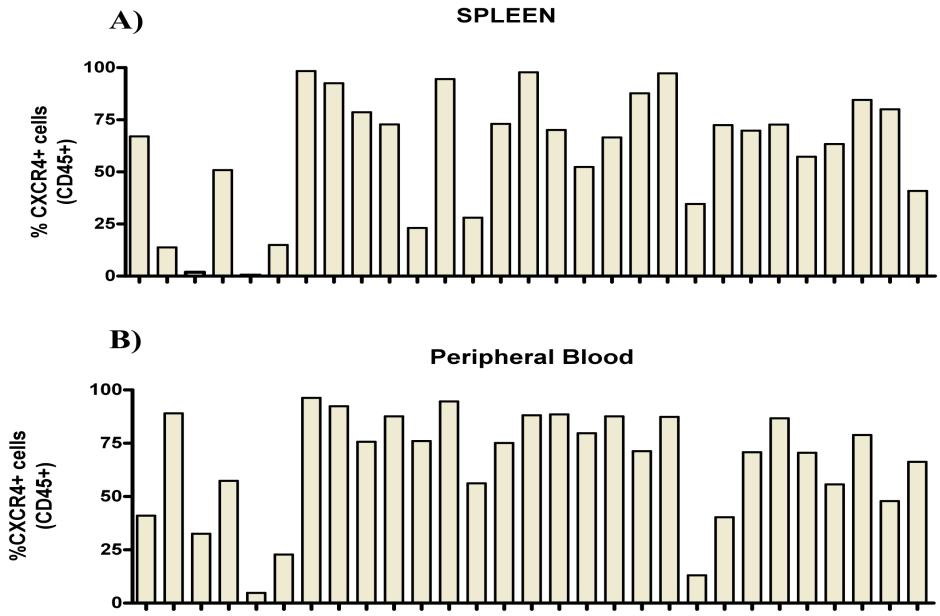

Figure 2: Graphics show the variable percentage of human CXCR4 positive cells (gated on CD45+) found in the spleen (A) and Peripheral Blood (B) of xenoengrafted mice. Data obtained by FCM. Each bar corresponds to mice xenografted with different patients. Y-axis shows the percentage of CXCR4+ cells, calculated on amount of CD45+ cells.

Influence of mouse microenvironment in CXCR4 expression at the T-cell surface

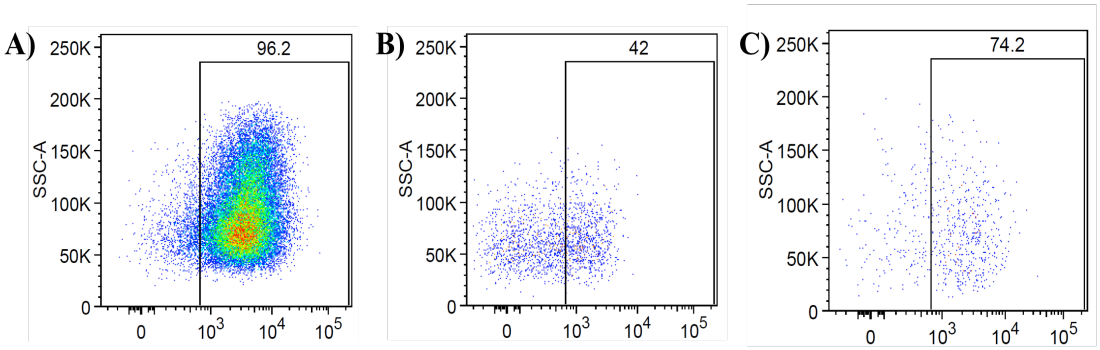

Figure 3: Figures show the variation of CXCR4 expression in the surface of Jurkat cells from *in vitro* culture (A) to *in vivo* environment (B/C). (A) Image shows that all Jurkat cells (100%) *in vitro* culture are positive for CXCR4; (B-C) figures show variation of CXCR4 expression when Jurkat cells are xenotransplanted in murine model; particularly, Jurkat cells extracted from the spleen (B) or peripheral blood (C) of xenografted mouse partially lose their positivity.

Variable amount of *CXCR4* are expressed by leukemic cells infiltrating mouse spleen

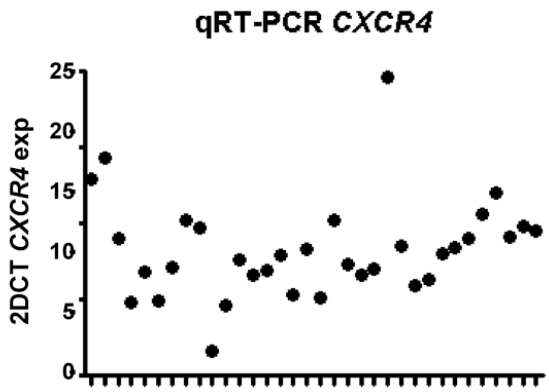

Figure 4: Dot plot show the expression levels of *CXCR4* in human T-ALL cells extracted from the spleen of different xenoengrafted mice. Data from qRT-PCR after normalization with the housekeeping gene, according to the formula formula $2^{-\Delta ct}$ [24]. Y-axis represents the RQ-value.

***CXCR4* transcription levels tend to correlate with the degree of CNS infiltration**

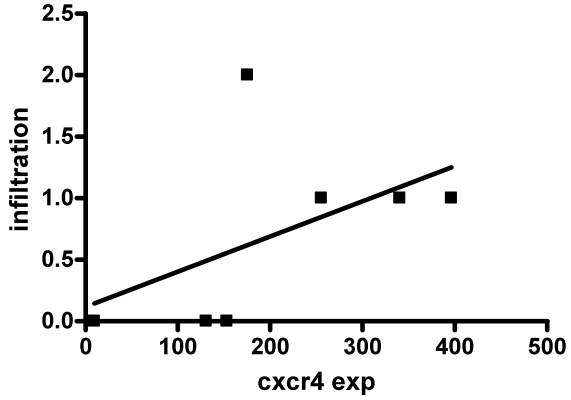

Figure 5: Preliminary data available for 7 cases. X-axis represents transcription level of *CXCR4*, Y-axis represents the degree of CNS infiltration at the meningeal level. Each dot corresponds to different sample. Pearson-correlation analysis was performed showing that results are not significant (*p*-value >.05).

TABLES

Table 1: Results of histological analysis for the first set of 18 xenografted mice are summarized in this table. The score associated to each different structures reflect its degree of infiltration.

#01		
Anatomical segment	**Structures**	**Degree of infiltration/colonization**
Head	Bone marrow	2
	Dental alveoli	0
	Oral and rhinopharingeal mucosa	0
	Orbital space	0
	Middle ear	0
	Meninges	0
Tot		2
#02		
Anatomical segment	**Structures**	**Degree of infiltration/colonization**
Head	Bone marrow	2
	Dental alveoli	0
	Oral and rhinopharingeal mucosa	1
	Orbital space	0
	Middle ear	0
	Meninges	1
Tot		4
#03		
Anatomical segment	**Structures**	**Degree of infiltration/colonization**
Head	Bone marrow	2
	Dental alveoli	0
	Oral and rhinopharingeal mucosa	1
	Orbital space	0
	Middle ear	1
	Meninges	1
Tot		5
#04		
Anatomical segment	**Structures**	**Degree of infiltration/colonization**
Head	Bone marrow	2
	Dental alveoli	0
	Oral and rhinopharingeal mucosa	1
	Orbital space	0
	Middle ear	1
	Meninges	1
Tot		5
#05		
Anatomical segment	**Structures**	**Degree of infiltration/colonization**
Head	Bone marrow	2
	Dental alveoli	1
	Oral and rhinopharingeal mucosa	1

	Orbital space	0
	Middle ear	2
	Meninges	2
Tot		8
#06		
Anatomical segment	**Structures**	**Degree of infiltration/colonization**
Head	Bone marrow	3
	Dental alveoli	0
	Oral and rhinopharingeal mucosa	2
	Orbital space	1
	Middle ear	2
	Meninges	2
Tot		10
#07		
Anatomical segment	**Structures**	**Degree of infiltration/colonization**
Head	Bone marrow	2
	Dental alveoli	0
	Oral and rhinopharingeal mucosa	0
	Orbital space	0
	Middle ear	0
	Meninges	2
Tot		4
#08		
Anatomical segment	**Structures**	**Degree of infiltration/colonization**
Head	Bone marrow	2
	Dental alveoli	0
	Oral and rhinopharingeal mucosa	0
	Orbital space	0
	Middle ear	0
	Meninges	0
Tot		2
#09		
Anatomical segment	**Structures**	**Degree of infiltration/colonization**
Head	Bone marrow	2
	Dental alveoli	0
	Oral and rhinopharingeal mucosa	0
	Orbital space	1
	Middle ear	1
	Meninges	1
Tot		5
#10		
Anatomical segment	**Structures**	**Degree of infiltration/colonization**
Head	Bone marrow	2
	Dental alveoli	0
	Oral and rhinopharingeal mucosa	0
	Orbital space	0
	Middle ear	0
	Meninges	1
Tot		3

#11		
Anatomical segment	**Structures**	**Degree of infiltration/colonization**
Head	Bone marrow	2
	Dental alveoli	0
	Oral and rhinopharingeal mucosa	1
	Orbital space	0
	Middle ear	0
	Meninges	1
Tot		4
#12		
Anatomical segment	**Structures**	**Degree of infiltration/colonization**
Head	Bone marrow	2
	Dental alveoli	0
	Oral and rhinopharingeal mucosa	1
	Orbital space	0
	Middle ear	0
	Meninges	2
Tot		5
#13		
Anatomical segment	**Structures**	**Degree of infiltration/colonization**
Head	Bone marrow	2
	Dental alveoli	0
	Oral and rhinopharingeal mucosa	1
	Orbital space	0
	Middle ear	1
	Meninges	1
Tot		5
#14		
Anatomical segment	**Structures**	**Degree of infiltration/colonization**
Head	Bone marrow	2
	Dental alveoli	0
	Oral and rhinopharingeal mucosa	0
	Orbital space	0
	Middle ear	0
	Meninges	1
Tot		3
#15		
Anatomical segment	**Structures**	**Degree of infiltration/colonization**
Head	Bone marrow	2
	Dental alveoli	0
	Oral and rhinopharingeal mucosa	0
	Orbital space	0
	Middle ear	0
	Meninges	0
Tot		2
#16		
Anatomical segment	**Structures**	**Degree of infiltration/colonization**
Head	Bone marrow	1
	Dental alveoli	0

	Oral and rhinopharingeal mucosa	0
	Orbital space	1
	Middle ear	0
	Meninges	0
Tot		2
#17		
Anatomical segment	**Structures**	**Degree of infiltration/colonization**
Head	Bone marrow	2
	Dental alveoli	0
	Oral and rhinopharingeal mucosa	0
	Orbital space	0
	Middle ear	0
	Meninges	0
Tot		2
#18		
Anatomical segment	**Structures**	**Degree of infiltration/colonization**
Head	Bone marrow	2
	Dental alveoli	0
	Oral and rhinopharingeal mucosa	0
	Orbital space	0
	Middle ear	0
	Meninges	0
Tot		2

Table2. Primers used for qRT-PCR

GENES	PRIMERS
CXCR4	Forward: 5'-CAGCAGGTAGCAAAGTGACG-3'
	Reverse: 5'-ATAGTCCCCTGAGCCCATTT-3'
GUS	Forward: 5'-GAAAATATGTGGTTGGAGAGC-3'
	Reverse: 5'-CGAGTGAAGATCCCCTTTTTA-3'

REFERENCES

1. Young, Jr, J.L., Ries, L.G., Silverberg, E., Horm, J.W. & Miller, R.W. (1986) Cancer incidence, survival, and mortality for children younger than age 15 years. Cancer, 58, 598±602.
2. Reiter, A., Schrappe, M., Ludwig, W.D., Hiddemann, W., Sauter, S., Henze, G., Zimmermann, M., Lampert, F., Havers, W. & Niethammer, D. (1994) Chemotherapy in 998 unselected childhood acute lymphoblastic leukemia patients. Results and conclusions of the multicenter trial ALL-BFM 86. Blood, 84, 3122±3133.
3. Bleyer, W.A. & Poplack, D.G. (1985) Prophylaxis and treatment of leukemia in the central nervous system and other sanctuaries. Seminars in Oncology, 12, 131±148.
4. Kreuger, A., Garwicz, S., Hertz, H., Jonmundsson, G., Lanning, M., Lie, S.O., Moe, P.J., Salmi, T.T., Schroder, H. & Siimes, M.A. (1991) Central nervous system disease in childhood acute lymphoblastic leukemia: prognostic factors and results of treatment. Pediatric Hematology and Oncology, 8, 291±299.
5. Pui CH, Relling MV, Downing JR. Acute lymphoblastic leukemia. N Engl J Med 2004;350(15):1535–48
6. Aifantis, I., Raetz, E. & Buonamici, S. Molecular pathogenesis of T-cell leukaemia and lymphoma. Nature Rev. Immunol. 8, 380–390 (2008).
7. Pui, C. H. & Howard, S. C. Current management and challenges of malignant disease in the CNS in paediatric leukaemia. Lancet Oncol. 9, 257–268 (2008).
8. Pui CH, Pei D, Sandlund JT, Ribeiro RC, Rubnitz JE, Raimondi SC, et al. Long-term results of St Jude Total Therapy Studies 11, 12, 13A, 13B, and 14 for childhood acute lymphoblastic leukemia. Leukemia 2009;24(2):371–82.
9. Holland M, Castro FV, Alexander S, Smith D, Liu J, Walker M, Bitton D, Mulryan K, Ashton G, Blaylock M, Bagley S, Connolly Y, Bridgeman J, Miller C, Krishnan S, Dempsey C, Masurekar A, Stern P, Whetton A, Saha V. RAC2, AEP, and ICAM1 expression are associated with CNS disease in a mouse model of pre-B childhood acute lymphoblastic leukemia. Blood. 2011 Jul 21;118(3):638-49. doi: 10.1182/blood-2010-09-307330. Epub 2011 May 23.
10. Buonamici S, Trimarchi T, Ruocco MG, Reavie L, Cathelin S, Mar BG, Klinakis A, Lukyanov Y, Tseng JC, Sen F, Gehrie E, Li M, Newcomb E, Zavadil J, Meruelo D, Lipp M, Ibrahim S, Efstratiadis A, Zagzag D, Bromberg JS, Dustin ML, Aifantis I.CCR7 signalling as an essential regulator of CNS infiltration in T-cell leukaemia. Nature. 2009 Jun 18;459(7249):1000-4. doi: 10.1038/nature08020.
11. Crazzolara R, Kreczy A, Mann G, Heitger A, Eibl G, Fink FM, Möhle R, Meister B. High expression of the chemokine receptor CXCR4 predicts extramedullary organ infiltration in childhood acute lymphoblastic leukaemia. Br J Haematol. 2001 Dec;115(3):545-53.
12. Christina Halsey, Mark TS Williams, Yasar Yousafzai, Klaus Rehe, Olaf Heidenreich, Josef Vormoor, Brenda Gibson[3]and Gerard Graham, Central Nervous System Involvement in a Xenograft Model of Pre-B Acute Lymphoblastic Leukaemia Is Associated with Dysfunctional CXCR4 Expression and Upregulation of the Neurotropic Chemokine Receptors CCR6 and CX3CR1, Blood, 2011: Abstract 3449.
13. Wu S, Gessner R, Taube T, et al. Chemokine IL-8 and chemokine receptor CXCR3 and CXCR4 gene expression in childhood acute lymphoblastic leukemia at first relapse. J. Pediatr. Hematol. Oncol. 2006; 28(4):216–220. [PubMed: 16679918]
14. SchenW, Bendall LJ, Gottlieb DJ, Bradstock KF (2001) The chemokine receptor CXCR4 enhances integrin-mediated in vitro adhesion and facilitates engraftment of leukemic precursor-B cells in the bone marrow. Exp Hematol 29: 1439–1447.
15. Lapidot T, Kollet O (2002) The essential roles of the chemokine SDF-1 and its receptor CXCR4 in human stem cell homing and repopulation of transplanted immune-deficient

NOD/SCID and NOD/SCID/B2mnull mice. Leukemia 16: 1992–2003.
16. Ma, Q., Jones, D., Borghesani, P.R., Segal, R.A., Nagasawa, T., Kishimoto, T., Bronson, R.T. & Springe, R.T.A. (1998) Impaired Blymphopoiesis, myelopoiesis, and derailed cerebellar neuron migration in CXCR4- and SDF-1-deficient mice. Proceedings of the National Academy of Sciences of the United States of America, 95, 9448±9453.
17. Rossi D, Zlotnik A. The biology of chemokines and their receptors. Annu Rev Immunol 2000;18:217–42.
18. Balkwill F. Cancer and the chemokine network. Nat Rev Cancer 2004;4(7):540–50. [PubMed: 15229479]
19. Mueller, A., Homey, B., Soto, H., Ge, N., Carton, D., Buchanan, M.E., McClanahan, T., Murphy, E., Yuan, W., Wagner, S.N., Barrera, J.L., Mohar, A., Verastegui, E. & Zlotnik, A. (2001) Involvement of chemokine receptors in breast carcinoma metastasis. Nature, 410, 50±56.
20. Stumm RK, Rummel J, Junker V, Culmsee C, Pfeiffer M, Krieglstein J, Hollt V, Schulz S (2002) A dual role for SDF-1/CXCR4 chemokine receptor system in adult brain: Isoform-selective regulation of SDF-1 expression modulates CXCR4-dependent neuronal plasticity and cerebral leukocyte
21. Mohle, R., Bautz, F., Rafii, S., Moore, M.A., Brugger, W. & Kanz, L. (1998) The chemokine receptor CXCR4 is expressed on CD341 hematopoietic progenitors and leukemic cells and mediates transendothelial migration induced by stromal cell-derived factor-1. Blood, 91, 4523±4530.
22. Mohle, R., Failenschmid, C., Bautz, F. & Kanz, L. (1999) Overexpression of the chemokine receptor CXCR4 in B cell chronic lymphocytic leukemia (B-CLL) is associated with increate functional response to stromal cell-derived factor-1. Leukemia, 13, 1954±1959.
23. Mohle, R., Schittenhelm, M., Failenschmid, C., Bautz, F., Kratz- Albers, K., Serve, H., Brugger, W. & Kanz, L. (2000) Functional response of leukaemic blasts to stromal cell-derived factor-1 correlates with preferential expression of the chemokine receptor CXCR4 in acute myelomonocytic and lymphoblastic leukaemia. British Journal of Haematology, 110, 563±572.
24. Meyer LH, Eckhoff SM, Queudeville M, Kraus JM, Giordan M, Stursberg J, Zangrando A, Vendramini E, Möricke A, Zimmermann M, Schrauder A, Lahr G, Holzmann K, Schrappe M, Basso G, Stahnke K, Kestler HA, Te Kronnie G, Debatin KM. Early relapse in ALL is identified by time to leukemia in NOD/SCID mice and is characterized by a gene signature involving survival pathways. Cancer Cell. 2011 Feb 15;19(2):206-17. doi: 10.1016/j.ccr.2010.11.014. Epub 2011 Feb 3.
25. Aiuti, A., Webb, I.J., Bleul, C., Springer, T. & Gutierrez-Ramos, J.C. (1997) The chemokine SDF-1 is a chemoattractant for human CD341 hematopoietic progenitor cells and provides a new mechanism to explain the mobilization of CD341 progenitors to peripheral blood. Journal of Experimental Medicine, 185, 111±120.

CHAPTER 3

Gene Expression Profiling analysis of ALL pediatric patients with Central Nervous System infiltration at diagnosis

ABSTRACT

Central nervous system (CNS) infiltration by leukemic cells in children with *de novo* acute lymphoblastic leukemia (ALL) is until the present day a major concern. Padiatric patients with this unfavorable characteristic have a lower event-free survival and undergo intensive therapy directed against the central nervous system. The molecular mechanisms contributing to central nervous system infiltration are unclear. In order to explore potential biologic properties of ALL cells infiltrating the central nervous system, we applied whole-genome gene expression profiling to identify differently expressed genes that may characterize this phenomenon comparing ALL patients with (CNS+) and without (CNS-) central nervous system infiltration. We analyzed the gene expression profiles of pediatric patients with *de novo* acute lymphoblastic leukemia committed to either the T- or B-cell lineage, of which 4 and 7 patients respectively, were positive for central nervous system infiltration at diagnosis. However we failed to find a strong signature that could identify CNS+ and CNS- patients. Results underlined the difficulty to study this phenomenon directly on human patients with this approach, as a high heterogeneity is present inside both T- and B-ALL and different mechanisms could drive blast cells in the CNS environment.

INTRODUCTION

Childhood Acute lymphoblastic leukemia (ALL) is an aggressive tumor characterized by abnormal proliferation of lymphoblastic progenitor cells. ALL is committed to either the B- (B-ALL ~85%) and the T- (T-ALL ~15%) cell lineage and represents a large heterogeneous group with distinct morphology, immunophenotype and genetic abnormalities that are used to stratify patients into risk-groups ranging from standard-risk to high-risk [1][2]. The presence of lymphoblasts infiltrating the Central nervous system (CNS) is an event that can be present both at diagnosis (<5%) and relapse (~30-40%)[3][4] in ALL patients and is an unfavorable feature that stratifies patients in the high risk group. The presence of CNS infiltration is not always accompanied by clinical symptoms and is usually detected through a lumbar puncture of the cerebrospinal fluid (CSF) [3]. Over the past years, the 5-year event free survival rate (EFS) of ALL pediatric patients has considerably improved due to more appropriate risk stratification and treatment. Although the overall EFS has increased significantly, reaching percentages above 85% [5], there are still patients that remain of major concern, such as patients with CNS infiltration [6]. In the seventies and eighties of last century, leukemic patients with CNS infiltration were mostly treated with cranial irradiation, even if cranial irradiation caused many secondary diseases, such as secondary cancer development. Recently, numerous efforts have been made to reduce the use of radiations and two studies demonstrated that cranial irradiation could be completely omitted using intensive triple intrathecal therapy (methotrezate, hydrocortisone and cytarabine) [3][4] [7]. Even if at reduced dosage, cranial irradiation is still recommended to treat patients that have been assigned to the high-risk group with CNS relapses, such as those that presented CNS leukemia at diagnosis (>5 White Blood Cells/μL with blasts) and/or T-cell phenotype ALL with high WBC counts [8].

Several studied investigated mechanisms used by lymphoblasts to infiltrate the CNS, but results are variable. Two studies tried to identify a common mechanism used by ALL cells to infiltrate the CNS, without distinguishing between B- and T- lineage ALL; Gunnar Cario and colleagues studied the differences in gene expression between children with- and without- CNS infiltration in ALL, proposing the up-regulation of interleukin-15 as predictor of the ability of blasts to infiltrate the CNS. However, these

results have not been reproduced in other studies [9]. Indeed, Crazzolara and colleagues focused their attention on CXCR4, showing that higher expression levels of this chemokine receptor could be predictive of blasts ability to infiltrate extramedullary organs in ALL pediatric patients. However, in their work, data regarding CNS infiltration were not shown [10]. On the contrary, other studies investigated possible mechanisms of CNS infiltration focusing in specific ALL subgroups; Buonamici and colleagues identified in the CCR7 expression the key signal directing T-lymphoblasts towards the CNS using a murine model xenografted with human T-ALL cell lines. Also the latter study lacks confirmation by and validation in further studies [11]. Holland and colleagues underlined an important role played by RAC2, AEP and ICAM1 expression in determining CNS involvement in a mouse model xenografted with human pre-B pediatric ALL cells [12]. Instead, in another study performed in a pre-B ALL murine model, CNS-homing cells showed CXCR4 down-regulation both at the transcriptional and protein level, complicating the understanding of the role played by CXCR4 in determining CNS infiltration [13]. Moreover, another study showed that in children with ALL relapses associated to testicles or CNS leukemia blast cells had a significantly lower CXCR4 level than blasts from children with relapsed disease isolated to the bone marrow [28].

In conclusion, different results have been found in these works and the mechanism/s used by ALL cell to infiltrate the CNS is/are still poorly understood. As the mechanisms related to pathogenesis of CNS infiltration are unknown, the creation of a target-directed therapy that could prevent this phenomenon is still a big challenge. In this study we aimed to investigate the presence of a specific gene expression signature that could characterize ALL patients with (CNS+) and without (CNS-) CNS infiltration at diagnosis. To achieve this aim we used the genome-wide Gene Expression Profiling approach on specimens of pediatric ALL patients enrolled in the "Associazione Italiana Ematologia-Oncologia Pediatrica" (AIEOP) ALL-2000 protocol and we separately analyzed a T-ALL and a B-ALL patients at diagnosis. For each cohort, we compared CNS+ and CNS- patients; in this way, differentially expressed genes between the two groups (CNS+ vs. CNS-) were addressed. Moreover, we investigated in patients our

results previously obtained from studies of zebrafish and murine models; in particular, we analyzed the expression levels of *CXCR4* in a T-ALL cohort.

MATERIAL AND METHODS

Human leukemia samples

Bone marrow or Peripheral Blood aspirates were collected from pediatric patients with B-ALL or T-ALL at diagnosis. All patients selected for this study were enrolled in the AIEOP ALL-2000 protocol. Patients' parents or legal guardians did provide written informed consent for the use of patient material for biomedical research in accordance with the Declaration of Helsinki. For gene expression profiling analysis we used the following two cohorts:

T-ALL cohort: 45 pediatric patients at diagnosis of T-ALL enrolled in the AIEOP 2000 protocol. PB or BM specimens were available to perform GEP. Four patients showed CNS infiltration at diagnosis with more than 5 lymphoid blasts/µl in the cerebrospinal fluid (CSF) and 41 without CNS Infiltration. In Table 1 we reported the biological and clinical features of T-ALL patients analyzed in this study.

B-ALL cohort: 58 pediatric patients at diagnosis of B-ALL, enrolled in the AIEOP 2000 protocol. PB or BM specimens were available to perform GEP. Seven patients showed CNS infiltration at diagnosis with more than 5 lymphoid blasts/µl in the cerebrospinal fluid (CSF) and 51 without CNS Infiltration. In Table 2 we reported the biological and clinical features of B-ALL patients analyzed in this study.

RNA isolation, quality controls and quantification

Mononucleated cells (MNC) were isolated via the Ficoll-Paque method (GE Healthcare companies, Buckinghamshire, United Kingdom), which is based on density gradient centrifugation. Total RNA from MNC derived from bone marrow (BM) or peripheral blood (PB) aspirates was extracted using Trizol (Invitrogen, Karlsruhe, Germany), according to manifactures' instructions. To perform gene expression experiments, extremely high quality of total RNA is required. To assess the quality of RNA, Agilent Bioanalyzer Expert 2100 (Agilent Technologies, Waldbronn, Germany) was used. RNA

concentration was determined using QBit 2.0 Fluorometer (Life Technology, Carlsbad, California, U.S.). NanoDrop ND-1000 spectrophotometer (NanoDrop Technologies Inc, Wilmington, DE). The instruments provide the sample concentration in ng/µl and the absorbance of the sample at 260nm and 280nm. The ratio (260/280) ranging from 1.8 to 2.1 indicate good quality of RNA (ratio < 1.8 means protein contamination and ratio > 2.1 RNA degradation and truncated transcripts).

Gene expression profiling

Only RNA samples that passed the high quality controls were diluted to 100ng in a total volume of 3µl DEPC treated water to perform gene expression experiments. *In vitro* transcription, hybridization and biotin labelling were performed according to GeneChip 3'IVT Express kit protocol (Affymetrix, Santa Clara, CA). The Affymetrix GeneChip Scanner was used to measure all intensities of the signals of each probe set on the GeneChip and stores all signals in a .DAT file (Raw image). Integrated software converts all raw signals into numbers, which were stored in a .CEL file. All GEP profiles used in these experiments were assessed for their comparability and quality, using different quality controls: Scale Factor, number of present calls, internal probe calls, Poly-A controls and the ratio GAPDH/β-actin 3'/5'.

Statistical analyis

Microarray data (.CEL files) were analyzed using Command Expression Console (Affymetrix). R-Bioconductor (Version 2.15.3) was used to analyze the .CEL files data in an unsupervised and supervised manner. Unsupervised analysis (Class Discovery) is a learning algorithm that clusters unspecified specimens together based on similar gene expression patterns and is therefore highly unbiased. Supervised analysis (Class Comparison, Class Prediction) is a learning algorithm that uses already defined (labeled) data in order to identify a set of genes that characterize the pre-specified data. The .CEL files first were normalized using the justRMA algorithm. justRMA is an algorithm fulfilling 2 steps, namely background adjustment of all the probe sets present on the GeneChip and quantile normalization to make the values of all the GeneChips comparable. In order to find differently expressed probe sets we applied a Shrinkage t-test on the normalized .CEL files [19]. We used a local false discovery rate (lfdr) as

correction of the p-value; a ldfr < 0,05 was considered significant for genes differently expressed between 2 groups. Differently expressed probe sets derived from the Shrinkage t-test were used for clustering analysis. Hierarchical clustering analysis was used to clusterize the specimens in an unsupervised manner using Euclidean Distance and Ward's Method. Euclidean Distance and Ward's Method compute the distance between two groups in a metric space. qRT-PCR statistical analyses and graphs were generated by GraphPad Prism software (Version 5.0.0).

Gene Ontology analysis

Differently expressed genes between CNS infiltrate (CNS+) and non-infiltrated (CNS-) ALL pediatric patients were analyzed using Database for Annotation, Visualization and Integrated Discovery (DAVID) v6.7.

RESULTS

Gene Expression Profiling of pediatric T-ALL and B-ALL patients at diagnosis

With this project we aimed to investigate the presence of a specific gene expression signature that could distinguish ALL patients with (CNS+) or without (CNS-) Central Nervous System infiltration at diagnosis. In order to identify different expression signatures between CNS+ and CNS- ALL patients at diagnosis, we performed Gene Expression Profiling (GEP) experiments (using Affymetrix HG U133 Plus 2.0 arrays) in 45 T-ALL and 58 B-ALL pediatric patients enrolled in the AIEOP 2000 protocol.

CNS infiltration in pediatric T-ALL patients

We started with the analysis of 45 T-ALL pediatric patients, including 4 CNS+ cases. Using supervised analysis (Shrinkage T-test, lfdr <0,05), we identified 582 probe sets differently expressed between CNS+ (n=4) versus CNS- (n=41) patients (lfdr < 0.05). Unsupervised hierarchical clustering analysis (using the 582 probe sets differently expressed) separated the 45 patients in two main branches (figure 1); the branch on the right comprised only CNS- patients, while in the left arm the CNS+ patients clustered together with a small group of 5 CNS- patients. Interestingly, the 4 CNS+ patients

clustered together based on a similar gene expression signature using the 582 probe sets (517 genes) differently expressed between CNS+ versus CNS- patients. Particularly, we found 125 and 391 genes up-regulated in CNS+ and CNS- patients, respectively (table 3). However, the majority of genes differently expressed between CNS+ and CNS- groups showed a low fold change (FC) which could be attributed to the small number of CNS+ samples available for this analysis and by the presence of a group of CNS- patients that behaved similar to CNS+ cases. The observation that some T-ALL CNS- patients behaved similar to CNS+ cases flattened differences between groups (CNS+ vs. CNS-) and contributes to the absence of a strong signature for patient with CNS infiltration at diagnosis. Moreover, these results lead to the assumption that CNS+ T-ALL patients are a heterogeneous group and mechanisms that drive their T-lymphoblasts towards the CNS could be diverse, impairing the extraction of a strong gene expression signature. This hypothesis is strengthened by results of unsupervised analysis (figure 2): CNS+ patients cluster independently of one another, suggesting a weak similarity in gene expression profiling. Interesting, the phenomenon of CNS infiltration at diagnosis in T-ALL seems not to depend on the cytogenetic subgroup of patients that was predicted using a GEP classifier for cytogenetic subgroup [16]. In fact, two patients with CNS infiltration presented a *TALLMO* signature, while the others were predicted to be *TLX1* and *TLX3*.

We further investigated the list of 517 genes differently expressed between CNS+ versus CNS- patients at the molecular level, in order to inquire more detailed information on potential gene networks that may be related to CNS infiltration. Gene ontology analysis using DAVID software revealed a significant (p-value=0,005) up-regulation of the Wnt/β-catenin pathway (figure 3) in CNS- patients.

In the light of a previous work [10] and results found in the chapter 1 and chapter 2, we decided to investigate the *CXCR4* expression in T-ALL pediatric patients. The dot plots showed how in general blast cells of the T-lineage express high levels of *CXCR4* (figure 5), independently from CNS infiltration. Of note, we can notice a patient with lower expression of *CXCR4* inside the group of CNS+ patient that strengths our hypothesis of more than one mechanism that can drive blast cells in the CNS environment. This analysis shows that *CXCR4* transcription in blast cells is very high both in patients with-

and without- CNS infiltration. We have to remember that with the previous results (chapter 1 and 2) we showed that expression levels of *CXCR4* are not necessary to infiltrate the CNS, but could confer an increased ability for lymphoblasts to infiltrate this environment.

CNS infiltration in pediatric B-ALL patient

We continued gene expression analysis in a cohort of 58 B-ALL patients, including 7 CNS+ and 51 CNS- cases. Supervised analysis using Shrinkage t-test with lfdr correction (lfdr<0.05) resulted in 460 probe sets differently expressed between CNS+ and CNS- B-ALL patients at diagnosis. The dendogram of hierarchical clustering revealed a highly similar gene expression signature for the 7 CNS+ B-ALL patients and 11 CNS- B-ALL patients that cluster together in one branch (figure 4). . We further investigated the list of probe sets (343 known genes) differently expressed between CNS+ versus CNS- patients. Particularly, 138 genes and 206 genes were up-regulated in the CNS+ and CNS- group respectively. Also in this case genes present low FCs that could be attributed to the presence of a group of CNS- patients with a signature similar to that of CNS+ cases. We performed gene ontology analysis, using DAVID software and identified in the B-ALL cohort, gene networks related to cytoskeleton remodeling pathways. In table 4 we reported genes and pathways related to cytoskeleton remodeling that were found to be down-regulated in CNS+ patients. This may indicate that pathways related to cytoskeleton remodeling could play a role in the mechanisms used by B-ALL cells to infiltrate the CNS.

Expression of IL-15 in T-ALL and B-ALL

CNS infiltration is more likely to occur in T-ALL than in B-ALL patients [8]. B- and T-ALL patients do not differ only in cell lineage but also in genetic landscape, transcriptome and treatment. At this point, we wanted investigate in both the T-ALL and B-ALL cohort, the expression of *Interleukin-15*, a gene that has been shown to be important in determining CNS invasion [9]. Moreover, we were interested in *IL-15* because it can enhance *CXCR4* transcription [27]. In our cohort, *IL-15* is significantly more expressed in T- compared to the B-lineage ALL samples (figure 6).

DISCUSSION

In the previous chapters of this thesis the gene networks that seem to facilitate the entrance of lymphoblasts in the CNS were studied in animal models (zebrafish and mouse xenografted with human T-ALL cells). Here we investigated this aspect in pediatric patients samples using whole transcriptome analysis. We examined the presence of gene expression profiling signatures that could distinguish patients with (CNS+) or without (CNS-) CNS involvement.

We started our analysis on a cohort of 45 T-ALL pediatric patients at diagnosis in which 4 cases where CNS+. Applying supervised analysis we identified 582 known genes differently expressed between CNS+ and CNS- T-ALL patients (lfdr<0.05), however these genes presented a low FC which is indicative of a limited distinction in gene expression profiling between the two groups (CNS+ vs. CNS-). Interesting, gene ontology analysis (DAVID) identified an up-regulation of the Wnt/β-catenin pathway in the group without CNS infiltration; in Chapter 1 of this thesis we already found that the activation of this pathway was present in the zf line (*hlk*), which showed low levels of CNS infiltration. One might speculate that an increased activation of the Wnt/β-catenin pathway determines a reduced ability of T-lymphocyte to infiltrate the CNS.

Next we applied a supervised analysis on patients with *de novo* B-ALL and we identified 460 probe sets differently expressed between CNS+ and CNS- B-ALL patients. However, also in this case the FCs were not high. For the B-ALL cohort gene ontology analysis showed that several genes up- (n=2) and down- (n=10) regulated were directly involved into cytoskeleton remodelling pathways, suggesting that CNS infiltration could be associated with alterations in the cytoskeleton. However, as indicated by the low FCs also for B-ALL we failed to find a strong signature that distinguished patients with- and without- CNS involvement.

Both these two gene expression analyses on a T- and B-ALL cohort failed to identify a strong signature that identified patients with CNS involvement at diagnosis. The intricacy to find a strong signature that identifies CNS+ cases in both T- and B-ALL cohorts could be due to several causes; 1) the small number of patient analyzed (n=4 CNS+T-ALL and n=7 CNS+ B-ALL); 2) the presence of a group of patients without

CNS infiltration that cluster together with the CNS+ cases, flattening the difference between CNS+ and CNS- and 3) the mechanisms that allow lymphoblasts to infiltrate the CNS could be many and entailing different gene networks activation and different gene expression profiles for samples of ALL patients with CNS disease.

It is surprising to observe how in both T- and B-ALL cohort, a group of patients without CNS infiltration had a very similar signature to CNS+ cases. In this respect we should remember that the current methodology to diagnosis the presence of CNS infiltration in pediatric ALL patients uses cytological analysis of a smear of CSF. Several studies have already shown the importance of using more sensitive techniques, such as flow cytometry (FCM) or PCR-methods, to detect CNS disease. In fact, using FCM and PCR for CSF analysis, several patients classified as CNS- resulted having a subclinical infiltration of the CSN [17][18][19][20][21] and the presence of small numbers of leukocytes in the CSF at diagnosis remains a controversial risk factor [22][23][24]. As the classification of CNS disease is not still perfect, we can speculate that also our cohorts might include patients with subclinical CNS infiltration among the CNS- group, which could partially explain the rather weak gene expression signature for CNS+ patients. Moreover, the CNS- cases that clustered together with the CNS+ cases could represent this group. Of course that is only a speculation and further studies need to be performed to clarify this hypothesis.

In this work, we also investigated if our previously results found to be related to an increased ability to infiltrate the CNS in animal models (Chapter 1 and 2) could be transferred to human ALL samples. Particularly, we investigate the levels of *CXCR4* transcription in the T- ALL cohort and we found a high expression of *CXCR4* both in CNS+ and CNS- patients. Notably, within the group of T-ALL CNS+ patients, we found 3 patients with very high- and one patient with lower- *CXCR4* expression levels. We can speculate that these patients reflect both the zebrafish models with high- (*hMYC-ER*) and low (*hlk)* expression of *CXCR4.* When we look back at chapter 1, the expression levels of *CXCR4* did not discriminate between CNS+ and CNS- specimens, but positive correlated with the seriousness of CNS infiltration. However, also patients without CNS infiltration showed high *CXCR4* transcription levels indicating that expression levels of *CXCR4* alone are not indicative of higher degrees of CNS

infiltration in human patients. At this point, it is necessary to underline that the phenomenon of CNS infiltration in human patients can not directly be compared to CNS infiltration in animal models: whereas CNS infiltration in zebrafish and murine models consisted of massive infiltration at the meningeal levels, CNS infiltration in human patients referred to blast cells (>5 WBC/μL with blasts) detected in the CSF and we might expect that the biological phenomenon we are observing is not exactly the same. In fact, in animal models we were in front of an extreme situation that could represent CNS leukemia in patients in the 1970s [25] fortunately no longer observed in human patients. The passage from animal model and human patients is not so linear. As several events related to microenvironment can influence *CXCR4* transcription [26], further analysis need to investigate not only the expression level of *CXCR4*, but also its regulation in human T-ALL.

Analysis of expression of *IL-15*, an interleukin related to the ability to infiltrate the CNS [9] and capable to increase *CXCR4* transcription, revealed increased expression levels in T- compared to B- lineage. Interesting, B-cells lose the ability to respond to CXCL12 during maturation, even if the chemokine receptor CXCR4 continues to be highly expressed on the membrane surface [14][15]. These observations suggest that T-lymphoblasts present both higher expression of *IL-15* and functional CXCR4, two factors that seem advantageous for lymphoblasts to infiltrate the CNS and which could partially suggest why the incidence of CNS infiltration is higher in T- compared to B-ALL.

Further studies are needed to understand if mechanisms favoring CNS invasion observed in animal models can be translated to human patients. Moreover, further studies are required that directly address CNS+ disease in human patients.

FIGURES

Supervised analysis of the T-ALL cohort using the 582 probe sets differently expressed between CNS+ and CNS- patients at diagnosis

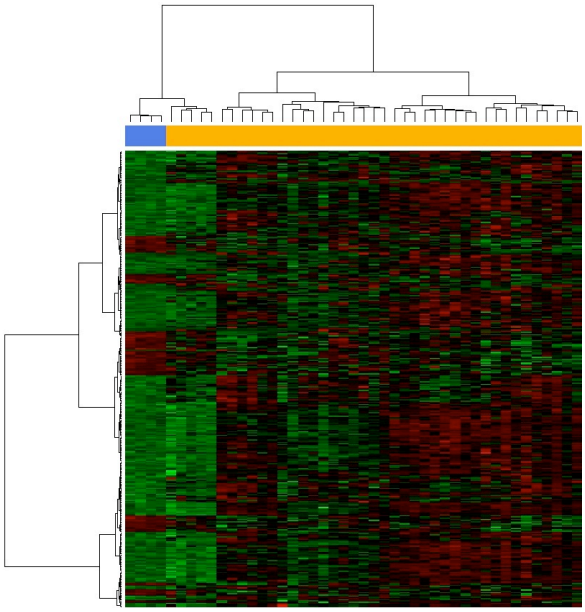

Figure 1: CNS+ patients are underlined in blue (n=4), CNS- patients in orange (n=41). Hierarchical clustering of the T-ALL patients (n=45) was made using the 582 probe sets found with the Shrinkage T-test with lfdr <0.05. X-axis represents patients while the Y-axis shows the probe sets of the list. Euclidean distance and Ward's method were used for clustering. The dendogram reveals two main branches; the branch on the right comprises only CNS- patients, while in the left branch the CNS+ patients clustered together with 5 CNS- patients.

Unsupervised analysis hierarchical clustering of T-ALL patients at diagnosis

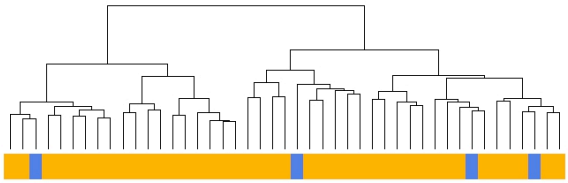

Figure 2: CNS+ patients are underlined in blue (n=4), CNS- patients in orange (n=41). CNS+ patients (blue) cluster independently in different branches in an unsupervised analysis, revealing a different gene expression profiling between samples.

Activation of Wnt/β-catenin pathway in CNS- T-ALL pediatric patients

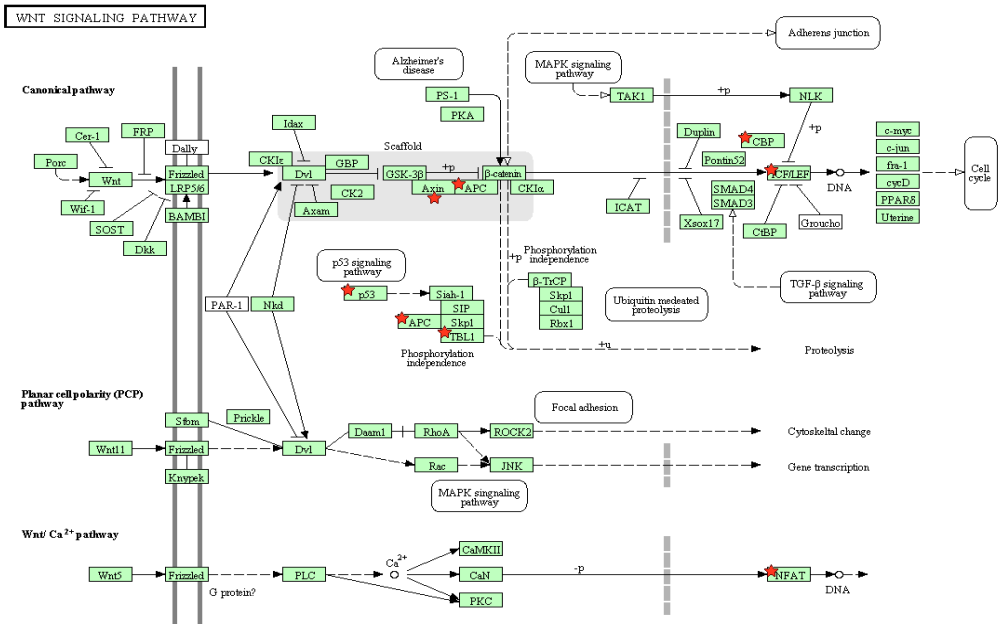

Figure 3: Pathway analyses tools DAVID 6.7 revealed a significant activation of the Wnt/β-catenin pathway in T-ALL patients without CNS infiltration. Red stars indicate genes of the Wnt/β-catenin pathway that resulted significantly upregulated in the gene list derived from the comparison between CNS- vs. CNS+ groups.

Supervised Analysis of the B-ALL cohort using the 460 probe sets differently expressed between CNS+ and CNS- patients at diagnosis

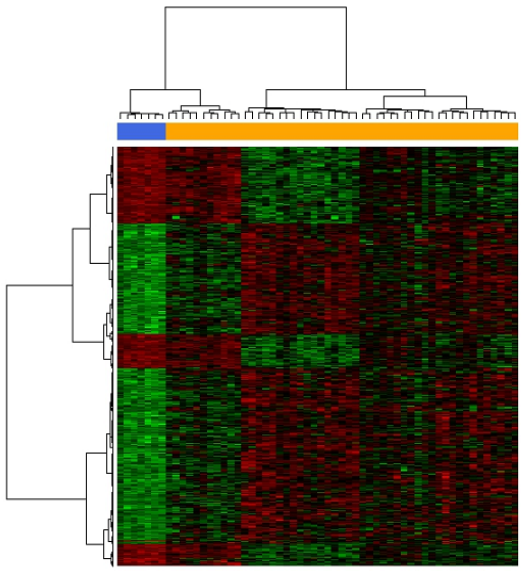

Figure 4: Hierarchical clustering of the B-ALL patients (n=58) with CNS infiltration (blue) and without CNS infiltration (orange) at diagnosis based on a list of 460 probe sets obtained after applying a Shrinkage T-test with lfdr <0.005. The CNS+ B-ALL patients cluster together with a highly similar gene expression signature. X-axis represents the patients and the Y-axis the genes. For clustering we used Euclidian distance and Ward's method.

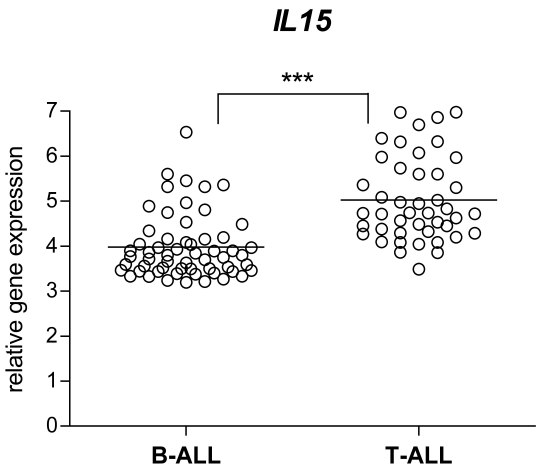

Figure 6: Dot plot for *IL-15* in T-ALL and B-ALL. The dot plot shows expression levels of *IL-15* for T-ALL and B-ALL patients. Data show higher expression levels in T- compare to B-lineage. X-axis represents the T- and B-ALL subgroups and the Y-axis the genes expression data for *IL-1*

***CXCR4* expression in a cohort of T-ALL**

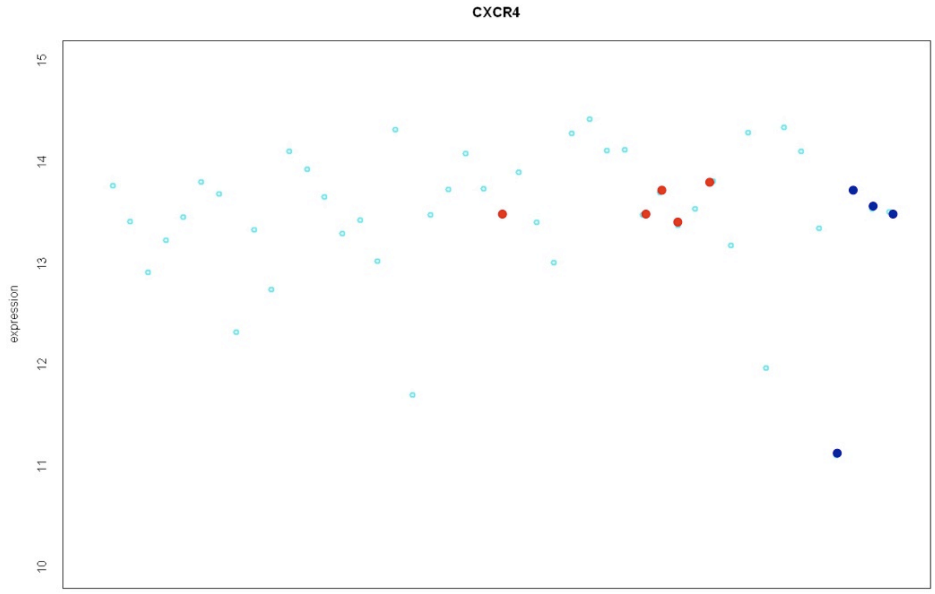

Figure 5: Graph represents gene expression profiling (GEP) data for the expression of a probe set representing the *CXCR4* gene. Each dot corresponds to one patient. The expression value of *CXCR4* for each patient is given in log2 scale after normalizing GEP data with justRMA algorithm normalization. X-axis represents patients and the Y-axis the genes expression. Dot plot shows *CXCR4* expression levels on a cohort of 45 T-ALL pediatric patients. The blue dots represent the 4 CNS+ cases. In red are underlined CNS- patients that clusterized with CNS+ cases in the supervised analysis.

TABLES

Characteristic	CNS + (n=4)		CNS - (n=41)	
	Number	%	Number	%
Age(years): 0 < 10	1	25	23	56,1
≥ 10	3	75	18	43,9
Subtype:				
TAL/LMO	2	50	21	51,2
TLX1	1	25	5	12,2
TLX3	1	25	8	19,5
HOXA	0	0	7	17,1
Gender:				
Male	3	75	34	82,9
Female	1	25	7	17,1
Relapse				
Yes	1	25	9	21,9
No	3	75	32	78,1
Prednisone Response:				
PGR	1	25	26	63,4
PPR	1	25	13	31,7
N.D.	2	50	2	4,9
RISK STRATIFICATION				
High	0	0	19	46,3
Medium	3	75	8	19,5
Standard	1	25	13	31,7
N.D	0	0	1	2,5
WBC at DIAGNOSIS				
< 10.000	0	0	3	7,3
10.000 < 50.000	1	25	10	24,4
50.000 < 100.000	1	25	6	14,6
≥ 100.000	0	0	20	48,8
N.D.	2	50	2	4,9

Table 1: Biological and clinical characteristics of T-ALL patients (n=45). Abbreviations: CNS = Central Nervous System, N.D. = No data, WBC = White blood count at diagnosis, PGR = prednisone good response; PPR = prednisone poor response.

Characteristic		CNS+ (n=7)		CNS- (n=51)	
		Number	%	Number	%
Age(years):	0 < 10	5	71,4	35	68,6
	≥ 10	2	28,6	16	31,4
Subtype:	- B-others	4	57,1	45	88,2
	- Hyperdiploïd	2	28,6	4	7,8
	- *AF4-MLL*	1	14,3	1	2,0
	- *ETV6-AML1*	0	0,0	1	2,0
	- *E2A-PBX1*	0	0,0	0	0,0
	- *BCR-ABL1*	0	0,0	0	0,0
Gender:	Male	6	85,7	33	64,7
	Female	1	14,3	18	35,3
Relapse:	Yes	2	28,6	20	39,2
	No	5	71,4	31	60,8
Prednisone Response:	PGR	1	14,3	10	19,6
	PPR	1	14,3	41	80,4
	N.D.	5	71,4	0	0,0
Risk stratification based on MRD:	- High	0	0,0	7	13,7
	- Medium	4	57,1	29	56,9
	- Standard	1	14,3	13	25,5
	- N.D.	2	28,6	2	4,0
WBC:	< 10.000	0	0,0	13	25,5
	10.000 < 50.000	1	14,3	23	45,1
	50.000 < 100.000	0	0,0	7	13,7
	≥ 100.000	3	42,9	8	15,7
	N.D.	3	42,9	0	0,0

Table 2: Biological and clinical characteristics of B-ALL patients (n=58). B-others: B-ALL patients without known translocations .Abbreviations: CNS = Central Nervous System, N.D. = No data, WBC = White blood count at diagnosis, PGR = prednisone good response; PPR = prednisone poor response.

Table 3. Genes differently expressed between CNS+ and CNS- T-ALL patients

Probe Set	Gene Symble	Up-regulated in	FC
217484_at	CR1	CNS+	1,34
214660_at	ITGA1	CNS+	1,34
205544_s_at	CR2	CNS+	1,31
1560359_at	PELO	CNS+	1,28
220307_at	CD244	CNS+	1,26
244710_at	LRGUK	CNS+	1,23
236910_at	MRPL39	CNS+	1,21
1555513_at	PIAS2	CNS+	1,19
1569827_at	ATG7	CNS+	1,19
235913_at	ZNF880	CNS+	1,19
224036_s_at	LMBR1	CNS+	1,19
1559042_at	NDUFB6	CNS+	1,17
1554999_at	RASGEF1B	CNS+	1,17
235473_at	MED6	CNS+	1,17
227751_at	PDCD5	CNS+	1,17
225651_at	UBE2E2	CNS+	1,16
214012_at	ERAP1	CNS+	1,15
1555610_at	AGK	CNS+	1,15
232026_at	HERC4	CNS+	1,15
220803_at	STAMBPL1	CNS+	1,14
218589_at	LPAR6	CNS+	1,14
1562271_x_at	ARHGEF7	CNS+	1,14
224596_at	SLC44A1	CNS+	1,14
204918_s_at	MLLT3	CNS+	1,14
215268_at	KIAA0754	CNS+	1,14
232295_at	GFM1	CNS+	1,14
1552835_at	DENND1B	CNS+	1,14
228506_at	NSMCE4A	CNS+	1,14
211200_s_at	EFCAB2	CNS+	1,13
218597_s_at	CISD1	CNS+	1,13
1554309_at	EIF4G3	CNS+	1,12
216115_at	NF1	CNS+	1,12
1556599_s_at	ARPP21	CNS+	1,12
1560734_at	LOC727924	CNS+	1,12
231995_at	C9orf82	CNS+	1,12
224173_s_at	MRPL30	CNS+	1,12
219366_at	AVEN	CNS+	1,12
227585_at	ATAD1	CNS+	1,12
235927_at	XPO1	CNS+	1,11
237856_at	RAP1GDS1	CNS+	1,11
202979_s_at	CREBZF	CNS+	1,11
218437_s_at	LZTFL1	CNS+	1,11
203211_s_at	MTMR2	CNS+	1,11

236481_at	FAH	CNS+	1,11
225278_at	PRKAB2	CNS+	1,11
235810_at	ZNF182	CNS+	1,11
243957_at	LOC400464	CNS+	1,10
238295_at	C17orf42	CNS+	1,10
226802_s_at	LOC96610	CNS+	1,10
226790_at	MORN2	CNS+	1,10
215425_at	BTG3	CNS+	1,10
204578_at	PPIP5K1	CNS+	1,10
214543_x_at	QKI	CNS+	1,10
205518_s_at	CMAHP	CNS+	1,10
226009_at	DPCD	CNS+	1,10
1556613_s_at	DPY19L4	CNS+	1,10
217633_at	URB1	CNS+	1,10
230516_at	C7orf30	CNS+	1,10
223591_at	RNF135	CNS+	1,10
215283_at	LOC339290	CNS+	1,10
232312_at	PPP6R3	CNS+	1,10
210219_at	SP100	CNS+	1,09
227187_at	CBLL1	CNS+	1,09
1553133_at	C9orf72	CNS+	1,09
215922_at	REPS1	CNS+	1,09
201436_at	EIF4E	CNS+	1,09
231970_at	C14orf118	CNS+	1,09
227575_s_at	C14orf102	CNS+	1,09
237076_at	NCSTN	CNS+	1,09
212572_at	STK38L	CNS+	1,09
214917_at	PRKAA1	CNS+	1,09
1557360_at	LRPPRC	CNS+	1,09
210531_at	NR2C1	CNS+	1,09
1563674_at	FCRL2	CNS+	1,09
242370_at	MTHFD2L	CNS+	1,09
217503_at	STK17B	CNS+	1,09
222444_at	ARMCX3	CNS+	1,09
202817_s_at	SS18	CNS+	1,08
227162_at	ZBTB26	CNS+	1,08
227766_at	LIG4	CNS+	1,08
221523_s_at	RRAGD	CNS+	1,08
1564482_at	ATP5O	CNS+	1,08
231066_s_at	CLCN4	CNS+	1,08
217427_s_at	HIRA	CNS+	1,08
228351_at	HEATR1	CNS+	1,08
1567213_at	PNN	CNS+	1,08
235162_at	MDM4	CNS+	1,08
211067_s_at	GAS7	CNS+	1,08

226036_x_at	CASP2	CNS+	1,08
219968_at	ZNF589	CNS+	1,07
210715_s_at	SPINT2	CNS+	1,07
234308_at	TUBGCP6	CNS+	1,07
242304_at	WIBG	CNS+	1,07
212959_s_at	GNPTAB	CNS+	1,07
213087_s_at	EEF1D	CNS+	1,07
227904_at	AZI2	CNS+	1,07
230706_s_at	CAMK2N2	CNS+	1,07
229317_at	KPNA5	CNS+	1,07
1554595_at	SYMPK	CNS+	1,07
202907_s_at	NBN	CNS+	1,07
214060_at	SSBP1	CNS+	1,07
217187_at	MUC5AC	CNS+	1,07
229141_at	WDR33	CNS+	1,07
233599_at	LOC728061	CNS+	1,07
238880_at	GTF3A	CNS+	1,06
1553493_a_at	TDH	CNS+	1,06
1563034_at	GPD1	CNS+	1,06
229803_s_at	NUDT3	CNS+	1,06
224759_s_at	C12orf23	CNS+	1,06
219931_s_at	KLHL12	CNS+	1,06
232253_at	C5orf56	CNS+	1,06
214197_s_at	SETDB1	CNS+	1,06
227274_at	SYNJ2BP	CNS+	1,06
225710_at	GNB4	CNS+	1,06
222204_s_at	RRN3	CNS+	1,06
227829_at	GYLTL1B	CNS+	1,06
207564_x_at	OGT	CNS+	1,05
221966_at	GPR137	CNS+	1,05
203152_at	MRPL40	CNS+	1,05
208715_at	TMCO1	CNS+	1,05
226412_at	PNISR	CNS+	1,05
231714_s_at	AP4B1	CNS+	1,05
218809_at	PANK2	CNS+	1,04
210968_s_at	RTN4	CNS+	1,03
200645_at	GABARAP	CNS-	1,04
214080_x_at	PRKCSH	CNS-	1,04
201606_s_at	PWP1	CNS-	1,05
210208_x_at	BAG6	CNS-	1,05
214656_x_at	MYO1C	CNS-	1,05
219261_at	C7orf26	CNS-	1,05
229270_x_at	SSBP4	CNS-	1,05
218533_s_at	UCKL1	CNS-	1,05
213937_s_at	FTSJ1	CNS-	1,05

223016_x_at	ZRANB2	CNS-	1,06
210428_s_at	HGS	CNS-	1,06
213655_at	YWHAE	CNS-	1,06
201914_s_at	SEC63	CNS-	1,06
222199_s_at	BIN3	CNS-	1,06
216032_s_at	ERGIC3	CNS-	1,06
211950_at	UBR4	CNS-	1,06
213649_at	SRSF7	CNS-	1,06
201717_at	MRPL49	CNS-	1,06
208938_at	PRCC	CNS-	1,06
225476_at	GPANK1	CNS-	1,06
201454_s_at	NPEPPS	CNS-	1,06
207124_s_at	GNB5	CNS-	1,06
202173_s_at	VEZF1	CNS-	1,07
204617_s_at	ACD	CNS-	1,07
209258_s_at	SMC3	CNS-	1,07
224676_at	TMED4	CNS-	1,07
207163_s_at	AKT1	CNS-	1,07
202109_at	ARFIP2	CNS-	1,07
232219_x_at	USP21	CNS-	1,07
211969_at	HSP90AA1	CNS-	1,07
200990_at	TRIM28	CNS-	1,07
201140_s_at	RAB5C	CNS-	1,07
212717_at	PLEKHM1	CNS-	1,07
216105_x_at	PPP2R4	CNS-	1,07
226108_at	ZC3H18	CNS-	1,07
208445_s_at	BAZ1B	CNS-	1,07
204789_at	FMNL1	CNS-	1,07
200767_s_at	FAM120A	CNS-	1,07
224979_s_at	USP36	CNS-	1,07
218300_at	C16orf53	CNS-	1,07
202161_at	PKN1	CNS-	1,07
200825_s_at	HYOU1	CNS-	1,07
218612_s_at	TSSC4	CNS-	1,07
212994_at	THOC2	CNS-	1,07
217866_at	CPSF7	CNS-	1,07
200852_x_at	GNB2	CNS-	1,07
226082_s_at	SCAF4	CNS-	1,07
202047_s_at	CBX6	CNS-	1,07
221512_at	TMEM222	CNS-	1,07
202480_s_at	DEDD	CNS-	1,08
218345_at	TMEM176A	CNS-	1,08
204104_at	SNAPC2	CNS-	1,08
200649_at	NUCB1	CNS-	1,08
201246_s_at	OTUB1	CNS-	1,08

1559397_s_at	PRR14	CNS-	1,08
208932_at	PPP4C	CNS-	1,08
215273_s_at	TADA3	CNS-	1,08
225090_at	SYVN1	CNS-	1,08
225025_at	IGSF8	CNS-	1,08
201593_s_at	ZC3H15	CNS-	1,08
223818_s_at	RSF1	CNS-	1,08
200613_at	AP2M1	CNS-	1,08
213669_at	FCHO1	CNS-	1,08
224250_s_at	SECISBP2	CNS-	1,08
222633_at	TBL1XR1	CNS-	1,08
203597_s_at	WBP4	CNS-	1,08
211874_s_at	KAT6B	CNS-	1,08
210125_s_at	BANF1	CNS-	1,08
205748_s_at	RNF126	CNS-	1,08
218681_s_at	SDF2L1	CNS-	1,08
224933_s_at	JMJD1C	CNS-	1,08
208830_s_at	SUPT6H	CNS-	1,08
221503_s_at	KPNA3	CNS-	1,08
217878_s_at	CDC27	CNS-	1,09
217903_at	STRN4	CNS-	1,09
226442_at	ABTB1	CNS-	1,09
233366_at	FBXO4	CNS-	1,09
202326_at	EHMT2	CNS-	1,09
217899_at	TMEM214	CNS-	1,09
202601_s_at	HTATSF1	CNS-	1,09
1553396_a_at	CCDC13	CNS-	1,09
200634_at	PFN1	CNS-	1,09
213467_at	RND2	CNS-	1,09
212783_at	RBBP6	CNS-	1,09
200727_s_at	ACTR2	CNS-	1,09
209113_s_at	HMG20B	CNS-	1,09
201082_s_at	DCTN1	CNS-	1,09
213665_at	SOX4	CNS-	1,09
210407_at	PPM1A	CNS-	1,09
211029_x_at	FGF18	CNS-	1,09
243414_at	PPIL2	CNS-	1,09
212167_s_at	SMARCB1	CNS-	1,09
223025_s_at	AP1M1	CNS-	1,09
207824_s_at	MAZ	CNS-	1,09
205460_at	NPAS2	CNS-	1,09
201040_at	GNAI2	CNS-	1,09
208364_at	INPP4A	CNS-	1,09
228204_at	PSMB4	CNS-	1,09
224775_at	IWS1	CNS-	1,09

201702_s_at	PPP1R10	CNS-	1,09
227402_s_at	UTP23	CNS-	1,09
236669_at	LOC100507495	CNS-	1,09
230106_at	ZXDC	CNS-	1,09
222616_s_at	USP16	CNS-	1,09
200745_s_at	GNB1	CNS-	1,09
201903_at	UQCRC1	CNS-	1,09
212028_at	RBM25	CNS-	1,09
227047_x_at	ZBTB4	CNS-	1,09
230213_at	C19orf43	CNS-	1,09
212107_s_at	DHX9	CNS-	1,09
201746_at	TP53	CNS-	1,09
200922_at	KDELR1	CNS-	1,09
244804_at	SQSTM1	CNS-	1,09
223132_s_at	TRIM8	CNS-	1,10
202805_s_at	ABCC1	CNS-	1,10
212081_x_at	PRRC2A	CNS-	1,10
211503_s_at	RAB14	CNS-	1,10
208114_s_at	ISG20L2	CNS-	1,10
212512_s_at	CARM1	CNS-	1,10
211358_s_at	CIZ1	CNS-	1,10
228337_at	PWWP2A	CNS-	1,10
218522_s_at	MAP1S	CNS-	1,10
203833_s_at	TGOLN2	CNS-	1,10
231860_at	BRWD1	CNS-	1,10
225979_at	PLEKHG2	CNS-	1,10
222508_s_at	ARGLU1	CNS-	1,10
241611_s_at	FNDC3A	CNS-	1,10
221972_s_at	SDF4	CNS-	1,10
223138_s_at	DHX36	CNS-	1,10
205322_s_at	MTF1	CNS-	1,10
234924_s_at	ZNF687	CNS-	1,10
236269_at	ZNF628	CNS-	1,10
203258_at	DRAP1	CNS-	1,10
226070_at	C9orf142	CNS-	1,10
202024_at	ASNA1	CNS-	1,10
1555125_at	GCFC1	CNS-	1,10
217656_at	SMARCA4	CNS-	1,10
203239_s_at	CNOT3	CNS-	1,10
212808_at	NFATC2IP	CNS-	1,10
223019_at	FAM129B	CNS-	1,10
1558782_a_at	LOC100130557	CNS-	1,10
213579_s_at	EP300	CNS-	1,10
214768_x_at	IGKV1-5	CNS-	1,10
203491_s_at	CEP57	CNS-	1,10

229765_at	ZNF207	CNS-	1,10
39835_at	SBF1	CNS-	1,10
214690_at	TAF1B	CNS-	1,10
1555730_a_at	CFL1	CNS-	1,10
208685_x_at	BRD2	CNS-	1,11
205740_s_at	RBM42	CNS-	1,11
209024_s_at	SYNCRIP	CNS-	1,11
214315_x_at	CALR	CNS-	1,11
227257_s_at	C10orf46	CNS-	1,11
200695_at	PPP2R1A	CNS-	1,11
236259_at	STK4	CNS-	1,11
241233_x_at	C21orf81	CNS-	1,11
240554_at	AKAP8L	CNS-	1,11
237333_at	RBBP4	CNS-	1,11
201101_s_at	BCLAF1	CNS-	1,11
206665_s_at	BCL2L1	CNS-	1,11
243295_at	RBM27	CNS-	1,11
225801_at	FBXO32	CNS-	1,11
202621_at	IRF3	CNS-	1,11
200702_s_at	DDX24	CNS-	1,11
58994_at	CC2D1A	CNS-	1,11
1566340_at	SNORD8	CNS-	1,11
208751_at	NAPA	CNS-	1,11
227393_at	ANO9	CNS-	1,11
228123_s_at	ABHD12	CNS-	1,11
225103_at	MRPL38	CNS-	1,11
238940_at	KLF12	CNS-	1,11
213957_s_at	CEP350	CNS-	1,11
227903_x_at	C19orf20	CNS-	1,11
222568_at	UGGT1	CNS-	1,11
57739_at	DND1	CNS-	1,11
221718_s_at	AKAP13	CNS-	1,11
203388_at	ARRB2	CNS-	1,12
225041_at	MPHOSPH8	CNS-	1,12
233559_s_at	WDFY1	CNS-	1,12
215188_at	STK24	CNS-	1,12
237741_at	SLC25A36	CNS-	1,12
208876_s_at	PAK2	CNS-	1,12
201683_x_at	TOX4	CNS-	1,12
204480_s_at	C9orf16	CNS-	1,12
212759_s_at	TCF7L2	CNS-	1,12
201264_at	COPE	CNS-	1,12
1553252_a_at	BRWD3	CNS-	1,12
222406_s_at	PNRC2	CNS-	1,12
227599_at	MB21D2	CNS-	1,12

217538_at	SGSM2	CNS-	1,12
204192_at	CD37	CNS-	1,12
229010_at	CBL	CNS-	1,12
209962_at	EPOR	CNS-	1,12
201224_s_at	SRRM1	CNS-	1,12
213799_s_at	PTPRA	CNS-	1,12
1569098_s_at	TP53BP1	CNS-	1,12
217539_at	C18orf25	CNS-	1,12
226176_s_at	USP42	CNS-	1,12
209996_x_at	PCM1	CNS-	1,12
227252_at	LRP10	CNS-	1,12
235828_at	PRELID2	CNS-	1,12
203506_s_at	MED12	CNS-	1,12
239382_at	HPS1	CNS-	1,12
231101_at	PPP2R5E	CNS-	1,12
220925_at	NAA35	CNS-	1,12
211947_s_at	PRRC2C	CNS-	1,12
221006_s_at	SNX27	CNS-	1,13
201183_s_at	CHD4	CNS-	1,13
218260_at	DDA1	CNS-	1,13
225124_at	PPP1R9B	CNS-	1,13
216563_at	ANKRD12	CNS-	1,13
230967_s_at	USP7	CNS-	1,13
222544_s_at	WHSC1L1	CNS-	1,13
1568680_s_at	YTHDC2	CNS-	1,13
209675_s_at	HNRNPUL1	CNS-	1,13
225294_s_at	TRAPPC1	CNS-	1,13
1553348_a_at	NFX1	CNS-	1,13
200598_s_at	HSP90B1	CNS-	1,13
220509_at	RBM26	CNS-	1,13
219158_s_at	NAA15	CNS-	1,13
200917_s_at	SRPR	CNS-	1,13
211022_s_at	ATRX	CNS-	1,13
241881_at	OR2W3	CNS-	1,13
223200_s_at	LSG1	CNS-	1,13
228433_at	NFYA	CNS-	1,13
222909_s_at	BAG4	CNS-	1,13
212451_at	SECISBP2L	CNS-	1,13
243995_at	PTAR1	CNS-	1,14
225393_at	GATAD2B	CNS-	1,14
222387_s_at	VPS35	CNS-	1,14
229265_at	SKI	CNS-	1,14
201868_s_at	TBL1X	CNS-	1,14
212332_at	RBL2	CNS-	1,14
208879_x_at	PRPF6	CNS-	1,14

229264_at	FLJ39739	CNS-	1,14
1559038_at	SEPT2	CNS-	1,14
207966_s_at	GLG1	CNS-	1,14
221705_s_at	SIKE1	CNS-	1,14
203496_s_at	MED1	CNS-	1,14
1553304_at	LSM14B	CNS-	1,14
214352_s_at	KRAS	CNS-	1,14
200964_at	UBA1	CNS-	1,14
212758_s_at	ZEB1	CNS-	1,14
1555057_at	NDUFS4	CNS-	1,14
235577_at	ZNF652	CNS-	1,14
209060_x_at	NCOA3	CNS-	1,14
227454_at	TAOK1	CNS-	1,14
222621_at	DNAJC1	CNS-	1,15
203444_s_at	MTA2	CNS-	1,15
235003_at	UHMK1	CNS-	1,15
204074_s_at	CEP104	CNS-	1,15
223254_s_at	G2E3	CNS-	1,15
243433_at	ARHGAP30	CNS-	1,15
223984_s_at	NUPL1	CNS-	1,15
229115_at	DYNC1H1	CNS-	1,15
215310_at	APC	CNS-	1,15
223611_s_at	LNX1	CNS-	1,15
209936_at	RBM5	CNS-	1,15
222082_at	ZBTB7A	CNS-	1,15
212487_at	GPATCH8	CNS-	1,15
203796_s_at	BCL7A	CNS-	1,15
208664_s_at	TTC3	CNS-	1,15
204535_s_at	REST	CNS-	1,15
208042_at	AGGF1	CNS-	1,15
219239_s_at	ZNF654	CNS-	1,15
201251_at	PKM2	CNS-	1,15
238013_at	PLEKHA2	CNS-	1,16
218273_s_at	PDP1	CNS-	1,16
219437_s_at	ANKRD11	CNS-	1,16
201996_s_at	SPEN	CNS-	1,16
228556_at	YTHDC1	CNS-	1,16
212113_at	ATXN7L3B	CNS-	1,16
212468_at	SPAG9	CNS-	1,16
229060_at	YPEL2	CNS-	1,16
1555180_at	LOC100132686	CNS-	1,16
229830_at	PDGFA	CNS-	1,16
240570_at	INADL	CNS-	1,16
200841_s_at	EPRS	CNS-	1,16
242979_at	IRS1	CNS-	1,16

210214_s_at	BMPR2	CNS-	1,16
201340_s_at	ENC1	CNS-	1,17
216361_s_at	KAT6A	CNS-	1,17
233937_at	GGNBP2	CNS-	1,17
224227_s_at	BDP1	CNS-	1,17
201039_s_at	RAD23A	CNS-	1,17
219387_at	CCDC88A	CNS-	1,17
213298_at	NFIC	CNS-	1,17
226075_at	SPSB1	CNS-	1,17
226054_at	BRD4	CNS-	1,17
208610_s_at	SRRM2	CNS-	1,17
212311_at	SEL1L3	CNS-	1,17
229966_at	EWSR1	CNS-	1,17
225377_at	C9orf86	CNS-	1,17
225525_at	KIAA1671	CNS-	1,18
204909_at	DDX6	CNS-	1,18
228998_at	TNRC6B	CNS-	1,18
237247_at	USP51	CNS-	1,18
227741_at	PTPLB	CNS-	1,18
201085_s_at	SON	CNS-	1,18
244133_at	USP49	CNS-	1,18
201793_x_at	SMG7	CNS-	1,18
229399_at	C10orf118	CNS-	1,18
208077_at	C9orf38	CNS-	1,19
224963_at	SLC26A2	CNS-	1,19
201861_s_at	LRRFIP1	CNS-	1,19
226571_s_at	PTPRS	CNS-	1,19
208624_s_at	EIF4G1	CNS-	1,19
1567013_at	NFE2L2	CNS-	1,19
1554873_at	CSPP1	CNS-	1,19
225806_at	JUB	CNS-	1,19
217867_x_at	BACE2	CNS-	1,19
235216_at	ESCO1	CNS-	1,19
40562_at	GNA11	CNS-	1,19
214519_s_at	RLN2	CNS-	1,20
220051_at	PRSS21	CNS-	1,20
220466_at	CCDC15	CNS-	1,20
1561923_a_at	SF3B14	CNS-	1,20
231235_at	NKTR	CNS-	1,20
241631_at	ARHGEF40	CNS-	1,20
35436_at	GOLGA2	CNS-	1,20
201360_at	CST3	CNS-	1,20
229193_at	LUC7L3	CNS-	1,21
243361_at	SREK1	CNS-	1,21
225937_at	CUX1	CNS-	1,21

205488_at	GZMA	CNS-	1,21
213926_s_at	AGFG1	CNS-	1,21
211965_at	ZFP36L1	CNS-	1,21
222527_s_at	RBM22	CNS-	1,21
208900_s_at	TOP1	CNS-	1,21
219878_s_at	KLF13	CNS-	1,22
244396_at	G3BP1	CNS-	1,22
1553107_s_at	C5orf24	CNS-	1,22
238435_at	LOC100506661	CNS-	1,22
201831_s_at	USO1	CNS-	1,22
239537_at	ST8SIA2	CNS-	1,22
242163_at	THRAP3	CNS-	1,22
1556204_a_at	ZNF814	CNS-	1,22
230057_at	LOC285178	CNS-	1,22
235009_at	BOD1L	CNS-	1,22
241620_at	SMCHD1	CNS-	1,22
236665_at	CCDC18	CNS-	1,22
224563_at	WASF2	CNS-	1,23
205889_s_at	JAKMIP2	CNS-	1,23
208003_s_at	NFAT5	CNS-	1,23
236645_at	LOC100506312	CNS-	1,23
212002_at	C1orf144	CNS-	1,23
236850_at	CAPRIN1	CNS-	1,24
213998_s_at	DDX17	CNS-	1,24
235653_s_at	THAP6	CNS-	1,24
236565_s_at	LARP6	CNS-	1,24
203874_s_at	SMARCA1	CNS-	1,24
244774_at	PHACTR2	CNS-	1,24
221276_s_at	SYNC	CNS-	1,25
1554679_a_at	LAPTM4B	CNS-	1,25
213446_s_at	IQGAP1	CNS-	1,25
1557529_at	C12orf51	CNS-	1,25
238848_at	OTUD4	CNS-	1,26
227152_at	C12orf35	CNS-	1,26
241403_at	CLK4	CNS-	1,26
1557227_s_at	TPR	CNS-	1,26
201278_at	DAB2	CNS-	1,26
235179_at	ZNF641	CNS-	1,27
235490_at	TMEM107	CNS-	1,27
1559528_at	LOC100129917	CNS-	1,27
229274_at	GNAS	CNS-	1,27
210057_at	SMG1	CNS-	1,27
205187_at	SMAD5	CNS-	1,27
210172_at	SF1	CNS-	1,27
242429_at	ZNF567	CNS-	1,28

213194_at	ROBO1	CNS-	1,28
227510_x_at	MALAT1	CNS-	1,28
225627_s_at	CACHD1	CNS-	1,28
1558173_a_at	LUZP1	CNS-	1,29
208683_at	CAPN2	CNS-	1,29
1566465_at	KCNK1	CNS-	1,30
227711_at	GTSF1	CNS-	1,32
209094_at	DDAH1	CNS-	1,32
214913_at	ADAMTS3	CNS-	1,34
215894_at	PTGDR	CNS-	1,35
227474_at	LOC654433	CNS-	1,36
240602_at	HBS1L	CNS-	1,36
204066_s_at	AGAP1	CNS-	1,37
236999_at	PPWD1	CNS-	1,38
206546_at	SYCP2	CNS-	1,40
226208_at	ZSWIM6	CNS-	1,41
235476_at	TRIM59	CNS-	1,41
1556499_s_at	COL1A1	CNS-	1,41
206142_at	ZNF135	CNS-	1,42
203828_s_at	IL32	CNS-	1,43
236085_at	CAPSL	CNS-	1,43
201215_at	PLS3	CNS-	1,44
214464_at	CDC42BPA	CNS-	1,51

Pathway	Gene Name	Description
Formation of actin bundles, filaments and cytoskeleton	*AKAP13* *ARRB1* *EZR* *MAPK8* *PDCD6IP* *PKN2* *RANBP9* *RICTOR* *SMARCA4* *TPR*	A kinase anchor protein 13 Arrestin, Beta 1 Ezrin Mitogen-activated protein kinase 8 Programmed Cell-Death 6 interacting protein Protein kinase N2 RAN binding protein 9 RPTOR independent companion of MTOR, complex 2 SWI/SNF-Related Matrix-Associated Actin-Dependent Regulator Of Chromatin Translocated promoter region
Binding & linkage of actin cytoskeleton	*EZR*	Ezrin
Formation of actin stress fibers	*AKAP13* *ARBB1* *PDCD6IP* *PKN2* *SMARCA4*	A kinase anchor protein 13 Arrestin, Beta 1 Programmed Cell-Death 6 interacting protein Protein kinase N2 SWI/SNF-Related Matrix-Associated Actin-Dependent Regulator Of Chromatin

Table 4: Differently expressed genes identified to be related to cytoskeleton remodeling. Pathway analyses tools DAVID 6.7 and IPA were used to identify gene networks that were directly related to CNS infiltration. This analysis revealed that many of the probe sets were directly or indirectly related to cytoskeleton remodeling. Genes listed in Table 4 could play a potential role in CNS infiltration. In addition, the genes can interact in multiple pathways.

REFERENCES

1. Pui CH, Carroll WL, Meshinchi S, Arceci RJ, Biology, risk stratification, and therapy of pediatric acute leukemias: an update, Journal of Clinical Oncology, 2011 Feb 10;29(5):551-65. DOI: 10.1200/JCO.2010.30.7405.
2. Swerdlow, S.H., Campo, E., Harris, N.L., Jaffe, E.S., Pileri, S.A., Stein, H., Thiele, J., Vardiman, J.W, WHO Classification of Tumours of Haematopoietic and Lymphoid Tissues, Fourth Edition, Lyon, France, IARC Press: 2008
3. Pui CH, Campana D, Pei D, Bowman WP, Sandlund JT, Kaste SC, Ribeiro RC, Rubnitz JE, Raimondi SC, Onciu M, Coustan-Smith E, Kun LE, Jeha S, Cheng C, Howard SC, Simmons V, Bayles A, Metzger ML, Boyett JM, Leung W, Handgretinger R, Downing JR, Evans WE, Relling MV, Treating childhood acute lymphoblastic leukemia without cranial irradiation, The New England Journal of Medicine, 2009 Jun 25;360: 2730-2741. DOI: 10.1056/NEJMoa0900386
4. C.H., Pui, Central Nervous System Disease in acute lymphoblastic leukemia: Prophylaxis and Treatment, ASH Education Book, 2006 Jan 1;2006(1):142-146. DOI: 10.1182/asheducation-2006.1.142
5. Pui CH, Mullighan CG, Evans WE, Relling MV, Pediatric acute lymphoblastic leukemia: where are we going and how do we get there? Blood, 2012 August 9;120(6);1165-1174. DOI: 10.1182/blood-2012-05-378943
6. Marta Pillon MD, Maurizio Aricò MD, Giuseppe Basso MD, Franco Locatelli MD, Marco Citterio MD, Concetta Micalizzi MD, Anna Maria Testi MD, Elena Barisone MD, Margherita Nardi MD, Alessandra Lombardi MD, Roberto Rondelli MD, Angelo Rosolen MD, On behalf of the NHL-Committee of the Italian Association of Pediatric Hematology, Oncology (AIEOP), Long-term results of AIEOP-8805 protocol for acute B-cell lymphoblastic leukemia of childhood, Pediatric Blood & Cancer, 2011 April;56(4):544–550. DOI: 10.1002/pbc.22787
7. Veerman AJ, Kamps WA, van den Berg H, van den Berg E, Bökkerink JP, Bruin MC, van den Heuvel-Eibrink MM, Korbijn CM, Korthof ET, van der Pal K, Stijnen T, van Weel Sipman MH, van Weerden JF, van Wering ER, van der Does-van den Berg A; Dutch Childhood Oncology Group, Dexamethasone-based therapy for childhood acute lymphoblastic leukaemia: results of the prospective Dutch Childhood Oncology Group (DCOG) protocol ALL-9 (1997-2004), The Lancet Oncology, 2009 Oct;10(10):957-966. DOI:10.1016/S1470-2045(09)70228-1
8. Pui CH, Howard SC, Current management and challenges of malignant disease in the CNS in pediatric leukemia, The Lancet Oncology, 2008 March;9(3):257-268. DOI:10.1016/S1470-2045(08)70070-6
9. Gunnar Cario, Shai Izraeli, Anja Teichert, Peter Rhein, Julia Skokowa, Anja Möricke, Martin Zimmermann, Andre Schrauder, Leonid Karawajew, Wolf-Dieter Ludwig, Karl Welte, Holger J. Schünemann, Brigitte Schlegelberger, Martin Schrappe and Martin Stanulla, High Interleukin-15 Expression Characterizes Childhood Acute Lymphoblastic Leukemia With Involvement of the CNS, Journal of Clinical Oncology, 2007 Oct 20;25:4813-4820. DOI: 10.1200/JCO.2007.11.8166
10. Crazzolara R, Kreczy A, Mann G, Heitger A, Eibl G, Fink FM, Möhle R, Meister B. High expression of the chemokine receptor CXCR4 predicts extramedullary organ infiltration in childhood acute lymphoblastic leukaemia. Br J Haematol. 2001 Dec;115(3):545-53.
11. Buonamici S, Trimarchi T, Ruocco MG, Reavie L, Cathelin S, Mar BG, Klinakis A, Lukyanov Y, Tseng JC, Sen F, Gehrie E, Li M, Newcomb E, Zavadil J, Meruelo D, Lipp M, Ibrahim S, Efstratiadis A, Zagzag D, Bromberg JS, Dustin ML, Aifantis I.CCR7 signalling as an essential regulator of CNS infiltration in T-cell leukaemia. Nature. 2009 Jun 18;459(7249):1000-4. doi: 10.1038/nature08020.

12. Holland M, Castro FV, Alexander S, Smith D, Liu J, Walker M, Bitton D, Mulryan K, Ashton G, Blaylock M, Bagley S, Connolly Y, Bridgeman J, Miller C, Krishnan S, Dempsey C, Masurekar A, Stern P, Whetton A, Saha V, RAC2, AEP, and ICAM1 expression are associated with CNS disease in a mouse model of pre-B childhood acute lymphoblastic leukemia, Blood, 2011 May 23;118(3):638-649. DOI: 10.1182/blood-2010-09-307330.
13. Christina Halsey, Mark TS Williams, Yasar Yousafzai, Klaus Rehe, Olaf Heidenreich, Josef Vormoor, Brenda Gibson[3]and Gerard Graham, Central Nervous System Involvement in a Xenograft Model of Pre-B Acute Lymphoblastic Leukaemia Is Associated with Dysfunctional CXCR4 Expression and Upregulation of the Neurotropic Chemokine Receptors CCR6 and CX3CR1, Blood, 2011: Abstract 3449.
14. Fedyk ER, Ryyan DH, Ritterman I, Springer TA. Maturation decreases responsiveness of human bone marrow B lineage cells to stromal-derived factor 1 (SDF-1). J Leukoc Biol 1999;66(4):667–73. [PubMed: 10534124]
15. Honczarenko M, Douglas RS, Mathias C, Lee B, Ratajczak MZ, Silberstein LE. SDF-1 responsiveness does not correlate with CXCR4 expression levels of developing human bone marrow B cells. Blood 1999;94(9):2990–8. [PubMed: 10556181]
16. La Starza R, Lettieri A, Pierini V, Nofrini V, Gorello P, Songia S, Crescenzi B, Te Kronnie G, Giordan M, Leszl A, Valsecchi MG, Aversa F, Basso G, Biondi A, Conter V, Cazzaniga G, Mecucci C. Linking genomic lesions with minimal residual disease improves prognostic stratification in children with T-cell acute lymphoblastic leukaemia. Leuk Res. 2013 Aug;37(8):928-35. doi: 10.1016/j.leukres.2013.04.005. Epub 2013 Jun 2.
17. de Haas V, Vet RJ, Verhagen OJ, et al. Early detection of central nervous system relapse by polymerase chain reaction in children with B-precursor acute lymphoblastic leukemia. Ann Hematol 2002;81:59–61.
18. Subir_a D, Casta~n_on S, Rom_an A, et al. Flow cytometry and the study of central nervous disease in patients with acute leukaemia. Br J Haematol 2001;112:381–384.
19. Biojone E, Queir_oz RD, Valera ET, et al. Minimal residual disease in cerebrospinal fluid at diagnosis: A more intensive treatment protocol was able to eliminate the adverse prognosis in children with acute lymphoblastic leukemia. Leuk Lymphoma 2012;53:89–95.
20. Scrideli CA, Queiroz RP, Takayanagui OM, et al. Polymerase chain reaction on cerebrospinal fluid cells in suspected leptomeningeal involvement in childhood acute lymphoblastic leukemia: Comparison to cytomorphological analysis. Diagn Mol Pathol 2003;12:124–127.
21. Pine SR, Yin C, Matloub YH, et al. Detection of central nervous system leukemia in children with acute lymphoblastic leukemia by real-time polymerase chain reaction. J Mol Diagn 2005;7:127–132.
22. Mahmoud HH, Rivera GK, Hancock ML, et al. Low leukocyte counts with blast cells in cerebrospinal fluid of children with newly diagnosed acute lymphoblastic leukemia. N Engl J Med 1993;329:314–319.
23. Smith M, Arthur D, Camitta B, et al. Uniform approach to risk classification and treatment assignment for children with acute lymphoblastic leukemia. J Clin Oncol 1996;14:18–24.
24. B€urger B, Zimmermann M, Mann G, et al. Diagnostic cerebrospinal fluid examination in children with acute lymphoblastic leukemia: Significance of low leukocyte counts with blasts or traumatic lumbar puncture. J Clin Oncol 2003;21:184–188.
25. Price RA, Johnson WW. The central nervous system in childhood leukemia. I. The arachnoid. Cancer. 1973 Mar;31(3):520-33.

26. Busillo JM, Benovic JL. Regulation of CXCR4 signaling. Biochim Biophys Acta. 2007 Apr;1768(4):952-63. Epub 2006 Nov 10.
27. Jourdan P, Vendrell JP, Huguet MF, Segondy M, Bousquet J, Pene J, Yssel H. Cytokines and cell surface molecules independently induce CXCR4 expression on CD4+ CCR7+ human memory T cells. J Immunol 2000;165(2):716–24. [PubMed: 10878344]
28. Wu S, Gessner R, Taube T, et al. Chemokine IL-8 and chemokine receptor CXCR3 and CXCR4 gene expression in childhood acute lymphoblastic leukemia at first relapse. J. Pediatr. Hematol. Oncol. 2006; 28(4):216–220. [PubMed: 16679918]

CHAPTER 4

Gene Expression Profiling defines T-ALL patients carrying *C-MYC* rearrangements within a group with high expression of *C-MYC*

ABSTRACT

GEP analysis performed on zebrafish models revealed the presence of a strong signature distinguishing the group overexpressing h*C-MYC* (h*MYC-ER*). Even if this part is not directly related to CNS invasion, these observations challenge us to clarify the importance and the role of *C-MYC* oncogene in T-ALL patients. Genetically, hT-ALLs are a heterogeneous group, distinguished in subgroups characterized by chromosomal rearrangements and related gene expression profiling signatures (*TALLMO, HOXA, TLX1, TLX3*). In pediatric T-ALL patients ~65% present *NOTCH1* mutations with consequent activation of the NOTCH1 pathway. MYC seems to have a critical role for tumor growth and maintenance, even if its overexpression is not sufficient to guide alone lymphomagenesis. In T-ALL, *MYC* overexpression is usually trigged by NOTCH1 activation, however there are some cases that present *MYC* upregulation independently from *NOTCH1* mutations: *MYC/TCR* translocations (~1% T-ALLs), *FBXW7* mutations (~5% T-ALLs), down-regulation/absence of *PTEN*, *MYC* translocation with unknown partner genes. Recently, it was shows how an activation of the Wnt/β-catenin pathway in T-cells trigged the development of T-ALL characterized by an overexpression of *C-MYC*, due to high percentages of both *MYC* secondary genomic rearrangements and loss of PTEN. This work underlines the presence of a subgroup of T-ALL independent from Notch1 activation but with a high expression of *C-MYC*. In this part of the work, we used a gene expression profiling approach to study T-ALL patients that have different *C-MYC* expression levels to define if *C-MYC* deregulation can have also a prognostic value. Moreover, we investigated the different events that triggered *C-MYC* upregulation (NOTCH1 activation, *FBOX* and *PTEN* mutations, *MYC* rearrangements) to understand the biological meaning of different causes that result all in *C-MYC* over-expression. Finally, were able to find a strong signature insight the group of patients with high expression of *C-MYC* that can discriminate patients with- and without- *C-MYC* rearrangements.

INTRODUCTION

T-cell Acute Lymphoblastic Leukemia (T-ALL) is an aggressive haematopoietic cancer resulting from an uncontrolled clonal proliferation of T-immature lymphoid cells that represents ~15% of pediatric and ~25% of adult T-ALLs [1]. Genetically, hT-ALLs represent a heterogeneous malignancy distinguished in main subgroups characterized by specific chromosomal rearrangements and related to distinct gene expression profiling signatures (*TALLMO, HOXA, TLX1, TLX3*) [2-4]. Independently from the subgroups, more than 50% of T-ALL patients carried *NOTCH1* mutations (*NOTCH1*^{m}) [5] with consequent constitutive NOTCH1 pathway activation and transcription of direct NOTCH1 target genes, suggesting an universal role of NOTCH1 in T-ALL pathogenesis. Several studies have already shown the central role played by NOTCH1 activation in promoting T-ALL development; moreover, these works identified *C-MYC* as a NOTCH1 directed target gene having a critical role in determining tumor growth and maintenance both in mouse- [6] and human- [7,8] NOTCH1-dependent T-ALL. *MYC* is involved in cell growth and proliferation in diverse solid and hematologic malignancies [9], but this oncogene can promote also apoptosis through the BIM and P53/P14ARF pathways [10,11]. However, the over-expression of *C-MYC* alone is not sufficient to determine T-ALL development and other events are required to initiate leukemogenesis [12,13]. The potential role of MYC activation in initiating T-ALL tumorigenesis was demonstrated both in transgenic zebrafish- [14,15] and mouse models [16-18], where the induced over-expression of *C-MYC* lead to T-ALL development with high penetrance and short latency. However, a recent work suggested that these animal models fail to reproduce the natural events that give rise to leukemia in human patients, as the accumulation of secondary hits is a slow process that is necessary for tumor development, according to a "multi-genomic alteration" model of hT-ALL pathogenesis [19]. Instead, transgenic animal models massively over-express *C-MYC* in specific target tissues, accelerating the leukemogenic process and moving away from human kinetics of oncogenesis. In Chapter 1 of this thesis, we used the transgenic *hMYC-ER* zebrafish model that over-expressed human *C-MYC* under the zebrafish *rag2* promoter [15]. Even if this model does not perfectly reflect the process of human leukemogenesis, it can be considered a very good model for studying the biology of T-ALL cases characterized by high *C-MYC* expression. In T-ALL human

patients, C-*MYC* over-expression is usually triggered by NOTCH1 activation. However, there are other events that can drive *C-MYC* up-regulation independently from *NOTCH1*^{m}; *C-MYC* translocations with *T-cell receptor* (~1% T-ALLs) [20] or unknown partner genes may directly cause an up-regulation of *C-MYC,* while *FBXW7*^{m} (~5% TALLs) [21-23] and down-regulation/absence of functional PTEN/AKT activation (~15-20% TALLs) [24-27] stabilize MYC impairing its degradation [28]. A recent study showed how MYC expression both at the mRNA and protein level resulted highly variable in a cohort of 164 mixed adult and pediatric T-ALL patients [28]. Even if the majority of T-ALL patients show a high expression of *C-MYC,* the role/importance or prognostic value of this oncogene is still not clear, among other things due to the complexity and variability of oncogenic networks that can occur in T-ALLs. A paper related T-ALL cell lines glucocorticoid resistance to up-regulation of cellular metabolism and proliferation due also to *C-MYC* signaling pathway activation [29], however the prognostic significance of *C-MYC* over-expression in T-ALL is still not understood. In fact, *C-MYC* over-expression is usually related to *NOTCH1*^{m} and activation of the NOTCH1 pathway has been associated to improved response to treatment in three different cohort of T-ALL, but showing different outcome that seems to be therapy-dependent [30-32]. However, patients with *C-MYC* over-expression due to loss of PTEN in the absence of *NOTCH1*^{m} were associated with resistance to chemotherapy and poor long-term outcome [27]. Recently, the activation of the Wnt/β-catenin pathway in T-cells has been shown to trigger the development of NOTCH1 independent T-ALL characterized by over-expression of *C-MYC* due to high incidence of *MYC* secondary genomic rearrangements and/or loss of PTEN [33]. This work underlines the presence of a subgroup of T-ALL independent from NOTCH1 activation but with a high expression of *C-MYC* that could be related to poor prognosis. *C-MYC* over-expression seems to have diverse values depending on different T-ALL contexts. In this part of the work, we focussed on T-ALL patients that have different *C-MYC* expression levels to define if this *C-MYC* deregulation is related to a specific gene expression profiling signature. Moreover, we investigated the different events that triggered *C-MYC* deregulation (NOTCH1 activation, *FBXW7* mutations, *MYC* rearrangements) to understand the biological meaning of different causes that result all in *C-MYC* over-expression.

MATERIAL AND METHODS

Human leukemia samples

Bone marrow or Peripheral Blood aspirates were collected from pediatric patients with or T-ALL at diagnosis. All patients selected for this study were enrolled in the AIEOP ALL-2000 protocol. Patients' parents or legal guardians did provide written informed consent for the use of patient material for biomedical research in accordance with the Declaration of Helsinki.

RNA isolation, quality controls and quantification

Mononucleated cells (MNC) were isolated via the Ficoll-Paque method (GE Healthcare companies, Buckinghamshire, United Kingdom), which is based on density gradient centrifugation. Total RNA from MNC derived from bone marrow (BM) or peripheral blood (PB) aspirates was extracted using Trizol (Invitrogen, Karlsruhe, Germany), according to manifactures' instructions. To perform gene expression experiments, extremely high quality of total RNA is required. To assess the quality of RNA, Agilent Bioanalyzer Expert 2100 (Agilent Technologies, Waldbronn, Germany) was used. RNA concentration was determined using QBit 2.0 Fluorometer (Life Technology, Carlsbad, California, U.S.). NanoDrop ND-1000 spectrophotometer (NanoDrop Technologies Inc, Wilmington, DE).

Fluorescence in situ hybridization (FISH)

Two break apart FISH assays were used to study CMYC rearrangements: the commercial LSI MYC dual color break apart rearrangement probe (Vysis, Abbott) and homebrew DNA clones mapping upstream (RP11-367L7) and downstream (RP11-26E5) CMYC (http://www.chori.org/BACPAC). TCRB was studied with RP11-1220K2 and RP11-556I13; TCRAD with RP11-242H9 and RP11-447G18. Double colour double fusion FISH assays were done to investigated cryptic translocations between CMYC and TCRB or TCRAD.

Gene expression profiling

Only RNA samples that passed the high quality controls were diluted to 100ng in a total volume of 3µl DEPC treated water to perform gene expression experiments. *In vitro* transcription, hybridization and biotin labelling were performed according to GeneChip 3'IVT Express kit protocol (Affymetrix, Santa Clara, CA). The Affymetrix GeneChip Scanner was used to measure all intensities of the signals of each probe set on the GeneChip and stores all signals in a .DAT file (Raw image). Integrated software converts all raw signals into numbers, which were stored in a .CEL file. All GEP profiles used in these experiments were assessed for their comparability and quality, using different quality controls: Scale Factor, number of present calls, internal probe calls, Poly-A controls and the ratio GAPDH/β-actin 3'/5'.

Statistical analysis

Microarray data (.CEL files) were analyzed using Command Expression Console (Affymetrix). R-Bioconductor (Version 2.15.3) was used to analyze the .CEL files data in an unsupervised and supervised manner. Unsupervised analysis (Class Discovery) is a learning algorithm that clusters unspecified specimens together based on similar gene expression patterns and is therefore highly unbiased. Supervised analysis (Class Comparison, Class Prediction) is a learning algorithm that uses already defined (labeled) data in order to identify a set of genes that characterize the pre-specified data. The .CEL files first were normalized using the justRMA algorithm. justRMA is an algorithm fulfilling 2 steps, namely background adjustment of all the probe sets present on the GeneChip and quantile normalization to make the values of all the GeneChips comparable. In order to find differently expressed probe sets we applied a Shrinkage t-test on the normalized .CEL files [35]. We used a local false discovery rate (lfdr) as correction of the p-value; a ldfr < 0,05 was considered significant for genes differently expressed between 2 groups. Differently expressed probe sets derived from the Shrinkage t-test were used for clustering analysis. Hierarchical clustering analysis was used to clusterize the specimens in an unsupervised manner using Euclidean Distance

and Ward's Method. Euclidean Distance and Ward's Method compute the distance between two groups in a metric space.

Gene Ontology and Protein-Protein Interacting Analyses

Differently expressed genes dereived by Shrinkage T-test analysis were analyzed using Database for Annotation, Visualization and Integrated Discovery (DAVID) v6.7 and Search Tool for the Retrieval of Interacting Genes/Proteins (STRING) v9.05. STRING, based on text mining, was used in order to investigate potential gene/protein networks within in the list of differently expressed genes. Gene ontology was performed with DAVID.

Gene Set Enrichment Analysis (GSEA)

Gene Set Enrichment Analysis (GSEA) is a method that can be used to identify groups of genes that share common biological functions or belong to the same gene pathways described in the public domain [36]. For each group of gene sets, GSEA calculates an enrichment score and evaluates statistical significance n the enrichment score (ES). The ES reflects the degree to which a gene set is over represented. For this stud we conducted GSEA analysis using the GSEA software [16] version 4.0 to identify gene sets in the public domain that share the expression pattern enriched in our current study. As recommended by GSEA guidelines, only gene sets with a false discovery rate (FDR) *q*-value lower than 0.05 were considered.

Sanger Sequencing

The screening of *NOTCH1* and *FBXW7* mutations was performed for 40 T-ALL specimens comprising patients of the two quartiles with high and low expression of *C-MYC* (table1), and 4 additional cases of T-ALL carrying *C-MYC* translocation (table2). Briefly, DNA was extracted from the bone marrow (BM) or peripheral blood (PB) of each patient using the Puregene DNA isolation kit according to the manufacturer's instructions (QIAGEN). 20 ng/µl of genomic DNA was used for PCR-amplified (primers reported in the Table3), using according to optimized protocols for each gene.

NOTCH1 and *FBXW7* PCR products were purified using illustra™ ExoStar™ enzymes (VWR International Ltd, Lutterworth, England). All PCR products were quantified using the NanoDrop ND-1000 Spectrophotometer (NanoDrop Technologies Inc, Wilmington, DE). Sanger sequencing was performed on both strands using BigDye Terminator v1.1 Sequencing kit (Applied Biosystems, Weiterstadt, Germany) and analyzed on an automated fluorescence-based analyzer according to the manufacturer's protocol.

RESULTS

C-MYC expression levels in a cohort of 78 T-ALL pediatric patients

This work aimed to clarify the biological significance of *C-MYC* oncogene expression in T-ALL development. Data of gene expression profiling considering a cohort of 78 T-ALL patients at diagnosis, revealed the presence of a broad range of variable expression levels of *C-MYC* among patients. The expression levels of *C-MYC* formed a continuum observing the entire cohort, but we could distinguish the presence of two opposite groups with "high" or "low" expression of *C-MYC* respectively (figure 1). We used a descriptive statistical method to define two opposite groups, calculating the quartiles based on *C-MYC* expression and we identified 20 patients with low (first quartile) and 20 patients with high (fourth quartile) expression of *C-MYC*.

Different gene expression profiling signatures between groups with Low and High C-MYC expression

To understand the different gene networks that move in relation to having high or low *C-MYC* expression, we performed a T-test on GEP data comparing the patients of the two opposite quartiles for *C-MYC* expression (Q1-Q4). Shrinkage T-test revealed the presence of 115 genes significantly differently expressed between Q1 and Q4 groups. Supervised analysis separated patients belonging to the Q1 and Q4 group, except for 4 patients with high expression of *C-MYC* that clustered together with the patients of Q1 (figure 2). However, genes that were differently expressed did not present high fold

changes (FCs) and explained the rather weak signature found between the two groups. The distinction between patients with high and low *C-MYC* expression levels is not related to a strong gene expression signature, which is maybe due to the high variability of events that regulate *C-MYC* expression in T-ALL patients. Moreover, Gene Set Enrichment Analysis (GSEA) did not reveal a particular enrichment of known gene sets when comparing the two groups. There is only a tendency for the group with high *C-MYC* expression to have an enrichment of the WNT and CXCR4 pathways, but the *p*-value is not significant (figure 3).

NOTCH1, FBXW7 mutation screening

Different events directly or indirectly induce *C-MYC* over-expression: $NOTCH1^{m}$ frequently sustain up-regulation of *C-MYC* [7,8], causing constitutive activation of the NOTCH1 pathway; $FBXW7^{m}$ can favour both indirect *C-MYC* over-expression (impairing active NOTCH1 degradation) and C-MYC protein stabilization directly preventing its proteasomal degradation [21-23]. We decided to investigate the causes that could be held responsible for *C-MYC* deregulation among the patientss with high MYC expression in our patient cohort. We screened *NOTCH1, FBXW7* mutations for each patient of the two quartiles with high or low expression of *C-MYC*. We analysed the regions frequently mutated in T-ALL for each of these genes: *NOTCH1* for the HD and PEST domains (26, 27, 28, 34T and 34P exons) while *FBXW7* was screened for mutations in exons 9 and 10. Moreover, to have an overview of effective NOTCH1 activation, we monitored the expression levels of NOTCH1 direct target genes (*HES1, DELTEX1 CR2* and *PTCRA*) using gene expression profiling data. (Table1). With this analysis we were able to identify 1 case (patient 36) with over-expression of *C-MYC* not related to *NOTCH1, FBXW7* mutations. These data suggested that this patient could carry other events that could explain *C-MYC* over-expression, such as a *C-MYC* rearrangements.

Rearrangements of C-MYC can cause the "high" expression of C-MYC

FISH [37,38] analysis using specific probes for *C-MYC* was performed for the 7/20 cases that presented low expression of *C-MYC* (Q1) and 13/20 cases with high

expression of *C-MYC* (Q4) (table 1). The aim of this analysis was to identify rearrangements of *C-MYC* that could explain the over-expression of this oncogene occurring in the presence or absence of *NOTCH1* and *FBXW7* mutations. *C-MYC* reciprocal translocations, i.e. an hybridization pattern characterized by 1 fusion signal and 2 separated green and orange signal occurred in 5 cases (figure 7) and involved *TCRB* or *TCRAD* in two samples. New as yet unidentified partner would be involved in the other 3 cases as cryptic rearrangements with *TCRB* or *TCRAD* were excluded. Inside the group with "high" *C-MYC* expression, we identified one patient (patient 36) with a *C-MYC* translocation (with an undefined partner gene).

Different signature among T-ALL patients with high expression of C-MYC related to C-MYC rearrangements

Recently, in a mouse model a subgroup of T-ALL was identified that was shown to be triggered by the activation of the Wnt/β-cathenin pathway, an event that seemed to be related to the development of secondary *C-MYC* rearrangements and loss of PTEN [33]. This mouse model developed a NOTCH1 independent T-ALL leukemia that migh identify a subgroup with bad prognosis, in fact the loss of PTEN in the absence of $NOTCH^{m}$ has been shown to be related to poor outcome [28]. To understand if also in human T-ALL there is a subgroup of patients with high *MYC* expression independent of NOTCH1 mutations or activation in general, we decided to increase our cohort of patient with high expression of *C-MYC* (Q4) with patients carrying *C-MYC* translocations. Using a gene expression profiling approach, we wanted to investigate the biological significance and possibly the prognostic impact of *C-MYC* over-expression due to distinct genomic aberrations (activation of NOTCH1, mutation of *FBXW7*, *C-MYC* translocations). We increased the high *C-MYC* group with 1 pediatric and 3 adult cases carrying *C-MYC* rearrangements in the absence of $NOTCH^{m}$ and $FBXW7^{m}$. FISH specific for C-MYC rearrangements had been performed for all patients and this technique allowed to detect and quantify also sub-clones carrying *C-MYC* rearrangements. All patients analyzed by GEP had the *C-MYC* rearrangement in the major clone. Analysis of *C-MYC* expression revealed that the 5 cases with *MYC* rearrangements had high expression of this oncogene (Figure 4). Shrinkage T-test revealed the presence of 174 genes differently expressed comparing *C-MYC* rearranged

vs. non *C-MYC* rearranged groups. We have to remember that the group without *C-MYC* rearrangement is enriched for *NOTCH1* and *FBXW7* mutations. Supervised analysis showed how patients carrying *C-MYC* translocations in absence of $NOTCH1^{m}$ clustered together, separately from the patients without translocations (Figure 5). Only one patient without a *C-MYC* translocation clustered in the group with *C-MYC* rearrangements.

To investigate the genes differently expressed between the two groups (*C-MYC* rearranged vs. non *C-MYC* rearranged) we performed gene ontology and protein-protein interaction analyses using DAVID and STRING software, respectively. Both DAVID and STRING analysis showed a significant enrichment for the NOTCH1 signaling pathway (*p*-value: 0.002) in the group without *C-MYC* rearrangements (Figure 6). This enrichment was confirmed also by Gene Set Enrichment analysis (GSEA).

DISCUSSION

In this chapter, we aimed to investigate the biological meaning of *C-MYC* aberrant expression in relation to T-ALL disease. Oncogenic *MYC* deregulation is a complex process involving multiple events (*MYC* rearrangements, *NOTCH1* and *FBXW7* mutations) that complicate the understanding of *C-MYC*- mediated oncogenesis in T-ALL. In a cohort of 78 pediatric T-ALL patients, we found different expression levels of *C-MYC*. Particularly, we identified two groups characterized by high and low expression levels of this oncogene. To deepen insight in the biological impact of *C-MYC* deregulation, we performed gene expression profiling analysis comparing these two groups. However, this analysis failed to identify a strong signature that could distinguish the two groups in a perfect way. This result can be attributed to the undeniable heterogeneity that characterize the T-ALLs and major subgroups with *C-MYC* deregulation; in fact a multiplicity of pathways and genetic alteration may control *C-MYC* transcription [34]. Moreover, we have to consider that also post-transcriptional control can play an important role in determining MYC protein levels and *C-MYC* transcription levels do not in all cases corresponds to protein levels [28].

Interestingly, inside the group with high expression of *C-MYC*, different molecular mechanisms can determine *C-MYC* overexpression or MYC stabilization (*MYC*

rearrangements, *NOTCH1* and *FBXW7* mutations). Usually the over-expression of *C-MYC* is related to activation of the NOTCH1 signalling pathway, an event related to improved response to treatment [30-32]. Analyzing NOTCH1 direct target genes expression, we were able to identify some patients with high expression of *C-MYC* not associated to *NOTCH1* and *FBXW7* mutations. One among these patients carried a *C-MYC* rearrangement. A recent work on a mouse model identified the presence of a NOTCH-independent subgroup of T-ALL characterized by high expression of *C-MYC* that can be related to poor prognosis. This subgroup was related to Wnt/β-catenin pathway activation and was characterized by a high incidence of *C-MYC* rearrangements and loss of PTEN. To explore the presence of this Wnt/β-catenin-dependent T-ALL subgroup also in T-ALL patients with high expression of *C-MYC*, we amplified our cohort introducing four patients carrying *C-MYC* rearrangements in the absence of *NOTCH1*^{m}. Analysis of gene expression profiling revealed a strong signature between patients with- or without- *C-MYC* rearrangements. Interestingly, this strong signature was associated to the presence of NOTCH1 pathway activation in the group of patients without *C-MYC* rearrangements. Although we failed to find activation of the Wnt/β-catenin pathway inside the group with *C-MYC* translocations, with this study we were able to show that inside the group of T-ALL characterized by an higher expression of *C-MYC* overexpression, the subgroup of patients carrying *C-MYC* rearrangements presents a NOTCH1-independent leukemia compared to the group without *C-MYC* rearrangement that seems to be strongly related to NOTCH1 pathway activation. Further analysis need to be performed increasing the number of patients carrying *C-MYC* rearrangements. Importantly, the screening of *PTEN* mutations is ongoing, to have a complete view of the major modulators of MYC deregulation at the protein level.

FIGURES

Dot plot showing the variable expression levels of *C-MYC* in a cohort of 78 T-ALL patients based on GEP data

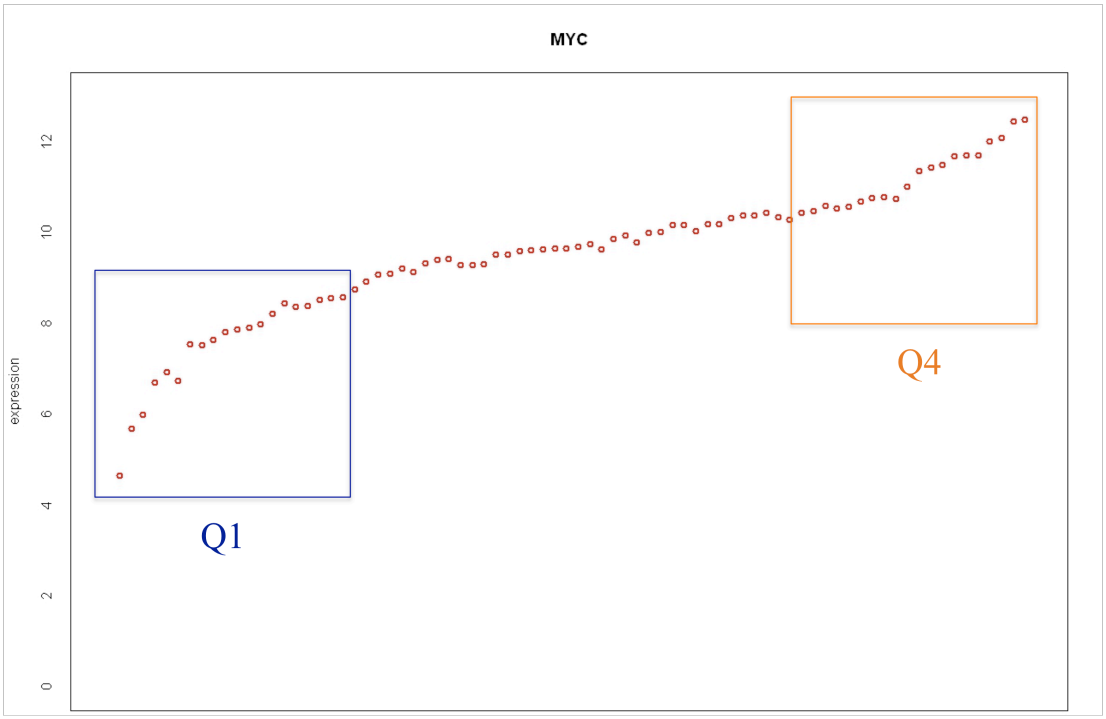

Figure 1: The expression value of the *C-MYC* probe set (202431_s_at) for each patient (single dot) is given in a log2 scale after normalizing all GEP data with the justRMA algorithm. Using descriptive statistics the cohort was divided in quartiles and identified two opposed groups characterized by low (blue square) or high (orange square) expression of *C-MYC* (Q1 and Q4 respectively).

Heatmap showing supervised analysis for groups with high (blue) or low (orange) expression of *C-MYC*

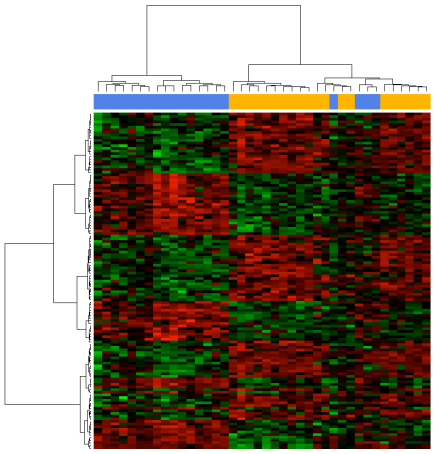

Figure 2: Hierarchical clustering based on a list of 115 probe sets obtained after Shrinkage T-test between groups with high (blue) and low (orange) *C-MYC* expression (lfdr<.05)**.**

Gene Set Enrichment Analysis for the group with high expression of *C-MYC*

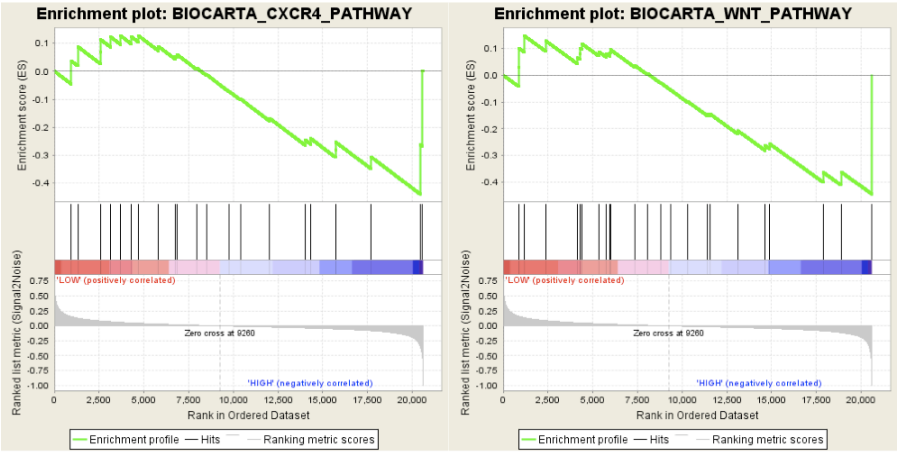

Figure 3. GSEA analyses showing the tendency for the group with HIGH expression of *C-MYC* to be enriched for the WNT and CXCR4 pathways. However, this enrichment is not sgnificative.

All *C-MYC* rearranged cases presented a high expression of *C-MYC* oncogene

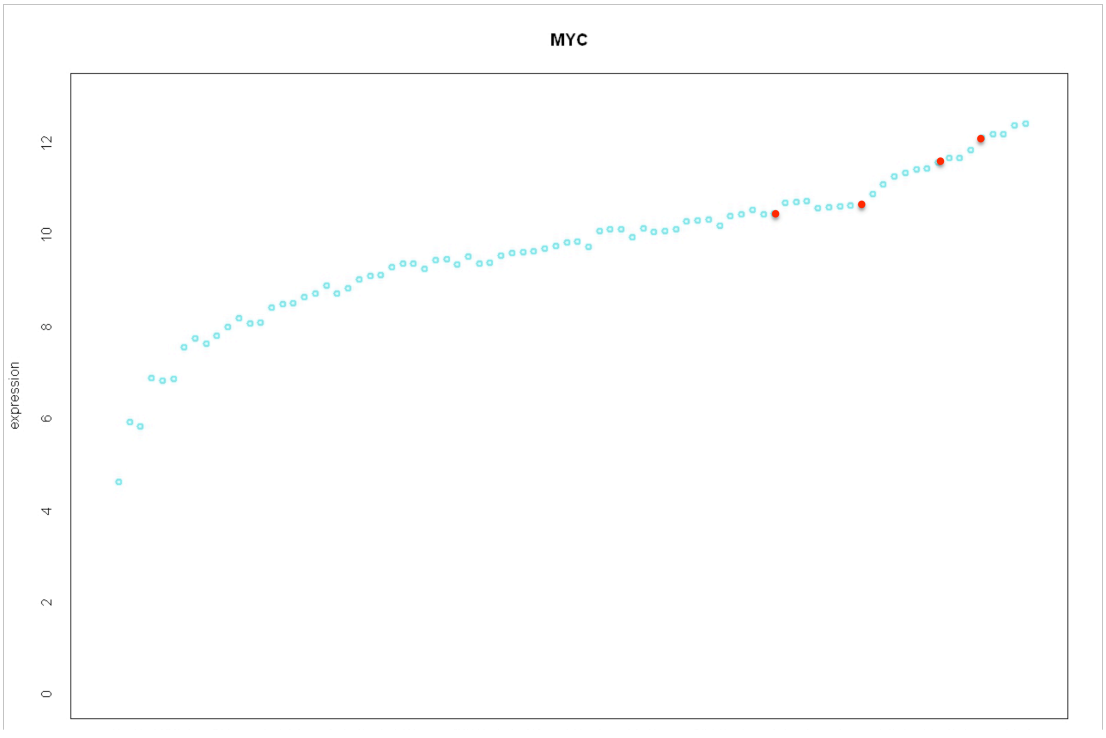

Figure 4: Dot plot showing the expression levels of *C-MYC* for the 4 new cases with a *C-MYC* rearrangements. In red are indicated the 4 additional cases (patients 41, 42, 43, 44) with *C-MYC* rearrangements that were included for new analysis.

Heatmap shows supervised analysis for groups with- (blue) and without (orange) *C-MYC* rearrangements

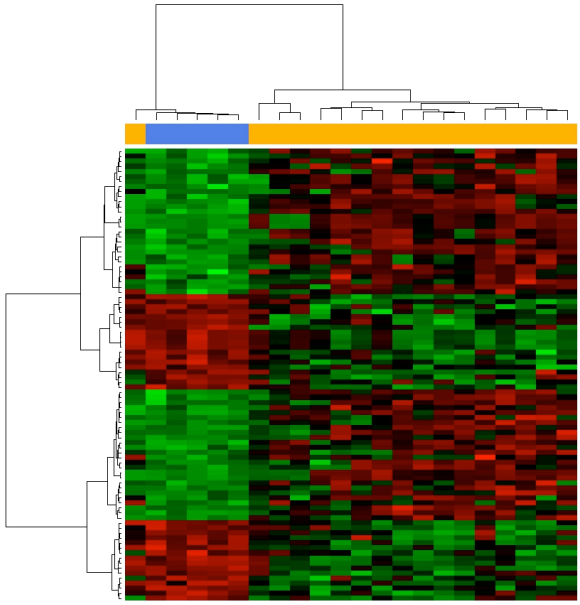

Figure 5: Hierarchical clustering based on a list of 174 probe sets obtained after Shrinkage T-test between groups with- (blue) and without (orange) *C-MYC* translocation (lfdr<.05)**.**

Protein-Protein Analysis with STRING 9.05 for the group with high expression of *C-MYC* in absence of *C-MYC* rearrangements

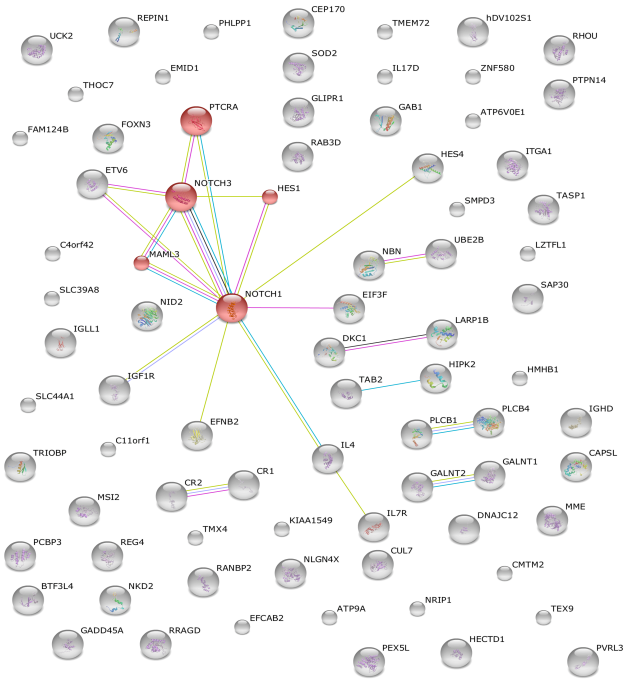

Figure 6: Analysis with STRING version 9.05 on genes significantly up-regulated in the group without *C-MYC* rearrangements shows enrichment in the NOTCH pathway (KEGG pathway) for the group without *MYC* translocations compared to the group where *MYC* is rearranged.

FISH assay with LSI CMYC break apart probe (Vysis-Abbott)

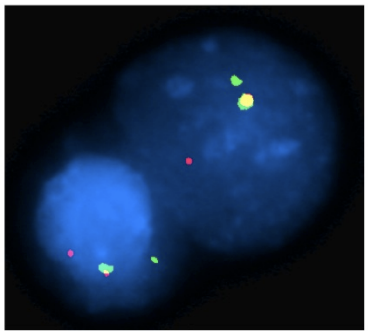

Figure 7: Two nuclei with *C-MYC* rearrangement. One Fusion signal corresponds to the *CMYC* wild type allele, two separated green and orange signals indicate a balanced *CMYC* translocation.

TABLES

Table 1. Patients belonging to the two groups with low (Q1) and high (Q4) expression of *C-MYC*

SAMPLES	SEX	QUARTILE	FISH	*HES1*	*DELTEX1*	*CR2*	*PTCRA*	*NOTCH1* STATUS	*FBXW7* STATUS
1	F	1		8,94	7,12	7,59	6,64	ongoing	ongoing
2	F	1	normal	6,27	5,87	5,07	6,14	**wt**	**wt**
3	M	1		4,89	6,66	4,26	6,64	ongoing	ongoing
4	M	1		4,15	6,24	3,31	6,13	**wt**	**wt**
5	M	1		8,64	5,83	6,04	6,11	ongoing	ongoing
6	F	1		5,25	6,21	4,76	6,57	ongoing	ongoing
7	M	1		5,64	6,78	6,15	6,45	ongoing	ongoing
8	M	1		5,64	7,17	9,29	7,56	**wt**	**wt**
9	M	1	normal	4,94	6,40	5,07	5,96	ongoing	**wt**
10	M	1		5,40	6,94	4,61	6,31	ongoing	ongoing
11	M	1	normal	6,18	6,45	9,51	8,05	ongoing	ongoing
12	M	1		7,78	6,60	7,94	6,53	ongoing	ongoing
13	M	1	normal	11,45	10,44	10,90	7,07	**mutated**	ongoing
14	M	1	normal	6,34	6,78	5,66	6,63	ongoing	ongoing
15	M	1	normal	6,30	6,09	4,54	6,59	ongoing	ongoing
16	M	1		5,53	6,54	7,65	7,13	**wt**	**wt**
17	M	1		6,00	6,82	8,38	8,00	ongoing	ongoing
18	M	1		7,89	6,31	7,75	7,07	ongoing	ongoing
19	M	1		9,63	7,30	8,15	8,68	ongoing	ongoing
20	M	1	normal	7,77	7,04	9,38	8,41	ongoing	ongoing
21	M	4	normal	8,86	7,29	8,77	9,52	**mutated**	**mutated**
22	M	4		8,38	11,06	10,66	9,63	ongoing	ongoing
23	F	4	normal	6,40	6,03	7,09	7,35	ongoing	ongoing
24	M	4		8,69	9,13	9,47	7,02	**mutated**	**wt**

25	F	4	normal	10,96	6,49	7,41	9,42	**mutated**	**wt**
26	M	4	normal	10,24	6,91	7,30	8,90	ongoing	ongoing
27	M	4		9,03	9,07	10,60	8,11	ongoing	ongoing
28	F	4	normal	10,84	7,84	7,67	6,92	ongoing	ongoing
29	M	4	normal	9,38	6,22	11,37	8,66	**mutated**	mutated
30	M	4	normal	8,30	6,68	6,80	6,42	ongoing	**wt**
31	M	4	normal	11,97	10,18	9,28	9,82	**mutated**	ongoing
32	F	4	normal	5,68	7,71	11,83	7,88	**mutated**	**wt**
33	M	4	normal	9,85	8,23	10,64	8,15	ongoing	ongoing
34	M	4		7,02	9,17	11,33	9,54	**mutated**	ongoing
35	F	4		5,39	6,25	5,49	6,84	ongoing	ongoing
36	M	4	**translocated**	6,00	6,61	5,54	6,54	**wt**	**wt**
37	F	4	normal	7,93	9,88	10,93	8,85	ongoing	ongoing
38	M	4		7,53	6,28	8,08	8,59	ongoing	ongoing
39	M	4	normal	11,20	8,31	11,85	10,06	ongoing	**wt**
40	F	4		11,27	10,89	11,03	6,68	ongoing	ongoing

Features of T-ALL patients carrying *C-MYC* rearrangements

SAMPLE	AGE	Type-MYC	FISH	STATUS	*NOTCH1* STATUS	*FBXW7* STATUS
36	11	NO TCR	del(1)(p32)/SIL-TAL1 (86%) **C-MYC-translocation (70%)**	DIED	wt	wt
41	5	NO TCR	**C-MYC-translocation** **t(**1;8)(q32;q24) del(4)(p15)	ND	ND	ND
42	56	NOTCR	del(9)(p21)/CDKN2A-B bial (95%) **C-MYC-translocation (62%)** MYB/6q23 gain MTCP1/Xq28 gain (34%) trisomy 7 (37%)	DIED	wt	wt
43	44	TCR	del(9)(p21)/CDKN2A-B bial (88.5%) del(1)(p32)/SIL-TAL1 (82%) **TCRA/D-C-MYC (90%)** LOSS: PTEN/10q23 (12%) GAIN:AF10/10p13 (86%)	ALIVE	wt	wt
44	25	TCR	del(9)(p21)/CDKN2A-B bial (72%) del(6q15)/CAS8AP2 (69%) del(1)(p32)/SIL-TAL1 (74%) t(7;11)(q34;p15)/TCRB-LMO1 (66%) **TCRAD-C-MYC (62%)**	DIED	wt	wt

Table 2: FISH details of 5 (2 pediatric and 3 adult) patients with *C-MYC* translocations. All 5 patients presented *C-MYC* rearrangements in the major clone. The *C-MYC* translocation involved both TCR and unknown rearranged partner genes. List of abbreviations: wt: wild-type; ND: not defined.

In Table 3 are listed the primers used for the screening of *NOTCH1* and *FBXW7*

Exons	Primers	Product Size
NOTCH1 ex26	for-5'_GCTGAGGGAGGACCTGAACTTGG_3'	812bp
	rev-5'_CCTGAGCTGGAATGCTGCCTCTA_3'	
NOTCH1 ex27	for-5'_CATGGGCCTCAGTGTCCT_3'	335bp
	rev-5'_TAGCAACTGGCACAAACAGC_3'	
NOTCH1 ex28	for-5'_GAGAGTGGGTGAGGAGGC_3'	346 bp
	rev-5'_GTGAGGATGCTCGGCCAG_3'	
NOTCH1 ex34P	for-5'_ACAGATGCAGCAGCAGAACC_3'	721 bp
	rev-5'_CCTGGGGCCAGATAAAACAGTACA_3'	
NOTCH1 ex34T	for-5'_GCTGGCCTTTGAGACTGG_3'	592 bp
	rev-5'_CTCCTGGGGCAGAATAGTGT_3'	
FBXW7 ex9	for-5'_TGATGGGATCATTTTATACGGATG_3'	495 bp
	rev-5'_GACAAAACGCTATGGCTTTCC_3'	
FBXW7 ex10	for-5'_CCCAACTTCCCATTCCCTTA _3'	583bp
	rev-5'_TTTCTTCATGCCAATTTTAACC_3'	

REFERENCES

1. Pui CH, Relling MV, Downing JR. Acute lymphoblastic leukemia. N Engl J Med 2004;350(15):1535–48.
2. Ferrando AA, Neuberg DS, Staunton J, Loh ML, Huard C, Raimondi SC, et al.Gene expression signatures define novel oncogenic pathways in T cell acutelymphoblastic leukemia. Cancer Cell 2002;1:75–87.
3. Soulier J, Clappier E, Cayuela JM, Regnault A, García-Peydró M, Dombret H, et al.HOXA genes are included in genetic and biologic networks defining humanacute T-cell leukemia (T-ALL). Blood 2005;106:274–86.
4. Clappier E, Cuccuini W, Kalota A, Crinquette A, Cayuela JM, Dik WA, et al. The C-MYB locus is involved in chromosomal translocation and genomic duplicationsin human T-cell acute leukemia (T-ALL), the translocation defining a new T-ALLsubtype in very young children. Blood 2007;110:1251–61.
5. Weng AP, Ferrando AA, Lee W, Morris IVth JP, Silverma LB, Sanchez-Irizarry C, Blacklow SC, Look AT, Aster JC. Activating mutations of NOTCH1 in human T cell acute lymphoblastic leukemia. Science 2004; 306:269-271.
6. Sharma VM, Calvo JA, Draheim KM, Cunningham LA, Hermance N, Beverly L, Krishnamoorthy V, Bhasin M, Capobianco AJ, Kelliher MA. Notch1 contributes to mouse T-Cell Leukemia by directly inducing the expression of c-myc. Mol Cell Biol 2006; 26:8022-8031.
7. Weng AP, Millholand JM, Yashiro-Ohtani Y, Arcangeli ML, Lau A, Wai C, Del Bianco C, Rodriguez CG, Sai H, Tobias J, Li Y, Wolfe MS, Shachaf C, Felsher D, Blacklow SC, Pear WS, Aster JC. c-Myc is an important direct target of Notch1 in T-cell acute lymphoblastic leukemia/lymphoma. Genes Dev 2006; 20:2096-2109.
8. Palomero T, Lim WK, Odom DT, Sulis ML, Real PJ, Margolin A, Barnes KC, O'Neil J, Neuberg D, Weng AP, Aster JC, Sigaux F, Soulier J, Look AT, Young RA, Califano A, Ferrando AA. NOTCH1 directly regulates c-MYC and activates a feed-forward-loop transcriptional network promoting leukemic cell growth. Proc Natl Acad Sci 2006; 103:18261-18266.
9. Pelengaris S, Khan M, Evan G. 2002. c-MYC: more than just a matter of life and death. Nat Rev Cancer 2:764–776.
10. Dang CV, O'Donnell KA, Juopperi T. 2005. The great MYC escape in tumorigenesis. Cancer Cell 8:177–178.
11. Meyer N, Penn LZ. 2008. Reflecting on 25 years with MYC. Nat Rev Cancer 8:976–990.
12. Girard , L. , Z. Hanna , N. Beaulieu , C.D. Hoemann , C. Simard , C.A. Kozak , and P. Jolicoeur. 1996 . Frequent provirus insertional mutagenesis of Notch1 in thymomas of MMTVD/myc transgenic mice suggests a collaboration of c-myc and Notch1 for oncogenesis. Genes Dev. 10 : 1930 – 1944.
13. Felsher , D.W. , and J.M. Bishop. 1999 . Reversible tumorigenesis by MYC in hematopoietic lineages. Mol. Cell . 4 : 199 – 207 .
14. Langenau DM, Traver D, Ferrando AA, Kutok JL, Aster JC, Kanki JP, Lin S, Prochownik E, Trede NS, Zon LI, Look AT. 2003. Myc-induced T cell leukemia in transgenic zebrafish. Science 299:887–890.
15. Gutierrez A, Grebliunaite R, Feng H, Kozakewich E, Zhu S, Guo F, Payne E, Mansour M, Dahlberg SE, Neuberg DS, Hertog J, Prochownik EV, Testa JR, Harris M, Kanki JP, Look AT. 2011. Pten mediates Myc oncogene dependence in a conditional zebrafish model of T cell acute lymphoblastic leukemia. J Exp Med 208:1595–1603.
16. Smith DP, Bath ML, Metcalf D, Harris AW, Cory S. 2006. MYC levels govern hernatopoietic tumor type and latency in transgenic mice. Blood 108:653–661.
17. Guo W, Lasky JL, Chang CJ, Mosessian S, Lewis X, Xiao Y, Yeh JE, Chen JY, Iruela-

Arispe ML, Varella-Garcia M, Wu H. 2008. Multi-genetic events collaboratively contribute to Pten-null leukaemia stem-cell formation. Nature 453:529–533.
18. Li X, Gounari F, Protopopov A, Khazaie K, von Boehmer H. 2008. Oncogenesis of T-ALL and nonmalignant consequences of overexpressing intracellular NOTCH1. J Exp Med 205:2851–2861.
19. Loosveld M, Bonnet M, Gon S, Montpellier B, Quilichini B, Navarro JM, Crouzet T, Goujart MA, Chasson L, Morgado E, Picard C, Hernandez L, Fossat C, Gabert J, Michel G, Nadel B, Payet-Bornet D. MYC fails to efficiently shape malignant transformation in T-cell acute lymphoblastic leukemia. Genes Chromosomes Cancer. 2014 Jan;53(1):52-66. doi: 10.1002/gcc.22117. Epub 2013 Oct 12.
20. Erikson J, et al. Deregulation of c-myc by trans location of the alpha-locus of the T-cell receptor in T-cell leukemias. Science. 1986;232(4752):884–886.
21. Thompson BJ, Buonamici S, Sulis ML, et al. The SCFFBW7 ubiquitin ligase complex as a tumor suppressor in T cell leukemia. J Exp Med. 2007; 204(8):1825-1835.
22. O'Neil J, Grim J, Strack P, et al. FBW7 mutations in leukemic cells mediate NOTCH pathway activation and resistance to {gamma}-secretase inhibitors. J Exp Med. 2007;204(8):1813-1824.
23. Asnafi V, Buzyn A, Le Noir S, et al. NOTCH1/ FBXW7 mutation identifies a large subgroup with favorable outcome in adult T-cell acute lymphoblastic leukemia (T-ALL): a Group for Research on Adult Acute Lymphoblastic Leukemia (GRAALL) study. Blood. 2009;113(17):3918-3924.
24. Palomero T, Sulis ML, Cortina M, Real PJ, Barnes K, Ciofani M, et al. Mutational loss of PTEN induces resistance to NOTCH1 inhibition in T-cell leukemia. Nat Med. 2007;13(10):1203-10.
25. Silva A, Yunes JA, Cardoso BA, Martins LR, Jotta PY, Abecasis M, et al. PTEN posttranslational inactivation and hyperactivation of the PI3K/Akt pathway sustain primary T cell leukemia viability. J Clin Invest. 2008;118(11):3762-74.
26. Remke M, Pfister S, Kox C, Toedt G, Becker N, Benner A, et al. High-resolution genomic profiling of childhood T-ALL reveals frequent copy-number alterations affecting the TGF-beta and PI3K-AKT pathways and deletions at 6q15-16.1 as a genomic marker for unfavorable early treatment response. Blood. 2009. 114(5):1053-62.
27. Bandapalli OR, Zimmermann M, Kox C, Stanulla M, Schrappe M, Ludwig WD, Koehler R, Muckenthaler MU, Kulozik AE.NOTCH1 activation clinically antagonizes the unfavorable effect of PTEN inactivation in BFM-treated children with precursor T-cell acute lymphoblastic leukemia. Haematologica. 2013 Jun;98(6):928-36. doi: 10.3324/haematol.2012.073585. Epub 2013 Jan 24.
28. Bonnet M, Loosveld M, Montpellier B, Navarro JM, Quilichini B, Picard C, Di Cristofaro J, Bagnis C, Fossat C, Hernandez L, Mamessier E, Roulland S, Morgado E, Formisano-Tréziny C, Dik WA, Langerak AW, Prebet T, Vey N, Michel G, Gabert J, Soulier J, Macintyre EA, Asnafi V, Payet-Bornet D, Nadel B. Posttranscriptional deregulation of MYC via PTEN constitutes a major alternative pathway of MYC activation in T-cell acute lymphoblastic leukemia. Blood. 2011 Jun 16;117(24):6650-9. doi: 10.1182/blood-2011-02-336842. Epub 2011 Apr 28.
29. Beesley AH, Firth MJ, Ford J, Weller RE, Freitas JR, Perera KU, Kees UR. Glucocorticoid resistance in T-lineage acute lymphoblastic leukaemia is associated with a proliferative metabolism. Br J Cancer. 2009 Jun 16;100(12):1926-36. doi: 10.1038/sj.bjc.6605072. Epub 2009 May 12.
30. Kox C, Zimmermann M, Stanulla M, Leible S, Schrappe M, Ludwig WD, et al. The favorable effect of activating NOTCH1 receptor mutations on long-term outcome in T-ALL patients treated on the ALL-BFM 2000 protocol can be separated from FBXW7

loss of function. Leukemia. 2010; 24(12):2005-13.
31. Clappier E, Collette S, Grardel N, Girard S, Suarez L, Brunie G, et al. NOTCH1 and FBXW7 mutations have a favorable impact on early response to treatment, but not on outcome, in children with T-cell acute lymphoblastic leukemia (T-ALL) treated on EORTC trials 58881 and 58951. Leukemia. 2010;24(12):2023-31.
32. Zuurbier L, Homminga I, Calvert V, te Winkel ML, Buijs-Gladdines JG, Kooi C, et al. NOTCH1 and/or FBXW7 mutations predict for initial good prednisone response but not for improved outcome in pediatric T-cell acute lymphoblastic leukemia patients treated on DCOG or COALL protocols. Leukemia. 2010;24(12):2014-22.
33. Kaveri D, Kastner P, Dembélé D, Nerlov C, Chan S, Kirstetter P. β-Catenin activation synergizes with Pten loss and Myc overexpression in Notch-independent T-ALL. Blood. 2013 Aug 1;122(5):694-704. doi: 10.1182/blood-2012-12-471904. Epub 2013 Jun 25.
34. Wierstra I, Alves J. The c-myc promoter: still MysterY and challenge. Adv Cancer Res. 2008;99: 113-333.
35. Rainer Opgen-Rhein and Korbinian Strimmer, Accurate Ranking of Differentially Expressed Genes by a Distribution-Free Shrinkage Approach, Statistical Applications in Genetics and Molecular Biology, 2007 Feb;6(1). DOI: 10.2202/1544-6115.1252
36. Subramanian A, Kuehn H, Gould J, Tamayo P, Mesirov JP. GSEA-P: a desktop application for Gene Set Enrichment Analysis. Bioinformatics. 2007 Dec 1;23(23):3251-3. Epub 2007 Jul 20.
37. Gorello P, La Starza R, Varasano E, Chiaretti S, Elia L, Pierini V, et al. Combined Interphase Fluorescence in situ Hybridization elucidates T-cell Acute Lymphoblastic Leukemia genetic heterogeneity in adults. Haematologica 2010;95(1):79-86.
38. La Starza R, Antonella Lettieri,Valentina Pierini, Valeria Nofrini, Paolo Gorello, Simona Songia, Barbara Crescenzi, Geertruy te Kronnie, Marco Giordan, Anna Leszl, Maria Grazia Valsecchi, Franco Aversa, Giuseppe Basso, Andrea Biondi, Valentino Conter, Giovanni Cazzaniga and Cristina Mecucci. Linking genomic lesions with Minimal Residual Disease improves prognostic stratification in children with T-cell acute lymphoblastic leukaemia. Leukemia Research 2013.

CHAPTER5

New *MLLT10* gene recombinations in pediatric T-Acute Lymphoblastic Leukemia

Lucia Brandimarte, PhD[1], Valentina Pierini, M.Sc.[1], Danika Di Giacomo, PhD[1], Chiara Borga, M.Sc.[2], Filomena Nozza, M.Sc.[1], Paolo Gorello, PhD[1], Marco Giordan, PhD[2], Giovanni Cazzaniga, PhD[3], Geertruy te Kronnie, PhD[2], Roberta La Starza, MD, PhD[1], Cristina Mecucci, MD, PhD[1].

[1] Hematology and Bone Marrow Transplantation Unit, University of Perugia, Italy
[2] Department of women's and children's health, University of Padova, Padova, Italy
[3] Centro Ricerca Tettamanti, Clinica Pediatrica, Università di Milano-Bicocca, Ospedale S. Gerardo, Monza, Italy.
Correspondence: Prof. Cristina Mecucci, Haematology and Bone Marrow Transplantation Unit, University Hospital, 06132 Perugia, Italy. Phone: +39.075.5783808. Fax: +39.075.5783691. E-mail: crimecux@unipg.it.

Published in Blood (2013) 121 (25), 5064-5067

ABSTRACT

MLLT10 gene, located at 10p13, is a known partner of *MLL* and *PICALM* in specific leukemic fusions generated from recurrent 11q23 and 11q14 chromosome translocations. Deep sequencing recently identified *NAP1L1*/12q21 as another *MLLT10* partner in T-ALL. In pediatric T-ALL we have identified two RNA processing genes, i.e., *HNRNPH1*/5q35 and *DDX3X*/Xp11.3 as new *MLLT10* fusion partners. Gene expression profile signatures of the *HNRNPH1*- and *DDX3X*- *MLLT10* fusions placed them in the *HOXA* subgroup. Remarkably they were highly similar only to *PICALM*-*MLLT10* positive cases. The present study showed *MLLT10* promiscuity in pediatric T-ALL and identified a specific *MLLT10* signature within the *HOXA* subgroup.

INTRODUCTION

New genomic technologies, including whole genome analysis and gene expression profiling (GEP) dramatically improved cytogenetic-molecular classification of T-cell Acute Lymphoblastic Leukemia (T-ALL) which affects about 15% of children with ALL.[1] At least 6 main genetic categories, i.e. *TAL/LMO*, *TLX1*, *TLX3*, *NKX2-1*/*NKX2-2*, *MEF2C*, and *HOXA* have been identified. The *HOXA* group includes cases with *TCRB-HOXA*, *SET-NUP214*, *MLL*-translocations, and *PICALM-MLLT10*.[1,2] In a case of Early T-cell Precursor-ALL (ETP-ALL) the *NAP1L1*/12q21 gene, member of the nucleosome assembly protein family, was recently identified as another *MLLT10* partner.[3]

Interestingly, PICALM-MLLT10, MLL-MLLT10, and NAP1L1-MLLT10 fusions all retained the OM-LZ domain at their C-terminal. [3-5] It exerts a leukemogenic effect by interacting with chromatin modifying proteins such as the H3K79 methyltransferase hDOT1L.[6,7]

The present study focuses on two new *MLLT10* fusion genes in pediatric T-ALL, placing them within the *HOXA* subgroup.

MATERIALS AND METHODS

A Combined Interphase (CI) FISH test (Supplementary Table 1) was applied in 42 pediatric T-ALL enrolled in the AIEOP ALL protocol (number NCT 00613457). Informed consent according to the Declaration of Helsinki was obtained from parents. To identify the new *MLLT10* fusions we used a 5'-RACE-PCR (Invitrogen, Carlsbad, CA, USA) and thermoscript RT-PCR System (Invitrogen) according to the manufacturer's instructions. Primers are listed in Supplementary Table 2. PCR products were subcloned into pGEM-T easy vector (Promega, Madison, WI, USA) and

sequenced with AB3500 Genetic analyzer (Applied Biosystem, Foster City, CA, USA). SNPs analysis was performed using Whole Genome Cytogenetic 2.7M array (Affymetrix, Santa Clara, CA, USA).

Statistical Methods for Microarray Data (Affymetrix hgu 133 plus 2 arrays) were analyzed using the Bioconductor package for R (v2.14.1). Data were deposited at GEO repository (Series Accession Number GSE42765; http://www.ncbi.nlm.nih.gov/geo/). Heatmaps were created using Ward's method and Euclidean distance. The heatmap for the unsupervised analysis was created using the probe sets with the highest variances (threshold 90%), while the heatmap for the supervised analysis was created with differentially expressed probe sets. Arrays were normalized using robust multiple-array average (RMA).[8] Batch effects were removed using ComBat.[9] Differentially expressed genes were identified by the shrinkage T-statistic.[10] False positive findings were prevented by the local False Discovery Rate (lFDR). Probe sets with local FDR below 0.05 were considered significant.[11,12]

RESULTS AND DISCUSSION

CI-FISH identified *MLLT10* rearrangements in 6/42 (14.3%) patients. Four of the total cohort (9.5%) showed the *PICALM-MLLT10* fusion and two (4.8%) *MLLT10* translocations to unknown partner(s). Clinical, hematological, cytogenetic and molecular data of these two patients are shown in Table 1. *MLLT10* FISH probe gave three signals in 55% of nuclei in case 1 and in 60% in case 2. In case 1 metaphase-FISH confirmed the split between the short and the long arms of one chromosome 10, resulting in the der(10)inv(10)(p12q25) seen at karyotype. The 10q breakpoint localized to band 25.3, in a ~12 kb region without genes (Supplementary Figure 1A).

The *MLLT10* gene breakpoint was narrowed to between exons 14 and 15 in patient 1 and between exons 1 and 3 in patient 2 (Supplementary Figure 1B and 1C). 5' RACE-PCR and sequencing showed an *HNRNPH1-MLLT10* in-frame transcript in the first case and a *DDX3X-MLLT10* fusion transcript in the second (Figure 1A and 1C). These results were confirmed by RT-PCR, cloning and sequencing. Subsequently a diagnostic double color double fusion test was developed in both cases (Figure 1B and 1D). The only common additional genetic lesion was a mutated *NOTCH1* gene (Table 1).

HNRNPH1 and *DDX3X* are involved in RNA processing. *HNRNPH1* encodes for a member of the ubiquitous heterogeneous nuclear ribonucleoprotein subfamily (hnRNPs). It is an RNA binding protein that is involved in pre-mRNA processing, and mRNA metabolism and transport.[13] A *HNRNPH1* frameshift mutation was previously described in gastric cancer[14] and a *HNRNPH1* splice variant with protein truncation was identified in murine breast cancer cells.[15] Interestingly, a variant HNRNPH1 protein, covalently modified by O-linked acetyl hexosamine (GlcnaC), was isolated in acute leukemia with 11q23 cytogenetic changes.[16]

DDX3X is a member of the large family of RNA helicases with a DEAD box domain (Asp-Glu-Ala-Asp), that is involved in RNA transcription, splicing, mRNA transport, translation initiation and cell cycle regulation.[17] DEAD box RNA helicases were implicated in diverse forms of leukemia. [18,19] Recently, mutations inside and outside the DEAD box domain were detected in around 3% of patients with Chronic Lymphocytic Leukemia.[20]

Structural analysis of *HNRNPH1-MLLT10* and *DDX3X-MLLT10* fusions showed HNRNPH1 maintained three RNA recognition motifs while DDX3X lost the DEAD box domain, at the N-terminal. At the C-terminal, MLLT10 lost 2/3 NLS domains in

patient 1 but maintained all 3 in patient 2 (Figure 1A and 1C). As in other MLLT10 fusions,[3-5] both cases retained the OM-LZ domain, which is needed to induce AML in mice bearing *PICALM-MLLT10* or *MLL-MLLT10*.[6,7] Interestingly DOT1L inhibitors binding the OM-LZ domain were successful in controlling *MLL-MLLT10* and *PICALM-MLLT10* murine leukemias.[21]

Whether these rare *MLLT10* partners are part of a functional complex or share a common regulation pathway remains to be investigated. The Net View Tools software (http://netview.tigem.it/netview_project/netview_tools.html)[22] showed *DDX3X* was significantly co-expressed and directly linked (Mutual Information >0.1) to *HNRNPH1*, *PICALM*, and *NAP1L1* (Supplementary Table 3).

We applied GEP to determine whether *HNRNPH1-MLLT10* and *DDX3X-MLLT10* shared leukemogenic properties with other *MLLT10* recombinations within the *HOXA* category of T-ALL.[23-24] In an unsupervised analysis of 11 T-ALL samples with the *HOXA* signature, the 6 cases with *MLLT10* rearrangements (4 *PICALM-MLLT10*, 1 *HNRNPH1-MLLT10*, and 1 *DDX3X-MLLT10*) clustered separately from the other 5 cases (1 *MLL-ENL*, 1 *MLL-AF6*, 2 *TCRB-HOXA*, and 1 *SET-NUP214*) (Figure 1E). T-test analysis revealed significant (lFDR<0.05) differences in expression of 280 probe sets (Supplementary Table 4). Supervised analysis with these probe sets confirmed two subgroups (Figure 1F). In the *HOXA* patients with *MLLT10* rearrangements *HHEX* gene expression was higher (> 1.5 fold-change) than in those without. *HHEX* is highly expressed in normal hematopoietic stem cells and down-regulated during normal T cell development.[25] *HHEX* over-expression was found in ETP (as seen in our case n. 1) and linked to up-regulation of *MEF2C* which directly binds the *HHEX* promoter.[2] Interestingly, *HHEX* is a member of the NK-like family of class II homeobox genes. In

the other sub-group of 5 patients without *MLLT10* rearrangements Gene Set Enrichment Analysis (GSEA) showed enrichment of *HOXA* class I homeobox genes and target genes (Supplementary Figure 2). Although these findings need to be confirmed in a larger series of T-ALL, present results suggest that *MLLT10* recombinations underlie a specific signature, within the *HOXA* category of T-ALL.

The present study provides insights into the biological pathways involved in *MLLT10* recombinations in pediatric T-ALL. Finding two new *MLLT10* fusion genes, involving *HNRNPH1* and *DDX3X,* highlights the role of the *MLLT10* gene, and particularly of its OM-LZ domain in this type of leukemia.

Acknowledgments

The authors would like to thank Dr. Diego Di Bernardo (University of Naples "Federico II", Naples, Italy) for assistance in the NetViewTools analysis. F.N. was on leave from Laboratory of Clinical Research, IRCCS-CROB Rionero in Vulture, Potenza, Italy;

L.B. is supported by a grant from "Beat Leukemia" ONLUS and "Società Italiana di Ematologia Sperimentale" (SIES); M.G. is supported by "Fondazione Città della Speranza" ONLUS; G.teK. is supported by "Fondazione Cariparo" progetto d'eccellenza; C.M. is partially supported by "Associazione Italiana per la Ricerca sul Cancro" (AIRC, IG-11512) and "Fondo per gli Investimenti della Ricerca di Base" (FIRB 2011 RBAP11TF7Z_005).

Author Contributions

F.N. and V.P. :performed karyotype analysis; V.P. selected DNA clones and performed FISH experiments; R.L.S. supervised FISH experiments and drafted the paper; L.B. designed and performed molecular experiments and drafted the paper; D.D.G. and P.G.

were involved in cloning and sequencing; C.B., M.G. and G.t.K. performed GEP studies; G.C. performed SNPs analysis; C.M. was responsible for the conception of the study, supervision and manuscript preparation.

Conflict of interest

The authors declare no conflict of interest.

Supplementary Information accompanies the paper on the Blood website (http://www.bloodjournal.org).

REFERENCES

1. Pieter Van Vlierberghe, Rob Pieters, H Berna Beverloo, Jules PP Meijerink. Molecular-genetic insights in paediatric T-cell acute lymphoblastic leukemia. British Journal of Haematology 2008;**143**:153-168.
2. Homminga I, Pieters R, Langerak AW, de Rooi JJ, Stubbs A, Verstegen M *et al.* Integrated transcript and genome analyses reveal NKX2-1 and MEF2C as potential oncogenes in T cell acute lymphoblastic leukemia. Cancer Cell 2011;**19**:484-97.
3. Zhang J, Ding L, Holmfeldt L, Wu G, Heatley SL, Payne-Turner D *et al.* The genetic basis of early T-cell precursor acute lymphoblastic leukaemia. Nature 2012;**481**:157-63.
4. Dreyling MH, Martinez-Climent JA, Zheng M, Mao J, Rowley JD, Bohlander SK. The t(10;11)(p13;q14) in the U937 cell line results in the fusion of the AF10 gene and CALM, encoding a new member of the AP-3 clathrin assembly protein family. Proc Natl Acad Sci U S A. 1996;**93**:4804-9.
5. Chaplin T, Ayton P, Bernard OA, Saha V, Della Valle V, Hillion J *et al.* A Novel Class of Zinc Finger/Leucine Zipper Genes Identified From the Molecular Cloning of the t(10; 11) translocation in Acute Leukemia. Blood 1995;**85**:1435-41.
6. Okada Y, Feng Q, Lin Y, Jiang Q, Li Y, Coffield VM et al. hDOT1L Links Histone Methylation to Leukemogenesis. Cell 2005;**121**:167-178.
7. Deshpande AJ, Rouhi A, Lin Y, Stadler C, Greif PA, Arseni N et al. The clathrin-binding domain of CALM and the OM-LZ domain of AF10 are sufficient to induce acute myeloid leukemia in mice. Leukemia 2011;**25**:1718-27.
8. Bolstad BM, Irizarry RA, Astrand M, Speed TP. A Comparison of Normalization Methods for High Density Oligonucleotide Array Data Based on Variance and Bias. Bioinformatics 2003;**19**:185-193.
9. Johnson WE, Li C, Rabinovic A. Adjusting batch effects in microarray expression data using empirical Bayes methods. Biostatistics 2007;**8**:118-27.
10. Opgen-Rhein R, Strimmer K. Accurate ranking of differentially expressed genes by a distribution-free shrinkage approach. Statist. Appl. Genet. Mol. Biol. 2007;**6**:Article9 (available from http://www.bepress.com/sagmb/vol6/iss1/art9/).
11. Strimmer K. A unified approach to false discovery rate estimation. BMC Bioinformatics 2008;**9**:303 (available from http://www.biomedcentral.com/1471-2105/9/303/).
12. Strimmer K. fdrtool: a versatile R package for estimating local and tail area- based false discovery rates. Bioinformatics 2008;24:1461-1462 (available from http://bioinformatics.oxfordjournals.org/cgi/content/abstract/24/12/1461).
13. Martinez-Contreras R, Cloutier P, Shkreta L, Fisette JF, Revil T, Chabot B. hnRNP proteins and splicing control. Advances in Experimental Medicine and Biology 2007;**623**:123-147.
14. Mori Y, Sato F, Selaru FM, Olaru A, Perry K, Kimos MC *et al.* Instabilotyping Reveals Unique Mutational Spectra in Microsatellite-Unstable Gastric Cancers. Cancer Research 2002;**62**:3641-5.
15. Bemmo A, Dias C, Rose AA, Russo C, Siegel P, Majewski J. Exon-Level Transcriptome Profiling in Murine Breast cancer reveals splicing changes specific to tumors with different metastatic abilities. PlosOne 2010;**5**:e11981.
16. Balkhi MY, Trivedi AK, Geletu M, Christopeit M, Bohlander SK, Behre HM *et al.* Proteomics of acute myeloid leukaemia: cytogenetic risk groups differ specifically in their proteome, interactome and post translational protein modifications. Oncogene

2006;**25**:7041-58.
17. Rosner A, Rinkevich B. The DDX3 subfamily of the DEAD box helicases: divergent roles as unveiled by studying different organisms and in vitro assays. Current Medicinal Chemistry 2007;**14**:2517-25.
18. Arai Y, Hosoda F, Kobayashi H, Arai K, Hayashi Y, Kamada N *et al.* The inv(11)(p15q22) chromosome translocation of de novo and therapy-related myeloid malignancies results in fusion of the nucleoporin gene, NUP98, with the putative RNA helicase gene, DDX10. Blood 1997;**89**:3936-44.
19. Payne EM, Bolli N, Rhodes J, Abdel-Wahab OI, Levine R, Hedvat CV *et al.* Ddx18 is essential for cell-cycle progression in zebrafish hematopoietic cells and is mutated in human AML. Blood 2011;**118**:903-15.
20. Wang L, Lawrence MS, Wan Y, Stojanov P, Sougnez C, Stevenson K *et al.* SF3B1 and other novel cancer genes in chronic lymphocytic leukemia. New England Journal of Medicine 2011;**365**:2497-506.
21. Chen L, Deshpande A, Banka D, Bernt KM, Dias S, Buske C *et al.* Abrogation of MLL-AF10 and CALM-AF10 mediated transformation through genetic inactivation or pharmacological inhibition of the H3K79 methyltransferase Dot1l. Leukemia 2012;e-pub ahead of print 9 November 2012; doi: 10.1038/leu.2012.327.
22. Belcastro V, Siciliano V, Gregoretti F, Mithbaokar P, Dharmalingam G, Berlingieri S *et al.* Transcriptional gene network inference from a massive dataset elucidates transcriptome organization and gene function. Nucleic Acids Research 2011;39:8677-88.
23. Dik WA, Brahim W, Braun C, Asnafi V, Dastugue N, Bernard OA et al. CALM-AF10 + T-ALL expression profiles are characterized by overexpression of HOXA and BMI1 oncogenes. Leukemia 2005;**19**:1948-1957
24. Soulier J, Clappier E, Cayuela JM, Regnault A, García-Peydró M, Dombret H et al. HOXA genes are included in genetic and biologic networks defining human acute T-cell leukemia (T-ALL). Blood 2005;**106**:274-86 .
25. Mack DL, Leibowitz DS, Cooper S, Ramsey H, Broxmeyer HE, Hromas R. Down-regulation of the myeloid homeobox protein Hex is essential for normal T-cell development. Immunology 2002;**107**:444-51.

Table 1. Clinical, immunophenotypic, hematologic, molecular and cytogenetic data.

Patients	Sex/ age	Diagnosis	WBC (x10^9/L)	*CALM-MLLT10*	*MLL-ENL*	*MLL-AF4*	*SIL-TAL1*	*NOTCH1*	*FLT3*	Karyotype	CI-FISH	SNPs	MRD +33/+78	Chemotherapy †	Follow-up (months)
1 (UPN 1036616)	F/7	ETP-ALL	10,55	n.a.	n.a.	neg	neg	mut*	neg	46,XX,inv(10) (p12q25)[2] /46,XX[17]	SPLIT: *MLLT10*/10p12 (55%) LOSS: *IKZF1*/7p12 (10%)	normal	+/+	High risk, no transplant donor	33+
2 (UPN 1023865)	M/11	Cortical T-ALL	152,8	neg	neg	n.a.	neg	mut**	neg	failed	SPLIT: *MLLT10/10p12* LOSS: *PAX5,CDKN2A/B,* *JAK2*/9p13-24 GAIN: RP11-501C14/17q21.31	LOSS 9p24.3-p11.2: from 0 to 47 508 608 bp GAIN 17q21.32-q25.3: from 45 273 751 to 78 786 769 bp	+/-	Standard risk	73+

F=female; M=male; WBC= White Blood Cell; n.a.= data not available; neg.=negative; mut= mutated; MRD=Minimal Residual Disease; * c.4766_4767insAGCAGAACCGGAGCAGCTGCGCAACAGCTC; p.S1589_F1590insAEPEQLRNSS; ** c.G4793C; p.R1598P; NOTCH1 mutation numbers refer to CCDS 43905.1 and NP_060087.3; † AIEOP LLA 2000 (Supplementary reference 1)

FIGURES

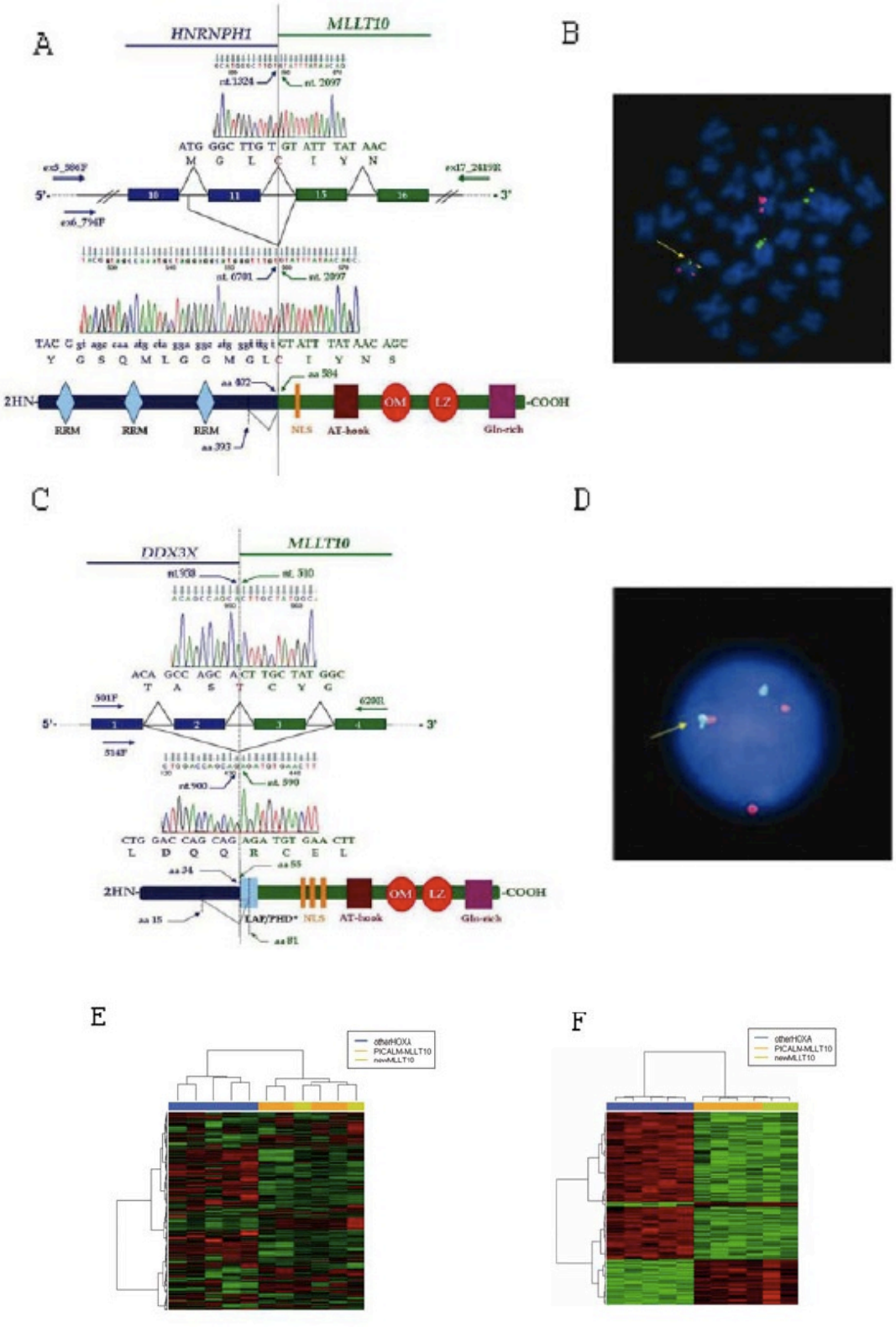
A
HNRNPH1
MLLT10
nt.1324
nt. 2097
ATG GGC TTG T GT ATT TAT AAC
M G L C I Y N
5'
3'
nt. 6701
nt. 2097
Y G S Q M L G G M G L C I Y N S
aa 332
aa 384
2HN-
-COOH
RRM
RRM
RRM
aa 393
NLS
AT-hook
OM
LZ
Gln-rich
B
C
DDX3X
MLLT10
nt.908
nt. 310
ACA GCC AGC ACT TGC TAT GGC
T A S T C Y G
501F
6200L
5'
3'
5143F
nt.900
nt. 590
CTG GAC CAG CAG AGA TGT GAA CTT
L D Q Q R C E L
aa 34
aa 55
2HN-
-COOH
aa 15
LAF/THD*
NLS
AT-hook
OM
LZ
Gln-rich
aa 81
D
E
otherHOXA
PICALM-MLLT10
newMLLT10
F
otherHOXA
PICALM-MLLT10
newMLLT10

Figure 1

Panel A: Two *HNRNPH1-MLLT10* splicing isoforms were identified in patient 1. Upper panel: direct sequencing showed an in-frame *HNRNPH1-MLLT10* isoform joining nucleotide 1324 (*HNRNPH1* exon 11) to nucleotide 2097 (*MLLT10* exon 15). Bottom panel: cloning and sequencing showed nucleotide 6701 (*HNRNPH1* intron 10) fused in-frame with nucleotide 2097 (*MLLT10* exon 15). Hypothetical fusion protein was shown in which HNRNPH1 maintained all three RNA Recognition Motifs (RRM) at the N-terminal and MLLT10 lost 2/3 Nuclear Localization Signals (NLS). MLLT10 mantained the critical OM-LZ domain at the C-terminal. Primer and sequence numbers refer to GenBank accession NC_000005.9, NM_005520.2, NP_005511.1 for *HNRNPH1* and NM_004641.3, NP_004632.1 for *MLLT10*.

Panel B: DCDF-FISH test: probes for *MLLT10* (RP11-418C1 and RP11-249M6) in orange and for *HNRNPH1* (CTD-3223H16 and RP11-410B18) in green, showed 1 fusion signal on der(10) (arrow).

Panel C: Two *DDX3X-MLLT10* splicing isoforms were identified in patient 2. Upper panel: sequencing showed an in-frame *DDX3X-MLLT10* isoform joining nucleotide 958 (*DDX3X* exon 2) to nucleotide 510 (*MLLT10* exon 3). Bottom panel: cloning and sequencing showed an in-frame isoform with nucleotide 900 (*DDX3X* exon 1) fused with nucleotide 590 (*MLLT10* exon 4). The hypothetical fusion protein lost the DDX3X DEAD box domain at the N-terminal and maintained part of the Plant Homeo Domain (PHD), all three NLS and the OM-LZ domain at the C-terminal. Primer and sequence numbers refer to GenBank accession NM_001356.3, NP_001347.3 for DDX3X and NM_004641.3, NP_004632.1 for MLLT10.

Panel D: DCDF-FISH with probes for *DDX3X* in green (RP11-1058N11, flanking 5',

and RP11-10K13, flanking 3') and *MLLT10* in red (RP11-418C1 and RP11-249M6), showed 1 fusion signal (arrow).

Panel E: Unsupervised analysis of 11 T-ALL *HOXA* patients. In such unsupervised analysis patients bearing *MLLT10* rearrangements and those without *MLLT10* rearrangements (1 *MLL-ENL*, 1 *MLL-AF6*, 2 *TCRB-HOXA*, and 1 *SET-NUP214*) are naturally clustered in two distinct groups. *PICALM-MLLT10* patients are indicated in orange; patient 1 and patient 2 (*HNRNPH1-MLLT10*, *DDX3X-MLLT10*) in green and patients without *MLLT10* rearrangements in blue.

Panel F: Supervised analysis was created using the significative probe sets from the comparison of *HOXA* patients with *MLLT10* rearrangements (4 with *PICALM-MLLT10* and the two new cases with *HNRNPH1-MLLT10*, *DDX3X-MLLT10*) vs patients without *MLLT10* rearrangements (1 *MLL-ENL*, 1 *MLL-AF6*, 2 *TCRB-HOXA*, and 1 *SET-NUP214*). Patients bearing *MLLT10* recombinations are indicated in orange or green while patients without *MLLT10* rearrangements are indicated in blue.

SUPPLEMENTARY

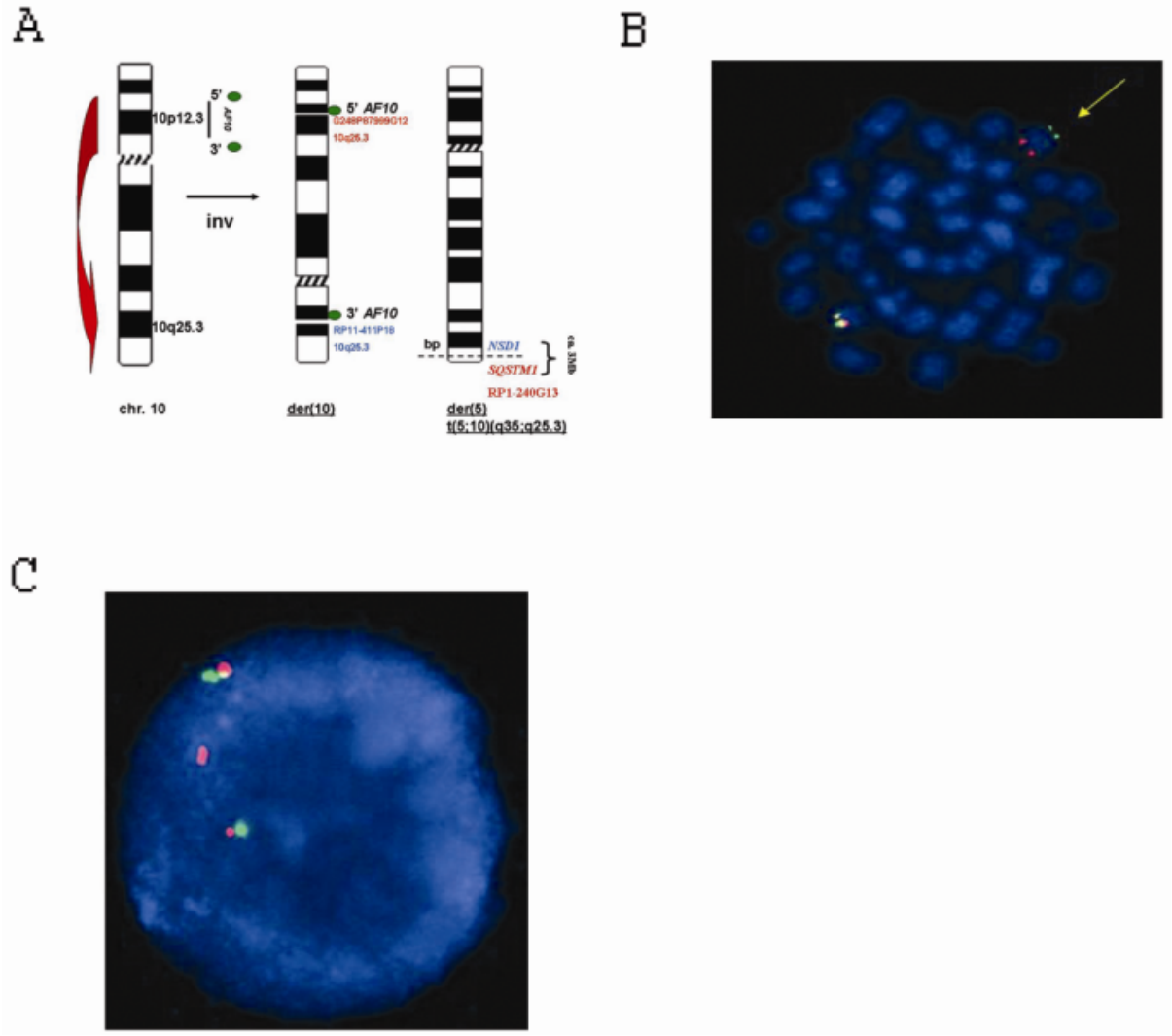

Supplementary Figure 1:

Panel A: Schema of der(10)inv(10)(p12q25)t(5;10)(q35;q25) in patient 1: the10q disruption was located at 10q25.3. A region of about 12 kb without genes (NCBI build 37.3) was flanked by fosmid G248P87999G12 and by RP11-411P18, which was translocated to chromosome 5. FISH located the 5q breakpoint at band 35.3 between *NSD1* (CTC-549A4) and *SQSTM1* (RP11-

379P7) which translocated to der(10) together with the 5q subtelomeric probe RP1-240G13.

Panel B: Metaphase analysis of inv(10) in patient 1: the *MLLT10* breakpoint was investigated with 6 fosmids: G248P86314F1, G248P8684D10, G248P87580B3, G248P89434C6, G248P88419G5, G248P89761F10, spanning the entire gene. Fosmids G248P89434C6 (*MLLT10* exons 10-14, green) and G248P88419G5 (*MLLT10* exons 15-23, red), gave split signals on der(10) (arrow).

Panel C: *MLLT10* break apart assay in patient 2 showed RP11-418C1 (red) gave a split signal indicating the breakpoint occurred within exons 1-3.

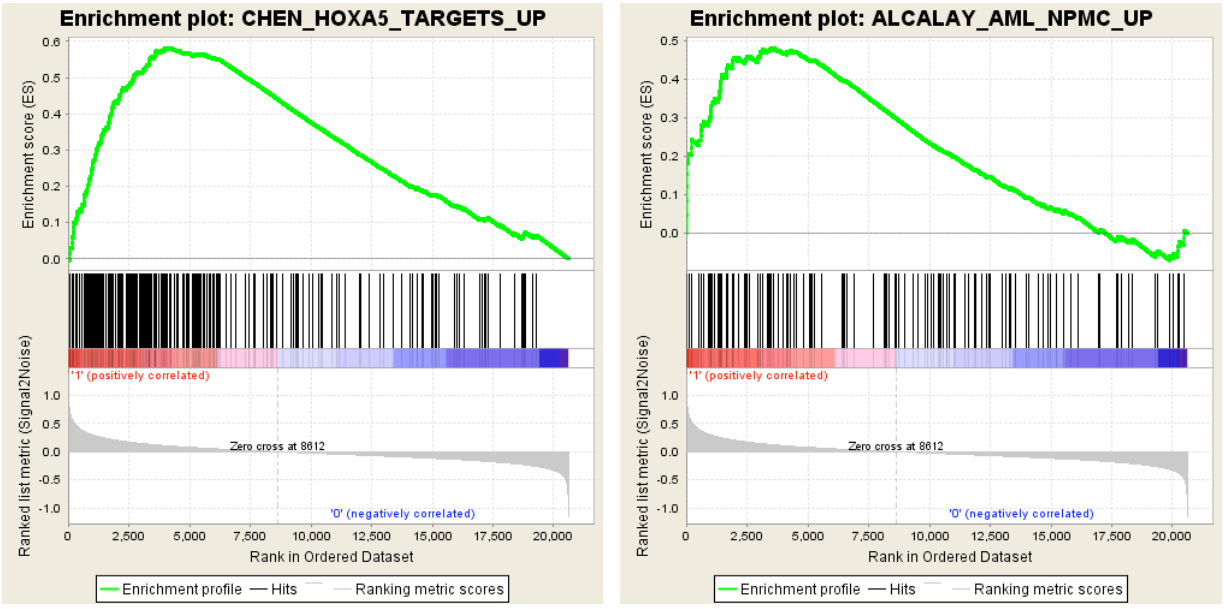

Supplementary Figure 2: Selected enriched gene sets from GSEA.

Figure showed positively enriched gene sets, containing genes upregulated in the "other HOXA" *group (number 1) compared with that bearing* MLLT10 *rearrangements (number 0). Left side: the first pathway was characterized by an upregulation of the* HOXA5 *targets genes; Right side: the second pathway was characterized by the upregulation of different* HOXA *genes (*HOXA1*,* HOXA2*,* HOXA5*,* HOXA6*,* HOXA9*,* HOXA10*). Green trace showed the enrichment score based on hits of genes (indicated by the band on the x axis) that are ordered depending on their level of correlation with one of the two phenotypes compared (in our case* "other HOXA" *vs* "MLLT10 rearrangements"*).*

Supplementary Table 1: FISH probes

CI-FISH (Supplementary reference 2)			
Gene/region	**Centromeric probe**	**Spanning probe**	**Telomeric probe**
SIL/*TAL1*/1p33	G248P80397F3		RP11-346M5
LEF1/4q25		G248P81593B3 G248P81094A7 RP11-840M18	
TLX3/5q35	RP11-182E4 RP11-453D13		RP11-117L6 CTB-31E20 RP11-266N12
CASP8AP2/6q15		RP11-81C7	
GRIK2/6q16		RP1-258B3	
MYB/6q23		RP1-32B1	
IKZF1/7p12		CTC-736O2	
HOXA@/7p15	RP1-170O19		RP1-167F23

TCRB@/7q34	RP11-1220K2		RP11-556I13
PAX5/9p13		RP11-243F8	
CDKN2A/B/9p21		G248P82010F5 G248P82557D2 RP11-149I2	
JAK2/9p24	RP11-39K24		RP11-125K10
ABL1/9q34	RP11-57C19		RP11-83J21
NUP214/9q34	RP11-143H20	RP11-544A12	
NOTCH1/9q34	RP11-83N9	RP11-413M3	RP11-251M1
MLLT10/10p12	RP11-249M6		RP11-418C1
PTEN/10q23		RP11-380G5	
LMO2/11p13	RP11-313G13		RP11-60G13
WT1/11p13		RP1-74J1	
LMO1/11p15	RP11-782G4		RP11-1065L8
NUP98/11p15	RP11-348A20		CTD-3234F16
PICALM/11q14	RP11-90K17		RP11-12D16
MLL/11q23	RP11-832A4	RP11-770J1	RP11-861M13 RP11-158I9
ETV6/12p13	RP11-418C2 RP11-297N18		RP11-434C1
NAP1L1/12q21	RP11-290L1		RP11-453D16
TCRAD@/14q11	RP11-242H9		RP11-447G18
BCL11B/14q32	RP11-74H1	RP11-431B1	
NF1/17q11	RP5-926B9		RP5-1002G3 RP11-501C14
PTPN2/18p11		CTD-2280F20	
AML1/21q22		RP5-1107L6	
PHF6/Xq26		G248P80005E1	

***MLLT10* narrowing**			
Gene/region	**Centromeric probe**	**Spanning probe**	**Telomeric probe**

MLLT10/10p12		G248P86314F1	
MLLT10/10p12		G248P8684D10	
MLLT10/10p12		G248P87580B3	
***MLLT10*/10p12 (exons 10-14)**		**G248P89434C6**	
***MLLT10*/10p12 (exons 15-23)**		**G248P88419G5**	
MLLT10/10p12		G248P89761F10	
10q narrowing			
Gene/region	**Centromeric probe**	**Spanning probe**	**Telomeric probe**
RET/10q11.21		RP11-351D16	
TET1/10q21.3	RP11-524O24		RP11-119F7
TLX1/10q24.31	RP11-108L7		RP11-107I14
ADD3/10q25.1	RP11-182C2		RP11-252O7
TCF7L2/10q25.2		RP11-139K1	
3' *CASP7*, *DCLRE1A*/10q25.3		RP11-211N11	
3' *NHLRC2*/10q25.3		G248P81309A4 G248P81596B5	
flanking 3' *NHLRC2*/10q25.3		G248P82625E6 G248P84642G1	
***ADRB1*/10q25.3**		**G248P87999G12**	
***MIR2110*/10q25.3**		**RP11-411P18**	
FAM160B1/10q25.3		RP11-106M7	
ATRNL1/10q25.3		RP11-359H22	
GFRA1/10q25.3		RP11-96N16	
flanking 3' *EMX2*/10q26.11		RP11-99L6	
5' *CASC2*/10q26.11		RP11-354M20	
BAG3/10q26.11	RP11-179H18		RP11-88I10
WDR11/10q26.12	RP11-323P17		RP11-95I16

FGFR2/10q26.13		RP11-62L18	
DMBT1/10q26.13		RP11-481L19	
BNIP3/10q26.3		RP11-50E23	
GPR123/10q26.3	RP11-97M24		CTD-2557L14

* In bold are indicated probes flanking 10p12 and 10q25 breakpoints in patient 1.

Supplementary Table 2: Primers used in 5'-RACE and RT-PCR experiments

Patients	**Primers used in 5'-RACE**	**Sequences (5'->3')**
1	MLLT10ex21_3191R	GGGTAGGGTTCTGGGACATT
2	MLLT10ex11_1529R	ATGACTGTTGGGAGTGAGAG
Patients	**Primers used in nested PCR**	**Sequences**
1	HNRNPH1ex5_586F	GTGCAGTTTGCTTCACAGGA
	HNRNPH1ex6_794F	CTGGCTTTGAGAGGATGAGG
	HNRNPH1ex8_965F	TCCAGAGCACAACAGGACAC
	MLLT10ex16_2319R	TGAGATGGTGCCTGACTGAG
	MLLT10ex17_2419R	TAGGTTGCGGCTATTGTCTC
2	DDX3X_501F	TAGGGTTTTAGCGGAGAGCAC
	DDX3X_514F	GAGAGCACGGGAAGTGTAG
	MLLT10ex4_620R	CTCCATCCTTATGGGGACAA

Primer numbers refer to Genbank accession: NM_005520.2 for *HNRNPH1*, NM_001356.3 for *DDX3X* and NM_004641.3 for *MLLT10*.

Supplementary Table 3: Connected genes ranked by Mutual Information (MI).

Probeset Id	**Gene Symbol**	**MI**	**MI**	**Probeset ID**	**Gene Symbol**
201210_at	DDX3X	0.142	0	201031_s_at	HNRNPH1
201210_at	DDX3X	0.103	0	208753_s_at	NAP1L1
201210_at	DDX3X	0.09	0	208754_s_at	NAP1L1
201210_at	DDX3X	0.07	0	204528_s_at	NAP1L1
201210_at	DDX3X	0.075	0	212511_at	PICALM
212514_x_at	DDX3X	0.16	0	215236_s_at	PICALM

Connections between DDX3X-HNRNPH1, DDX3X-PICALM and DDX3X-NAP1L1 are significant (MI>0.1).

(http://netview.tigem.it/netview_project/netview_tools.html).

Supplementary Table 4: List of genes with significantly different expression (p <0.05) in the "other *HOXA*" and the "*MLLT10* rearranged" groups, after t-test analysis on gene expression results.

Probe	Symbol	Cytoband	p-value	FC
232424_at	PRDM16	1p36.23-p33	0.005259157	2.41
244413_at	CLECL1	12p13.31	9.59E-09	2.15
213506_at	F2RL1	5q13	0.001086216	1.90
1557167_at	HCG11	6p21	0.043036153	1.83
1556261_a_at			0.000192345	1.76
237458_at			0.033178575	1.69
231747_at	CYSLTR1	Xq13.2-q21.1	0.005259157	1.61
240413_at	PYHIN1	1q23.1	6.39E-05	1.59
215933_s_at	**HHEX**	**10q23.33**	**0.001086216**	**1.58**
1569479_at	ZNF718	4p16.3	0.023225169	1.57
204689_at	**HHEX**	**10q23.33**	**0.001086216**	**1.55**
221045_s_at	PER3	1p36.23	0.000192345	1.52
233903_s_at	ARHGEF26	3q25.2	0.000393532	1.51
238127_at	FLJ41484	13q34	0.023225169	1.50
227889_at	LPCAT2	16q12.2	0.023225169	1.50
232686_at	SIGLECP3	19q13.3	0.033178575	1.48
229822_at			0.001086216	1.47
206120_at	CD33	19q13.3	0.000192345	1.44
1562067_at			0.002392781	1.44
209108_at	TSPAN6	Xq22	0.011065268	1.42
37966_at	PARVB	22q13.2-q13.33	0.023225169	1.42
228538_at	ZNF662	3p22.1	0.001086216	1.40
212686_at	PPM1H	12q14.1	0.023225169	1.40
241696_at	CNTLN	9p22.2	0.000413972	1.39
204638_at	ACP5	19p13.3-p13.2	0.000192345	1.38
202449_s_at	RXRA	9q34.3	0.002392781	1.38
243113_at			0.033178575	1.37
1563226_at	SLC38A10	17q25.3	0.023225169	1.37
215695_s_at	GYG2	Xp22.3	0.012520058	1.36
215813_s_at	PTGS1	9q32-q33.3	0.013232319	1.36
225255_at	MRPL35	2p11.2	0.019228939	1.35

205418_at	FES	15q26.1	0.003034408	1.35
205222_at	EHHADH	3q26.3-q28	4.47E-05	1.35
237497_at			0.005259157	1.34
223487_x_at	GNB4	3q26.33	0.008376883	1.34
57082_at	LDLRAP1	1p36-p35	0.008376883	1.34
240661_at	LOC284475	1p13.1	0.023225169	1.31
1561899_at	CLECL1	12p13.31	0.012520058	1.31
239062_at	LOC100131096	17q25.3	0.000393532	1.31
203128_at	SPTLC2	14q24.3	0.014162154	1.31
210964_s_at	GYG2	Xp22.3	0.038059584	1.30
233467_s_at	TSPAN32	11p15.5	1.18E-07	1.29
1558105_a_at			0.043036153	1.28
221879_at	CALML4	15q23	0.033178575	1.27
1566040_at			0.043036153	1.27
214235_at	CYP3A5	7q21.1	0.012520058	1.27
227999_at	PWWP2B	10q26.3	0.012520058	1.26
233428_at			0.013232319	1.26
1569401_at	CLEC12A	12p13.2	0.019228939	1.25
39318_at	TCL1A	14q32.1	0.013232319	1.25
242966_x_at			6.39E-05	1.24
1556116_s_at	TNPO1	5q13.2	0.038059584	1.24
234645_at			0.023225169	1.24
223467_at	RASD1	17p11.2	0.033178575	1.24
205505_at	GCNT1	9q13	0.000545837	1.24
220558_x_at	TSPAN32	11p15.5	0.002696521	1.23
224708_at	KIAA2013	1p36.22	0.003034408	1.22
223995_at	SLC12A9	7q22	0.014162154	1.22
228066_at	C17orf96	17q12	0.012520058	1.22
204394_at	SLC43A1	11p11.2-p11.1	0.001906421	1.21
211582_x_at	LST1	6p21.3	0.023225169	1.21
236501_at	SALL4	20q13.2	0.008376883	1.20
214181_x_at	LST1	6p21.3	0.023225169	1.20
241466_at			0.023225169	1.19
232309_at	LOC202181	5q35.3	0.023225169	1.19
204336_s_at	RGS19	20q13.33	0.023225169	1.18
229686_at	P2RY8	Xp22.33	0.002852378	1.18
227344_at	IKZF1	7p13-p11.1	0.003034408	1.17
236454_at	RNF212	4p16.3	0.001086216	1.17
201954_at	ARPC1B	7q22.1	0.005259157	1.15
220600_at	C3orf75	3p21.31	0.033178575	1.15
208736_at	ARPC3	12q24.11	4.47E-05	1.14
201143_s_at	EIF2S1	14q23.3	0.019228939	1.13
201651_s_at	PACSIN2	22q13.2-q13.33	0.043036153	1.11
221267_s_at	FAM108A1	19p13.3	0.001906421	1.10
217839_at	TFG	3q12.2	0.033178575	-1.08

224630_at	ERLEC1	2p16.2	0.043036153	-1.08
221493_at	TSPYL1	6q22.1	0.038059584	-1.09
203279_at	EDEM1	3p26.1	0.000192345	-1.11
217858_s_at	ARMCX3	Xq21.33-q22.2	0.023225169	-1.11
201738_at	EIF1B	3p22.1	0.013232319	-1.11
218497_s_at	RNASEH1	2p25	0.001086216	-1.12
227141_at	TYW3	1p31.1	0.043036153	-1.12
209067_s_at	HNRPDL	4q21.22	1.18E-07	-1.12
203261_at	DCTN6	8p12-p11	0.023225169	-1.12
218740_s_at	CDK5RAP3	17q21.32	0.023225169	-1.12
203484_at	SEC61G	7p11.2	0.033178575	-1.12
210178_x_at	SRSF10	1p36.11	0.011065268	-1.12
223766_at	LOC100133130	10q11.22	0.003034408	-1.14
230659_at	EDEM1	3p26.1	0.002392781	-1.14
207079_s_at	MED6	14q24.2	0.001086216	-1.14
226285_at	CAPRIN1	11p13	0.033178575	-1.14
218582_at	MARCH5	10q23.32-q23.33	0.012520058	-1.14
213447_at			0.003034408	-1.14
222307_at	LOC282997	10q25.2	0.012520058	-1.14
217825_s_at	UBE2J1	6q15	0.000192345	-1.14
218178_s_at	CHMP1B	18p11.21	0.033178575	-1.14
201057_s_at	GOLGB1	3q13	0.012520058	-1.14
225811_at	C11orf58	11p15.1	0.043036153	-1.14
228349_at	KIAA1958	9q32	0.013232319	-1.15
227640_s_at			0.023225169	-1.15
213594_x_at	SRSF10	1p36.11	3.94E-05	-1.15
202583_s_at	RANBP9	6p23	0.000393532	-1.15
202557_at	HSPA13	21q11	0.019228939	-1.16
223486_at	GTPBP8	3q13.2	0.023225169	-1.16
222435_s_at	UBE2J1	6q15	0.011065268	-1.16
1554678_s_at	HNRPDL	4q21.22	0.000192345	-1.16
235566_at	TMF1	3p21-p12	0.011065268	-1.16
225284_at	DNAJC3	13q32.1	0.023225169	-1.17
1555832_s_at	KLF6	10p15	0.014162154	-1.17
202798_at	SEC24B	4q25	0.023225169	-1.17
205068_s_at	ARHGAP26	5q31	0.008376883	-1.18
204299_at	SRSF10	1p36.11	3.39E-06	-1.18
219335_at	ARMCX5	Xq22.1-q22.3	0.023225169	-1.18
209712_at	SLC35D1	1p32-p31	0.012520058	-1.18
223117_s_at	USP47	11p15.3	0.033178575	-1.18
210285_x_at	WTAP	6q25-q27	0.000413972	-1.18
39729_at	PRDX2	19p13.2	0.023225169	-1.18
235112_at			0.014162154	-1.18
224606_at	KLF6	10p15	1.08E-06	-1.18
1553686_at	C18orf25	18q21.1	0.023225169	-1.18

213372_at	PAQR3	4q21.21	3.94E-05	-1.19
202842_s_at	DNAJB9	14q24.2-q24.3	0.011065268	-1.19
213074_at	PHIP	6q14	0.043036153	-1.19
212542_s_at	PHIP	6q14	0.033178575	-1.20
214289_at	PSMB1	6q27	0.012520058	-1.20
239562_at	MTHFD2L	4q13.3	0.013232319	-1.20
223602_at	USP30	12q24.11	0.023225169	-1.20
235526_at			0.014162154	-1.20
1560029_a_at	C11orf57	11q23.1	0.013232319	-1.20
231269_at	ASCC3	6q16	0.006117516	-1.20
206181_at	SLAMF1	1q23.3	0.033178575	-1.20
238946_at			0.011065268	-1.20
238114_at	PCMTD1	8q11.23	0.012520058	-1.21
232126_at	COQ2	4q21.23	0.023225169	-1.21
235103_at	MAN2A1	5q21-q22	8.44E-06	-1.21
228857_at	GNL1	6p21.3	0.001906421	-1.21
200732_s_at	PTP4A1	6q12	0.008376883	-1.21
228330_at	ZUFSP	6q22.1	0.023225169	-1.21
213212_x_at			0.013232319	-1.21
227160_s_at	C20orf7	20p12.1	0.002852378	-1.21
1555562_a_at	ZCCHC7	9p13.2	0.038059584	-1.21
201799_s_at	OSBP	11q12-q13	0.000545837	-1.22
218696_at	EIF2AK3	2p12	0.011065268	-1.22
203097_s_at	RAPGEF2	4q32.1	0.008376883	-1.22
1554661_s_at	CNST	1q44	0.036210511	-1.22
218013_x_at	DCTN4	5q31-q32	0.013232319	-1.22
1555274_a_at	EPT1	2p23.3	0.000545837	-1.22
227018_at	DPP8	15q22	8.44E-06	-1.22
222519_s_at	IFT57	3q13.13	0.023225169	-1.23
204526_s_at	TBC1D8	2q11.2	3.94E-05	-1.23
200898_s_at	MGEA5	10q24.1-q24.3	0.023225169	-1.23
233952_s_at	ZNF295	21q22.3	0.023225169	-1.23
228789_at	MTMR6	13q12	0.008376883	-1.23
244828_x_at	NAF1	4q32.2	0.001958125	-1.23
201775_s_at	KIAA0494	1pter-p22.1	0.023225169	-1.23
1553749_at	FAM76B	11q21	0.005259157	-1.23
1565651_at	ARF1	1q42	0.008376883	-1.24
202722_s_at	GFPT1	2p13	0.023225169	-1.24
204334_at	KLF7	2q32	0.008376883	-1.24
203017_s_at	SSX2IP	1p22.3	4.47E-05	-1.24
210048_at	NAPG	18p11.22	0.019228939	-1.24
1559862_at	COPA	1q23-q25	0.013232319	-1.25
222303_at			1.28E-09	-1.25
1561965_at	SNRPB2	20p12.1	0.001906421	-1.25
1553133_at	C9orf72	9p21.2	0.001906421	-1.25

223846_at	AZI2	3p24.1	0.023225169	-1.25
229790_at	TERF2	16q22.1	0.000413972	-1.25
225539_at	ZNF295	21q22.3	0.023225169	-1.25
219631_at	LRP12	8q22.2	0.000393532	-1.25
239124_at			0.001086216	-1.26
244360_at	FBXL17	5q21.3	6.39E-05	-1.26
242325_at	YWHAH	22q12.3	0.000192345	-1.26
240432_x_at	KLF7	2q32	0.023225169	-1.26
235369_at	C14orf28	14q21.2	0.023225169	-1.27
1556144_at	DHX30	3p21.31	0.023225169	-1.27
1559023_a_at	KIAA0494	1pter-p22.1	0.012520058	-1.27
1555448_at	MUDENG	14q22.3	0.011065268	-1.27
212225_at	EIF1	17q21.2	0.000545837	-1.27
233138_at	C18orf1	18p11.21	0.023225169	-1.27
227767_at	CSNK1G3	5q23	0.002575538	-1.27
228370_at			0.001086216	-1.28
232483_at	MED17	11q14	0.000192345	-1.28
242776_at	ZCCHC6	9q21	0.000413972	-1.28
231833_at	RBM33	7q36.3	0.023225169	-1.28
231793_s_at	CAMK2D	4q26	0.023225169	-1.28
243982_at	KLHL28	14q21.2	0.013232319	-1.28
237495_at	MPP7	10p12.1	0.033178575	-1.28
1569450_at	CAPZA2	7q31.2-q31.3	0.011065268	-1.29
242073_at			0.012520058	-1.29
231953_at	BPTF	17q24.3	0.038059584	-1.29
201776_s_at	KIAA0494	1pter-p22.1	0.005259157	-1.29
233035_at			0.033178575	-1.29
202766_s_at	FBN1	15q21.1	0.008376883	-1.30
1554038_at	LARP1B	4q28.2	0.001086216	-1.30
239862_at			0.013232319	-1.30
227384_s_at			0.023225169	-1.31
202558_s_at	HSPA13	21q11	0.005259157	-1.31
230764_at			0.033178575	-1.33
243649_at	FBXO7	22q12-q13	0.012520058	-1.33
213292_s_at	SNX13	7p21.1	0.001086216	-1.33
221211_s_at	C21orf7	21q22.3	0.023225169	-1.33
231042_s_at			0.003034408	-1.34
233480_at	TMEM43	3p25.1	0.023225169	-1.34
242999_at	ARHGEF7	13q34	0.033178575	-1.34
240513_at	EIF3M	11p13	0.012520058	-1.34
1568665_at	RNF103	2p11.2	8.44E-06	-1.35
1568627_at	SMEK2	2p16.1	0.033178575	-1.35
213093_at	PRKCA	17q22-q23.2	0.005259157	-1.36
202375_at	SEC24D	4q26	0.023225169	-1.36
239540_at			1.08E-06	-1.36

239200_at			0.023225169	-1.37
242756_at			0.001086216	-1.37
226750_at	LARP1B	4q28.2	1.28E-09	-1.37
225019_at	CAMK2D	4q26	0.023225169	-1.37
1554339_a_at	COG3	13q14.13	0.019228939	-1.38
1554785_at	CCDC82	11q21	0.023225169	-1.38
200731_s_at	PTP4A1	6q12	0.008376883	-1.39
227755_at			0.000192345	-1.39
207850_at	CXCL3	4q21	0.008376883	-1.40
228555_at	CAMK2D	4q26	0.023225169	-1.40
1555279_at	ARMC8	3q22.3	0.023225169	-1.41
222167_at			0.012520058	-1.41
226393_at	CYP2U1	4q25	3.39E-06	-1.41
232615_at			0.008376883	-1.41
244700_at	SEC61B	9q22.32-q31.3	6.39E-05	-1.41
207068_at	ZFP37	9q32	0.011065268	-1.42
240485_at			8.44E-06	-1.42
224994_at	CAMK2D	4q26	0.000192345	-1.43
216121_at			0.023225169	-1.43
202083_s_at	SEC14L1	17q25.2	0.008376883	-1.44
239415_at	MAP9	4q32.1	0.005259157	-1.44
215351_at	RTCD1	1p21.2	0.013232319	-1.45
1554290_at	HERC3	4q21	0.023225169	-1.45
215209_at	SEC24D	4q26	0.023225169	-1.47
219532_at	ELOVL4	6q14	0.013232319	-1.47
1560846_at			0.023225169	-1.49
212254_s_at	DST	6p12.1	0.043036153	-1.49
1555281_x_at	ARMC8	3q22.3	8.44E-06	-1.49
1568609_s_at			0.000545837	-1.49
60084_at	CYLD	16q12.1	0.023225169	-1.50
226120_at	TTC8	14q31.3	0.000393532	-1.50
239005_at	FLJ39739	1q21.1	0.000192345	-1.51
212602_at	WDFY3	4q21.23	0.001086216	-1.53
202381_at	ADAM9	8p11.22	0.008376883	-1.54
220576_at	PGAP1	2q33.1	6.39E-05	-1.55
222142_at	CYLD	16q12.1	0.012520058	-1.56
229139_at	JPH1	8q21	0.008376883	-1.57
212606_at	WDFY3	4q21.23	0.002696521	-1.57
232304_at	PELI1	2p13.3	0.002575538	-1.60
236260_at	LOC100287598	16p13.2	1.08E-06	-1.60
1556911_at			6.39E-05	-1.60
208015_at	SMAD1	4q31	0.001086216	-1.61
212526_at	SPG20	13q13.3	0.011065268	-1.61
207738_s_at	NCKAP1	2q32	0.023225169	-1.61
241801_at	PGAP1	2q33.1	8.44E-06	-1.62

207705_s_at	NINL	20p11.22-p11.1	0.008376883	-1.62
204201_s_at	PTPN13	4q21.3	0.012520058	-1.63
212263_at	QKI	6q26	0.014162154	-1.65
216693_x_at	HDGFRP3	15q25.2	0.011065268	-1.70
237491_at			9.59E-09	-1.70
232098_at	DST	6p12.1	8.44E-06	-1.72
235391_at	FAM92A1	8q22.1	0.012520058	-1.74
235451_at	SMAD5	5q31	0.023225169	-1.76
213469_at	PGAP1	2q33.1	0.012520058	-1.76
209526_s_at	HDGFRP3	15q25.2	0.005259157	-1.79
239725_at	PGAP1	2q33.1	1.16E-11	-1.80
218847_at	IGF2BP2	3q27.2	4.47E-05	-1.81
228266_s_at	HDGFRP3	15q25.2	0.011065268	-1.84
217963_s_at	NGFRAP1	Xq22.2	0.033178575	-1.86
202351_at	ITGAV	2q31-q32	0.011065268	-1.91
207781_s_at	ZNF711	Xq21.1	0.012520058	-1.94
242457_at			0.023225169	-1.98
201579_at	FAT1	4q35	6.39E-05	-2.05
228423_at	MAP9	4q32.1	1.18E-07	-2.06
220145_at	MAP9	4q32.1	0.000545837	-2.07
210517_s_at	AKAP12	6q24-q25	0.013232319	-2.18
228988_at	ZNF711	Xq21.1	1.56E-06	-2.18
209524_at	HDGFRP3	15q25.2	0.008376883	-2.21

Supplementary references

1. Schrappe M, Valsecchi MG, Bartram CR, Schrauder A, Panzer-Grümayer R, Möricke A *et al.* Late MRD response determines relapse risk overall and in subsets of childhood T-cell ALL: results of the AIEOP-BFM-ALL 2000 study. Blood 2011;**118**:2077-84.

2. Gorello P, La Starza R, Varasano E, Chiaretti S, Elia L, Pierini V *et al.* Combined interphase fluorescence in situ hybridization elucidates the genetic heterogeneity of T-cell acute lymphoblastic leukemia in adults. Haematologica 2010;**95**:79-86.

CONCLUSIONS

Acute Lymphoblastic Leukemia (ALL) is an aggressive malignancy of lymphopoietic cells characterized by a clonal proliferation of blast cells originated from lymphoid precursors arrested at early stages of differentiation. ALL is the most common cancer and the most successfully treated malignancy in children, with long-term survival rates reaching over 80% as result of risk-directed treatment and intensifies cure protocols. Although advances in genomic and molecular analysis have improved the ability to stratify patients in risk groups that receive appropriate treatment, still a quarter of children experience relapse and have poor outcomes, failing to achieve a complete remission. Relapse in ALL is characterized by disease recurrence at extramedullary sites, such as the Central Nervous System. At diagnosis <2% of ALL patients present CNS disease, but at relapse >30% have infiltration at this site. Reaching leukemic cells in the so-called "sanctuary-sites", such as the CNS, require specific therapies that can be invasive (i.e: cranial irradiation) and related to several deleterious effects. Modern diagnostic techniques improved the ability to categorize risk, allowing clinicians to optimize therapy including that directed to the CNS. Moreover, numerous efforts have been made to reduce or avoid the use of cranial irradiation. The need to use cranial irradiation in the cure of patient with CNS disease is still debated, in fact some studies propose to avoid this treatment. However, cranial irradiation is still recommended for 2-20% of ALL at high risk of CNS relapse, such as patients with CNS infiltration at diagnosis or presenting T-immunophenotype with high WBC count. This overview shows the importance to understand molecular mechanisms that allow or predispose blast cells to infiltrate the CNS in order to improve the CNS-directed treatment.

With this work we aimed to deep insight into molecular mechanisms that allow T-ALL cells to infiltrate the CNS. Particularly, to gain in this aim we used a whole transcriptome analysis approach (gene expression profiling) starting from animal

models to arrive to T-ALL patients. We studied T-cell Acute Lymphoblastic Leukemia (T-ALL) as the incidence of CNS infiltration is higher in T-ALL compared to B-ALL.

We identify for the first time the presence of CNS infiltration in two zebrafish models that develop T-ALL (*hMYC-ER* and *hlk*). These two zf lines are genetically different and could represent different subgroup of human T-ALL; *hMYC-ER* model overexpress the human *C-MYC* as a larger number of T-ALL patients, while *hlk* line carries an unknow mutation. Interesting, the type of CNS invasion in these models was very similar to CNS infiltration found in pediatric patients at time to dead in 1970s. In fact, we found different degree of infiltration at the meningeal level, often correlated to optic nerve involvement. These data underline the ability of these zf models to mimic the human CNS disease. This discovery is very important, not only for the study of mechanisms that predispose T-ALL cell to enter in the CNS, but also to perform pharmacological test in a high-throughput manner. Another important aspect was the presence of a different trend of CNS infiltration that was characteristic for each zf line: *hMYC-ER* zf line presented higher levels of CNS infiltration compare to *hlk* model. GEP analysis allowed us to identify two different molecular networks active in *hMYC-ER* and *hlk* cancer, suggesting the idea that T-ALL cells could use different mechanisms to infiltrate the CNS. Particularly, we found a positive correlation between the degree of CNS infiltration and the expression levels of the chemokine receptor *cxcr4*. This result suggests that higher expression levels of *cxcr4* increase the ability of T-ALL cells to infiltrate the CNS. Interesting, in zebrafish the transcription of *cxcr4* was also related to high expression levels of *C-MYC* oncogene.

At this point we decided to validate the results found in zebrafish using another animal model closer to human patients: we used murine models xenografted with primary T-ALL cells coming from pediatric patients. We demonstrated that also in xenografted mice, human T-ALL cells could mimic the phenomenon of CNS infiltration. Importantly, we found another useful model to study the phenomenon of CNS. Moreover, mice xenografted with different patients presented variable degree of CNS infiltration, suggesting a different predisposition of T-ALL cells to invade the CNS environment. Results found in murine model were very similar to previous ones obtain in zebrafish. At this point we decided to investigate also in xenografted model the

CXCR4 as one possible molecular mechanism that predispose T-ALL cells to invade the CNS. Preliminary results seem to validate the relation between higher *CXCR4* expression levels and the increased ability of blast cells to invade the CNS. Other analyses on a larger cohort of xenoengrafted mice are ongoing. Once confirmed the importance of this chemokine receptor in regulating the phenomenon of CNS invasion, we could start to test specific inhibitor for *CXCR4*, such as ADM3100, in murine model xenografted with T-ALL cells that we know to infiltrate the CNS.

We do not limit the study of CNS infiltration to animal models, but we preceded this work performing a whole transcriptome analysis on human pediatric T-ALL patients with- and without- CNS infiltration at diagnosis. The study of CNS infiltration directly in human patient is not easy, as little material is available for research and it is not possible to study cells directly extracted from the cerebrospinal fluid. GEP analysis failed to find a strong signature that could distinguish patients with- and without CNS involvement. Moreover, in T-ALL human patients we were not able to find the correlation between higher expression levels of *CXCR4* and the CNS infiltration, as almost all CNS- patients highly expressed the *CXCR4*. The passage from animal model to human patients is not so linear. First, the biological process we are observing in patients and animal models is not exactly the same, in fact, animal models present an extreme infiltration that might happen in human if disease is not treated and that could partially change the gene expression profiling of blast cells. Second, it is possible that a group of patients is underestimated for CNS disease and is classified among CNS- cases; that increases the complexity to study this phenomenon in human patients. Third, different mechanisms could be used by T-ALL cells to infiltrate the CNS; in fact, we proposed the CXCR4/CXCL12 axis as one possible mechanisms or a predisposing factor to enter in the CNS, but not as the absolute mechanisms that can discriminate between CNS+ and CNS- cases. Further studies are necessary to better understand the role of *CXCR4* in human patients, maybe studying also the activation of this chemokine receptor in T-ALL cells.

Another aspect we investigated inside the human pediatric T-ALL group was related to *C-MYC* expression levels. Previously, we have seen that *hMYC-ER* line is also a zebrafish model that can mimic human T-ALL overexpressing *C-MYC*. The prognostic

significance of *C-MYC* activation is not still understood. Analysis of *C-MYC* expression on a cohort of T-ALL patients revealed different expression level of *C-MYC* oncogene; particularly it is possible identify a group with high- and low- expression of *C-MYC*. However, GEP analysis failed to found a signature that can distinguish these groups. Once again we are in front of this problem; human T-ALL is a complex disease in which multiple events can occur to contribute and give rise to leukemogenesis process. In fact, many factors can contribute to *C-MYC* deregulation (*NOTCH1, FBXW7, PTEN* mutations and *C-MYC* rearrangements). To give a prognostic significance to *C-MYC* deregulation, it is probably necessary to investigate not only the deregulation of the single gene but contextualize its expression in different T-ALL contexts. To understand the biological meaning to have *C-MYC* upregulated by different causes, we compared patients with *C-MYC* rearrangement in absence of $NOTCH1^{m}$ and patients without *C-MYC* rearrangement but possible *NOTCH1, FBXW7, PTEN* mutations. A strong signature separated cases with-and without *C-MYC* rearrangement. Of note, the subgroup of patients carrying *C-MYC* rearrangements presents a NOTCH1-independent leukemia compared to the group without *C-MYC* rearrangement that seems to be strongly related to NOTCH1 pathway activation.

In this thesis work we tested the ability of GEP analysis in distinguish signatures also inside specific T-ALL subgroups, such us in the subgroup of T-ALL patients with high expression of *C-MYC*. This power of GEP was already tested in another study, where we were able to identified a specific signature for patients carrying *MLLT10* rearrangements, inside the *HOXA* subgroup in pediatric T-ALL.